



**Dissertation zur Erlangung des Doktorgrades
der Fakultät für Chemie und Pharmazie
der Ludwig-Maximilians-Universität München**

Biofunctionalized Mesoporous Silica for Controlled Release Applications

vorgelegt von
Axel Schloßbauer
aus
München

2010

Erklärung

Diese Dissertation wurde im Sinne von § 13 Abs. 3 bzw. 4 der Promotionsordnung vom 29. Januar 1998 von Herrn Professor Thomas Bein betreut.

Ehrenwörtliche Versicherung

Diese Dissertation wurde selbständig, ohne unerlaubte Hilfe erarbeitet.

München, am

.....

(Unterschrift des Autors)

Dissertation eingereicht am:

1. Gutacher: Prof. Dr. Thomas Bein

2. Gutachter: Prof. Dr. Christoph Bräuchle

Mündliche Prüfung am: 14.12.2010

Danksagung

Für die freundliche Aufnahme in seinen Arbeitskreis, das Vertrauen und die bereitgestellte Freiheit, welche ich während meinen Forschungsarbeiten genießen durfte möchte ich mich bei meinem Doktorvater Professor Thomas Bein herzlich bedanken. Das interessante Forschungsthema und das freundliche Arbeitsklima in seiner Gruppe haben mich über die gesamte Zeit sehr motiviert. Außerdem bedanke ich mich für die bereitgestellten Empfehlungsschreiben für die Römer-Preise für Diplom- und Doktorarbeit sowie für meinen anstehenden Post-Doc-Aufenthalt in Kalifornien.

Professor Christoph Bräuchle möchte ich ebenfalls sehr herzlich danken für die interessanten Kooperationsmöglichkeiten mit einem meist sehr erfolgreichen Ausgang. Die bereitgestellten Empfehlungsschreiben für meinen Post-Doc-Aufenthalt in Santa Barbara waren äußerst hilfreich. Zusätzlich bedanke ich mich für die Erstellung des Zweitgutachtens zu dieser Arbeit.

Ich bedanke mich sehr bei Anna M. Sauer aus dem Arbeitskreis Prof. Bräuchle für ihre unermüdliche Ausdauer am Mikroskop, die uns ein paar schöne Erfolge beschert hat. In diesem Zusammenhang bedanke ich mich auch bei Dr. Nadia Ruthardt für die wichtigen Diskussionen.

Ich möchte mich auch bei meinen Kooperationspartnern aus der Pharmazie bedanken, Professor Ernst Wagner, David Schaffert und Christian Dohmen, welche immer wohlwollend meine Vorschläge aufgegriffen, verbessert und mit mir gemeinsam in die Realität umgesetzt haben.

Eine weitere erfolgreiche Kooperation gab es zwischen unserem Arbeitskreis, dem Arbeitskreis von Professor Thomas Carell und der Firma Baseclick GmbH, namentlich Simon Warncke und Philipp Gramlich. Die große Unterstützung in der Bereitstellung der hochfunktionellen DNA hat eine tolle Publikation ermöglicht.

Das angenehme Arbeitsklima im AK Bein ist natürlich auch den netten Kollegen zu verdanken, welche ich glücklicherweise in der Doktorarbeit kennenlernen durfte.

Dr. Johann Kecht hat mich bis zum Ende seiner Promotion wirklich erstklassig betreut und eingearbeitet.

Dr. Valentina Cauda danke ich für die Spitzenkooperationen und wünsche ihr viel Glück in ihrem neuen, alten Leben.

Mein Büro mit Mirjam und Jörg (wir haben es tatsächlich geschafft, den Dreierpack) war immer gut für ne kleine Auszeit. Ich wünsche euch weiterhin viel Glück!

Schon weg, aber ebenfalls sehr nette Kollegen waren Hendrik, Johannes, Camilla, Anderl, Lea (danke fürs empfehlen), Monika und Olivier, welche alle immer mit ihrer Altdoktoranden bzw. Post-Doc Weisheit mit Rat und Tat zur Seite standen.

Noch da, und ebenfalls äußerst nette Kollegen waren Benni (der mich das ganze Studium begleitet hat), Christian, Alexandra, Fabian, Vesna, Yan, Yujing, Stefan, Florian Auras, Hans, Norma, Johann, Alesja, Dina, Karin, Flo HiHo (die Band passt schon!), Andi und Kun. Danke euch für die netten Kaffeepausen und Konferenzen

Danke an Markus und Steffen für diverse TEM-Sessions (waren viele Rotzproben, ich weiss...)

Ein besonderer Dank gilt Bastian Rühle für die tollen Grafiken in 3D für meine Paper und das Angewandte-Titelblatt.

Ralf und Doro (Das Paper kommt schon noch raus!), danke euch auch fürs Kontakthalten. Hoffentlich kommt ihr im Dezember noch mal vorbei!

Großen Dank auch an Regina, die in meinem Papierkramchaos immer den Überblick behalten hat, Tina Reuther für viele Messungen und Unterstützung in der Besorgung exotischer Labormaterialien.

CeNS möchte ich danken für die finanzielle Unterstützung meiner Forschung, ebenso großen Dank an die Dr.-Klaus-Römer-Stiftung für die großzügige Vergabe von Preisgeldern.

Der größte Dank gilt meiner Familie, welche durch ihre Unterstützung mein Studium und die Doktorarbeit erst ermöglicht hat.

Abstract

Host-Guest chemistry based on mesoporous silica materials has attracted increasing attention in the past two decades. Potential applications for these functionalized materials are in the fields of controlled drug delivery, catalysis, separation or encapsulation of functional biomolecules.

The present work is focused on the synthesis of nanosized, mesoporous drug delivery devices, which are able to release a preloaded drug as a result of a certain trigger action, e.g. during the endocytosis in a cancer cell. For this purpose, several different synthesis strategies had to be developed in order to incorporate the different required functional groups within one mesoporous silica nanoparticle.

A spatial separation of two different functionalities was achieved by the development of a sequential co-condensation approach. With this approach, core-shell bifunctionalized colloidal mesoporous silica could be synthesized. The obtained particles are an important prerequisite for other systems presented in this work.

The applicability of the copper-(I)-catalyzed Huisgen reaction (click reaction) as mild synthetic tool for the immobilization of biomolecules in the channels of mesoporous silica was investigated. In this joint project between our group and the research group of Prof. Ernst Wagner (LMU), it was shown that a sensitive enzyme can be immobilized with this strategy in the pores of SBA-15. It was demonstrated that the recoverability and long-term stability of the active enzyme benefits from the encapsulation in the host.

The well-known strong biotin-avidin interaction was used for the construction of a protease-responsive cap system for controlling the release from colloidal mesoporous silica. Fluorescein was released from the nanoparticles as a model compound for small drug molecules. In order to monitor the release, a custom-made two-compartment fluorescence cuvette was designed. Thermoresponsive opening through protein denaturation was demonstrated for temperatures higher than 90 °C.

A programmable opening temperature for this concept became possible by using DNA-linkers between the silica surface and the avidin cap. It was demonstrated that the length of the double-stranded DNA controls the opening temperature of the avidin cap. This work was carried out as a joint project between our group, the research group of Prof. Thomas Carell (LMU) and the baseclick GmbH.

Redox-responsive drug delivery was investigated in living cells. In this context, the release of disulfide-linked, dye-labeled cysteine from the core of colloidal mesoporous silica was monitored by confocal fluorescence microscopy at a single cell level, in collaboration with the research group of Prof. Christoph Bräuchle. It was shown by photoinduced endosomal rupture that the endosomal escape is a bottleneck in redox-based drug delivery.

This concept was extended through the synthesis of photosensitizer-functionalized, PEGylated colloidal mesoporous silica. It was demonstrated that particle-loaded endosomes collapse under irradiation with 405 nm light and release the particles into the cytosol.

In another joint project between the groups of Prof. Bein, Prof. Bräuchle, Prof. Rädler and Prof. Leonhardt together with Dr. Ulrich Rothbauer (all LMU), the novel photosensitizer-functionalized porous nanoparticles were used as carriers for the delivery of small GFP-binding antibodies from *Camelidae sp.* into GFP-tubulin expressing HuH7 cancer cells. Additionally, the particles were encapsulated by a supported lipid bilayer. The attached photosensitizer was shown to play a key role in the delivery mechanism. Light-irradiation was used to destroy both surrounding membranes (supported lipid bilayer and endosomal membrane).

Finally, the pH-responsive release of the membrane-intercalating peptide mellitin from a mesoporous SBA-15 host was demonstrated. This was possible through the use of pH-sensitive acetal linkers. The release of the peptide was shown by the lysis of mouse erythrocytes. This work was carried out in collaboration with the group of Prof. Ernst Wagner.

To summarize, mesoporous silica materials were functionalized with different biomolecules in order to generate novel materials for potential applications in drug delivery or other controlled release applications. The newly developed concepts provide a basis for future work on mesoporous silica as a powerful and versatile drug delivery platform.

Table of Contents

1. Introduction	1
1.1 Ordered mesoporous materials and their evolution.....	1
1.2 Synthesis of mesoporous silica.....	2
1.3 Formation mechanism of mesoporous silica.....	4
1.4 Functionalization of mesoporous silica.....	5
1.5 Synthesis of mesoporous silica nanomaterials.....	6
1.6 Targeted drug delivery with porous silicates.....	8
1.7 Site-selective functionalization of mesoporous silica structures.....	10
1.8 Stimuli-responsive gatekeeper and molecular valves for mesoporous silica.....	12
1.8.1 Enzyme-responsive valves.....	12
1.8.2 Redox-responsive opening of molecular valves.....	14
1.8.3 UV-light responsive molecular release mechanisms.....	15
1.8.4 pH-responsive molecular valves.....	17
1.8.5 Supported lipid bilayers on mesoporous silica nanoparticles.....	20
1.9 Targeting of cancer cells with nanoparticles.....	21
1.10 Polyethylene glycol in drug delivery applications.....	22
1.11 References.....	23
2. Characterization	34
2.1 X-ray Diffraction.....	34
2.2 Infrared (IR) and Raman spectroscopy.....	37
2.3 Thermogravimetric analysis and Differential Scanning Calorimetry.....	38
2.4 Nitrogen sorption.....	39
2.5 Dynamic Light Scattering.....	42
2.6 Zeta Potential.....	45
2.7 Fluorescence Spectroscopy.....	46
2.8 Transmission electron Microscopy (TEM).....	47
2.9 References.....	48
3. Multiple Core-Shell Functionalized Colloidal Mesoporous Silica Nanoparticles	50
3.1 Introduction.....	50
3.2 Experimental Section.....	53
3.2.1 Applied Chemicals.....	53
3.2.2 Synthesis of unfunctionalized CMS (Un-CMS).....	53
3.2.3 Synthesis of CMS by co-condensation and post-grafting.....	53
3.2.4 Synthesis of bifunctional CMS by sequential co-condensation.....	54
3.2.5 Synthesis of core-bifunctional CMS by sequential co-condensation.....	54
3.2.6 Extraction of template.....	55
3.2.7 Post-grafting of the samples CMS(A)-Cl _{OUT} and CMS(A)-NH _{OUT}	55
3.2.8 Fluoresceine isothiocyanate labeling.....	56
3.2.9 Synthesis of dodecanethiolate gold nanoparticles.....	56
3.3 Results and Discussion.....	57
3.4 Conclusion.....	68
3.5 References.....	68
4. Click-Chemistry for High-Density Biofunctionalization of Mesoporous Silica	71
4.1 Introduction.....	71
4.2 Experimental Section.....	73

4.2.1 Applied Chemicals	73
4.2.2 Preparation of large pore SBA-15 spherical particles	73
4.2.3 Preparation of 3-chloropropyl-functionalized large pore SBA-15 (SBA-Cl).....	74
4.2.4 Preparation of azide-functionalized SBA-15 (SBA-N ₃).....	74
4.2.5 Acetylene functionalization of trypsin	74
4.2.6 Preparation of trypsin-functionalized large pore SBA-15 (SBA-trypsin)	75
4.2.7 Preparation of 3-chloropropyl-functionalized Cab-o-Sil aerogel	75
4.2.8 Preparation of azide-functionalized Cab-o-Sil aerogel.....	75
4.2.9 Preparation of trypsin-functionalized Cab-o-Sil aerogel.....	76
4.2.10 Preparation of the applied PBS buffer	76
4.2.11 Preparation of the applied TRIS buffer.....	76
4.2.12 Preparation of the applied MES buffer	76
4.2.13 BCA assay for protein quantification.....	77
4.2.14 Trypsin activity determination	78
4.2.15 Procedure for the applied leaching test	82
4.3 Results and Discussion	83
4.4 Conclusion	91
4.5 References.....	92

5. Biotin-Avidin as Protease-Responsive Cap-System for Controlled Guest Release from Colloidal Mesoporous Silica94

5.1 Introduction.....	94
5.2 Experimental Section	95
5.2.1 Applied Chemicals	95
5.2.2 Preparation of colloidal mesoporous silica nanoparticles (CMS).....	96
5.2.3 General Procedure for the selective functionalization of CMS with 3-mercaptopropyl moieties by co-condensation (CMS-SH)	96
5.2.4 Extraction of CMS.....	96
5.2.5 Biotin-functionalized colloidal mesoporous silica nanoparticles (CMS-BIO)	97
5.2.6 Fluorescein-loaded CMS and CMS-BIO.....	97
5.2.7 Avidin-capped, fluorescein loaded CMS (CMS-AVI).....	97
5.2.8 Fluorescence Spectroscopy Setup	98
5.3 Results and Discussion	98
5.4 Conclusion	109
5.4 References.....	109

6. A Programmable DNA-Based Molecular Valve for Colloidal Mesoporous Silica111

6.1 Introduction.....	111
6.2 Experimental Section	113
6.2.1 Applied Chemicals	113
6.2.2 Preparation of colloidal mesoporous silica nanoparticles (CMS).....	113
6.2.3 Extraction of CMS.....	114
6.2.4 Synthesis of azide-functionalized CMS (CMS-N ₃)	114
6.2.5 Attachment of Alkyne-modified oligonucleotides to CMS-N ₃ (CMS-DNA)	115
6.2.6 Fluorescein loading and avidin capping of CMS-DNA.....	115
6.3 Results and Discussion	115
6.4 Conclusion	123
6.5 References.....	123

7. Role of Endosomal Escape for Disulfide-Based Drug Delivery from Colloidal Mesoporous Silica Evaluated by Live-Cell Imaging126

7.1 Introduction.....	126
7.2 Experimental Section	129

7.2.1 Applied Chemicals	129
7.2.2 Synthesis of CMS-SH _{core} -NH _{2shell} by sequential co-condensation	129
7.2.3 Template Extraction	130
7.2.4 Fluorescence labeling procedure for CMS-SH _{core} -NH _{2shell}	130
7.2.5 Fluorescence labeling procedure for the amino group of cysteine.....	130
7.2.6 Attachment of ATTO633-labeled cysteine to CMS-SH _{core} -ATTO488 _{shell} via disulfide bridge (CMS-CysATTO633 _{core} -ATTO488 _{shell})	131
7.2.7 Attachment of ATTO633 to CMS-SH _{core} -ATTO488 _{shell} (CMS-ATTO633 _{core} -ATTO488 _{shell})	131
7.2.8 Cell Culture	131
7.2.9 Spinning Disk confocal microscope	132
7.2.10 Long-term incubation and imaging of CMS nanoparticles in living cells.....	132
7.2.11 Wide-field fluorescence microscope	133
7.2.12 Dye-release at single particle level on glass	133
7.2.13 Photochemical release of CMS nanoparticles in HuH7 cells	133
7.2.14 Evaluation of the fluorescence intensity of CMS nanoparticles in vitro and in cells	134
7.3 Results and Discussion	134
7.4 Conclusion.....	148
7.5 References.....	149

8. Photosensitizer-Functionalized PEGylated Colloidal Mesoporous Silica153

8.1 Introduction.....	153
8.2 Experimental Section	155
8.2.1 Applied Chemicals	155
8.2.2 Synthesis of CMS-NH _{2core} -SH _{shell} by sequential co-condensation	155
8.2.3 Template Extraction from CMS.....	156
8.2.4 PEGylation of CMS-NH _{2core} -SH _{shell} with maleinimido-3-oxo- 7,10,13,16,19,22,25,28-octaoxa-4-azahentriacontan-31-oic acid (Mal-dPEG(8)-COOH, sample CMS-NH _{2core} -PEG _{shell})	156
8.2.5 Dye Labeling of CMS-NH _{2core} -PEG _{shell}	156
8.2.6 Synthesis of Protoporphyrin-IX-bis(phenyleneaminoamide) (PP-NH ₂)	157
8.2.7 Attachment of PP-NH ₂ to CMS-Atto _{core} -PEG _{shell}	157
8.2.8 Cell Culture	157
8.3 Results and Discussion	158
8.4 Conclusion.....	165
8.5 References.....	165

9. Light-Induced Delivery of Chromobodies from Lipid-Bilayer Coated Colloidal Mesoporous Silica169

9.1 Introduction.....	169
9.2 Experimental Section	173
9.2.1 Applied Chemicals	173
9.2.2 Synthesis of bi-functionalized colloidal mesoporous silica (CMS-NH _{2core} -SH _{shell}) ..	173
9.2.3 Extraction of the CMS samples.....	174
9.2.4 Preparation of non-porous, aminofunctionalized silica nanoparticles (Stöber-NH ₂)	174
9.2.5 PEGylation of CMS-NH _{2core} -SH _{shell} with maleinimido-3-oxo- 7,10,13,16,19,22,25,28-octaoxa-4-azahentriacontan-31-oic acid (Mal-dPEG(8)-COOH, sample CMS-NH _{2core} -PEG _{shell})	175
9.2.6 Synthesis of Protoporphyrin-IX-bis(phenyleneaminoamide) (PP-NH ₂)	175
9.2.7 Attachment of PP-NH ₂ to CMS-NH _{2core} -PEG _{shell}	176
9.2.8 Loading of silica nanoparticles with Atto594-labeled chromobodies.....	176

9.2.9 Supported Lipid Bilayer Preparation (CMS-NH ₂ core-PS _{shell} -DOPC)	176
9.2.10 Spinning Disk confocal microscope.....	177
9.3 Results and Discussion	177
9.4 Conclusion.....	185
9.5 References.....	185
10. pH-Responsive Release of Acetal-Linked Mellitin from SBA-15 Mesoporous Silica	188
10.1 Introduction.....	188
10.2 Experimental Section.....	190
10.2.1 Applied Chemicals	190
10.2.2 Preparation of large-pore SBA-15 spherical particles.....	190
10.2.3 Preparation of mercaptopropyl-functionalized SBA.15 (SBA-SH)	190
10.2.4 Maleimide-linker attachment (SBA-MK, SBA-BM)	191
10.2.5 Attachment of mellitin to SBA-15 (SBA-MK-Mel, SBA-BM-Mel).....	191
10.2.6 Erythrocyte leaching assay	192
10.3 Results and Discussion.....	193
10.4 Conclusion	199
10.5 References	200
11. General Conclusions and Outlook.....	201
12. Appendix.....	204
13. Curriculum Vitae	223
14. Publications and Presentations	225

1. Introduction

1.1 Ordered porous materials and their evolution

Before the early 1990's, zeolites (crystalline aluminosilicates exhibiting microporosity) were considered to be the prototype ordered porous materials. This materials class was copiously investigated for many applications like ion exchangers, molecular sieves and catalysts.^{1,2} Apart from these traditional zeolite application fields, newer areas of research include medical applications,³⁻⁵ photovoltaics,^{6,7} heat storage,⁸ chemical sensors⁹⁻¹¹ or hydrogen storage materials.¹²⁻¹⁴ Porous materials to be used as carriers for enzymes or for the controlled release of larger molecules require larger pores, thus the small pores of zeolites between 0.5 and 1 nm exclude this materials class as possible option for such applications. In 1992, the Mobil Oil corporation introduced a novel type of silica-based molecular sieve, the M41S family.^{15,16} The main characteristics of this material include the long range order of mesopores, formed by amorphous silica walls, its high internal surface area of around $1000 \text{ cm}^2\text{g}^{-1}$, and pore diameters around 3-5 nm, respectively. This materials class was soon extended by the development of different synthesis strategies. Today, mesoporous silica materials with pore diameters in the range between about 2-50 nm are accessible. This flexibility allows the construction of tailor-made materials for diverse applications such as controlled release,¹⁷ catalysis based on immobilized enzymes^{18,19} or the growth of nanowires in the confined environment of mesopores.²⁰⁻²²

Another class of porous materials was introduced by Yaghi *et al.* in 1995, i.e., the so-called metalorganic frameworks (MOF).²³ A MOF consists typically of di-, tri- or tetravalent metal centers, which are connected by organic linkers with corresponding complexing ligand moieties. MOFs with larger cages were published a few years later, featuring pore sizes of about 2 nm. These so-called MILs (Materiaux de Institute Lavoisier) were the first crystalline mesoporous solids.^{24,25} Another class of porous hybrid materials with covalent bonds was

developed by Yaghi et al. in 2005: covalent organic frameworks (COFs). This class of material can be obtained by the condensation of organoboronic acids with diol-moieties.²⁶

The widely discussed field of multifunctional mesoporous silica-based drug delivery devices emerged after the development of nanosized mesoporous silica particles.

The following work will highlight the progress of the synthesis of such a drug delivery device based on mesoporous silica. Several aspects like biocompatible synthesis strategies and tuning the behavior of the particle in a cancer cell will be considered. The different prerequisites for the function of the nanodevice to be generated are studied in detail and a solution to each of the issues will be proposed.

1.2 Synthesis of mesoporous silica

The formation of mesoporous materials such as the M41S-family is driven by a cooperative self-assembly of organic surfactants and inorganic species. As structure-directing surfactants, micelles of quaternary ammonium salts (hexadecyltrimethylammonium bromide) that form liquid crystalline micelles are used. Silica precursors like tetraethyl orthosilicate can be hydrolyzed under hydrothermal conditions in basic media, resulting in silica materials with high internal surface area and highly ordered pore structures with pore diameters around 4 nm, surrounded by amorphous pore walls. The obtained materials were classified based on the geometrical arrangement of the cylindrical pores. The MCM-41 material exhibits a 2D hexagonal arrangement of pores, while MCM-48 has a 3D cubic pore system. A 1D array of layered sheets is called MCM-50 (Figure 1.2.1).²⁷

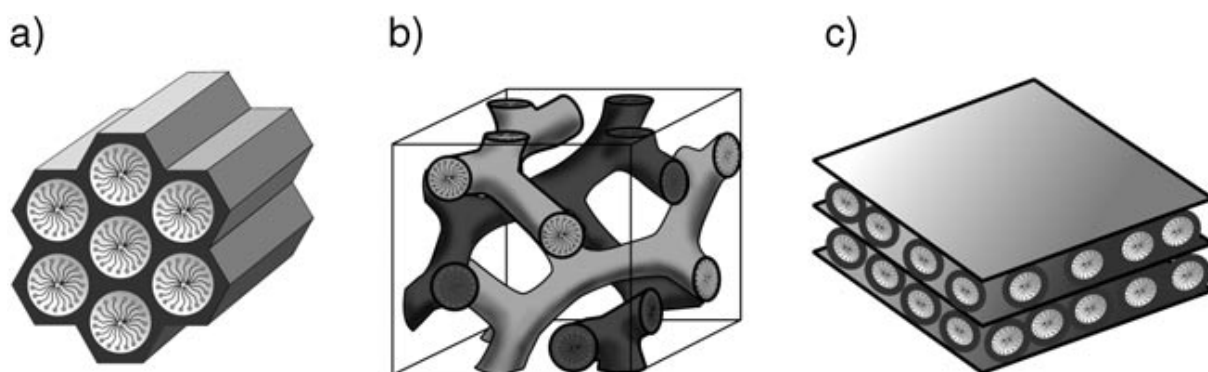


Figure 1.2.1. Structures of mesoporous M41S materials: (a) MCM-41, (b) MCM-48, and (c) MCM-50. Picture taken from reference 27.

Other strategies to create mesoporous silica structures use neutral surfactants. In the materials introduced by Pinnavaia *et al.*, non-ionic interactions between the organic template and the inorganic silica precursor are responsible for the formation of the porous materials.^{28,29} HMS (Hexagonal Mesoporous Silica) materials use primary amines as template to create mesoporous silica structures.³⁰ Poly(ethylene oxides) are used as a template in the formation of MSU materials (Michigan State University).³¹ Accessible pore diameters using this strategy are in the range of 4 nm to 14 nm. The advantage of the neutral surfactants used in HMS and MSU materials is the easy recoverability of the template.²⁸

Another very prominent type of mesoporous silica materials was presented by Stucky *et al.* in 1998, the SBA materials (Santa Barbara materials).^{32,33} Triblock copolymers of the Pluronic family were used as template. The structure of the template consists of poly(ethylene oxide)_x-poly(propylene oxide)_y-poly(ethylene oxide)_x units with variable chain lengths x and y. The synthesis environment for the SBA materials is strongly acidic. A main feature of the obtained mesoporous materials is the improved hydrothermal stability, due to the formation of thicker pore walls compared to MCM-materials.³⁴ The obtainable pore diameters are up to 18 nm and the pore walls do contain additional microporosity, due to the embedding of poly(ethylene oxide) side chains in the structure.^{32,35}

1.3 Formation mechanism of mesoporous silica

In general, four ingredients are necessary to form a mesoporous silica material: a surfactant, a silica source, an acid- or base catalyst and a solvent like ethanol or water. Based on this generalized recipe, many different synthesis procedures have been developed and were extensively reviewed in the recent years.^{27,36-38} For cationic surfactants, the formation mechanism of mesoporous silica is strongly influenced by ionic interactions between anionic oligosilicates and the cationic headgroup of the template (e. g. CTAB), and no initial liquid crystalline phase is necessary for the synthesis.^{39,40} In a first step, Coulomb forces lead to an assembly of silicate polyanions at the positively charged headgroups of the cationic surfactants. As a result, the charge density changes dramatically at this interface, which leads to the formation of micelles in a structure depending on the applied reaction conditions. The final mesostructure is formed by crosslinking and polymerization of the silicate species. The product is a result of the optimized interfacial energy of the organic surfactant and the inorganic silica.

In contrast to this cooperative self-assembly process, another formation mechanism called “true” liquid crystal templating is known (TLCT). In the latter case, the liquid-crystalline phase is already present at the applied reaction conditions.⁴¹ The inorganic precursor is added and polymerized thereafter. A schematic overview showing the two possible general formation mechanisms is presented in figure 1.3.1.

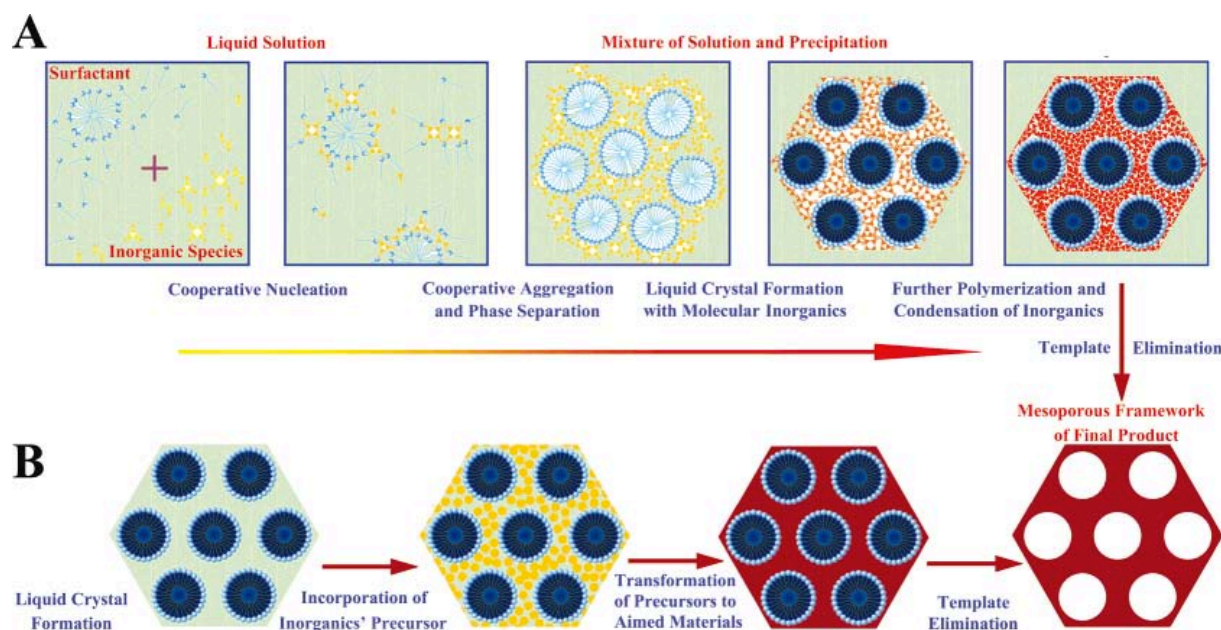


Figure 1.3.1. Schematic overview about mesoporous silica formation mechanisms: (A) cooperative self-assembly and (B) true liquid crystal templating (Figure taken from reference 36).

A subsequent removal of the template can be achieved either by calcination at high temperatures or by extraction procedures. A typical extraction procedure used in the present work uses ethanolic ammonium nitrate solutions. The exchange of template with ammonium is highly efficient due to the high similarity of surfactant head group and extraction reagent.⁴² Other extraction methods apply supercritical CO₂, plasma or microwave irradiation.⁴³⁻⁴⁵

1.4 Functionalization of mesoporous silica

In order to manipulate and tune the silica surface to be used in specific applications, organic moieties that are covalently attached to the surface serve well. In general, there are two different approaches to achieve such functionalization: Post-synthetic grafting of the surface with chloro- or alkoxy-silanes or direct co-condensation of the organic functionality during the synthesis.^{46,47} More recently, metalorganic reagents like Grignard – or organolithium compounds were introduced as alternative route to achieve organic functionality on

mesoporous silica surfaces, resulting in direct Si-C bond formation.^{48,49} This method allows, for example, the incorporation of multiply bonded residues in a one-step reaction. Post-synthetic grafting is achieved by attaching organotrialkoxysilanes to the pore walls of pre-synthesized, template-free mesoporous silica. Co-condensation includes copolymerization of an organosilane with the silica precursor in the presence of the templating surfactant. The metalorganic functionalization route is based on the substitution at silicon atoms with metalorganic compounds, resulting in the formation of direct Si-C bonds.

1.5 Synthesis of mesoporous silica nanomaterials

After the introduction of the M41S materials family in 1992 by Mobil Oil, a number of research groups have searched for strategies to obtain mesoporous silica materials with particle sizes in the nanometer range.^{15,16} In 1999, Brinker *et al.* developed a self-assembly approach to obtain mesoporous particles in an aerosol-based synthesis.⁵⁰ The used reactor is shown in Figure 1.5.1.

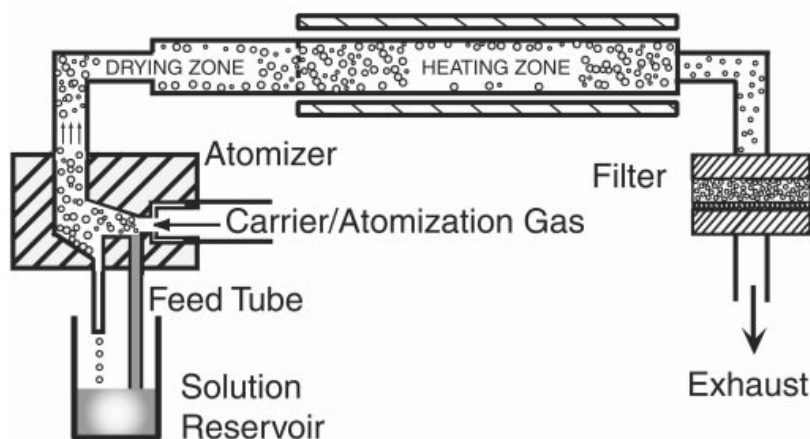


Figure 1.5.1. A diagram of the applied aerosol reactor. Figure was taken from reference 50.

An atomizer creates silica precursor/surfactant droplets with a size distribution characterized by a geometric standard deviation of 2. Finally, the produced particles are collected on a Teflon filter or directly on a TEM grid. Depending on the applied template type, lamellar,

cubic or hexagonally ordered mesoporous silica particles were obtained. The synthesized particles showed a size distribution around 120 nm and tunable pore sizes between 3 and 40 nm. Another approach uses neutralization of the synthesis solution after a short period of particle growth.⁵¹ CTAB-templated mesoporous silica particles featuring particle sizes between 10 and 100 nm were obtained, but the yield was relatively low. Hexagonal arrangement of the pores was only observed for particles featuring a diameter of 60 nm or larger.

Imai *et al.* have developed a synthesis route using complementary, immiscible surfactant systems.^{52,53} While one of the applied surfactants acts as templating agent defining the mesostructure, the growing particles are surrounded by a second surfactant. This hinders the diffusion of growth species to the growing surface and leads to a slowed down particle growth. A schematic representation to illustrate the functions of the two surfactants is given in Figure 1.5.2.

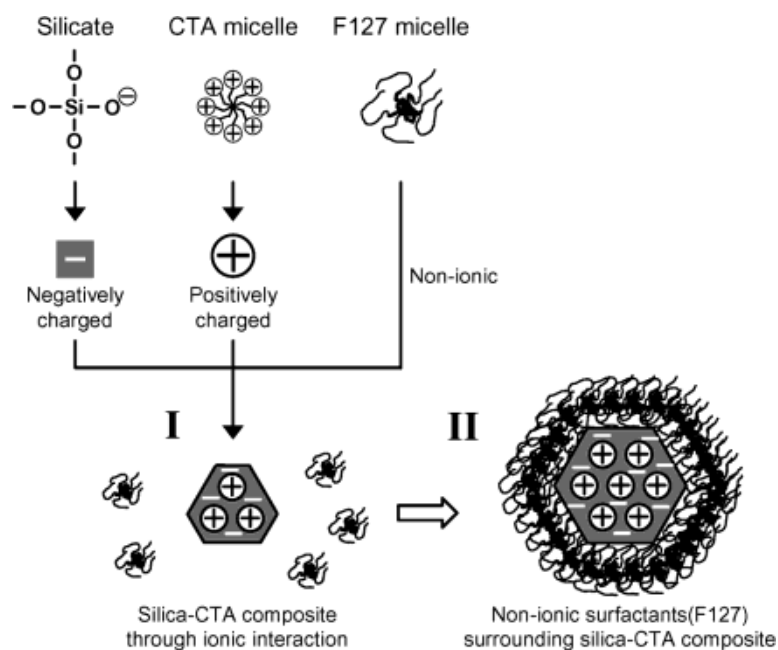


Figure 1.5.2. Schematic representation of the functions of two surfactants. Figure was taken from reference 52.

A typical surfactant mixture uses CTAB/Pluronic F127. An exceptionally great variety of pore structures and sizes can be achieved by applying mixtures of triblock-copolymers such as Pluronic P123 or F127 combined with fluorocarbon surfactants.⁵⁴ Round-shaped MCM-41 nanoparticles with particle sizes around 200 nm were obtained in a microwave heating approach including the addition of ethylene glycol as another dielectric medium in the synthesis.⁵⁵ Other strategies to limit the particle growth include the use of complexation agents such as triethanolamine (TEA).⁵⁶⁻⁵⁹ The chelating capabilities of TEA leading to silatrane complexes in the synthesis solution⁶⁰ prevents a fast condensation reaction of the silica.^{61,62} In the present work, the latter strategy for the synthesis of colloidal mesoporous silica was applied. The obtained high particle concentrations and narrow size distributions make this approach ideal for the introduction of subsequent functionalization steps.

1.6 Targeted drug delivery with porous silicates

Currently, functional nanomaterials are widely discussed as drug carriers in cancer therapy or other medical applications. The use of nanocarriers that are able to transport a drug directly to tumor tissue within a living system can help to reduce the drug dose and therefore reduce unwanted side effects. Liposomes have been used to transport cytostatics or therapeutics to cancer tissue with many different cargos such as doxorubicin or DNA plasmids. Some of the loaded liposomes have already been approved after clinical trials.⁶³ Other groups use nanosized polymeric conjugates to deliver genes, peptides or toxins into cancer cells.⁶⁴⁻⁶⁷ Zeolites were also investigated for their potential in drug delivery and controlled release applications.^{68,69} As an example, the potential use of commercially available zeolite Y was studied as carrier for anthelmintic drugs. It was shown that the loaded zeolite was able to improve the killing rates of adult worms *in vivo*.⁷⁰ Mesoporous silica nanoparticles were widely investigated for potential applications in targeted drug delivery.⁷¹⁻⁷⁵ Silica itself is non-toxic and exhibits an excellent biocompatibility.⁷⁶⁻⁷⁸ Additionally, the incorporated mesopores

with tunable diameters between about 3 and 20 nm offer enough space for the loading with even spacious therapeutic molecules like nucleic acids, peptides or antibiotics.⁷⁹⁻⁸³ However, for a mesoporous silica nanoparticle to serve as a sophisticated drug delivery vehicle, it has to fulfill a couple of important prerequisites. In order to overcome the synthetic challenges, a number of multidisciplinary approaches are necessary.

In Figure 1.6.1, the ultimate goal of the research of the present work is presented as a cartoon.

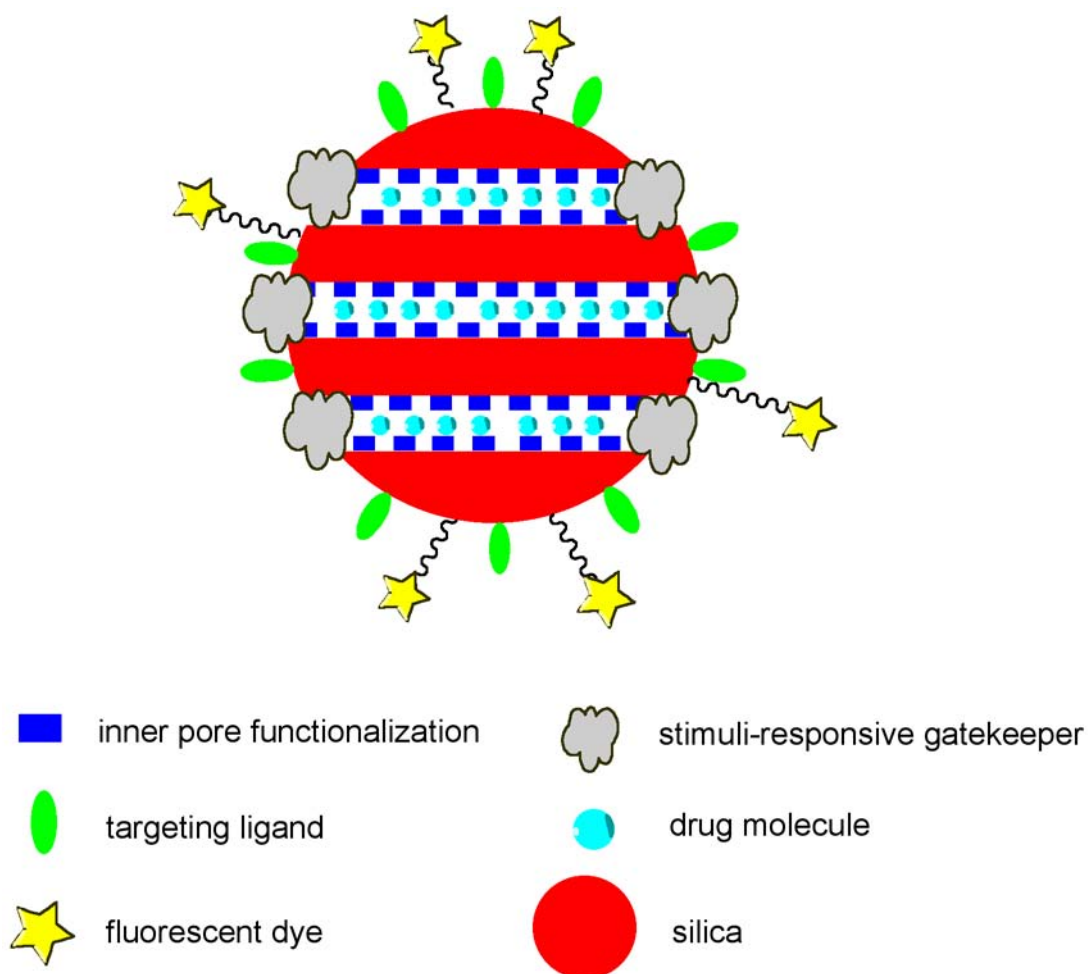


Figure 1.6.1. Cartoon of an ideal mesoporous silica based drug delivery nanodevice.

In the cartoon, a number of different functionalizations are visible. First, an inner core functionalization is necessary in order to tune the interaction of a loaded guest molecule with the pore walls. However, on the outer particles' surface, a number of different additional

groups need to be attached selectively. A targeting ligand enables the particle to bind to specific receptors, which are overexpressed on the desired cancer cell surface. The function of the stimuli-responsive gatekeeper is to release the cargo only as a result of a certain trigger effect, e.g. after cell entrance. A fluorescent label on the surface of the particle allows monitoring the mechanisms of cellular uptake with fluorescence microscopy. If it is possible to access such multifunctional nanodevices, we anticipate that they will permit the reduction of the applied drug doses in cancer therapy, as the drugs are transported and released directly to the desired locus of activity. This will largely reduce unwanted side effects and enables the use of more powerful tools to kill cancer tissue within the organism.

1.7 Site-selective functionalization of mesoporous silica structures

The challenge of introducing molecular functionality at defined loci within one particle of mesoporous material is subject of the current research. Molecular functionality attached to the inorganic surfaces can change the properties of the obtained material dramatically. This is crucial not only in host-guest chemistry, but also in the fields of catalysis and sorption.^{84,85} First attempts to control the locus of incorporated functionalization were published by Chen *et al.*⁸⁶ The control was achieved by a partial cleavage of P123 surfactant in the mesopores of SBA-15, leaving the micropores unextracted. Subsequent functionalization with trimethylchlorosilane and further template removal allowed the deposition of metals selectively in the micropore volume of SBA-15. A selective functionalization of the outer surface was achieved by the addition of (3-mercaptopropyl)trimethoxysilane to radially growing mesoporous silica microspheres.⁸⁷ The obtained material showed a hydrophilic/hydrophobic core/shell structure, characterized by the reductive deposition of aqueous platinum precursors to the inner core of the silica sphere. One approach to distinguish between a preferential post-synthetic functionalization on the outer surface and the inner pore walls is varying the ratio of added functionalized silanes, assuming the most

accessible silanols to be present on the outer surface.⁸⁸ By adding only a fractional amount of grafting agent compared to the present silanols, a preferential functionalization on the outer surface takes place. Other research groups showed an outer surface functionalization by leaving the template unextracted during functionalizations steps, thus hindering the access to the interior pore surface.⁸⁹⁻⁹¹ However, independently achieved results from different groups have shown that chloro- and trialkoxysilanes can efficiently replace surfactant molecules and can even produce completely extracted materials.⁹²⁻⁹⁵ We have recently shown that the functionalization of template-filled pores occurs already at room temperature conditions after 4 hours.⁹⁶ Therefore, we have developed a site-selective co-condensation approach for colloidal mesoporous silica nanoparticles, allowing us to introduce molecular functionality dispersed throughout the whole particle volume or concentrate it towards the outer shell (Figure 1.7.1.).

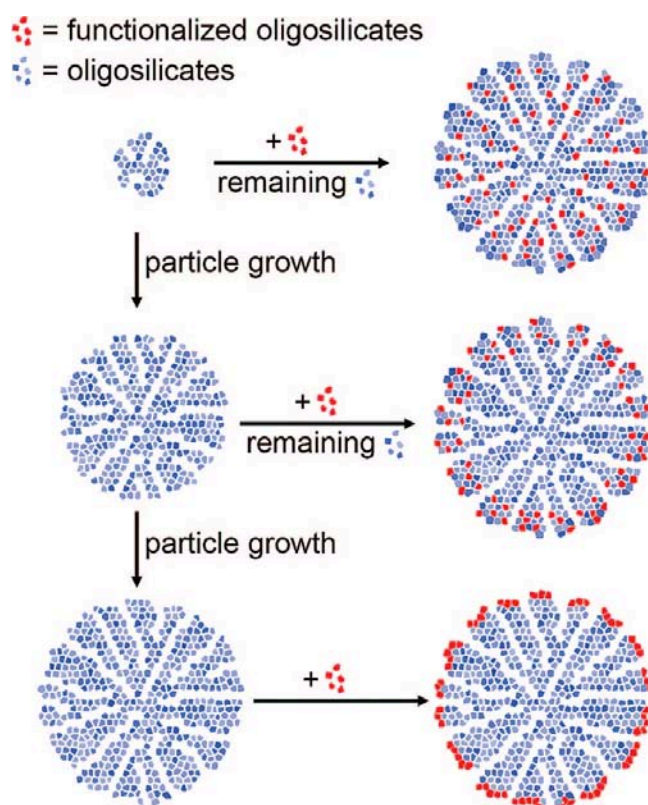


Figure 1.7.1. The functional groups are dispersed within the particle volume depending on the addition time of the organosilane component. Figure was taken from reference 96.

In the present work, the existing approach was successfully extended to yield multifunctional, core-shell structured mesoporous silica nanoparticles via a sequential co-condensation process, allowing a differentiation between the outer and inner organic functional groups (joint project with Dr. Valentina Cauda).⁹⁷ The synthesized core-shell particles are an important prerequisite for the manufacturing of our version of a mesoporous silica-based drug delivery device.

1.8 Stimuli-responsive gatekeeper and molecular valves for mesoporous silica

For an effective drug delivery device, it is important to release the medication only under defined conditions, e.g. upon entrance into a cancer cell. The synthesis of such valves has become an interesting and widely investigated field of research, attracting scientists from multiple disciplines around the world.

In the literature, the reported molecular valve concepts are mainly based on the following triggers:

1. Enzyme responsive
2. Redox-responsive
3. UV-light responsive
4. pH-responsive

Another elegant approach uses supported lipid bilayers as biocompatible shell carried by the surface of colloidal mesoporous silica.

1.8.1 Enzyme-responsive valves

Stoddart *et al.* presented an esterase-responsive “snap-top” release mechanism for mesoporous silica nanoparticles (MSN), based on a cyclodextrin (CD) cap (Figure 1.8.1).⁹⁸ In this case, the surface of MSN was reacted with tri(ethylene glycol) linkers, onto which the CD

threads. A terminal azide group was subsequently reacted with an ester-linked adamantyl stopper, preventing the CD cap from leaving the MSN surface. The release of Rhodamin B was not detected before esterase addition.

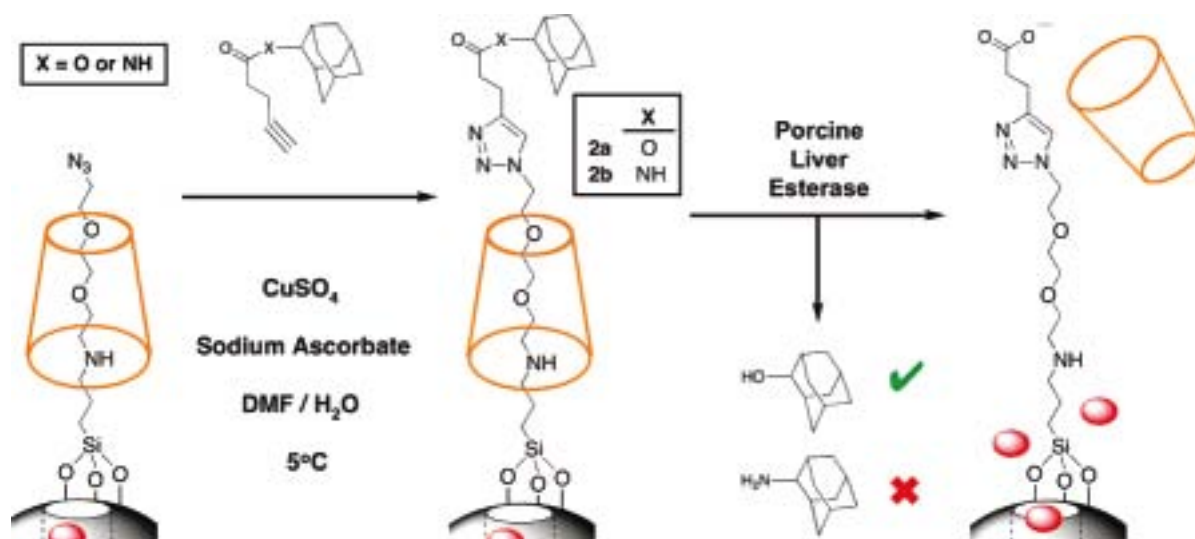


Figure 1.8.1. Synthesis of a snap-top cover for mesoporous silica nanoparticles. The figure was taken from reference 98.

Others have shown the synthesis of lactose-capped mesoporous silica nanoparticles, which open upon β -galactosidase action.⁹⁹ MCM-41 was loaded with $[Ru(bipy)_3]Cl_2$ in order to monitor the release. As molecular cap, they used a lactose derivative consisting of β -D-galactose and β -D-glucose linked through a glycosidic bond. The cleavage of this bond by β -galactosidase led to a removal of the steric barrier and the dye could be released.

In the present work, I will report on biotin-functionalized colloidal mesoporous silica, which is capped by avidin proteins. A release of fluorescein molecules is triggered by the addition of the protease trypsin.¹⁰⁰

1.8.2 Redox-responsive opening of molecular valves

Molecular valve mechanisms that react on reductive environments offer a great potential in drug delivery. Disulfide-based mechanisms have already demonstrated their potential in this field, e.g. in polymer conjugates.¹⁰¹

Disulfide-based controlled release mechanisms were also studied in mesoporous silica nanoparticles (MSN). The snap-top covered MSN system described under 1.8.1 (ref. 98) was extended to a redox-responsive valve very recently.¹⁰² The applied adamantyl-stoppers for the cyclodextrin-caps were linked with a disulfide-bridge instead of an esterase-sensitive ester-bond. This leads to an opening of the valves upon creation of a reductive milieu.

Lin *et al.* have attached disulfide-bridged cadmium sulfide (CdS) nanoparticles to the pore openings of MSN (Figure 1.8.2).¹⁰³

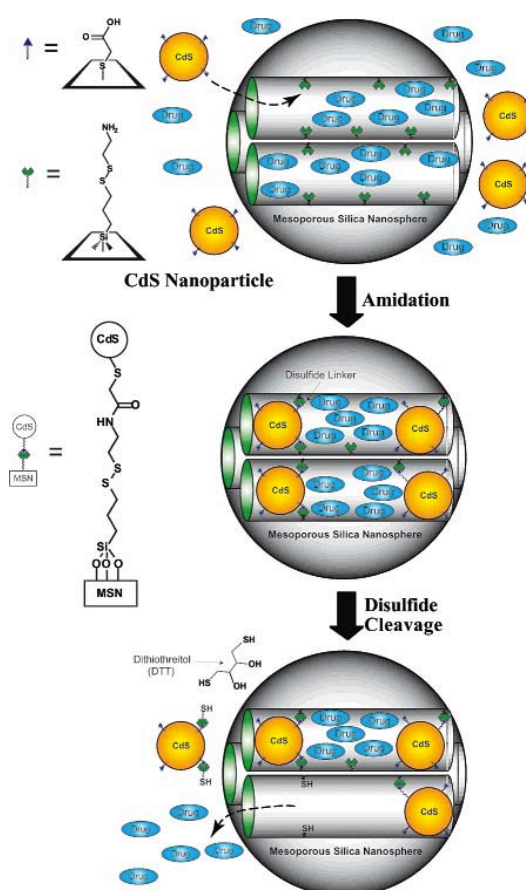


Figure 1.8.2. Concept for the redox-responsive release of vancomycin from CdS-capped mesoporous silica nanoparticles. Figure taken from reference 103.

They were able to show a release of vancomycin and adenosine triphosphate at the presence of a reducing agent such as mercaptoethanol or dithiothreitol (DTT). In order to avoid the toxic CdS, the same group has applied a redox-sensitive bond to attach superparamagnetic iron oxide nanoparticles on MCM-41.¹⁰⁴ The functionality was again demonstrated by the release of fluorescein upon addition of DTT. In another work of Lin *et al.*, membrane-impermeable cysteine was delivered into living cells.¹⁰⁵ For this purpose, the cysteine was directly linked to the silica wall by a disulfide bridge. The advantage of this approach is that synthetically demanding caps are not necessary, as the delivered species themselves are reversibly attached to the pore walls. A closer look into the mechanism of this approach by live-cell imaging is provided in the present work, as a joint project with the research group of Prof. Bräuchle.¹⁰⁶

Cystamine crosslinks of poly(*N*-acryloxysuccinimide) shells for MSN's were shown to release cargo on demand. The presence of DTT acts as a trigger.¹⁰⁷ Another approach uses ferrocenedicarboxylic acid coupled to (3-aminopropyl)-modified MSN surfaces. After loading the particles with Rhodamin B, the pores were closed with a cyclodextrin (CD).¹⁰⁸ Electrochemical oxidation of the ferrocene units lowers the interaction between the CD and the functionalized particle surface and thus, the incorporated dye gets released.

1.8.3 UV-light responsive molecular release mechanisms

In the synthesis of UV-light responsive valves, photocleavable molecules that link the capping agent to the pore openings are used. As an example, cyclodextrin caps were linked to the silica surface by *o*-nitrobenzylesters. Irradiation of the functionalized particles resulted in a release of the cargo.¹⁰⁹ Zink *et al.* have reported in several publications on the acceleration of release by the incorporation of light-driven “nanoimpellers”. This interesting functionality is given by light-induced *cis-trans* isomerization of azobenzenes, pushing out loaded molecules like rhodamine B or camptothecin from the inside of the pores (Figure 1.8.3).¹¹⁰⁻¹¹²

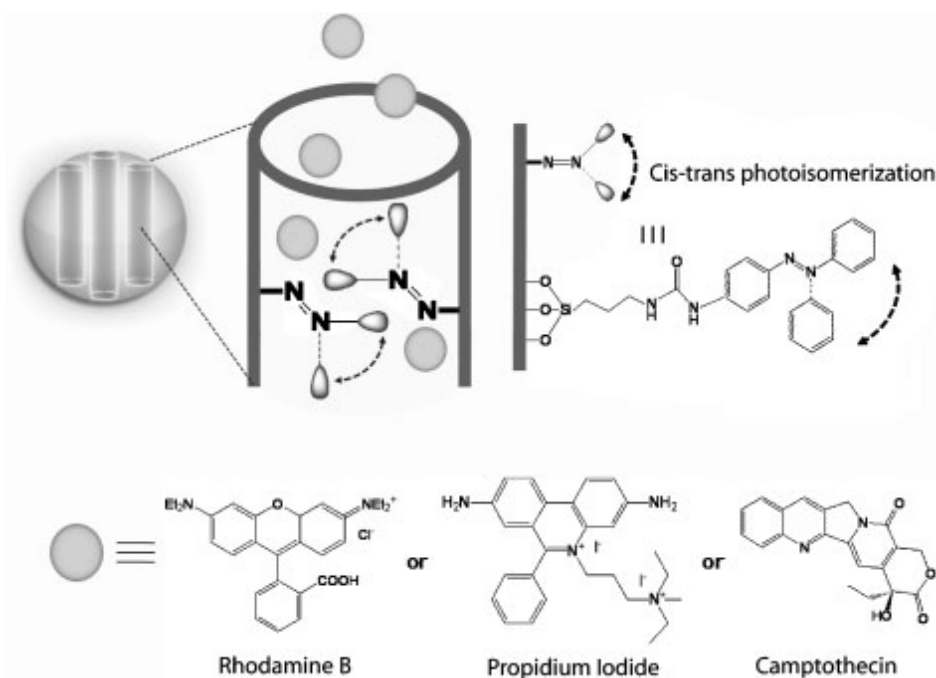


Figure 1.8.3. Molecular structure of the incorporated, light driven nanoimpellers. Figure was taken from reference 110.

The high affinity of β -cyclodextrines (β -CD) to the trans-form of azobenzenes was also used in the construction of a photoresponsive gatekeeper mechanism. Irradiation of the β -CD-capped material leads to isomerization of the applied azobenzene-linker and thus detaching of the β -CD cap.¹¹³ Coumarin-derivatives can act as photo-responsive gatekeeper molecules for MCM-41.¹¹⁴ UV-light irradiation ($\lambda > 310$ nm) of the coumarin-functionalized silica surface causes a [2+2] photocycloaddition between two coumarin molecules, leading to an efficient closing of the pores. Reopening is achieved by irradiation at higher energy ($\lambda = 250$ nm). Another group has combined this mechanism with the azobenzene nanoimpellers to control the release kinetics of cholesterol from mesoporous silica.¹¹⁵

Photoresponsive release of fluorescein in cells was introduced by Lin *et al.* with gold nanoparticle-capped MSN. The utilized gold nanoparticles were functionalized with thioundecyltetraethyleneglycoester-*o*-nitrobenzylethyldimethylammonium bromide (TUNA),

which functions as a photochemical linker. Being irradiated with UV-light, the TUNA linker is converted into a negatively charged carboxylate, leading to an electrostatically driven dissociation of the gold from the also negatively charged silica surface (Figure 1.8.4).¹¹⁶

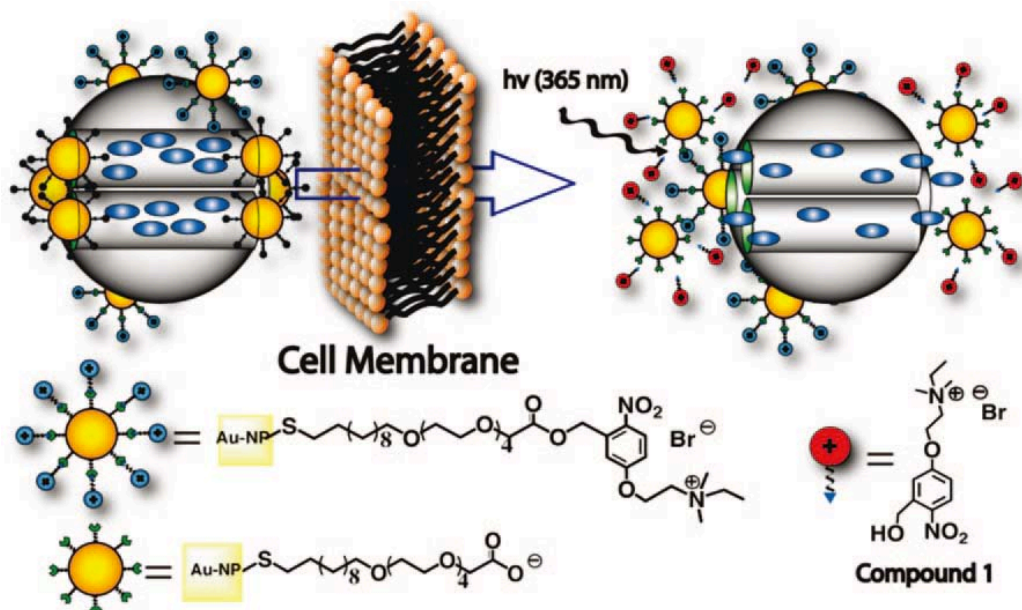


Figure 1.8.4. Construction and function of the UV-light driven controlled release from mesoporous silica. Figure was taken from reference 116.

1.8.4 pH-responsive molecular valves

One of the reported pH-responsive systems uses a crown-ether to encircle a naphthalene-containing dialkylammonium center. The release of coumarin from this system was shown by the addition of base, leading to a proton abstraction from the used linker, thus weakening the interaction between the applied crown-ether and the surface.¹¹⁷ Kim *et al.* have introduced a pH-responsive pseudorotaxane-based cap system, which is composed of biocompatible materials only.¹¹⁸ The surface of the MSN was post-synthetically modified with polyethyleneimine (PEI), which was subsequently complexed by cyclodextrines. Lowering

the pH led to a positively charged PEI backbone, thus the cyclodextrine caps were detached from the surface (Figure 1.8.5).

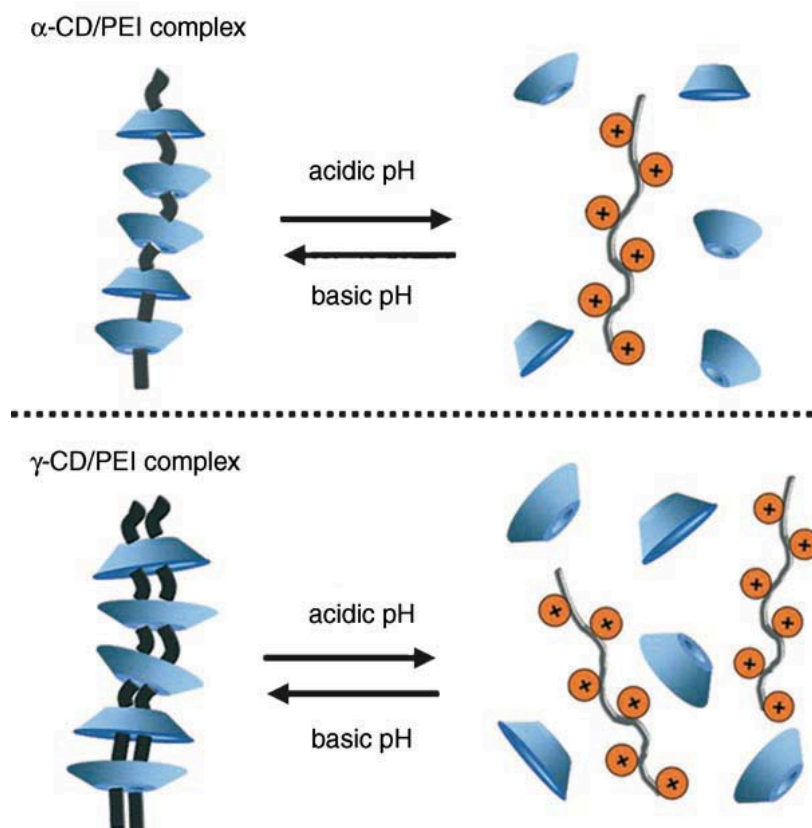


Figure 1.8.5. Schematic illustration of complexation from PEI with cyclodextrines. Figure taken from reference 118.

Zink *et al.* have reported base-activated Cucurbit[6]uril (CB[6]) pseudorotaxane caps, attached to the silica surface by an azide-alkyne cycloaddition. This reaction was self-catalyzed by the CB[6] and resulted in a triazol-ring surrounded by the CB[6] moiety. Upon deprotonation at pH 10, the CB[6] was detached and was no longer able to hinder the release of Rhodamine B into the solution.¹¹⁹ This principle was successfully extended to the construction of an acid-activated cap system by the same group.¹²⁰ The CB[6] unit is now sitting around a organic chain which contains three ammonium groups. Two of the contained

ammonium groups are tetramethylene ammoniums while the third and terminal group is an anilinium unit (Figure 1.8.6).

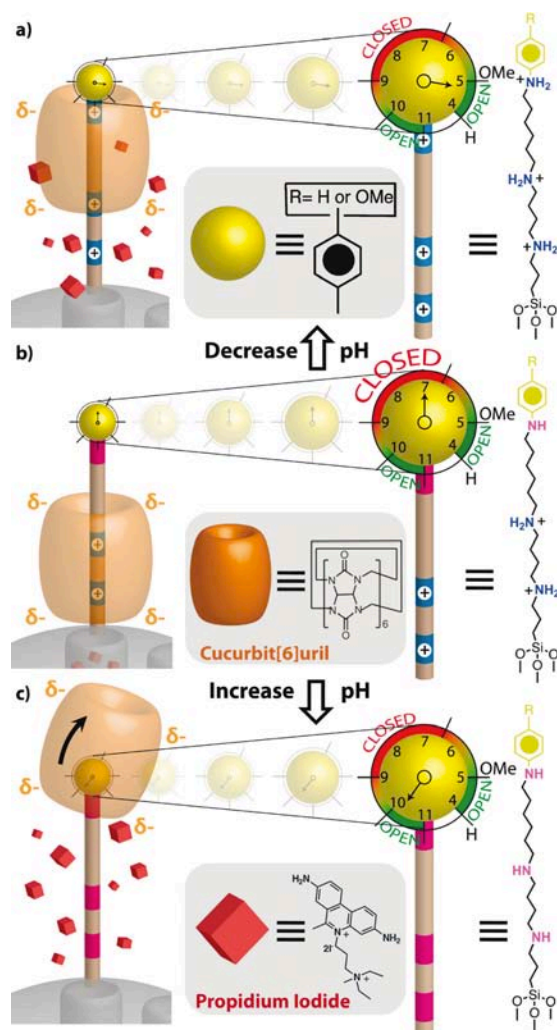


Figure 1.8.6. Concept of an acid-activated, Cucurbit[6]uril capped mesoporous silica particle.

Figure taken from reference 120.

A lowering of pH to the point where the anilinium ion gets protonated leads to a release of the CB[6], followed by the release of the incorporated guest molecules. A combination of the light-driven nanoimpellers and the CB[6] based cap system in one particle gives AND-logic controllable release behaviors.¹²¹ For an effective release of the incorporated compound, two stimuli are required. Base addition leads to an opening of the CB[6]-caps as described for reference 118, but the encapsulated guest is not released until the photoinduced cis-trans

isomerization of the incorporated nanoimpellers described in reference 109, Figure 1.8.3 is activated.

Cucurbit[7]uril was used as capping agent by ferrocene-functionalized MSNs at low pH values. The stability of the complex is weakened at $\text{pH} > 4$ and therefore, an incorporated guest molecule can be released.¹⁰⁸

Our group has recently shown a pH-dependent release of Ibuprofen from core-shell functionalized colloidal mesoporous silica CMS.¹²² CMS with an outer-surface aminopropyl-functionality was further reacted with 4-sulfophenyl isothiocyanate. The ionic interaction between the attached sulfonic acid groups and the remaining protonated aminogroups of the surface led to a closure of the pores, preventing Ibuprofen from leaching out of the particle. An opening was achieved by proton abstraction from the surface (addition of base), leading to an electrostatic repulsion of the sulfonic acid gatekeeper. Another group has applied a layer of polyamines to the surface of mesoporous silica.¹²³ Protonation of the linear amine-chains created a rigid layer structure, blocking the access to the pores.

A polyelectrolyte multilayer was shown to seal effectively the pores of hollow mesoporous silica spheres at high pH values.¹²⁴ In the present work, we have investigated the applicability of acetal linkers for a pH-responsive release of mellitin peptides from SBA-15, in a joint project with the group of Prof. Wagner from the pharmaceutical department of the University of Munich (LMU).¹²⁵

1.8.5 Supported lipid bilayers on mesoporous silica nanoparticles

Another interesting possibility to control the delivery of drugs with mesoporous silica nanoparticles is to combine the easy functionalization capabilities of the silica surface with the exceptional biocompatibility of phospholipid bilayers. Brinker *et al.* have introduced such supported bilayers made from a mixture of 1,2-dioleoyl-*sn*-glycero-3-[phospho-L-serine] (DOPS) and 1,2-dioleoyl-3-trimethylammoniumpropane (DOTAP) prepared by an

electrostatically driven lipid exchange mechanism.¹²⁶ It was demonstrated that these so-called protocells are able deliver doxorubicin and other compounds into cells. Our group in cooperation with the groups of Prof. Bräuchle and Prof. Rädler (both LMU Munich) has recently shown that particles coated with a lipid bilayer can deliver the plant toxin colchicine into living cells.

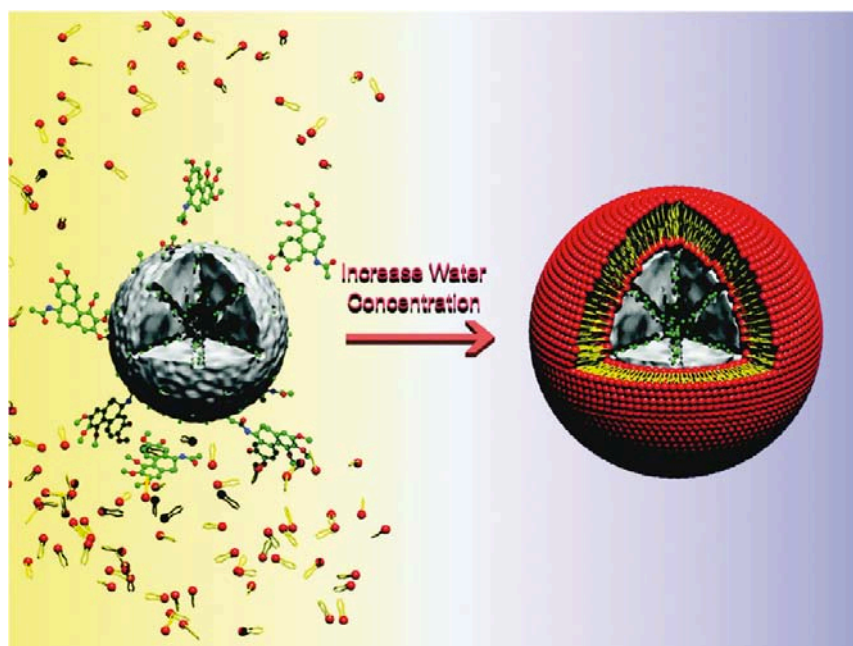


Figure 1.8.7. Synthesis scheme of a lipid bilayer coated, colchicine-loaded colloidal mesoporous silica particle. Figure was taken from reference 80.

The successful delivery was evaluated by live-cell imaging. Specifically, the depolymerization of GFP-labeled microtubules was observed.⁸⁰

1.9 Targeting of cancer cells with nanoparticles

The specific entry of nanoparticles into cancer cells can be enhanced by attaching ligands to the surface that interact with cell receptors being overexpressed in cancer cells. Prominent examples for such receptors are the epidermal growth factor receptor (EGFR),¹²⁷ the folate receptor¹²⁸ or the integrin $\alpha v \beta 3$ -receptor.^{129,130}

Linden *et al.* have studied the folate receptor as target for drug delivery with mesoporous silica nanoparticles.¹³¹ They constructed polyethyleneimine (PEI)-coated MSN's that were further reacted with folic acid to yield the targeting system. They showed an efficient uptake of folic acid-modified nanoparticles compared to the unfunctionalized case. They further investigated the delivery of membrane-staining dyes with these targeting systems. As a result, they could show that HeLa-cells with a highly expressed folate receptor do preferentially take up the particles, made visible by a high fluorescence intensity of the membrane.¹³² Another group has initially investigated the efficiency of targeting the $\alpha v \beta 3$ -receptor using arginine-glycine-aspartate tripeptide (RGD) functionalized mesoporous silica nanoparticles with a positive result.¹³³ They observed a more effective endocytosis by using targeting particles. A similar result was achieved by functionalizing gold nanoparticles or polymers with the RGD peptide.^{134,135} The specific targeting of the epidermal growth factor receptor with the EGF peptide is another way to directly target cellular surfaces. One group has synthesized conjugates of 2-methacryloyloxyethyl phosphorylcholine with EGF, loaded with paclitaxel, showing a preferential uptake in tumor cells *in vitro* and *in vivo*.¹³⁶ Wagner *et al.* have shown the synthesis of DNA-polyplexes conjugated with the EGF peptide, including investigations of the uptake and gene transfection efficiency in cells.¹³⁷

1.10 Polyethylene glycol in drug delivery applications

In the field of systemic drug delivery, it has been known for decades that polyethylene glycol (PEG)-carrying conjugates show a prolonged blood circulation time *in vivo*. The inert polymer represents a steric barrier to the surface of the nanocarrier and can minimize protein binding.¹³⁸ This effect, often referred to as stealth effect, reduces the effectivity of the reticuloendothelial system to recognize the circulating nanomaterials and thus improves the pharmacokinetics. So far, PEGylation has been applied on various potential drug carriers like liposomes,¹³⁹ polymeric drug and DNA conjugates,^{140,141} or even viral capsids.¹⁴² In the

context of mesoporous silica, the effect of PEGylation of the silica surface was studied recently.¹⁴³ The post-synthetically modified mesoporous silica nanoparticles (MSN) were investigated in terms of protein adsorption. It was shown that PEGylated MSNs adsorb far less human serum protein on their surface than the unfunctionalized reference material. Hemolysis was additionally studied, showing a very low hemolysis percentage of 0.9 %, compared to more than 14 % of the unfunctionalized reference material.

In our group we have initially shown that CMS nanoparticles with an outer co-condensed PEG-shell are stabilized against degradation by biologically relevant anions such as phosphate. The results indicate that the PEG shell conserves the mesoporous structure up to a week of immersion in Simulated Body Fluid¹⁴⁴ (SBF) at 37°C whereas unfunctionalized particles degrade within a couple of hours.¹⁴⁵ In further studies, it was demonstrated that the density and the chain length of a co-condensed PEG-chain (see Figure 1.10.1) has an influence on the degradation behavior of the CMS nanoparticles.¹⁴⁶

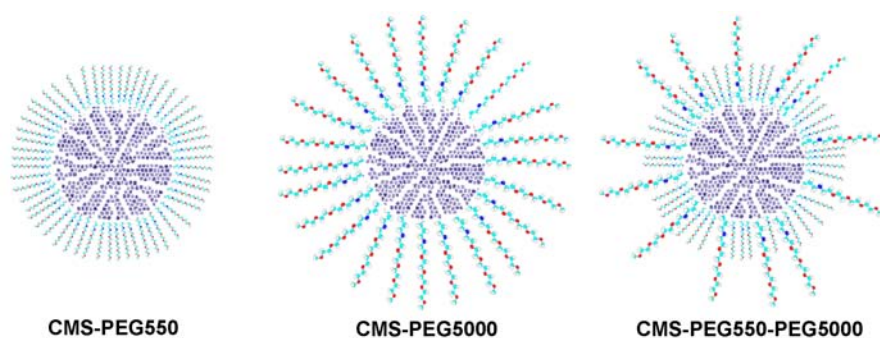


Figure 1.10.1 Colloidal mesoporous silica nanoparticles with an outer shell of different PEG chain lengths.

By varying these parameters, it is even possible to tune the degradation behaviour to the desired application. This is of great interest for future injectable blood-persistent biomedical systems and site-specific drug delivery devices.

In the present work, we use functional PEG-linkers attached to the silica surface for further

functionalization with organic molecules on the outer surface of the particle.

1.11 References

- (1) Rees, L. V. C. *Reports on the Progress of Applied Chemistry* **1969**, *54*, 655.
- (2) Townsend, R. P. *Studies in Surface Science and Catalysis* **1986**, *28*, 273.
- (3) Platas-Iglesias, C.; Vander Elst, L.; Zhou, W.; Muller, R. N.; Geraldes, C. F. G. C.; Maschmeyer, T.; Peters, J. A. *Chemistry--A European Journal* **2002**, *8*, 5121.
- (4) Vallet-Regi, M.; Balas, F.; Colilla, M.; Manzano, M. *Solid State Sciences* **2007**, *9*, 768.
- (5) Zarkovic, N.; Zarkovic, K.; Kralj, M.; Borovic, S.; Sabolovic, S.; Blazi, M. P.; Cipak, A.; Pavelic, K. *Anticancer Research* **2003**, *23*, 1589.
- (6) Caro, J. *Microporous and Mesoporous Materials* **2009**, *125*, 79.
- (7) Calzaferri, G.; Bruhwiler, D.; Megelski, S.; Pfenniger, M.; Pauchard, M.; Hennessy, B.; Maas, H.; Devaux, A.; Graf, U. *Solid State Sciences* **2000**, *2*, 421.
- (8) Tchernev, D. I. *Reviews in Mineralogy & Geochemistry* **2001**, *45*, 589.
- (9) Schaf, O.; Ghobarkar, H.; Knauth, P. *Encyclopedia of Sensors* **2006**, *10*, 491.
- (10) Xu, X.; Wang, J.; Long, Y. *Sensors* **2006**, *6*, 1751.
- (11) Ozin, G. A.; Kuperman, A.; Stein, A. *Angewandte Chemie* **1989**, *101*, 373.
- (12) Yu, M.; Li, S.; Falconer, J. L.; Noble, R. D. *Microporous and Mesoporous Materials* **2008**, *110*, 579.
- (13) Nijkamp, M. G.; Raaymakers, J. E. M. J.; Van Dillen, A. J.; De Jong, K. P. *Applied Physics A: Materials Science & Processing* **2001**, *72*, 619.
- (14) Kazansky, V. B.; Borovkov, V. Y.; Serich, A.; Karge, H. G. *Microporous and Mesoporous Materials* **1998**, *22*, 251.

- (15) Beck, J. S.; Vartuli, J. C.; Roth, W. J.; Leonowicz, M. E.; Kresge, C. T.; Schmitt, K. D.; Chu, C. T. W.; Olson, D. H.; Sheppard, E. W.; et al. *Journal of the American Chemical Society* **1992**, *114*, 10834.
- (16) Kresge, C. T.; Leonowicz, M. E.; Roth, W. J.; Vartuli, J. C.; Beck, J. S. *Nature (London)* **1992**, *359*, 710.
- (17) Lopez, T.; Ortiz, E.; Alexander-Katz, R.; Basaldella, E.; Bokhimi, X. *Nanomedicine (New York, NY, United States)* **2009**, *5*, 170.
- (18) Wang, Y.; Caruso, F. *Chemistry of Materials* **2005**, *17*, 953.
- (19) Galarneau, A.; Phuoc, L. T.; Falcimaigne, A.; Renard, G.; Fajula, F. *Studies in Surface Science and Catalysis* **2007**, *165*, 637.
- (20) Ke, J.; Su, W.; Howdle, S. M.; George, M. W.; Cook, D.; Perdjon-Abel, M.; Bartlett, P. N.; Zhang, W.; Cheng, F.; Levason, W.; Reid, G.; Hyde, J.; Wilson, J.; Smith, D. C.; Mallik, K.; Sazio, P. *Proceedings of the National Academy of Sciences of the United States of America* **2009**, *106*, 14768.
- (21) Bao, R.; Jiao, K.; He, H.; Zhuang, J.; Yue, B. *Studies in Surface Science and Catalysis* **2007**, *165*, 267.
- (22) Eliseev, A. A.; Gorozhankin, D. F.; Zaitsev, D. D.; Lukashin, A. V.; Knotko, A. V.; Tretyakov, Y. D.; Goernert, P. *Journal of Magnetism and Magnetic Materials* **2005**, *290-291*, 106.
- (23) Yaghi, O. M.; Li, G.; Li, H. *Nature (London)* **1995**, *378*, 703.
- (24) Ferey, G.; Serre, C.; Mellot-Draznieks, C.; Millange, F.; Surble, S.; Dutour, J.; Margiolaki, I. *Angewandte Chemie, International Edition* **2004**, *43*, 6296.
- (25) Ferey, G.; Mellot-Draznieks, C.; Serre, C.; Millange, F.; Dutour, J.; Surble, S.; Margiolaki, I. *Science (Washington, DC, U. S.)* **2005**, *309*, 2040.
- (26) Cote, A. P.; Benin, A. I.; Ockwig, N. W.; O'Keeffe, M.; Matzger, A. J.; Yaghi, O. M. *Science (Washington, DC, U. S.)* **2005**, *310*, 1166.

- (27) Hoffmann, F.; Cornelius, M.; Morell, J.; Froeba, M. *Angewandte Chemie, International Edition* **2006**, *45*, 3216.
- (28) Tanev, P. T.; Pinnavaia, T. J. *Science (Washington, D. C.)* **1995**, *267*, 865.
- (29) Bagshaw, S. A.; Prouzet, E.; Pinnavaia, T. J. *Science (Washington, D. C.)* **1995**, *269*, 1242.
- (30) Cassiers, K.; van der Voort, P.; Vansant, E. F. *Chemical Communications (Cambridge)* **2000**, 2489.
- (31) Herrier, G.; Blin, J.-L.; Su, B.-L. *Langmuir* **2001**, *17*, 4422.
- (32) Zhao, D.; Feng, J.; Huo, Q.; Melosh, N.; Frederickson, G. H.; Chmelka, B. F.; Stucky, G. D. *Science (Washington, D. C.)* **1998**, *279*, 548.
- (33) Zhao, D.; Huo, Q.; Feng, J.; Chmelka, B. F.; Stucky, G. D. *Journal of the American Chemical Society* **1998**, *120*, 6024.
- (34) Taguchi, A.; Schueth, F. *Microporous and Mesoporous Materials* **2004**, *77*, 1.
- (35) Imperor-Clerc, M.; Davidson, P.; Davidson, A. *Journal of the American Chemical Society* **2000**, *122*, 11925.
- (36) Wan, Y.; Zhao, D. *Chemical reviews* **2007**, *107*, 2821.
- (37) Huo, Q.; Margolese, D. I.; Ciesla, U.; Feng, P.; Gier, T. E.; Sieger, P.; Leon, R.; Petroff, P. M.; Schueth, F.; Stucky, G. D. *Nature (London)* **1994**, *368*, 317.
- (38) Huo, Q.; Margolese, D. I.; Ciesla, U.; Demuth, D. G.; Feng, P.; Gier, T. E.; Sieger, P.; Firouzi, A.; Chmelka, B. F.; et al. *Chemistry of Materials* **1994**, *6*, 1176.
- (39) Chen, C. Y.; Burkett, S. L.; Li, H. X.; Davis, M. E. *Microporous Materials* **1993**, *2*, 27.
- (40) Monnier, A.; Schuth, F.; Huo, Q.; Kumar, D.; Margolese, D.; Maxwell, R. S.; Stucky, G. D.; Krishnamurty, M.; Petroff, P.; et al. *Science (Washington, DC, United States)* **1993**, *261*, 1299.
- (41) Attard, G. S.; Glyde, J. C.; Goltner, C. G. *Nature (London)* **1995**, *378*, 366.

- (42) Lang, N.; Tuel, A. *Chemistry of Materials* **2004**, *16*, 1961.
- (43) Kawi, S. *Chemical Communications (Cambridge)* **1998**, 1407.
- (44) Gomez-Vega, J. M.; Teshima, K.; Hozumi, A.; Sugimura, H.; Takai, O. *Surface and Coatings Technology* **2003**, *169-170*, 504.
- (45) Tian, B.; Liu, X.; Yu, C.; Gao, F.; Luo, Q.; Xie, S.; Tu, B.; Zhao, D. *Chemical Communications (Cambridge, United Kingdom)* **2002**, 1186.
- (46) Lim, M. H.; Stein, A. *Chemistry of Materials* **1999**, *11*, 3285.
- (47) Yokoi, T.; Yoshitake, H.; Tatsumi, T. *Journal of Materials Chemistry* **2004**, *14*, 951.
- (48) Angloher, S.; Kecht, J.; Bein, T. *Chemistry of Materials* **2007**, *19*, 3568.
- (49) Angloher, S.; Kecht, J.; Bein, T. *Chemistry of Materials* **2007**, *19*, 5797.
- (50) Lu, Y.; Fan, H.; Stump, A.; Ward, T. L.; Rieker, T.; Brinker, C. J. *Nature (London)* **1999**, *398*, 223.
- (51) Fowler, C. E.; Khushalani, D.; Lebeau, B.; Mann, S. *Advanced Materials (Weinheim, Germany)* **2001**, *13*, 649.
- (52) Suzuki, K.; Ikari, K.; Imai, H. *Journal of the American Chemical Society* **2004**, *126*, 462.
- (53) Ikari, K.; Suzuki, K.; Imai, H. *Langmuir* **2006**, *22*, 802.
- (54) Han, Y.; Ying, J. Y. *Angewandte Chemie, International Edition* **2005**, *44*, 288.
- (55) Park, S.-E.; Kim, D. S.; Chang, J.-S.; Kim, W. Y. *Catalysis Today* **1998**, *44*, 301.
- (56) El Haskouri, J.; Ortiz de Zarate, D.; Guillem, C.; Beltran-Porter, A.; Caldes, M.; Marcos, M. D.; Beltran-Porter, D.; Latorre, J.; Amoros, P. *Chemistry of Materials* **2002**, *14*, 4502.
- (57) Kobler, J.; Moeller, K.; Bein, T. *ACS Nano* **2008**, *2*, 791.
- (58) Moeller, K.; Kobler, J.; Bein, T. *Advanced Functional Materials* **2007**, *17*, 605.
- (59) Moeller, K.; Kobler, J.; Bein, T. *Journal of Materials Chemistry* **2007**, *17*, 624.
- (60) Frye, C. L.; Vincent, G. A.; Finzel, W. A. *J. Amer. Chem. Soc.* **1971**, *93*, 6805.

- (61) Verkade, J. G. *Accounts of Chemical Research* **1993**, *26*, 483.
- (62) Cabrera, S.; El Haskouri, J.; Guillem, C.; Latorre, J.; Beltran-Porter, A.; Beltran-Porter, D.; Marcos, M. D.; Amoros, P. *Solid State Sciences* **2000**, *2*, 405.
- (63) Torchilin, V. P. *Nature Reviews Drug Discovery* **2005**, *4*, 145.
- (64) Ogris, M.; Brunner, S.; Schuller, S.; Kircheis, R.; Wagner, E. *Gene Therapy* **1999**, *6*, 595.
- (65) Merkel, O. M.; Germershaus, O.; Wada, C. K.; Tarcha, P. J.; Merdan, T.; Kissel, T. *Bioconjugate Chemistry* **2009**, *20*, 1270.
- (66) Weiss, S. I.; Sieverling, N.; Niclasen, M.; Maucksch, C.; Thuenemann, A. F.; Moehwald, H.; Reinhardt, D.; Rosenecker, J.; Rudolph, C. *Biomaterials* **2006**, *27*, 2302.
- (67) Boeckle, S.; Fahrmeir, J.; Roedl, W.; Ogris, M.; Wagner, E. *Journal of Controlled Release* **2006**, *112*, 240.
- (68) Rimoli Maria, G.; Rabaioli Maria, R.; Melisi, D.; Curcio, A.; Mondello, S.; Mirabelli, R.; Abignente, E. *Journal of biomedical materials research. Part A* **2008**, *87*, 156.
- (69) Strassert, C. A.; Otter, M.; Albuquerque, R. Q.; Hoene, A.; Vida, Y.; Maier, B.; De Cola, L. *Angewandte Chemie, International Edition* **2009**, *48*, 7928.
- (70) Dyer, A.; Morgan, S.; Wells, P.; Williams, C. *Journal of Helminthology* **2000**, *74*, 137.
- (71) Coti, K. K.; Belowich, M. E.; Liong, M.; Ambrogio, M. W.; Lau, Y. A.; Khatib, H. A.; Zink, J. I.; Khashab, N. M.; Stoddart, J. F. *Nanoscale* **2009**, *1*, 16.
- (72) Vallet-Regi, M.; Balas, F.; Arcos, D. *Angewandte Chemie, International Edition* **2007**, *46*, 7548.
- (73) Aznar, E.; Martinez-Manez, R.; Sancenon, F. *Expert Opinion on Drug Delivery* **2009**, *6*, 643.

- (74) Trewyn, B. G.; Slowing, I. I.; Giri, S.; Chen, H.-T.; Lin, V. S. Y. *Accounts of Chemical Research* **2007**, *40*, 846.
- (75) Slowing, I. I.; Vivero-Escoto, J. L.; Wu, C.-W.; Lin, V. S. Y. *Advanced Drug Delivery Reviews* **2008**, *60*, 1278.
- (76) Korteso, P.; Ahola, M.; Karlsson, S.; Kangasniemi, I.; Yli-Urpo, A.; Kiesvaara, J. *Biomaterials* **2000**, *21*, 193.
- (77) Chia, S.; Urano, J.; Tamanoi, F.; Dunn, B.; Zink, J. I. *Journal of the American Chemical Society* **2000**, *122*, 6488.
- (78) Radin, S.; El-Bassyouni, G.; Vresilovic Edward, J.; Schepers, E.; Ducheyne, P. *Biomaterials* **2005**, *26*, 1043.
- (79) Slowing, I. I.; Trewyn, B. G.; Lin, V. S. Y. *Journal of the American Chemical Society* **2007**, *129*, 8845.
- (80) Cauda, V.; Engelke, H.; Sauer, A.; Arcizet, D.; Braeuchle, C.; Raedler, J.; Bein, T. *Nano Letters* **2010**, *10*, 2484.
- (81) Han, Y.-J.; Stucky, G. D.; Butler, A. *Journal of the American Chemical Society* **1999**, *121*, 9897.
- (82) Tourne-Peteilh, C.; Lerner Dan, A.; Charnay, C.; Nicole, L.; Begu, S.; Devoisselle, J.-M. *Chemphyschem : a European journal of chemical physics and physical chemistry* **2003**, *4*, 281.
- (83) Doadrio, J. C.; Sousa, E. M. B.; Izquierdo-Barba, I.; Doadrio, A. L.; Perez-Pariente, J.; Vallet-Regi, M. *Journal of Materials Chemistry* **2006**, *16*, 462.
- (84) Ford, D. M.; Simanek, E. E.; Shantz, D. F. *Nanotechnology* **2005**, *16*, 458.
- (85) Stein, A.; Melde, B. J.; Schroden, R. C. *Advanced Materials (Weinheim, Germany)* **2000**, *12*, 1403.
- (86) Yang, C.-M.; Lin, H.-A.; Zibrowius, B.; Spliethoff, B.; Schueth, F.; Liou, S.-C.; Chu, M.-W.; Chen, C.-H. *Chemistry of Materials* **2007**, *19*, 3205.

- (87) Yano, K.; Nakamura, T. *Chemistry Letters* **2006**, *35*, 1014.
- (88) Shephard, D. S.; Zhou, W.; Maschmeyer, T.; Matters, J. M.; Roper, C. L.; Parsons, S.; Johnson, B. F. G.; Duer, M. J. *Angewandte Chemie, International Edition* **1998**, *37*, 2719.
- (89) De Juan, F.; Ruiz-Hitzky, E. *Advanced Materials (Weinheim, Germany)* **2000**, *12*, 430.
- (90) Rosenholm, J. M.; Duchanoy, A.; Linden, M. *Chemistry of Materials* **2008**, *20*, 1126.
- (91) Angelos, S.; Johansson, E.; Stoddart, J. F.; Zink, J. I. *Advanced Functional Materials* **2007**, *17*, 2261.
- (92) Bourlinos, A. B.; Karakostas, T.; Petridis, D. *Journal of Physical Chemistry B* **2003**, *107*, 920.
- (93) Antochshuk, V.; Jaroniec, M. *Chemical Communications (Cambridge)* **1999**, 2373.
- (94) Antochshuk, V.; Jaroniec, M. *Chemistry of Materials* **2000**, *12*, 2496.
- (95) Antochshuk, V.; Araujo, A. S.; Jaroniec, M. *Journal of Physical Chemistry B* **2000**, *104*, 9713.
- (96) Kecht, J.; Schlossbauer, A.; Bein, T. *Chemistry of Materials* **2008**, *20*, 7207.
- (97) Cauda, V.; Schlossbauer, A.; Kecht, J.; Zurner, A.; Bein, T. *Journal of the American Chemical Society* **2009**, *131*, 11361.
- (98) Patel, K.; Angelos, S.; Dichtel, W. R.; Coskun, A.; Yang, Y.-W.; Zink, J. I.; Stoddart, J. F. *Journal of the American Chemical Society* **2008**, *130*, 2382.
- (99) Bernardos, A.; Aznar, E.; Marcos, M. D.; Martinez-Manez, R.; Sancenon, F.; Soto, J.; Barat, J. M.; Amoros, P. *Angewandte Chemie, International Edition* **2009**, *48*, 5884.
- (100) Schlossbauer, A.; Kecht, J.; Bein, T. *Angewandte Chemie, International Edition* **2009**, *48*, 3092.
- (101) West, K. R.; Otto, S. *Current Drug Discovery Technologies* **2005**, *2*, 123.
- (102) Ambrogio, M. W.; Pecorelli, T. A.; Patel, K.; Khashab, N. M.; Trabolsi, A.; Khatib, H. A.; Botros, Y. Y.; Zink, J. I.; Stoddart, J. F. *Organic Letters* **2010**, *12*, 3304.

- (103) Lai, C.-Y.; Trewyn, B. G.; Jeftinija, D. M.; Jeftinija, K.; Xu, S.; Jeftinija, S.; Lin, V. S. Y. *Journal of the American Chemical Society* **2003**, *125*, 4451.
- (104) Giri, S.; Trewyn, B. G.; Stellmaker, M. P.; Lin, V. S. Y. *Angewandte Chemie, International Edition* **2005**, *44*, 5038.
- (105) Mortera, R.; Vivero-Escoto, J.; Slowing, I. I.; Garrone, E.; Onida, B.; Lin, V. S. Y. *Chemical Communications (Cambridge, United Kingdom)* **2009**, 3219.
- (106) Sauer, A. M.; Schlossbauer, A.; Ruthardt, N.; Cauda, V.; Bein, T.; Brauchle, C. *Nano Letters* **2010**, *10*, 3684.
- (107) Liu, R.; Zhao, X.; Wu, T.; Feng, P. *J. Am. Chem. Soc.* **2008**, *130*, 14418.
- (108) Khashab, N. M.; Trabolosi, A.; Lau, Y. A.; Ambrogio, M. W.; Friedman, D. C.; Khatib, H. A.; Zink, J. I.; Stoddart, J. F. *European Journal of Organic Chemistry* **2009**, 1669.
- (109) Park, C.; Lee, K.; Kim, C. *Angewandte Chemie (International ed. in English)* **2009**, *48*, 1275.
- (110) Lu, J.; Choi, E.; Tamanoi, F.; Zink, J. I. *Small* **2008**, *4*, 421.
- (111) Sierocki, P.; Maas, H.; Dragut, P.; Richardt, G.; Voegtle, F.; De Cola, L.; Brouwer, F.; Zink, J. I. *Journal of Physical Chemistry B* **2006**, *110*, 24390.
- (112) Angelos, S.; Choi, E.; Voegtle, F.; De Cola, L.; Zink, J. I. *Journal of Physical Chemistry C* **2007**, *111*, 6589.
- (113) Ferris, D. P.; Zhao, Y.-L.; Khashab, N. M.; Khatib, H. A.; Stoddart, J. F.; Zink, J. I. *Journal of the American Chemical Society* **2009**, *131*, 1686.
- (114) Mal, N. K.; Fujiwara, M.; Tanaka, Y. *Nature (London, United Kingdom)* **2003**, *421*, 350.
- (115) Zhu, Y.; Fujiwara, M. *Angewandte Chemie, International Edition* **2007**, *46*, 2241.
- (116) Vivero-Escoto, J. L.; Slowing, I. I.; Wu, C.-W.; Lin, V. S. Y. *Journal of the American Chemical Society* **2009**, *131*, 3462.

- (117) Nguyen, T. D.; Leung, K. C. F.; Liong, M.; Pentecost, C. D.; Stoddart, J. F.; Zink, J. I. *Organic Letters* **2006**, *8*, 3363.
- (118) Park, C.; Oh, K.; Lee, S. C.; Kim, C. *Angewandte Chemie, International Edition* **2007**, *46*, 1455.
- (119) Angelos, S.; Yang, Y.-W.; Patel, K.; Stoddart, J. F.; Zink, J. I. *Angewandte Chemie, International Edition* **2008**, *47*, 2222.
- (120) Angelos, S.; Khashab, N. M.; Yang, Y.-W.; Trabolosi, A.; Khatib, H. A.; Stoddart, J. F.; Zink, J. I. *Journal of the American Chemical Society* **2009**, *131*, 12912.
- (121) Angelos, S.; Yang, Y.-W.; Khashab, N. M.; Stoddart, J. F.; Zink, J. I. *Journal of the American Chemical Society* **2009**, *131*, 11344.
- (122) Cauda, V.; Argyo, C.; Schlossbauer, A.; Bein, T. *Journal of Materials Chemistry* **2010**, *20*, 4305.
- (123) Casasus, R.; Marcos, M. D.; Martinez-Manez, R.; Ros-Lis, J. V.; Soto, J.; Villaescusa, L. A.; Amoros, P.; Beltran, D.; Guillem, C.; Latorre, J. *Journal of the American Chemical Society* **2004**, *126*, 8612.
- (124) Zhu, Y.; Shi, J.; Shen, W.; Dong, X.; Feng, J.; Ruan, M.; Li, Y. *Angewandte Chemie, International Edition* **2005**, *44*, 5083.
- (125) Schlossbauer, A. D., Christian; Schaffert, David; Wagner, Ernst; Bein, Thomas *Journal of the American Chemical Society* **2010**.
- (126) Liu, J.; Jiang, X.; Ashley, C.; Brinker, C. J. *Journal of the American Chemical Society* **2009**, *131*, 7567.
- (127) Carbone, D. P. *Journal of Clinical Oncology* **2003**, *21*, 4268.
- (128) Kularatne, S. A.; Low, P. S. *Methods in Molecular Biology (Totowa, NJ, United States)* **2010**, *624*, 249.
- (129) Liu, S. *Bioconjugate Chemistry* **2009**, *20*, 2199.

- (130) Ross, J. S.; Schenkein, D. P.; Pietrusko, R.; Rolfe, M.; Linette, G. P.; Stec, J.; Stagliano, N. E.; Ginsburg, G. S.; Symmans, W. F.; Pusztai, L.; Hortobagyi, G. N. *American Journal of Clinical Pathology* **2004**, *122*, 598.
- (131) Rosenholm, J. M.; Meinander, A.; Peuhu, E.; Niemi, R.; Eriksson, J. E.; Sahlgren, C.; Linden, M. *ACS Nano* **2009**, *3*, 197.
- (132) Rosenholm, J. M.; Peuhu, E.; Eriksson, J. E.; Sahlgren, C.; Linden, M. *Nano Letters* **2009**, *9*, 3308.
- (133) Fang, I. J.; Slowing, I. I.; Wu, C.-W.; Lin, V. S. Y. *Abstracts of Papers, 238th ACS National Meeting, Washington, DC, United States, August 16-20, 2009* **2009**, INOR.
- (134) Wang, S.; Chen, K.-J.; Wu, T.-H.; Wang, H.; Lin, W.-Y.; Ohashi, M.; Chiou, P.-Y.; Tseng, H.-R. *Angewandte Chemie, International Edition* **2010**, *49*, 3777.
- (135) Lu, J.; Shi, M.; Shoichet, M. S. *Bioconjugate Chemistry* **2009**, *20*, 87.
- (136) Shimada, T.; Ueda, M.; Jinno, H.; Chiba, N.; Wada, M.; Watanabe, J.; Ishihara, K.; Kitagawa, Y. *Anticancer Research* **2009**, *29*, 1009.
- (137) Kloeckner, J.; Boeckle, S.; Persson, D.; Roedl, W.; Ogris, M.; Berg, K.; Wagner, E. *Journal of Controlled Release* **2006**, *116*, 115.
- (138) Li, S.-D.; Huang, L. *Journal of Controlled Release* **2010**, *145*, 178.
- (139) Carstens, M. G.; Romberg, B.; Oussoren, C.; Storm, G.; Laverman, P.; Boerman, O. *C. Liposome Technology (3rd Edition)* **2007**, *3*, 79.
- (140) Fichter, K. M.; Zhang, L.; Kiick, K. L.; Reineke, T. M. *Bioconjugate Chemistry* **2008**, *19*, 76.
- (141) Lee, M.; Kim, S. W. *Pharmaceutical Research* **2005**, *22*, 1.
- (142) Comellas-Aragones, M.; de la Escosura, A.; Dirks, A. J.; van der Ham, A.; Fustecune, A.; Cornelissen, J. J. L. M.; Nolte, R. J. M. *Biomacromolecules* **2009**, *10*, 3141.
- (143) He, Q.; Zhang, J.; Shi, J.; Zhu, Z.; Zhang, L.; Bu, W.; Guo, L.; Chen, Y. *Biomaterials* **2010**, *31*, 1085.

- (144) Kokubo, T.; Kushitani, H.; Sakka, S.; Kitsugi, T.; Yamamuro, T. *Journal of Biomedical Materials Research* **1990**, *24*, 721.
- (145) Cauda, V.; Schlossbauer, A.; Bein, T. *Microporous and Mesoporous Materials* **2010**, *132*, 60.
- (146) Argyo, C.; Cauda, V.; Bein, T. *Journal of Materials Chemistry* **2010**, *20*, 8693.

2. Characterization

2.1 X-ray Diffraction

Electromagnetic radiation with wavelengths between 10 and 0.01 nm is defined as X-rays. To generate X-rays, a cooled metal anode is bombarded with a highly energetic and focused electron beam. When the electrons hit the target, their loss of energy is partly emitted as a continuous background spectrum called “Bremsstrahlung”. Additionally, narrow lines that are characteristic for the applied target appear in the spectrum, resulting from a X-ray fluorescence process. The impact of primary electrons can create holes in energetically low shells of the target atoms. Electrons from higher shells are then falling into these holes. The energy is released as X-ray photons. Monochromatic X-ray radiation can be created by blocking filters, isolating a single emission from these processes.

X-rays are used to determine structural properties of crystalline solid materials.¹ As the wavelengths of the X-ray photons lie in the Ångström range, the wavelength lies in the same order of magnitude as the distances of atoms in solid matter. Thus, structural information of the ordered lattice of crystals can be gained by interpreting the constructive and destructive interferences of X-rays scattered by the lattice planes (Figure 2.1.1).

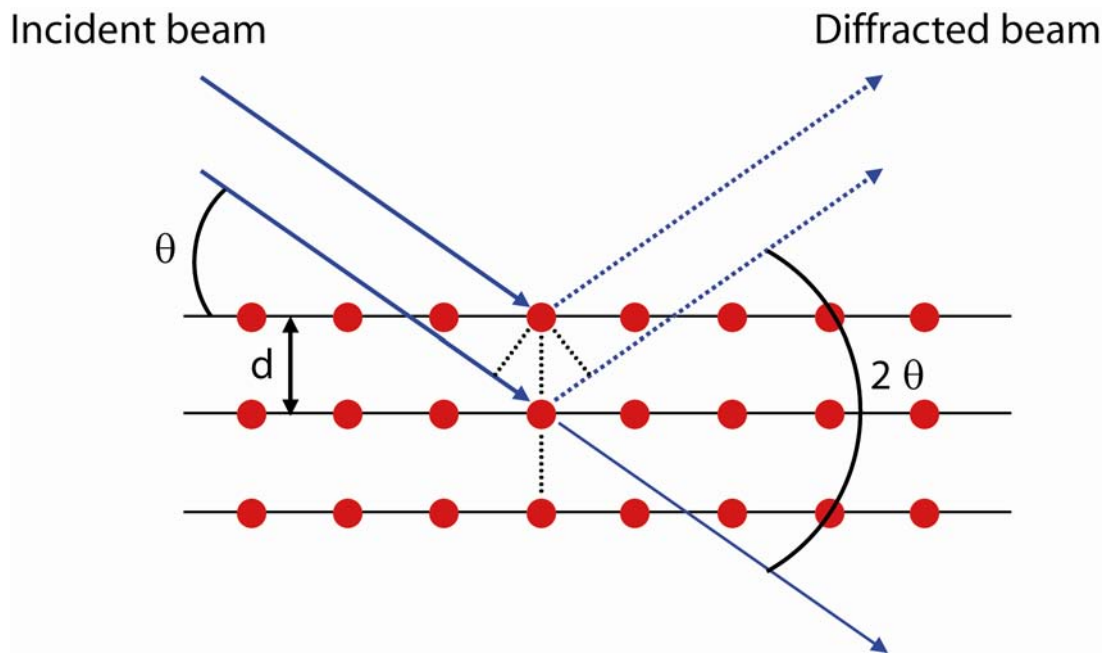


Figure 2.1.1 Illustration of the Bragg relation. A constructive interference occurs when the path difference is a multiple integer of the X-ray wavelength.

Bragg's law defines the conditions at which constructive interference of scattered X-rays is observed (equation 2.1.1).

$$n\lambda = 2 d \sin \theta \text{ (eq. 2.1.1)}$$

n : order of interference

λ : X-ray wavelength

d : lattice spacing

θ : angle of incidence

In the present work, ordered mesopores in amorphous silica frameworks are characterized by X-ray diffraction. In this case, the walls of the ordered mesopores define the lattice planes of the material.

2.2 Infrared (IR) and Raman spectroscopy

Infrared (IR)² and Raman³ vibrational spectroscopy are methods to characterize the chemical bonding of the elements contained in a sample. The characteristic vibrational modes of functional groups can be used to gain this information. Radiation of the infrared region of the electromagnetic spectrum is used to excite these modes. Usually, electromagnetic radiation between 200- 4000 cm^{-1} is used. The absorbed light from the sample is characteristic for the contained functionalities. To be visible in IR spectroscopy, a vibrational mode of a molecule needs to change the dipole moment of the compound during the vibration. Thereby, the molecule itself does not need to have a permanent dipole.

However, in Raman spectroscopy, inelastic scattering of monochromatic light is detected. The scattering of the light occurs upon interaction with the electron clouds around chemical bonds. Since this relies on a different physical process than IR spectroscopy, the general selection rules of observable vibrational states are different. For a vibrational mode visible in Raman spectroscopy, the polarizability of the bond is changed during the vibration. The amount of deformation of the electron cloud determines the signal intensity.

Photons are able to excite a given vibrational state into a virtual energy state. Photons can be re-radiated in all directions after relaxation of the electrons (Figure 2.2.1).

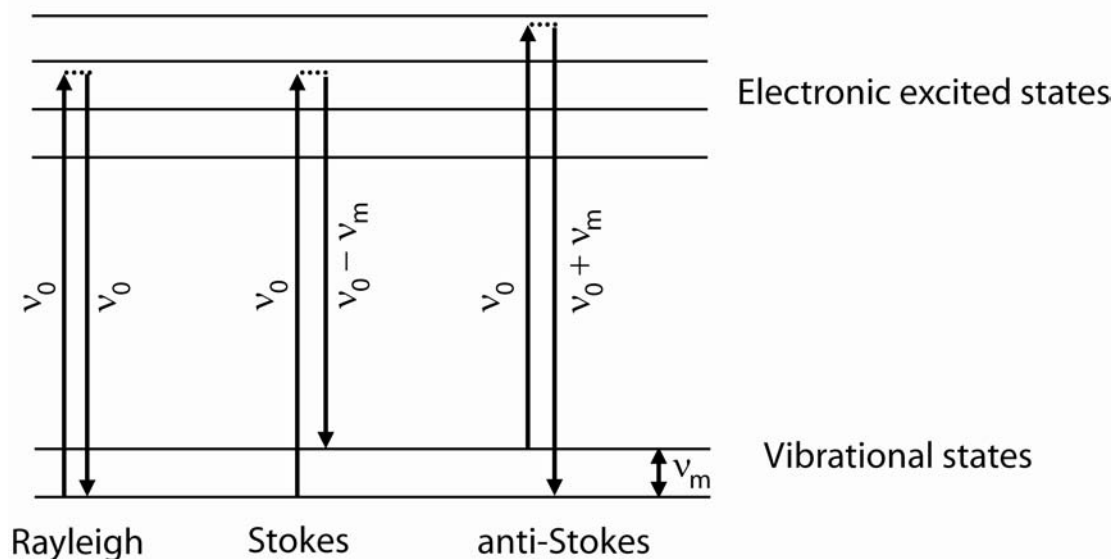


Figure 2.2.1 Rayleigh-, Stokes-, and anti-Stokes scattering.

Most of the incident light is scattered and released without changing the frequency, i.e. as Rayleigh scattering. Photons with lower energy are scattered if the excited system was in an energetically low state and relaxes back into higher vibrational states. This “Stokes scattering” results in weak bands at lower frequencies. On the other hand, “anti-Stokes scattering” result from relaxation into vibrational states of lower energy than the original. Although both Stokes and anti-Stokes scattering can be used to measure molecular vibrations, Stokes scattering is mainly used. This is due to the required excited vibrational states for anti-Stokes scattering, which typically results in lower intensities.

2.3 Thermogravimetric analysis and Differential Scanning Calorimetry

Thermogravimetric analysis investigates the mass loss of a sample related to the temperature of a heating ramp. Thereby, the temperature is raised with a constant heating rate. During this process, evaporation and pyrolysis reactions can occur among other possible processes. Oxidation reactions can be either excluded or included, controlled through the use of an inert gas atmosphere such as argon or nitrogen or a synthetic air mixture, respectively. In the present work, oxidation reactions were included, as we investigate the combustion of organic groups on the inorganic silica framework. The used gas mixture passes the sample with an approximately laminar flow, leading to a removal of desorbed components. The obtained thermograms include information about the temperature stability of the samples and quantitative information about the amount of organic groups included in the sample.

Additionally, Differential Scanning Calorimetry (DSC) can be performed during the TGA measurement. With this technique, the difference of heat needed to heat the sample and an inert reference is determined. From this, information about endothermic or exothermic processes during sample heating is gained. For example, it is possible to distinguish between combustion (exothermic) and evaporation (endothermic) steps. Thermogravimetric analyses of the samples were performed on a Netzsch STA 440 C TG/DSC.

2.4 Nitrogen Sorption

Sorption of nitrogen molecules on surfaces is commonly used for the determination of pore characteristics and surface areas of porous solids.^{4,5} From the measured amount of adsorbed nitrogen at different pressures and constant temperature, adsorption and desorption isotherms can be generated. As defined by IUPAC, there are six major types of isotherms (Figure 2.4.1).

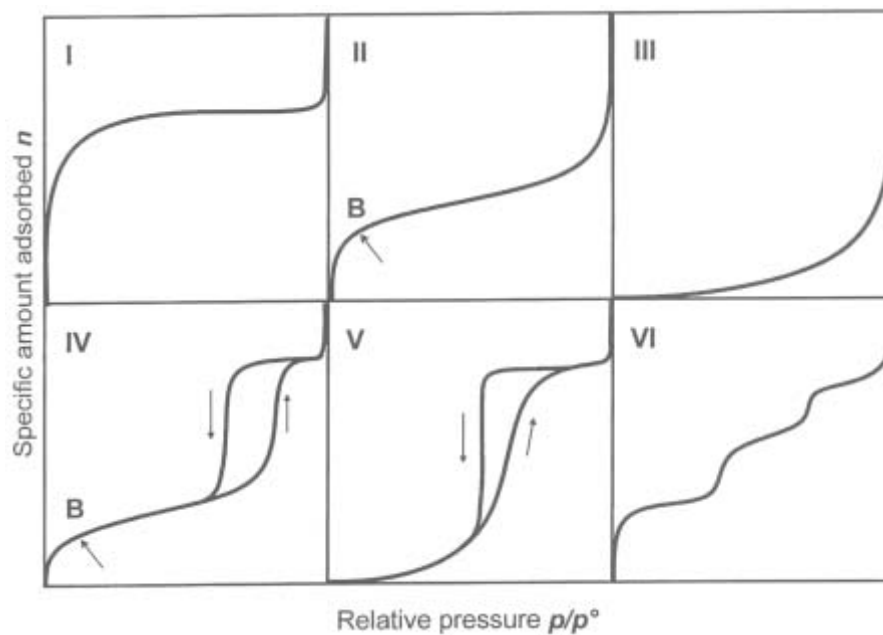


Figure 2.4.1 The six types of gas sorption (IUPAC) isotherms.

Every type displayed in Figure 2.4.1 is characteristic for a certain type of solid material (Table 2.4.1).

Table 2.4.1 Classification of adsorption isotherms

Isotherm Type	Corresponding Material
I	Microporous material, remains static after complete pore filling
II	Nonporous or macroporous material, high adsorption energy
III	Nonporous or macroporous material, low adsorption energy, weak interaction between adsorbate and adsorbens
IV	Mesoporous material
V	Mesoporous material with very weak interaction between adsorbate and adsorbens
VI	Stepwise multilayer adsorption on nonporous, uniform material

During a nitrogen sorption experiment, the gas is added at 77 K. In the case of mesoporous silica materials, the applied adsorbate is bound to the surface (adsorptive) by van-der-Waals forces, leading to physisorbed nitrogen molecules. The adsorbed amount of gas is plotted against the relative pressure in order to obtain an isotherm. The obtained isotherm can then be interpreted to gain information on the porous features of the investigated sample. Three different models are most commonly applied in the literature to describe isotherms. They are named after its developers, Langmuir, Freundlich or Brunauer-Emmett-Teller, respectively.

The simplest method for the characterization of isotherms is the Langmuir interpretation. It is based on a few simple approximations:

1. Adsorption leads only to a monolayer of adsorbed molecules
2. The surface is uniform, every binding site is equal
3. The ability of a molecule to bind specific surface sites is independent from the occupancy of neighboring binding sites.

These simple approximations are expressed in Langmuir's equation (eq. 2.4.1)

$$\frac{n}{n_m} = \frac{B \cdot p}{1 + B \cdot p} \quad \text{eq. 2.4.1)}$$

n: amount of adsorbate, n_m : capacity of one monolayer, p: pressure, B: constant

While the Freundlich interpretation is generally based on the same approximations, Brunauer-Emmett-Teller's model (BET) also incorporates multilayer adsorption.⁶ Therefore, the initial monolayer serves as a substrate for further adsorption processes. As a result from these approximations, the BET-equation can be expressed (eq. 2.4.2).

$$\frac{n}{n_m} = \frac{C \cdot \frac{P}{P_0}}{\left(1 - \frac{P}{P_0}\right) \left(1 + C - \frac{P}{P_0}\right)} \quad \text{(eq. 2.4.2)}$$

n: amount of adsorbate, n_m : capacity of one monolayer, C: BET constant, p: equilibrium pressure, p_0 : saturation vapor pressure of adsorbate.

Based on Kelvin's equation, a model for calculating the pore diameters was developed by Barrett, Joyner and Halenda (BJH - diameter).^{4,5} However, for small mesopores in the range of 4 nm, the pore diameters calculated from BJH are typically 1 nm smaller than the real diameters. This can be attributed to the existence of an adsorption potential within the pores leading to an enhanced stability of incumbent fluid phases against capillary driving forces.⁷ For the applicability of microscopic methods such as grand canonical Monte-Carlo simulations and density functional theory, specific knowledge about the structure and surface atoms of the investigated material is essential.

DFT techniques include site-wise attraction between surface atoms and the adsorbate molecules and adsorbate-adsorbate attractions, among numerous other factors. The obtained system's free energy is then minimized by primarily changing the number density as a function of distance from the surface. A differentiation has to be made between local and non-

local density functional theory (NLDFT). While local density functional theory assumes a fluid to be structureless when calculating long-range interactions between adsorbate particles, NLDFT is used for strongly interacting boundaries. As the solid walls of mesoporous silica have an influence on the number density, NLDFT is used for calculating the pore size distribution in this work. Nitrogen sorption measurements were performed on a Quantachrome Instruments Nova 4000e at -196°C.

2.5 Dynamic Light Scattering

Hydrodynamic radii of particles in colloidal solutions can be determined by Dynamic Light Scattering (DLS).^{8,9} Thereby, the Brownian motion of the particles is measured and then mathematically correlated to the particle size. In the experiment, the particle solutions are illuminated with a laser. The resulting intensity fluctuations in the scattered light are analyzed. Laser light that was scattered from small particles results in a speckle pattern on the detector, resulting from constructive and destructive interference. As the particles in suspension are constantly moved by Brownian motion, the speckle pattern is also permanently changing on the detector. With the help of a digital correlator in the instrument, changes of the speckle pattern are measured with time. A second-order autocorrelation curve is derived from the measured intensity trace (eq. 2.5.1).

$$g^2(q; \tau) = \frac{\langle I(t)I(t + \tau) \rangle}{\langle I(t)^2 \rangle} \quad (\text{eq. 2.5.1})$$

q: wave detector

τ : delay time

I: intensity

Siegert's equation is used to relate the normalized scattered electric field autocorrelation function to the second order correlation curve. (eq. 2.5.2)

$$g^2(q;\tau) = 1 + \beta [g^1(q;\tau)] \quad (\text{eq. 2.5.2})$$

q: wave detector

τ : delay time

β : correction factor

The obtained first order autocorrelation curve is then fitted by a number of algorithms to give a number of single exponential decays related to the translational diffusion coefficients of different particle size populations in polydisperse samples. Thus, a monodisperse sample gives a single exponential function. (eq. 2.5.3, eq. 2.5.4)

$$g^1(q;\tau) = e^{-\Gamma\tau} \quad (\text{eq. 2.5.3})$$

$$\Gamma = \frac{D}{\frac{4n_0\pi}{\lambda} \sin\left(\frac{\theta}{2}\right)^2} \quad (\text{eq. 2.5.4})$$

D: diffusion coefficient

n_0 : refractive index of the solution

λ : wavelength of laser

θ : angle of scattering experiment

As the above experimental conditions are defined, the diffusion coefficient D of the investigated sample can be calculated. Furthermore, the hydrodynamic diameter of the colloidal sphere is calculated by using Stoke-Einstein's equation (eq. 2.5.5).

$$D = \frac{kT}{3\pi\eta d} \quad (\text{eq. 2.5.5})$$

D: diffusion coefficient

k: Boltzmann constant

T: temperature

η : solvent viscosity

d: hydrodynamic diameter

Most samples display a broad distribution of particle sizes. While the scattering from larger particles needs to be described by Mie theory, the scattering intensity of small particles in a beam of unpolarized light can be described by Rayleigh scattering (eq. 2.5.6).

$$I = I_0 \frac{1 + \cos^2 \theta}{2R^2} \left(\frac{2\pi}{\lambda} \right)^4 \left(\frac{n^2 - 1}{n^2 + 2} \right)^2 \left(\frac{d}{2} \right)^6 \quad (\text{eq. 2.5.6})$$

I: Intensity of the scattered light

I_0 : Intensity of the incoming light

θ : Scattering angle

R: Distance to the particle

λ : Wavelength of the incoming light

n: Refractive index of the particle

d: Particle diameter

The obtained distribution curves are often dominated by a small amount of larger aggregates or particles, as the scattering intensity is proportional to d^6 . In order to gain better information of the synthesized nanoparticle suspensions, it is more likely to give the volume-weighted or number-weighted distributions. They are proportional to d^3 or d , respectively.

The DLS measurements in this work were performed on a Malvern Zetasizer Nano equipped with a 4 mW He-Ne laser (633nm) and an avalanche photodiode detector.

2.6 Zeta Potential

The zeta potential of a particle is the potential that exists on the boundary called hydrodynamic shear or slipping plane. This potential denotes the electrostatic potential at the interfacial layer of a colloid as compared to that of the bulk fluid.¹⁰ When colloids are dispersed in ion containing solutions, the charged surface affects the distribution in the areas near the interface. This leads to the formation of an electric double layer. The inner region of the double layer consists of strongly bound ions and is called Stern layer. The outer region contains diffuse ions, which are less firmly bound to the surface (Figure 2.6.1).

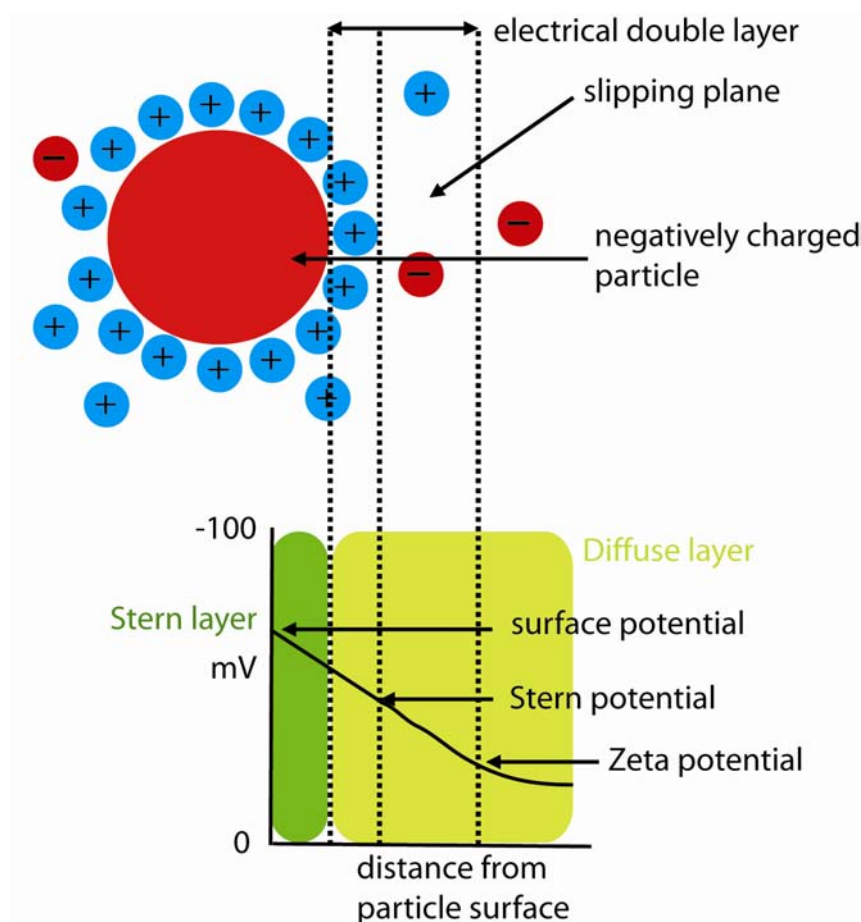


Figure 2.6.1. Scheme of electric double layer around a negatively charged colloid

The zeta potential is determined indirectly by measuring the electrophoretic mobility. Henry's equation describes the relation between the electrophoretic mobility and the zeta potential (eq. 2.6.1).

$$U_E = \frac{2\varepsilon z f(Ka)}{3\eta} \quad (\text{eq. 2.6.1})$$

U_E : Electrophoretic mobility

ε : Dielectric constant

z : Zeta potential

$f(Ka)$: Henry's function

η : Viscosity

To obtain the electrophoretic mobility, the particles' velocity is determined by Laser Doppler Velocimetry (LDV).¹⁰ The LDV applies an electrical field of known strength across the sample, through which a laser is then passed. The electrophoretic mobility determines the velocity with which the particle moves. This will then induce a frequency shift in the incident laser beam. Henry's function is commonly set to $f(Ka)=1.5$, according to Smoluchowski's approximation. This approximation applies, when the electric double layer is very thin compared to the particles diameter. Hückel's approximation uses $f(Ka) = 1.0$ and is used by thick double layers compared to the particles diameter or dispersions in organic media.

2.7 Fluorescence Spectroscopy

Fluorescence spectroscopy is a type of electromagnetic spectroscopy that analyzes the fluorescence of the investigated sample. Fluorescence itself is the process of light emitting deactivation of electronically excited states (Fig. 2.7.1).¹¹

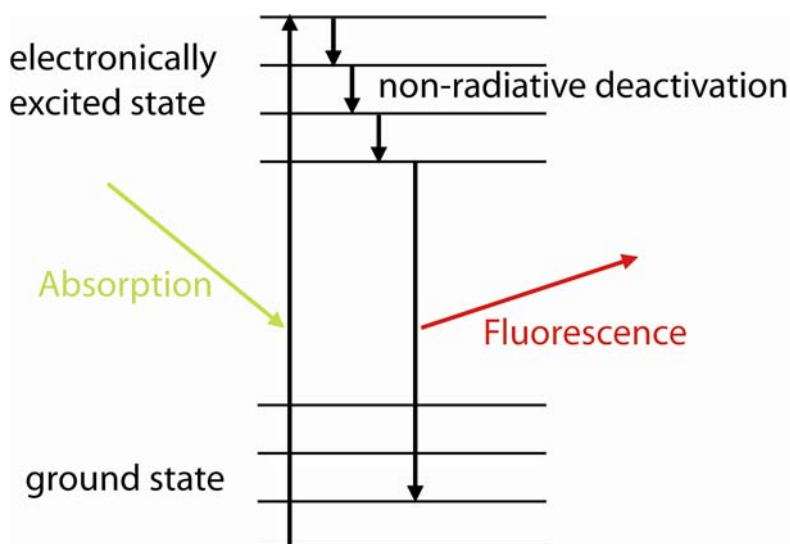


Figure 2.7.1 Mechanism of the fluorescence process

Absorption of incoming light results in a vertical electronic excitation according to Franck-Condon's rule. The excited molecule loses energy upon collisions with its environment until it reaches the vibrational ground state of the excited electronic state. The released energy upon the transition into the electronic ground state results in a photon emission. The energy of the emitted photon is of lower energy compared to the absorbed photon due to the occurred non-radiative deactivation.

In this work, this method is used for the spectroscopic characterization of fluorescence-labeled particles or guest molecules. Most important for very limited amounts of sample, the functionalization can be more easily detected while the sample remains intact.

2.8 Transmission Electron Microscopy (TEM)¹²

Conventional light microscopes are limited to magnifications of 1000 and resolutions down to about 0.2 μm . Max Knoll and Ernst Ruska built the first electron microscope in 1931. A transmission electron microscope (Figure 2.8.1) uses the same basic principles as the light microscope but uses an electron beam instead of light.

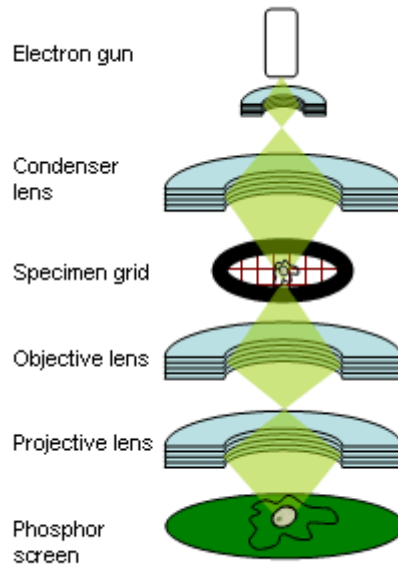


Figure 2.8.1 Scheme of a Transmission Electron Microscope

The used electron beam, generated by a tungsten filament or a field emission gun, is accelerated by a potential difference between about 40 and 1000 keV and then focused by electrostatic and/or electromagnetic lenses. When hitting the specimen, the diameter of the electron beam has typically reached a few nm. Microscopes using a high acceleration voltage offer a higher resolution and a better transillumination of the samples. The electron beam that has transmitted the specimen carries information about the inner structure of the sample. The spatial variation of this information is magnified by a series of electrostatic/electromagnetic lenses and then recorded by a phosphor screen or a CCD camera. The resolution of TEM is usually limited by spherical aberration. However, the new generation of aberration correctors allows resolutions down to the atomic level.

2.9 References

- (1) Toney, M. F. In *Encyclopedia of Materials Characterization - Surfaces, Interfaces, Thin Films* Manning Publications: Greenwich, 1992.
- (2) Cox, J. N. In *Encyclopedia of Materials Characterization - Surfaces, Interfaces, Thin Films*; Manning Publications: Greenwich, 1992.
- (3) White, W. B. In *Encyclopedia of Materials Characterization - Surfaces, Interfaces, Thin Films*; Manning Publications: Greenwich, 1992.

- (4) Condon, J. B. *Surface Area and Porosity Determinations by Physisorption - Measurements and Theory*; Elsevier: Amsterdam 2006.
- (5) F. Rouquerol, J. R., K. Sing *Adsorption by Powders and Porous Solids - Principles, Methodology and Application*; Academic Press: San Diego, 1999.
- (6) Brunauer, S.; Emmett, P. H.; Teller, E. *Journal of the American Chemical Society* **1938**, *60*, 309.
- (7) Kruk, M.; Jaroniec, M.; Sayari, A. *Langmuir* **1997**, *13*, 6267.
- (8) Santos, N. C.; Castanho, M. A. R. B. *Biophysical Journal* **1996**, *71*, 1641.
- (9) El Haskouri, J.; Ortiz de Zarate, D.; Guillem, C.; Beltran-Porter, A.; Caldes, M.; Marcos, M. D.; Beltran-Porter, D.; Latorre, J.; Amoros, P. *Chemistry of Materials* **2002**, *14*, 4502.
- (10) *Malvern Instruments, Zetasizer Nano Series - User Manual*, 2003.
- (11) Atkins, P. W. In *Physikalische Chemie*; Wiley-VCH: Weinheim, 2001.
- (12) Sickafus, K. E. In *Encyclopedia of Materials Characterization- Surfaces, Interfaces, Thin Films*; Manning Publications: Greenwich, 1992.

3. Multiple Core-Shell Functionalized Colloidal Mesoporous Silica

Nanoparticles

The following work based on the publication indicated below:

Valentina Cauda, Axel Schlossbauer, Johann Kecht, Andreas Zürner, and Thomas Bein;

Journal of the American Chemical Society **2009**, *131*, 11361-11370

3.1 Introduction

Although many different approaches for the synthesis of mesoporous silica featuring particle sizes in the nanometer range were proposed,¹⁻⁵ the spatially defined incorporation of functionality is still a critical issue. By controlling the location of two or more different molecular functionalities on the inner and outer surface of the spherical mesoporous particles, it is possible to control many key properties like host-guest interactions and interactions with the environment in a differentiated and defined way. The external surface of such a particle can be, for example, equipped with anchor groups for tumor cell targeting or gatekeepers.⁶⁻⁸ Moreover, the functionalization of the inner pore walls can be used to control the diffusional behavior of bioactive cargo molecules along with providing stability to sensitive guest species.⁹⁻¹¹ Recent examples of site-selective functionalization of silica structures are the generation of Janus particles or sequential grafting procedures before and after template extraction.^{12,13} It was shown that a preferential distribution of functional groups towards the pore openings occurs even in calcined pores.¹⁴ In our group, we have recently found a way to selectively add functionality on the outer surface of the particle. A delayed co-condensation approach allows the control of the distribution of the functionality on the inner or outer surface of radially growing colloidal mesoporous silica (CMS) with a worm-like pore structure.¹⁵ Not only the distribution of functional groups within one particle, but also the density of functional groups can be controlled. The present work includes the synthesis of

3. Multiple Core-Shell Functionalized Colloidal Mesoporous Silica Nanoparticles

CMS exhibiting two different functional groups on the inner and external surface of each particle. A novel sequential co-condensation protocol controlling the incorporation of the silica precursors at different stages of the particle growth was developed. Additionally, we investigated another approach, which uses post-synthetic grafting of previously outer-surface functionalized particles. The different approaches are highlighted in Figure 3.1.1.

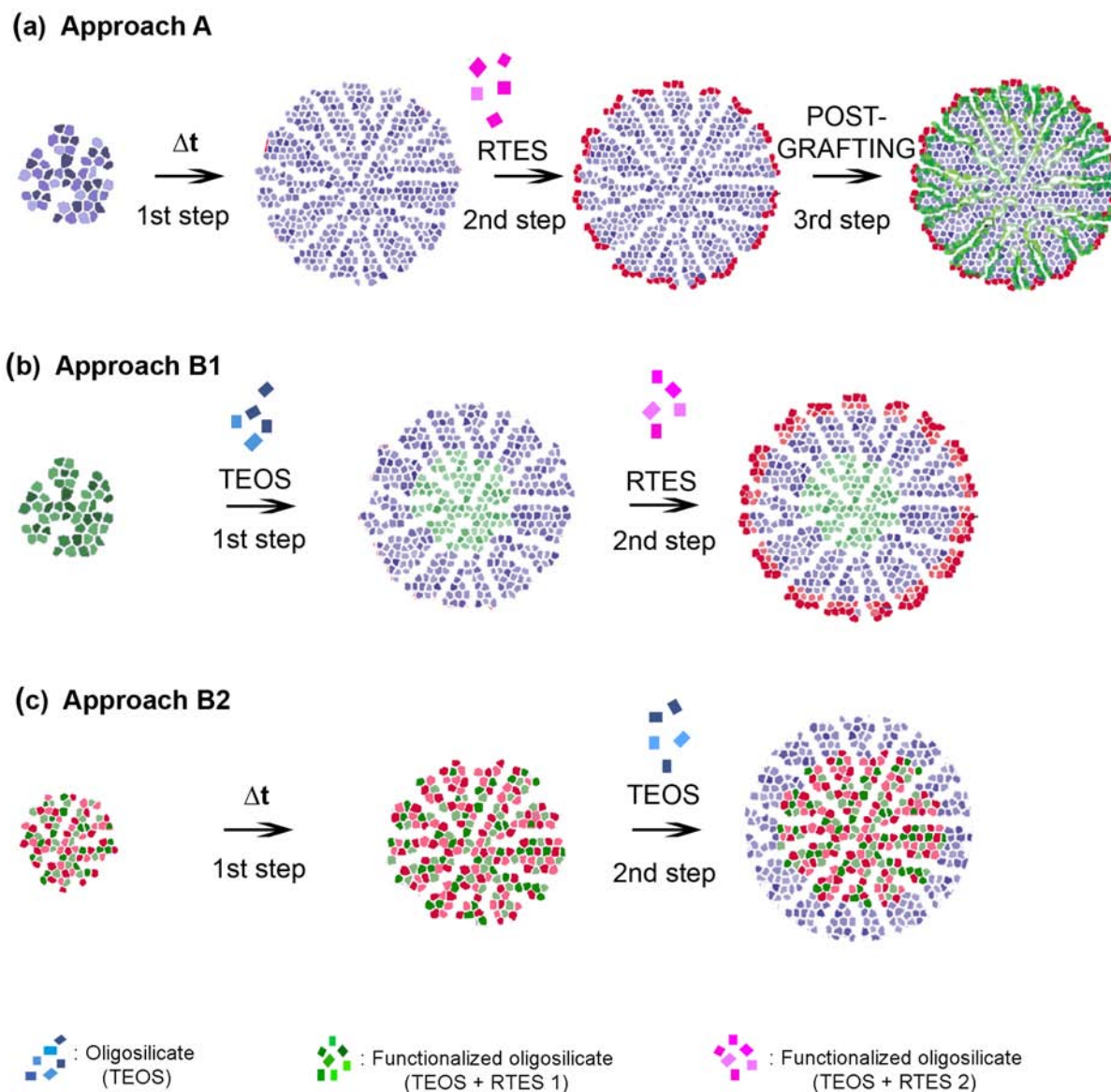


Figure 3.1.1 Synthesis scheme of the two applied approaches. (a) Delayed co-condensation approach, followed by template extraction and grafting of a second functional group. (b) Sequential co-condensation approach with two different and separated functionalizations. (c) Sequential co-condensation approach with two different functionalizations both incorporated in the core of the particle.

The project was a joint project with the group member Dr. Valentina Cauda. The experimental protocols and analytical ideas are the result of the collaboration.

3.2 Experimental Section

3.2.1 Applied Chemicals

Tetraethylorthosilicate (TEOS, Fluka, >98%), triethanolamine (TEA, Aldrich, 98%), cetyltrimethylammonium chloride (CTAC, Fluka, 25 wt% in H₂O), bidistilled water from a Millipore system (H₂O from Milli-Q Academic A10), (3-chloropropyl)trimethoxysilane (CIPTES, Fluka, 98%), (3-aminopropyl)trimethoxysilane (APTES, ABCR, 96%), phenyltriethoxysilane (PTES, Aldrich, 98%), fluorescein isothiocyanate (FITC, Fluka, >90%), tetraoctylammonium bromide (Aldrich, 98%), toluene (Aldrich, 99.8 %), hydrogen tetrachloroaurate (HAuCl₄•3 H₂O, Sigma, 99.99%), dodecanethiol (Fluka, >97%), sodium borohydride (Aldrich, >98%). All chemicals were used as received without further purification.

3.2.2 Synthesis of unfunctionalized CMS (Un-CMS)

Mesoporous silica nanoparticles were prepared according to a previously published procedure.⁵ A mixture of TEOS (1.92 g, 9.22 mmol) and TEA (14.3 g, 95.6 mmol) was heated for 20 minutes at 90°C under static conditions in a 100 mL polypropylene reactor. A solution of CTAC (25 wt% in water, 2.41 mL, 1.83 mmol) and water (21.7 g, 1.21 mol) preheated to 60 °C was added, and the resulting mixture was stirred at room temperature for 12 hours. The resulting molar composition of the mixture was 1 TEOS : 0.20 CTAC : 10.4 TEA : 130.2 H₂O. After addition of 50 mL of ethanol, the mesoporous silica nanoparticles were separated by centrifugation (43.146 rcf, 20 min) and redispersed in ethanol.

3.2.3 Synthesis of CMS by co-condensation and post-grafting (Approach A, samples CMS(A)-Cl_{OUT} and CMS(A)-NH_{OUT})

A mixture of TEA (14.3 g, 95.6 mmol) and TEOS (1.92 g, 9.22 mmol) was heated for exactly 20 min at 90°C without stirring in a 100 mL polypropylene reactor (solution 1). After 20

3. Multiple Core-Shell Functionalized Colloidal Mesoporous Silica Nanoparticles

minutes, a mixture of CTAC (2.41 mL, 7.29 mmol) and H₂O (21.7 g, 1.21 mol), preheated to 60°C was added to solution 1 and stirred for 30 min at 500 rpm. The resulting molar composition of the mixture was 1 TEOS: 0.20 CTAC: 10.4 TEA: 130.2 H₂O. After 30 minutes, a 1:1 mixture of TEOS and functionalized trialkoxysilane (RTES) was added (0.0922 mmol TEOS and 0.0922 mmol RTES). The RTES reagents used here were CIPTES and APTES for samples CMS(A)-Cl_{OUT} and CMS(A)-NH_{OUT}, respectively. After addition of 50 mL ethanol, CMS nanoparticles were separated by centrifugation (43.146 rcf, 20 min), redispersed in ethanol, and extracted according to the procedure described below.

3.2.4 Synthesis of bifunctional CMS by sequential co-condensation (core-shell functionality, Approach B1, sample CMS(B)-Ph_{IN}-NH_{OUT})

A mixture of TEA (14.3 g, 95.6 mmol), TEOS (1.56 g, 7.48 mmol) and PTES (111 mg, 0.46 mmol) was heated for exactly 20 min at 90°C without stirring in a 100 mL polypropylene reactor (solution 1). After 20 minutes, a mixture of CTAC (2.41 mL, 7.29 mmol) and H₂O (21.7 g, 1.21 mol), preheated to 60°C was added to solution 1 and stirred for 20 min at 500 rpm. Then, TEOS (183 mg, 0.922 mmol) was quickly poured into the mixture. The reaction was stirred for another 40 minutes. After that time, a 1:1 mixture of TEOS (19.2 mg, 92.2 μmol) and APTES (20.4 mg, 92.2 μmol) was added. After addition of 50 mL of ethanol, the mesoporous silica nanoparticles were separated by centrifugation (43.146 rcf, 20 min) and redispersed in ethanol.

3.2.5 Synthesis of core-bifunctional CMS by sequential co-condensation (Approach B2, sample CMS(B)-Ph/NH_{IN})

A mixture of TEA (14.3 g, 95.6 mmol), TEOS (1.47 g, 7.37 mmol), PTES (111 mg, 0.46 mmol), and APTES (82.7 mg, 0.46 mmol) was heated for exactly 20 min at 90 °C without stirring in a 100 mL polypropylene reactor (solution 1). After 20 minutes, a mixture of CTAC

3. Multiple Core-Shell Functionalized Colloidal Mesoporous Silica Nanoparticles

(2.41 mL, 7.29 mmol) and H₂O (21.7 g, 1.21 mol), preheated to 60 °C was added to solution 1 and stirred for 20 min at 500 rpm. Next, TEOS (183 mg, 0.0922 mmol) was added to the mixture, divided into 4 equal aliquots (46 mg each), which were added every 3 minutes. The resulting reaction mixture was stirred overnight at room temperature. After addition of 50 mL of ethanol, the mesoporous silica nanoparticles were separated by centrifugation (43.146 rcf, 20 min) and redispersed in ethanol.

3.2.6 Extraction of the template

The extraction of the template from the obtained CMS materials was performed by heating the samples (1 g) under reflux at 90 °C for 45 minutes in a solution containing 2 g ammonium nitrate in 100 mL ethanol, followed by 45 minutes under reflux at 90 °C in a solution of 4 g concentrated hydrochloric acid in 100 mL ethanol. The extracted CMS nanoparticles were collected by centrifugation and washed with 100 mL ethanol after each extraction step. The samples were obtained as clear ethanolic suspensions.

3.2.7 Post-grafting of the samples CMS(A)-Cl_{OUT} and CMS(A)-NH_{OUT}

In order to achieve inner pore wall functionalization, the samples CMS(A)-Cl_{OUT} and CMS(A)-NH_{OUT} were post-grafted with organotrialkoxysilanes. To the extracted samples CMS(A)-Cl_{OUT} and CMS(A)-NH_{OUT} (50 mg in 5 mL of ethanolic suspension), the amount of 0.5 mmol of the respective organotrialkoxysilane (APTES for sample CMS(A)-Cl_{OUT}, CITES for sample CMS(A)-NH_{OUT}) was added. The resulting mixture was stirred for 4 hours under reflux conditions. The functionalized CMS were collected by centrifugation, washed with 10 mL of ethanol and redispersed in 5 mL of ethanol.

3.2.8 Fluorescein isothiocyanate labeling

FITC-labeling was performed on the samples synthesized in 3.2.4 and 3.2.5, following a literature procedure.¹⁶

The amount of 85 mg of CMS dispersed in 10 mL of ethanol was added to a 10 mL solution of FITC in ethanol. The resulting suspension was stirred in the dark for 24 hours at room temperature. The labeled CMS were collected by centrifugation, washed two times with each 20 mL of ethanol and redispersed in 10 mL of ethanol.

3.2.9 Synthesis of dodecanthiolate gold nanoparticles

The gold nanoparticles were synthesized by following a literature procedure.^{17,18} Tetraoctylammonium bromide (0.75 g, 1.25 eq.) was vigorously stirred at room temperature in 40 mL of toluene. Hydrogen tetrachloroaurate (0.15 g, 0.5 eq.) was dissolved in 12.5 mL water and added to the tetraoctylammonium bromide solution and stirred for 30 minutes. The organic phase was separated from the water, and dodecanethiol (0.56 g, 2.79 mmol) was added to the organic phase (AuCl_4^- -solution). The reaction temperature was adjusted to -78°C using a dry ice/acetone bath. Sodium borohydride (0.38 g, 10 eq.) was suspended in 25 mL of absolute ethanol and slowly added over a period of 15 minutes to the stirred AuCl_4^- -solution. Stirring was continued for 1 hour at -78°C followed by 3 hours of room temperature. The solvent was removed in vacuo and the black product was redispersed in 30 mL of ethanol and sonicated in order to remove byproducts. Finally, the dodecanthiolate gold nanoparticles were washed on a glass frit with 80 mL of ethanol and 150 mL of acetone and were then redispersed in 40 mL of toluene.

3.3 Results and discussion

As a first approach to gain bifunctionalized core-shell structured mesoporous silica nanoparticles, our previously published delayed co-condensation approach was used to yield starting materials with molecular functionality exclusively on the outer surface (Approach A).¹⁵ Tetraethylorthosilicate (TEOS) was hydrolyzed in a reaction mixture containing cetyltrimethylammoniumchloride (CTAC) and triethanolamine (TEA). 30 minutes after seed generation, a second set of reactants consisting of a 1:1 mixture of TEOS and CITES/APTES, respectively, was added to the reaction mixture. As a result, colloidal mesoporous silica particles with either chloropropyl- or aminopropyl moieties placed on the outer surface of the particles were obtained after template extraction (samples CMS(A)-Cl_{OUT}, CMS(A)-NH_{OUT}). In order to introduce a second functional group on the inner surface (pore walls), a post-grafting approach was applied. As the outer surface is already carrying organic functionality, a preferential grafting of the inner pore walls is anticipated. The sample CMS(A)-Cl_{OUT} was grafted with APTES, the sample CMS(A)-NH_{OUT} with CITES. The two obtained samples can therefore be considered as complementary (samples CMS(A)-Cl_{OUT}-NH_{IN}, CMS(A)-NH_{OUT}-Cl_{IN}). Nitrogen sorption isotherms were recorded to determine surface area and porosity of the synthesized samples. The isotherms can be found in the Appendix (Figures A-1.1, A-1.2), the BET surface areas and NLDFT pore characteristics are displayed in Table 3.3.1.

Table 3.3.1 Calculations from the nitrogen sorption measurements from samples in Approach A

Sample	NLDFT pore size [nm]	NLDFT pore volume	BET surface area
		[cm ³ g ⁻¹]	[m ² g ⁻¹]
Un-CMS	3.77	0.86	1134
CMS(A)-Cl _{OUT}	3.77	0.80	1184
CMS(A)-Cl _{OUT} -NH _{IN}	3.77	0.80	1077
CMS(A)-NH _{OUT}	3.77	0.75	1050
CMS(A)-NH _{OUT} -Cl _{IN}	3.77	0.55	439

For characterization of the location of the groups, zeta potential measurements were performed. If the post-grafting of functional groups affected only the inner pore walls of the particles, this process should not affect the zeta potential curves. However, a different result was obtained (Figure 3.3.1).

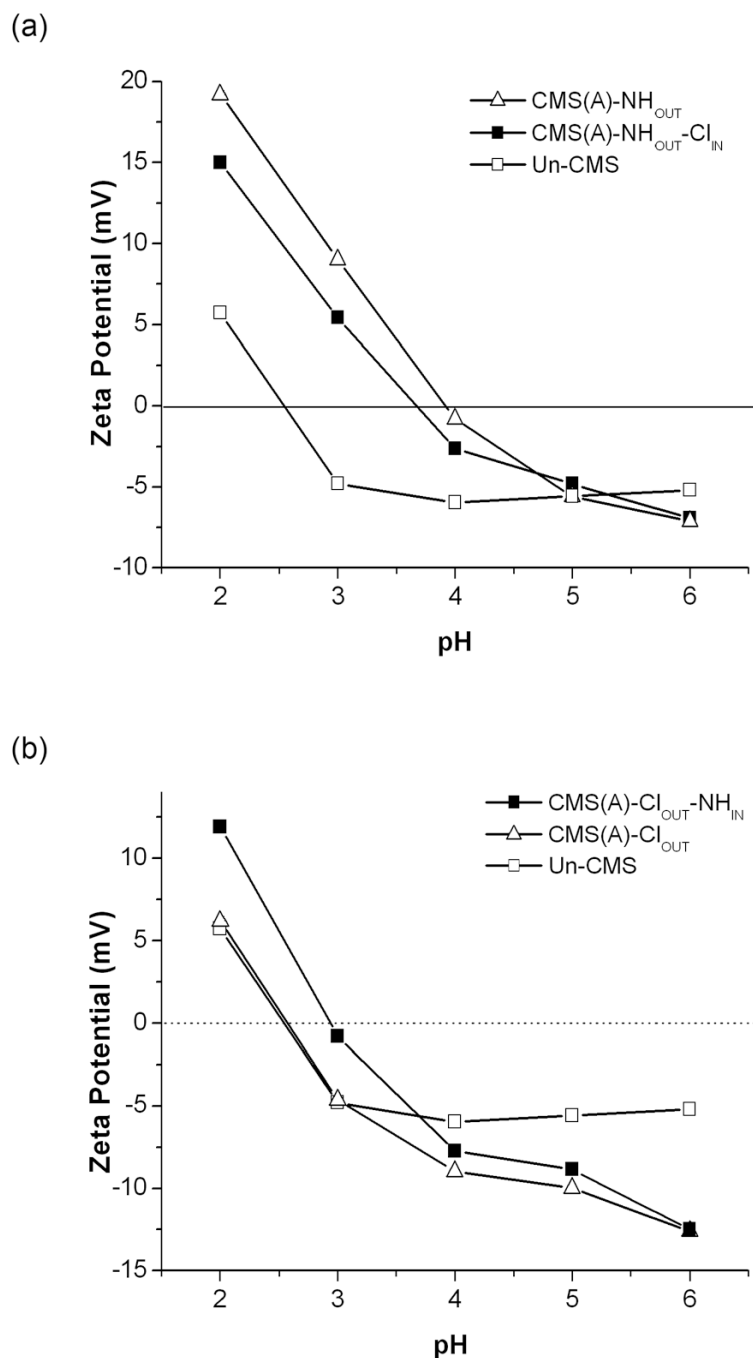


Figure 3.3.1 Zeta potential measurements of the samples produced in approach A in comparison to the unfunctionalized sample Un-CMS. (a) shows a comparison of CMS(A)-NH_{OUT}, CMS(A)-NH_{OUT}-Cl_{IN}, and Un-CMS, (b) shows a comparison of CMS(A)-Cl_{OUT}, CMS(A)-Cl_{OUT}-NH_{IN}, and Un-CMS

In Figure 3.3.1a (triangles), the sample CMS(A)-NH_{OUT} carries a positive surface charge at low pH values, due to the protonation of the amino groups. On the contrary, since the

3. Multiple Core-Shell Functionalized Colloidal Mesoporous Silica Nanoparticles

chloropropyl groups are uncharged at high or low pH values, the zeta potential curve of the sample CMS(A)-Cl_{OUT} (Figure 3.3.1b, triangles), is similar to that of the unfunctionalized CMS. This shows that different functional groups can affect the physical properties of the external surface of the particle. However, post-grafting of the sample CMS(A)-Cl_{OUT} with (3-aminopropyl)triethoxysilane increased the zeta potential, meaning that the outer surface of the particle is still accessible for further functionalization (Figure 3.3.1 b). Additionally, grafting of the sample CMS(A)-NH_{OUT} with CITES leads to a decrease of the zeta potential, confirming the findings described above. The performed zeta potential measurements imply that a complete spatial separation of two functional groups within one particle is not possible by following Approach A. The experiments in this direction were abandoned after these results.

Therefore, another approach was developed, following a sequential co-condensation protocol based on our previously reported findings (Approach B, Figure 3.1.1 b, c).¹⁵ In particular, the two functional groups phenyl- and (3-aminopropyl-) were introduced during the synthesis. In approach B1 (Figure 3.1.1. b) the phenyl-groups were condensed in the core of the particle, spatially separated from the (3-aminopropyl-) functions attached on the outer surface (sample CMS(B)-Ph_{IN}-NH_{OUT}). On the contrary, approach B2 creates mesoporous silica nanoparticles with both functions (Phenyl/3-aminopropyl) in the core, surrounded by a shell of pure mesoporous silica (sample CMS(B)-)Ph/NH_{IN}).

In the synthesis protocol for approach B1, the synthesis was started with a co-condensed core made from two different precursors, TEOS and phenyltriethoxysilane (PTES). 20 minutes after the start of the hydrolysis, a small amount of pure TEOS was added to the reaction, yielding a shell of pure silica around the functionalized core. Another 40 min later, the shell functionality was introduced by adding a 1:1 mixture of APTES and TEOS to the solution. After template extraction, the sample CMS(B)-Ph_{IN}-NH_{OUT} was isolated by centrifugation. The overall molar amount of Si in the synthesis was the same than in our conventional unfunctionalized CMS synthesis.⁵

3. Multiple Core-Shell Functionalized Colloidal Mesoporous Silica Nanoparticles

Approach B2 starts with a co-condensation of three compounds, TEOS, APTES and PTES. 20 minutes after the seed generation, a shell made from hydrolyzed TEOS was grown by adding 4 small aliquots of TEOS to the synthesis in 3-minute steps. After the synthesis, the template was also extracted, giving sample CMS(B)-(Ph/NH)_{IN}.

The morphology of the obtained materials was investigated by transmission electron microscopy. Representative TEM images can be found in Figure 3.3.2.

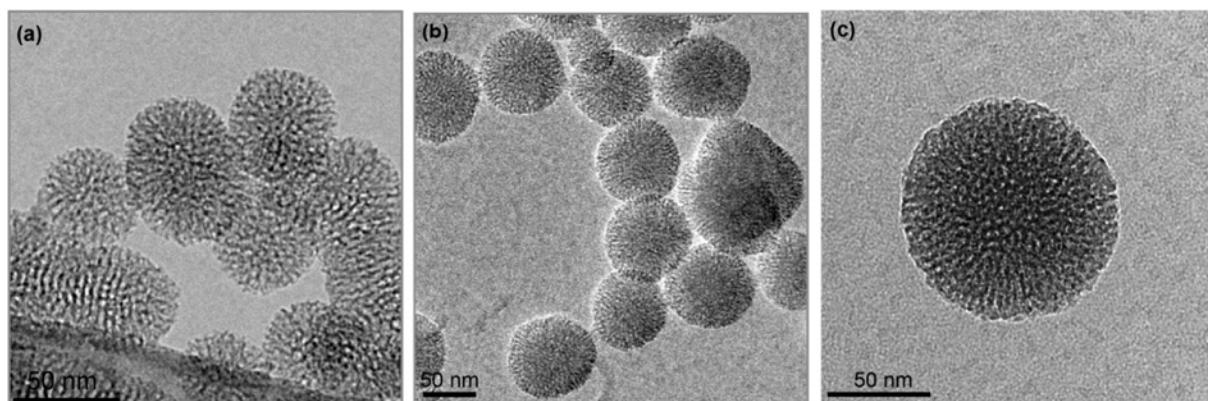


Figure 3.3.2 TEM images of the samples (a) Un-CMS, (b) CMS(B)-Ph_{IN}-NH_{OUT}, and (c) CMS(B)-(Ph/NH)_{IN}

It can be seen that all synthesized materials are composed of nanosized particles (around 80 nm) and that they exhibit mesostructured surfaces with worm-like pores.

The mesoporous structure of all samples was investigated by nitrogen sorption. The structural parameters calculated from the obtained isotherms can be found in Table 3.3.2. The corresponding isotherms and NLDFT pore size distributions can be found in the Appendix (Figure A-1.3).

Table 3.3.2. Data derived from nitrogen sorption for the samples from approach B

Sample	NLDFT pore volume		BET surface area [m ² g ⁻¹]
	NLDFT pore size [nm]	[cm ³ g ⁻¹]	
Un-CMS	3.77	0.86	1314
CMS(B)-Ph _{IN} -NH _{OUT}	3.65	0.77	1302
CMS(B)-(Ph/NH) _{IN}	3.54	0.60	1059

As can be seen, the synthesized samples show the typical pore sizes and high surface areas. A slight reduction of pore volume with increasing core functionality is observed. This can be taken as a first hint for a spatial control over the incorporated functionalization. In order to investigate the surface charge, zeta potential measurements were performed. It is expected that the locus of the amino groups has a strong influence on the zeta potential. An overview over the derived data can be found in Figure 3.3.3.

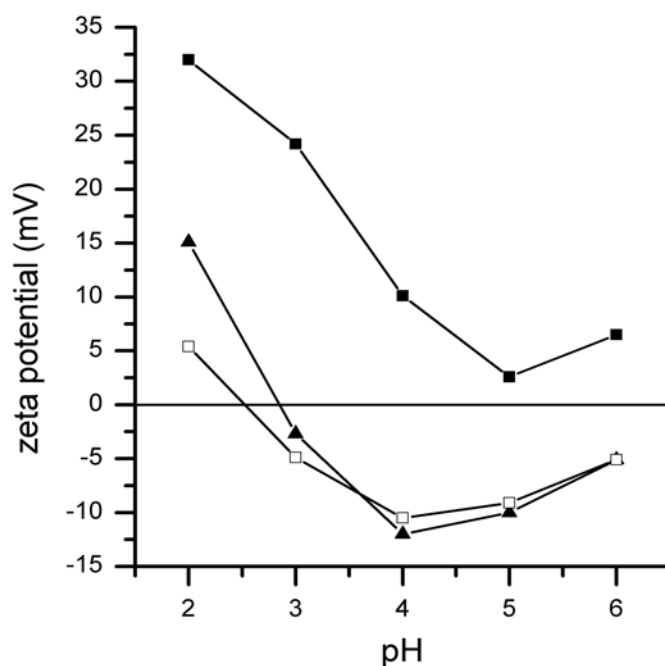


Figure 3.3.3 Zeta potential of the samples derived from approach B: (■) CMS(B)-Ph_{IN}-NH_{OUT}, (▲) CMS(B)-(Ph/NH)_{IN}, (□) Un-CMS.

3. Multiple Core-Shell Functionalized Colloidal Mesoporous Silica Nanoparticles

The highest zeta potential is measured for the sample CMS(B)-Ph_{IN}-NH_{OUT}, indicating that the amino groups are incorporated on the outer shell of the particles and thus are contributing to the high value.

The two very similar curves for the unfunctionalized CMS and the sample CMS(B)-(Ph/NH)_{IN} show that the amino groups are not present on the outer surface of the particles. The material interacts with the external environment like an unfunctionalized particle.

Raman spectroscopy serves to confirm the presence of phenyl groups in the sample. The Raman spectra of the samples CMS(B)-Ph_{IN}-NH_{OUT} and CMS(B)-(Ph/NH)_{IN} can be found in Figure 3.3.4.

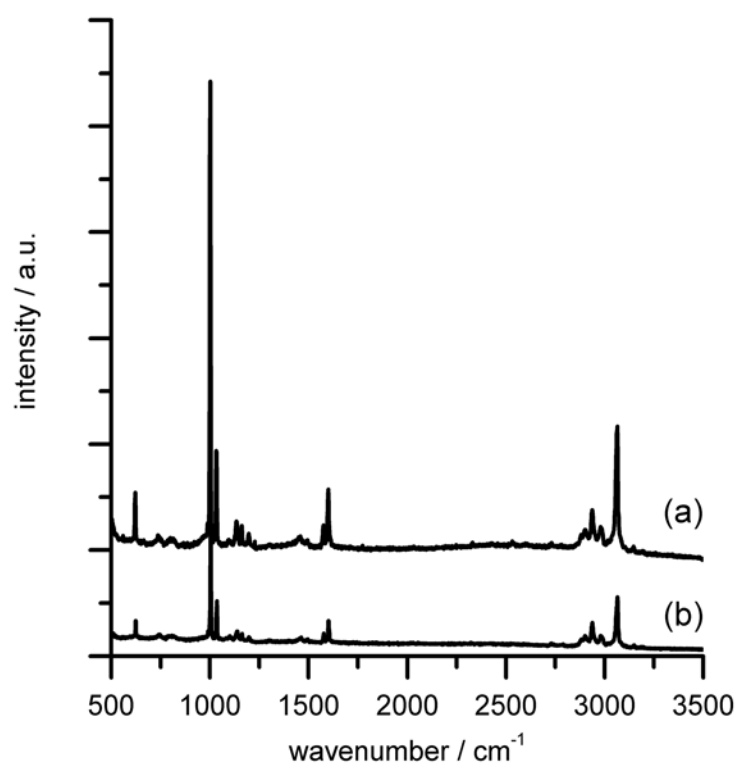


Figure 3.3.4 Raman spectra of the samples (a) CMS(B)-Ph_{IN}-NH_{OUT} and (b) CMS(B)-(Ph/NH)_{IN}.

3. Multiple Core-Shell Functionalized Colloidal Mesoporous Silica Nanoparticles

The strong signal at 1000 cm^{-1} in both spectra corresponds to the C-H in-plane deformation vibration from the aromatic ring. This result is underlined by the signal at 3080 cm^{-1} , also present in both samples, which is caused by the aromatic =C-H stretching vibration.

The following characterization of the synthesized materials with fluorescent methods was performed and analyzed in cooperation by Dr. Valentina Cauda from our group.

Although the above-mentioned zeta potential and nitrogen sorption measurements provide many hints about the loci of the different functional groups, we have developed a procedure based on fluorescence quenching. For this purpose, the amino-groups of the particles were labeled with FITC, forming a thiourea linkage between the dye and the functionalized particle (see Figure 3.3.5).

3. Multiple Core-Shell Functionalized Colloidal Mesoporous Silica Nanoparticles

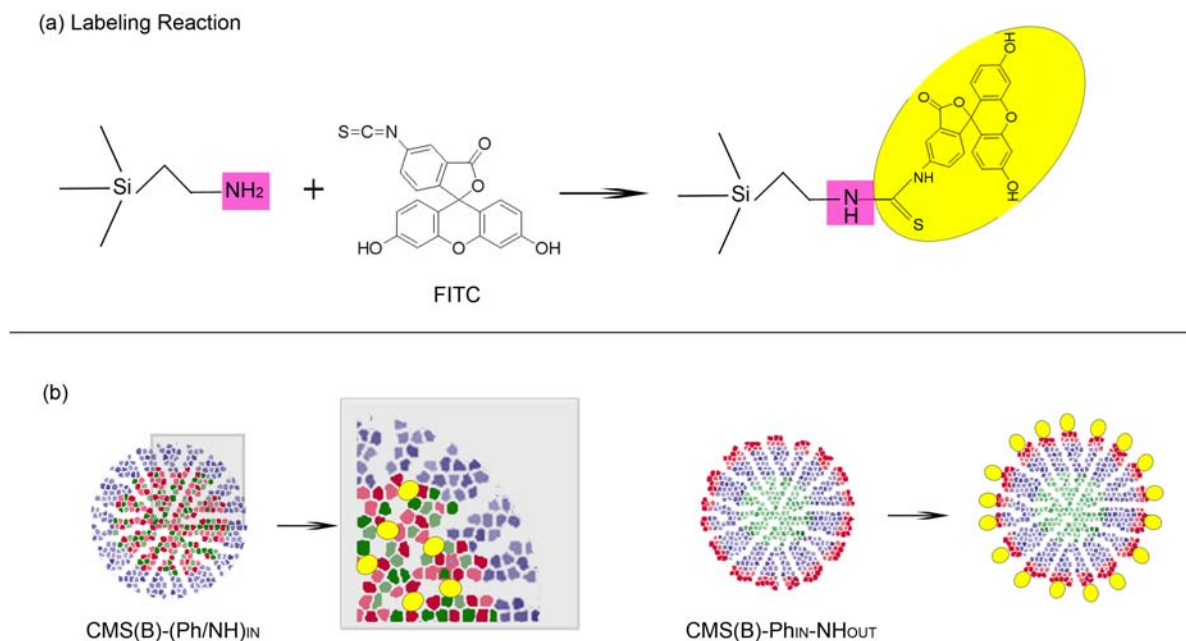


Figure 3.3.5 (a) Reaction scheme between the aminopropyl groups of the CMS nanoparticle and fluorescein isothiocyanate. (b) Expected spatial distribution of the attached fluorescent dyes within the two samples.

As indicated by our synthesis procedures from approach B1 and B2, the sample CMS(B)-Ph_{IN}-NH_{OUT} carries the fluorescent dye on the outer surface whereas the sample CMS(B)-(Ph/NH)_{IN} has the fluorescence dye attached at the inner pore walls.

Gold nanoparticles (AuNP) were synthesized according to a literature procedure, yielding nanoparticles with about 4 nm in diameter.¹⁸ A representative TEM image of the synthesized gold nanoparticles can be found in Figure 3.3.6.

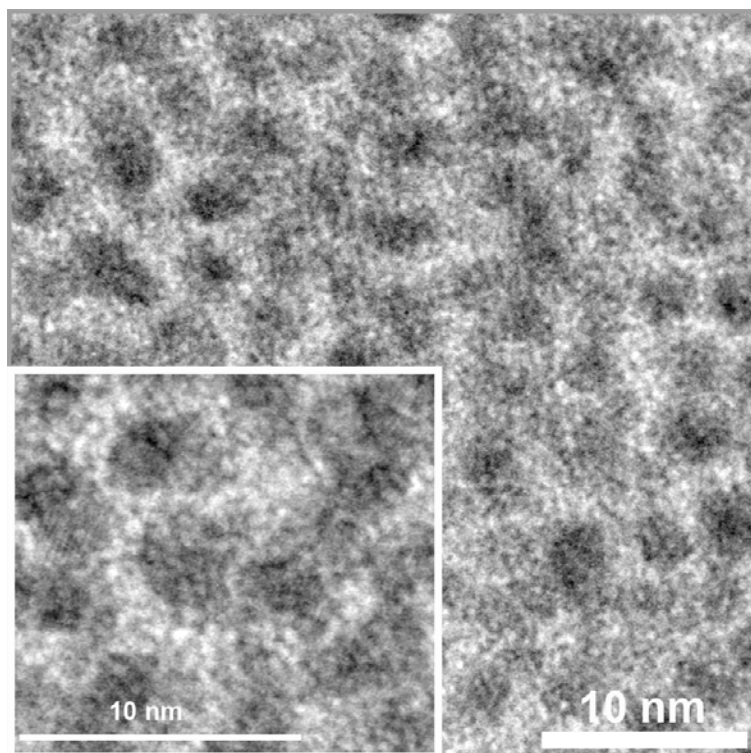


Figure 3.3.6 Transmission electron micrograph of colloidal dodecane thiolate gold nanoparticles used for the fluorescence quenching experiments.

As reported in the literature, gold nanoparticles can be used as efficient quencher of fluorescence, due to an energy transfer between the dye and the AuNP.¹⁹ We have prepared three solutions containing different concentrations of AuNP (SOL1: 5.56 nM; SOL2: 5.56 μ M; SOL3: 5.56 mM) in order to gradually quench the fluorescence emission of the FITC-labeled samples. Figure 3.3.7 shows the changing fluorescence emission intensities related to an increasing AuNP concentration in solution. It should be noted that the emission spectrum of the sample CMS(B)-Ph_{IN}-NH_{OUT} shows an emission band at 550 nm in addition to the expected fluorescein emission at 519 nm. The red-shifted additional emission can be attributed to the formation of so-called J-aggregates. The J-band occurs due a delocalized coherent excitonic state caused by a head-to-tail alignment of transition dipoles of the dye.²⁰ This can be associated with the high local concentration of FITC on the outer surface of the particles in the sample CMS(B)-Ph_{IN}-NH_{OUT}. This arrangement of dyes cannot take place in

3. Multiple Core-Shell Functionalized Colloidal Mesoporous Silica Nanoparticles

the pores due to the confined environment. A gradual reduction of fluorescence intensity upon addition of AuNP to the sample CMS(B)-Ph_{IN}-NH_{OUT} is observed (Figure 3.3.7a).

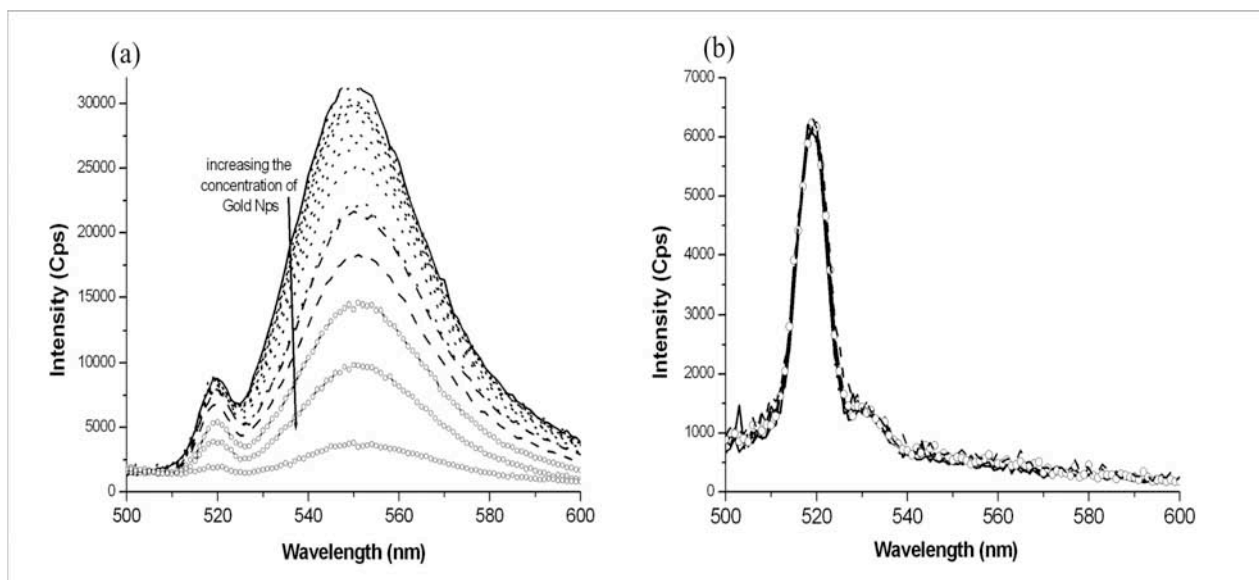


Figure 3.3.7 Fluorescence emission spectra (excitation at 450 nm) for FITC-labeled CMS quenched by gold nanoparticles. The intensities decrease with increasing amount of gold nanoparticles added to the solution. The different lines represent curves obtained from the experiments with the different gold nanoparticle solutions. SOL1: dotted line, SOL2: dashed line, SOL3: empty circles. Sample CMS(B)-Ph_{IN}-NH_{OUT} is shown in (a), sample CMS(B)-(Ph/NH)_{IN} is shown in (b).

The energy of the dye is successfully transferred to the metal surface, where emissionless surface-plasmon excitations and electron hole pair excitations take place. This mechanism is not effective over distances greater than 8 nm.²¹ However, in the sample CMS(B)-(Ph/NH)_{IN}, no influence of the presence of AuNP is observed (Figure 3.3.6b). Due to their size, the AuNP cannot enter the pore system. Therefore, the required short distance between the dye and the AuNP for an effective energy transfer is not given, as the dye molecules are attached in the core of the particle. This experiment clearly shows that we are able to control the spatial distribution of functional groups within one mesoporous silica nanoparticle.

3.4 Conclusion

We have investigated two different approaches toward spatially controlled functionalization of colloidal mesoporous silica. In one case, a delayed co-condensation approach to functionalize the external surface exclusively was followed by a post-grafting of the internal surface. It was demonstrated by zeta potential measurements that a precise separation of two functions in core- and shell regions of a particle was not efficiently achieved. The second method uses a sequential co-condensation approach. An initial co-condensation was mantled with a shell of pure silica. Finally, a shell carrying a different functionality was grown. We have demonstrated by several methods like zeta potential, nitrogen sorption and fluorescence quenching with gold nanoparticles that this approach is a highly effective way to incorporate core-shell functionality into our colloidal mesoporous silica. As will be highlighted in this work, this strategy opens the gate for the design of numerous, multifunctional nanodevices based on our mesoporous silica nanoparticles.

3.5 References

- (1) Lu, Y.; Fan, H.; Stump, A.; Ward, T. L.; Rieker, T.; Brinker, C. J. *Nature (London)* **1999**, *398*, 223.
- (2) Fowler, C. E.; Khushalani, D.; Lebeau, B.; Mann, S. *Advanced Materials (Weinheim, Germany)* **2001**, *13*, 649.
- (3) Suzuki, K.; Ikari, K.; Imai, H. *Journal of the American Chemical Society* **2004**, *126*, 462.
- (4) El Haskouri, J.; Ortiz de Zarate, D.; Guillem, C.; Beltran-Porter, A.; Caldes, M.; Marcos, M. D.; Beltran-Porter, D.; Latorre, J.; Amoros, P. *Chemistry of Materials* **2002**, *14*, 4502.
- (5) Moeller, K.; Kobler, J.; Bein, T. *Advanced Functional Materials* **2007**, *17*, 605.

- (6) Park, C.; Oh, K.; Lee Sang, C.; Kim, C. *Angewandte Chemie (International ed. in English)* **2007**, *46*, 1455.
- (7) Lin, Y.-S.; Tsai, C.-P.; Huang, H.-Y.; Kuo, C.-T.; Hung, Y.; Huang, D.-M.; Chen, Y.-C.; Mou, C.-Y. *Chemistry of Materials* **2005**, *17*, 4570.
- (8) Lai, C.-Y.; Trewyn, B. G.; Jeftinija, D. M.; Jeftinija, K.; Xu, S.; Jeftinija, S.; Lin, V. S. Y. *Journal of the American Chemical Society* **2003**, *125*, 4451.
- (9) Lebold, T.; Muehlstein, L. A.; Blechinger, J.; Riederer, M.; Amenitsch, H.; Koehn, R.; Peneva, K.; Muellen, K.; Michaelis, J.; Braeuchle, C.; Bein, T. *Chemistry--A European Journal* **2009**, *15*, 1661.
- (10) Manzano, M.; Aina, V.; Arean, C. O.; Balas, F.; Cauda, V.; Colilla, M.; Delgado, M. R.; Vallet-Regi, M. *Chemical Engineering Journal (Amsterdam, Netherlands)* **2008**, *137*, 30.
- (11) Rosenholm, J. M.; Linden, M. *Journal of Controlled Release* **2008**, *128*, 157.
- (12) Hong, L.; Jiang, S.; Granick, S. *Langmuir : the ACS journal of surfaces and colloids* **2006**, *22*, 9495.
- (13) De Juan, F.; Ruiz-Hitzky, E. *Advanced Materials (Weinheim, Germany)* **2000**, *12*, 430.
- (14) Lim, M. H.; Stein, A. *Chemistry of Materials* **1999**, *11*, 3285.
- (15) Kecht, J.; Schlossbauer, A.; Bein, T. *Chemistry of Materials* **2008**, *20*, 7207.
- (16) Salmio, H.; Bruehwiler, D. *Journal of Physical Chemistry C* **2007**, *111*, 923.
- (17) Brust, M.; Walker, M.; Bethell, D.; Schiffrin, D. J.; Whyman, R. *Journal of the Chemical Society, Chemical Communications* **1994**, 801.
- (18) Hostetler, M. J.; Wingate, J. E.; Zhong, C.-J.; Harris, J. E.; Vachet, R. W.; Clark, M. R.; Londono, J. D.; Green, S. J.; Stokes, J. J.; Wignall, G. D.; Glish, G. L.; Porter, M. D.; Evans, N. D.; Murray, R. W. *Langmuir : the ACS journal of surfaces and colloids* **1998**, *14*, 17.

3. Multiple Core-Shell Functionalized Colloidal Mesoporous Silica Nanoparticles

- (19) Huang, T.; Murray, R. W. *Langmuir : the ACS journal of surfaces and colloids* **2002**, *18*, 7077.
- (20) Kitahama, Y.; Yago, T.; Furube, A.; Katoh, R. *Chemical Physics Letters* **2008**, *457*, 427.
- (21) Whitmore, P. M.; Robota, H. J.; Harris, C. B. *Journal of Chemical Physics* **1982**, *77*, 1560.

4. Click-Chemistry for High-Density Biofunctionalization of Mesoporous Silica

The following work is based on the publication indicated below.

Axel Schlossbauer, David Schaffert, Johann Kecht, Ernst Wagner, and Thomas Bein; *Journal of the American Chemical Society* **2008**, *130*, 12558-12559

4.1 Introduction

In order to design effective, multifunctional silica nanoparticles, the investigation of mild, biocompatible and high-yield reactions for the purpose of surface functionalization are of essential interest.¹⁻⁴ In this context, surface-based click chemistry is attracting increasing attention.⁵⁻⁷ The mild reaction conditions of the copper-(I)-catalyzed azide-alkyne cycloaddition and its very high yield make this reaction suitable for the functionalization of surfaces with sensitive biomolecules.^{3,7} Recent publications have used the click approach to immobilize peptides,⁷ DNA⁸ or carbohydrates⁹ for various applications. One possibility to demonstrate the potential of the click approach as biocompatible reaction on mesoporous silica surfaces is the immobilization of sensitive enzymes in the pores of mesoporous silica by using this reaction. Supported enzymes on mesoporous solids have many possible applications in biotechnology, including synthesis and purification of fine chemicals, catalysis for green chemistry or sensing.^{10,11} It has been shown that the stability and recoverability of enzymes benefit from encapsulation in mesoporous hosts.¹² In earlier work, lysozyme was adsorbed into the pores of SBA-15.¹³ However, the non-covalent interactions between mesoporous silica materials and proteins are too weak to prevent the adsorbed biomolecules from leaching out of the pore system during further washing and reaction steps, thus leading to relatively low loading levels.^{14,15} Organic modification of the pore walls of a mesoporous

host or glutaraldehyde-based cross-linking can sometimes prevent the absorbed enzymes from leaching out of the pore system.^{12,16} However, these methods are typically limited to certain proteins and carry the risk of deactivating the enzyme.

First attempts at covalent enzyme immobilization in mesoporous silica have claimed the binding of penicillin-G-acylase onto glycidopropyl-functionalized mesoporous silica, although no proof of covalent attachment was provided.¹⁷ Another approach encapsulates enzymes by a layer-by-layer assembly of oppositely charged species around mesoporous silica spheres loaded with enzymes. It was shown that the activity can be conserved during various recovery cycles, but the loading level was poor and leaching tests were not performed.¹⁸ In the present work, the stable covalent immobilization of the protease trypsin in the channel system of a large-pore SBA-15 host by a click-chemistry approach is presented (Figure 4.1.1).

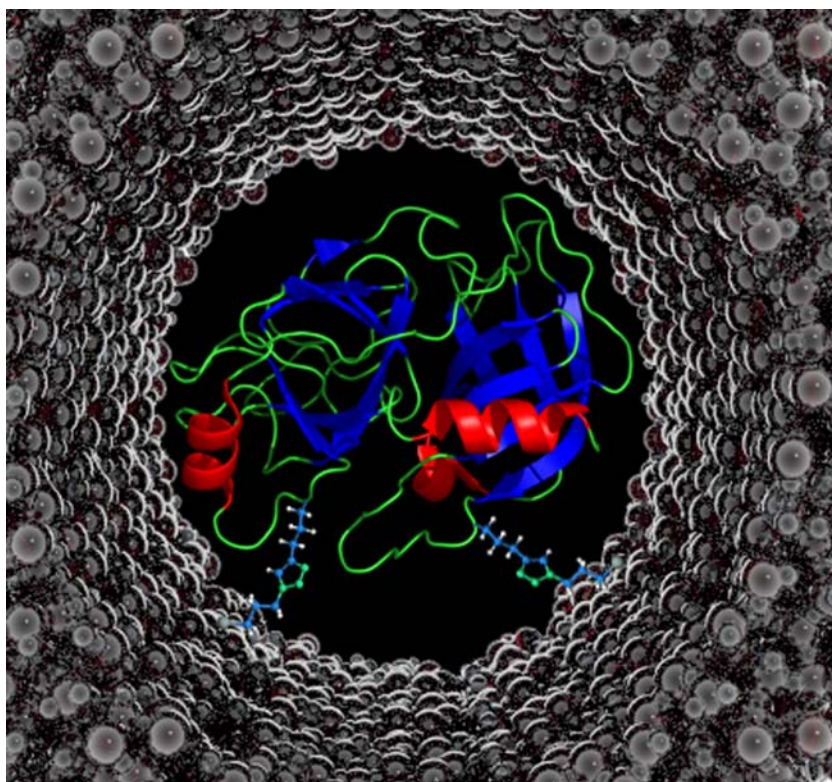


Figure 4.1.1 Illustration of immobilized trypsin in a pore of SBA-15 mesoporous silica

This versatile and mild method for the covalent immobilization of functional biomolecules on mesoporous supports allows for unprecedented functionalization densities while retaining enzyme activity and preventing protein leaching from the mesoporous support. This work was carried out in cooperation with David Schaffert from the research group of Prof. Ernst Wagner, Department of Pharmacy at the University of Munich (LMU).

4.2 Experimental Section

4.2.1 Applied Chemicals

Tetraethyl orthosilicate (TEOS, Fluka, >98%), cetyltrimethylammonium bromide (CTAB, Aldrich, 95%), (3-chloropropyl)trimethoxysilane (CTMS, Fluka, 95 %), Mesitylene (Aldrich, 98%), sodium azide (Fluka, 99 %), 4-pentynoic acid (Fluka, 97%), N-(3-dimethylaminopropyl)-N-ethylcarbodiimide (EDC, Fluka, 97%), trypsin from bovine pancreas (Sigma, lyophilized, essentially salt-free, TPCK treated), N_α-p-tosyl-L-arginine methyl ester hydrochloride (Sigma), phosphate buffer solution (Sigma), tris(hydroxymethyl) aminomethane (TRIS, Sigma, 99.8 %), 2-(N-morpholino)ethanesulfonic acid (MES, Sigma, 99.5 %). All chemicals were used as received without any further purification.

4.2.2 Preparation of large pore SBA-15 spherical particles

Large pore SBA-15 was synthesized according to literature.¹⁹ Pluronic 123 (3 g) was dissolved in 1.5 M HCl (60 mL). CTAB (0.6 g) and mesitylene (1.5 g) were first mixed with 25 mL of distilled water separately, before the two solutions were combined and stirred thoroughly as Ethanol (20 mL absolute) was added. The resulting solution is referred to as the surfactant solution. To the surfactant solution, the amount of 10 mL TEOS was added dropwise. The resulting mixture was vigorously stirred (500 rpm) at 35°C for 45 min before being transferred to a Parr autoclave and being heated to 75°C for 12 hours at static conditions. Subsequently, the mixture is aged at 125°C for another 12 h. The resulting white

powder was filtered off, was washed with 100 mL of water and 100 mL of ethanol and dried at 60°C overnight. Removal of the template was obtained through calcination at 550°C for 5 hours (heating rate 1°C/min).

4.2.3 Preparation of 3-chloropropyl-functionalized large pore SBA-15 (SBA-Cl)

Freshly calcined SBA-15 (200 mg) was dried at 110°C under vacuum conditions for 90 minutes. Afterwards, dry toluene was added under nitrogen atmosphere. After addition of 3-chloropropyltrimethoxysilane (1.5 mmol, 276 µl), the reaction mixture was allowed to stir for 4 hours under reflux conditions. The now functionalized SBA-15 (SBA-Cl) was filtered off and washed with each 50 mL of toluene, methanol and water before being dried at 60°C overnight.

4.2.4 Preparation of azide-functionalized SBA-15 (SBA-N₃)

The amount of 100 mg SBA-Cl was added to 5 mL of a saturated solution of sodium azide in DMF. The resulting mixture was stirred at 90°C for 3 hours. The material was then filtered off and was stirred in PBS buffer solution (for preparation, see 3.2.10) for another 3 hours to remove remaining DMF from the pore walls. After being filtered off again, the material was washed with 50 mL of water and 50 mL of ethanol before being dried at 60°C overnight.

4.2.5 Acetylene functionalization of trypsin

The amount of 10 mL of a solution containing trypsin (1mg/ml) in MES buffer (for preparation, see 3.2.12) was prepared. Subsequently, the amount of 500 µl of an aqueous stock solution containing 4-pentynoic acid (0.1 M) was added to the solution. The resulting mixture was vortexed for 2 minutes and then stored at 4°C for 15 minutes. The amount of 5 mg EDC powder was added subsequently. The resulting mixture was vortexed for 2 minutes. The reaction mixture was stored at 4°C for 4 hours, after which the sample was dialyzed in a

cold room at 6°C against sodium phosphate buffer (10 mM, pH 7.2) for a period of 24 hours. The resulting acetylene-functionalized trypsin was used for the click reaction without further purification.

4.2.6 Preparation of trypsin-functionalized large pore SBA-15 (SBA-trypsin)

To a solution containing 7 mg of acetylene-functionalized trypsin, the amount of 50 mg SBA-N₃ was added. To a freshly prepared aqueous solution of CuSO₄·5 H₂O (1 mM, 5 mL), 1 mg of ascorbic acid was added and stirred at room temperature for 10 minutes. Then, 10 µl of the solution is added to the reaction mixture. The resulting mixture was allowed to stir at 4°C for 14 hours. Subsequently, the suspension was centrifuged and washed two times with PBS buffer solution (50 mM, pH 7.1).

4.2.7 Preparation of 3-chloropropyl-functionalized Cab-o-Sil aerogel (Cab-o-Sil-Cl)

500 mg of Cab-o-Sil (Grade EH-2) were dried at 100°C under vacuum conditions for 4 hours. Afterwards, the amount of 15 mL toluene was added. After addition of 3-chloropropyltrimethoxysilane (1.9 mmol, 345 µl), the reaction mixture was allowed to stir for 4 hours under reflux conditions. The functionalized Cab-o-Sil (Cab-o-Sil-Cl) was washed with 50 mL of toluene, methanol and water by multiple centrifugation and redispersion cycles before being dried at 60°C for 12 hours.

4.2.8 Preparation of azide-functionalized Cab-o-Sil aerogel (Cab-o-Sil-N₃)

The amount of 100 mg Cab-o-Sil -Cl was added to 5 mL of a saturated solution of sodium azide in DMF. The resulting mixture was stirred at 90°C for 3 hours. The material was filtered off and stirred in PBS buffer solution for 3 hours in order to remove remaining DMF from the mesopores. The material was washed with 50 mL of each water and ethanol by centrifugation before being dried at 60°C for 12 hours.

4.2.9 Preparation of trypsin-functionalized Cab-o-Sil aerogel (Cab-o-Sil-trypsin)

To a solution containing 7 mg of acetylene-functionalized trypsin (7 mL) in PBS buffer (pH 7.4), the amount of 50 mg Cab-o-Sil-N₃ was added. The amount of 1 mg ascorbic acid was added to a freshly prepared aqueous solution of CuSO₄·5 H₂O (1 mM, 5 mL) and the resulting mixture stirred at room temperature for 10 minutes. Subsequently, 12.5 µl of the copper-containing solution were added to the reaction mixture. The resulting mixture was allowed to stir at 4°C for 24 hours. The trypsin-functionalized Cab-o-Sil was recovered by centrifugation and washed five times with 20 mL PBS buffer solution (50 mM, pH 7.1).

4.2.10 Preparation of the applied PBS buffer

The amounts of 8 g sodium chloride (NaCl), 0.2 g potassium chloride (KCl), 1.44 g disodiumhydrogen phosphate (Na₂HPO₄), and 0.24 g potassiumdihydrogen phosphate (KH₂PO₄) were dissolved in 800 mL water. The pH was adjusted to 7.4 mL using 1 M hydrochloric acid (HCl). Then, water was added to 1 L of volume.

4.2.11 Preparation of the applied TRIS buffer

The amount of 5.57 g Tris(hydroxymethyl)-aminomethane (TRIS, C₄H₁₁NO₃) and 0.169 g calcium chloride-dihydrate (CaCl₂ · 2 H₂O) was dissolved in 60 mL of water. The pH was adjusted to 8.1 using 1 M hydrochloric acid (HCl). Water was added to 100 mL of volume.

4.2.12 Preparation of the applied MES buffer

The amount of 1.95 g 2-(N-morpholino)ethanesulfonic acid (MES, C₆H₁₃NO₄S) was dissolved in 500 mL water. The pH was adjusted to 5.5 using 1 M hydrochloric acid (HCl). Then, water was added to 1 L of volume.

4.2.13 BCA Assay for protein quantification

For the quantification of trypsin in solution, a Pierce BCA (bicinchoninic acid) Protein Assay was used. A trypsin stock solution was prepared containing 2 mg/mL trypsin in PBS buffer solution. For a calibration curve, the following samples featuring different trypsin concentrations were prepared according to Table 4.2.1.

Table 4.2.1 Prepared solutions for a trypsin calibration curve

concentration [$\mu\text{g/mL}$]	0	5	10	15	20	25
$\mu\text{L PBS}$	100	97.5	95	92.5	90	87.5
$\mu\text{L trypsin stock}$	0	2.5	5	7.5	10	12.5

5 μL of the investigated sample were diluted in 95 μL PBS buffer ($2 < c_{\text{max}} < 0.1 \text{ mg/mL}$). BCA-Kit solution B and A were mixed 1:50. 500 μL of the resulting BCA assay mixture was added to every sample. The samples were incubated at 60°C for 30 minutes in a thermocycler. 150 μL of every sample were transferred into a well plate, absorption was measured at 590 nm using a TECAN well plate reader.

By using the linear equation of the calibration curve, the concentration of each investigated sample can be determined. The obtained calibration curve can be found in Figure 4.2.1.

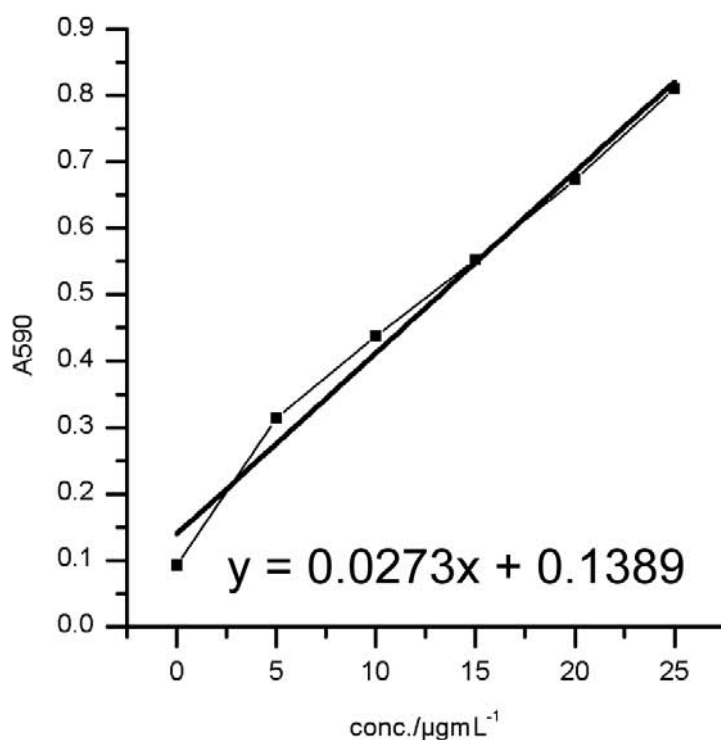


Figure 4.2.1. Trypsin calibration curve for protein quantification.

4.2.14 Trypsin activity determination

The activity of trypsin, acetylene-modified trypsin (sp-trypsin), and silica supported trypsin (SBA-trypsin) was quantified by the release of N_{α} -p-tosyl-L-arginine from the substrate N_{α} -p-tosyl-L-arginine methyl ester hydrochloride (TAME) according to a procedure developed by Hummel.²⁰ The reaction is monitored photometrically by measuring the increase of extinction at 247 nm.

In the following, one unit is defined as the amount of enzyme releasing 1 μmol N_{α} -p-tosyl-L-arginine per minute under the denoted conditions.

A TAME stock solution is prepared containing 189 mg TAME in 50 mL water. The enzyme is dissolved in 0.001 n HCl with an enzyme concentration of 5.5 $\mu\text{g/mL}$.

For the activity determination, a 1.5 mL cuvette with 75 μL TAME solution, 200 μL enzyme solution (1.1 μg enzyme), and 1225 μL Tris buffer was prepared. For the sample SBA-trypsin,

4. Click-Chemistry for High-Density Biofunctionalization of Mesoporous Silica

the amount of 55 μg sample containing 6.6 μg of enzyme (data from TGA and BCA assay) was dispersed in a mixture of 75 μl TAME solution, 100 μl 0.001 n HCl, and 1325 μl Tris buffer.

For the sample Cab-o-Sil-trypsin, 14 μg solid sample containing 2 μg of enzyme (data from TGA and BCA assay) was dispersed in the mixture described for SBA-trypsin. The extinction at 247 nm was acquired at intervals of one minute. Between each acquisition, the SBA-containing suspension was homogenized by shaking. The enzyme activity was determined from the slope of the obtained linear curve (eq. 4.2.1).

$$\frac{E_{247}}{0.54 \cdot E_w} \cdot 1.5 \quad \text{eq. 4.2.1}$$

E_{247} : Increase in extinction at 247 nm

0.54: Extinction of 1 μmol N_α -p-tosyl-L-arginine

E_w : Initial weight of enzyme in mg per 0.1 mL solution

1.5: Total volume of sample in mL

The curve measured for trypsin can be found in Figure 4.2.2. The resulting slope of the linear regression is 0.0091 min^{-1} .

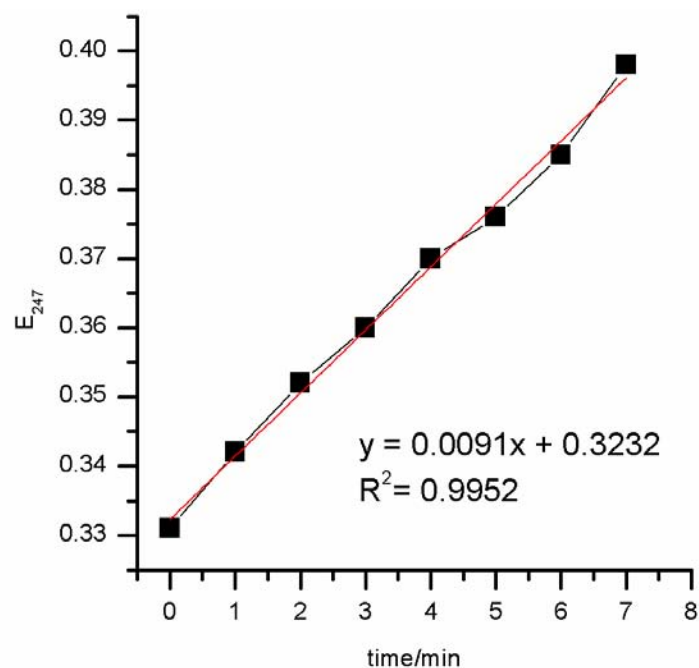


Figure 4.2.2 Activity determination curve for native trypsin.

By using equation 1, an activity of 346.3 units was found for native trypsin. The curve measured for sp-trypsin is shown in Figure 4.2.3. The resulting slope of the linear regression is 0.0088 min^{-1} . This corresponds to 334.9 units for sp-trypsin.

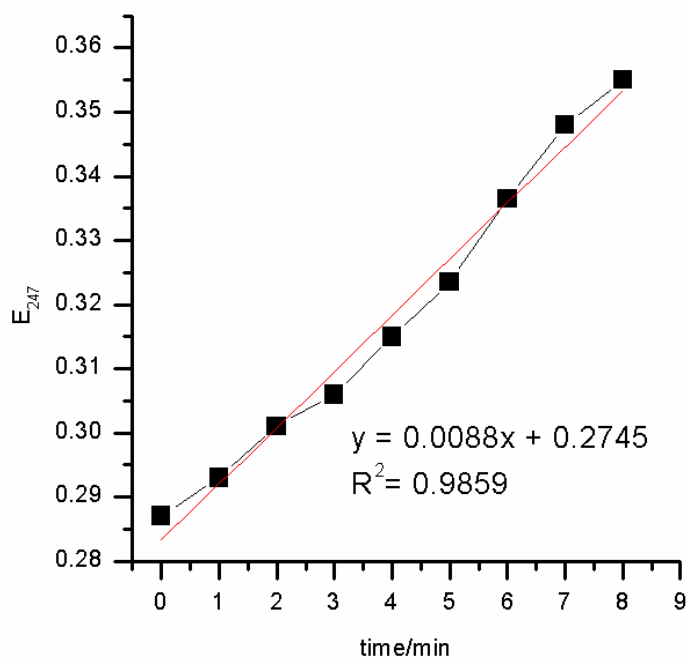


Figure 4.2.3. Activity determination curve for sp-trypsin.

The curve measured for SBA-trypsin is shown in Figure 4.2.4.

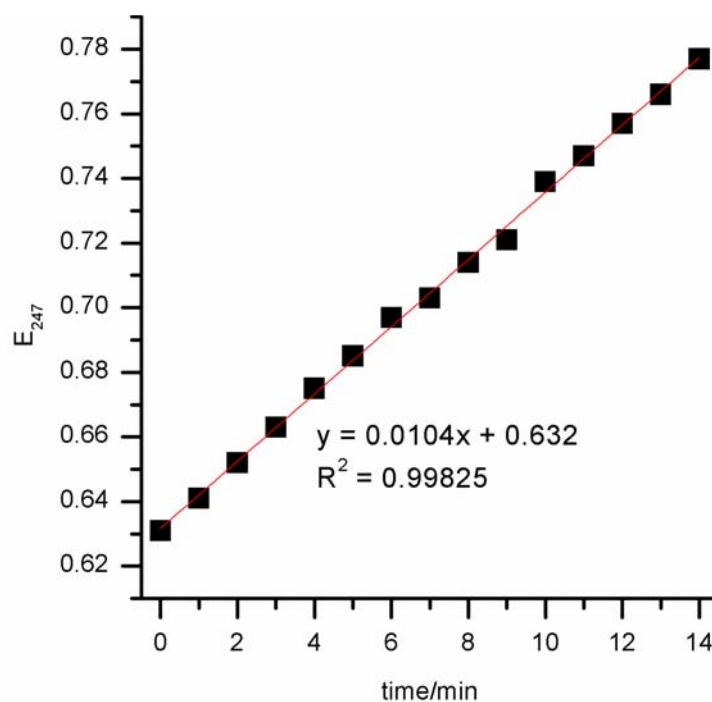


Figure 4.2.4. Activity determination curve of SBA-trypsin.

The slope of 0.0104 in Figure 4.2.4 and a loading of 123 mg enzyme per 1 g SBA-15 (TGA and BCA quantification) correspond to an enzyme activity of 65.6 units per mg enzyme.

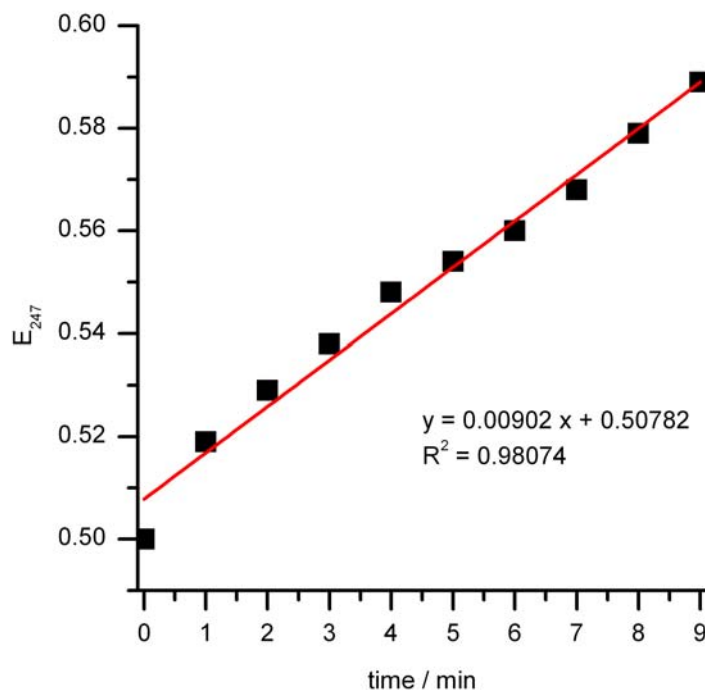


Figure 4.2.5. Activity determination curve of Cab-o-Sil-trypsin.

With the slope of 0.00902 in Figure 4.2.5 and the determined enzyme loading of 141 mg enzyme per 1 g of Cab-o-Sil, the remaining enzymatic activity can be calculated to 84 u/mg.

4.2.15 Procedure for the applied leaching test

The sample SBA-trypsin was re-suspended in Tris-buffer solution for 4 hours. The supernatant and the powder were then separated by centrifugation. Then, the absorption at 279 nm of the protein in the supernatant was measured. A previously acquired calibration curve (Figure 4.2.6) was used to quantify the amount of enzyme leached out of the pores.

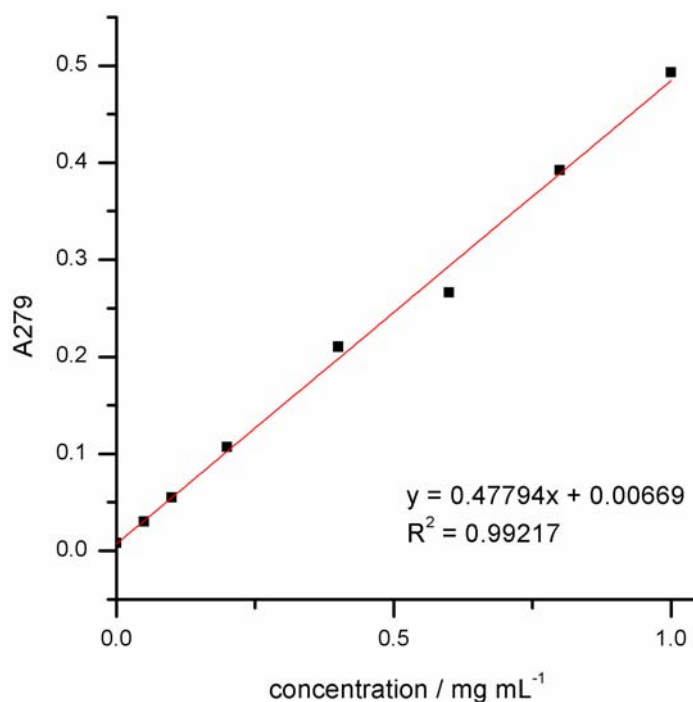


Figure 4.2.6. Calibration curve for the determination of trypsin concentrations in the performed leaching experiment.

4.3 Results and Discussion

Large-pore SBA-15 was synthesized according to previously published procedures.¹⁹ Tetraethyl orthosilicate (TEOS) was hydrolyzed in a reaction mixture containing Pluronic 123 as template, cetyltrimethylammonium bromide (CTAB) as co-template, mesitylene as swelling agent, potassium chloride, and hydrochloric acid. Removal of the template was achieved by calcination at 550 °C for 5 hours (heating rate 1 °C/min). Mesoporous silica spheres featuring diameters of 6 μm with a surface area of 700 m^2g^{-1} and pore sizes of around 9 nm were obtained. A choice of SEM images of the synthesized material can be found in Figure 4.3.1.

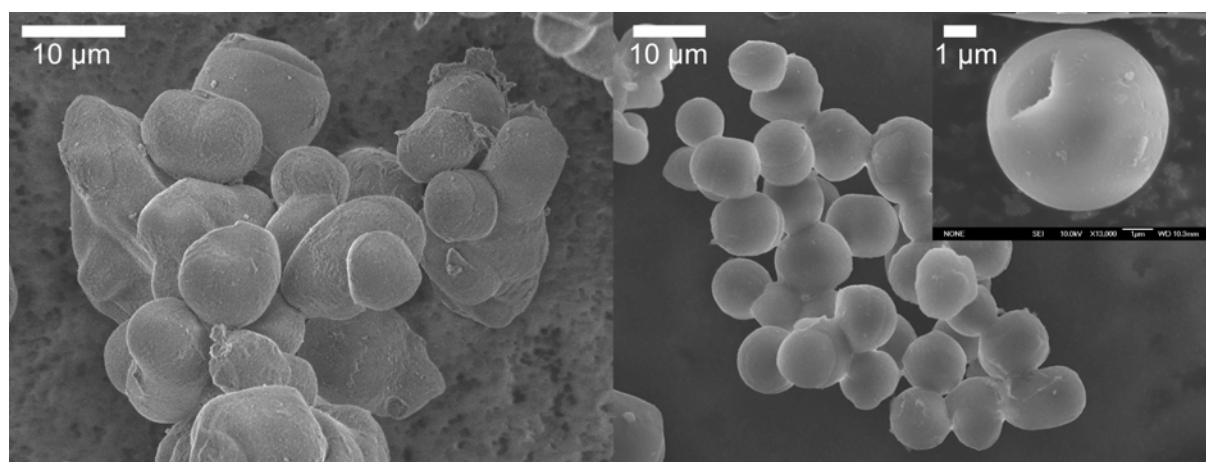


Figure 4.3.1. SEM-Pictures of the obtained SBA-15 microspheres.

The silica surface was functionalized with (3-chloropropyl)-trimethoxysilane (sample SBA-Cl) using a post-synthetic grafting approach. The mesostructure of the resulting materials was demonstrated by small-angle X-ray diffraction (Figure 4.3.2)

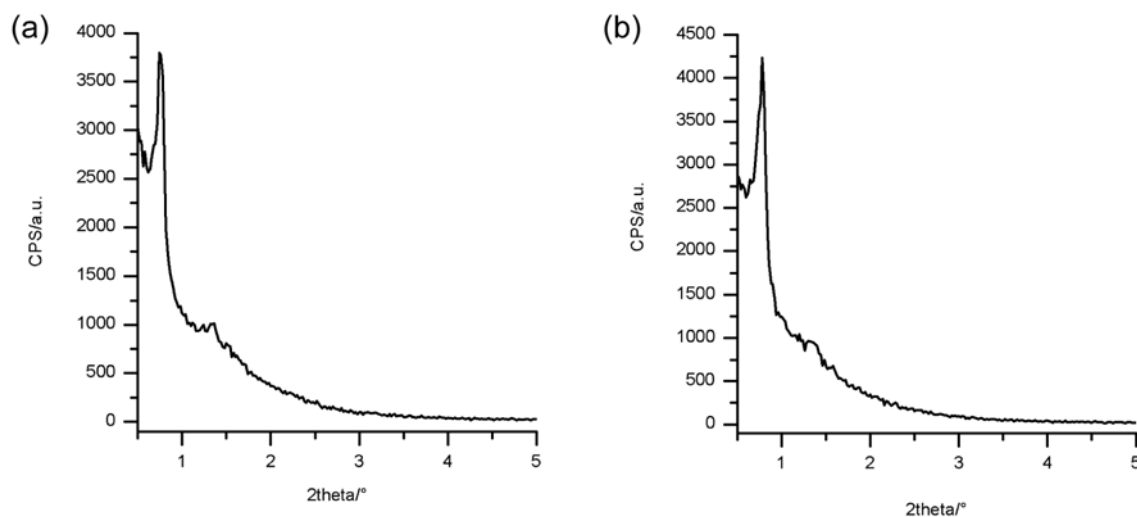


Figure 4.3.2 XRD-patterns of the sample (a) SBA-15 and (b) SBA-Cl.

By a substitution reaction with sodium azide (NaN_3) in *N,N*-dimethylformamide (DMF), an azide-functionalized mesoporous silica surface was created (SBA- N_3). Acetylene-modified trypsin (sp-trypsin) was synthesized according to previously reported procedures, using 4-

4. Click-Chemistry for High-Density Biofunctionalization of Mesoporous Silica

pentynoic acid as reagent and *N*-(3-dimethylaminopropyl)-*N*-ethylcarbodiimide (EDC) as activating agent.²¹

Subsequently, SBA-N₃ was reacted with sp-trypsin in a copper(I)-catalyzed Huisgen reaction (Click reaction) at 4 °C in aqueous medium followed by vigorous washing steps, resulting in trypsin-functionalized mesoporous silica (SBA-trypsin, Figure 4.3.3).

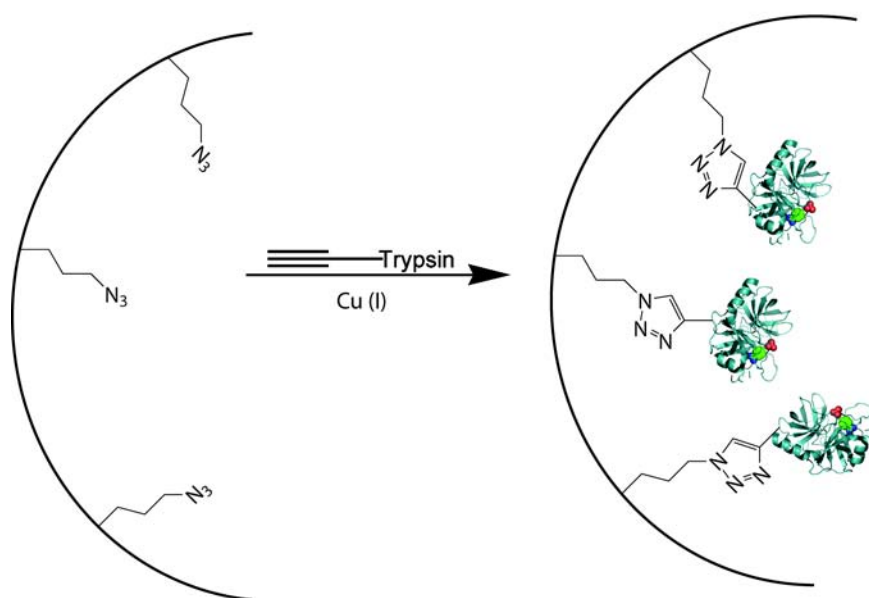


Figure 4.3.3 Covalent attachment of trypsin into the mesoporous system of large-pore SBA-15 achieved by Click chemistry (schematic).

The result of the click reaction and the presence of trypsin in the sample were monitored by IR spectroscopy (Figure 4.3.4). The almost complete loss of intensity of the azide stretch signal (2105 cm^{-1} , Figure 4.3.4 a, b) indicates the covalent attachment of trypsin to the surface. The emerging strong absorption bands located at 1667 cm^{-1} and 1531 cm^{-1} are assigned to the amide bonds of the attached protein (Figure 4.3.4 b, c).

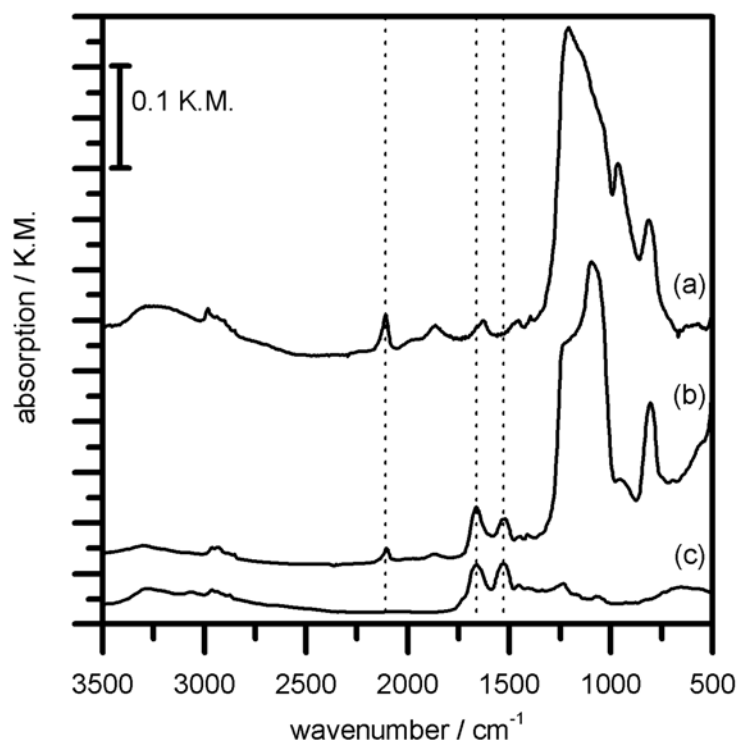


Figure 4.3.4. IR spectra of the samples (a) SBA-N₃, (b) SBA-trypsin, and (c) trypsin.

Nitrogen sorption measurements of samples SBA-15, SBA-Cl and SBA-trypsin confirm the presence of the large trypsin molecules attached to the pore walls (Figure 4.3.5, Table 4.3.1).

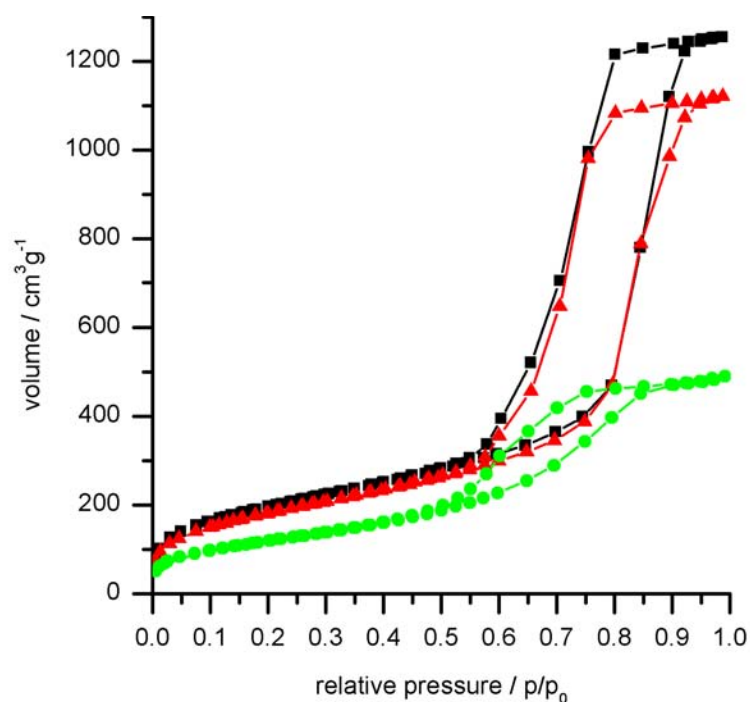


Figure 4.3.5 Nitrogen sorption isotherms of the sample (black) SBA-15, (red) SBA-Cl, and (green) SBA-trypsin.

Table 4.3.1 Nitrogen sorption data of the synthesized samples

sample name	BET surface [m ² g ⁻¹]	pore size [nm]	pore volume [cm ³ g ⁻¹]
SBA-15	701	8.91	1.89
SBA-Cl	651	8.40	1.69
SBA-trypsin	430	6.95	0.73

The considerable decrease in surface area, NLDFT pore volume, and pore diameter in sample SBA-trypsin clearly indicates functionalization with the enzyme on the inner surface. The functionalization density was determined by thermogravimetric analysis (TGA, Figure 4.3.6) and confirmed by a bicinchoninic acid assay (BCA-assay).

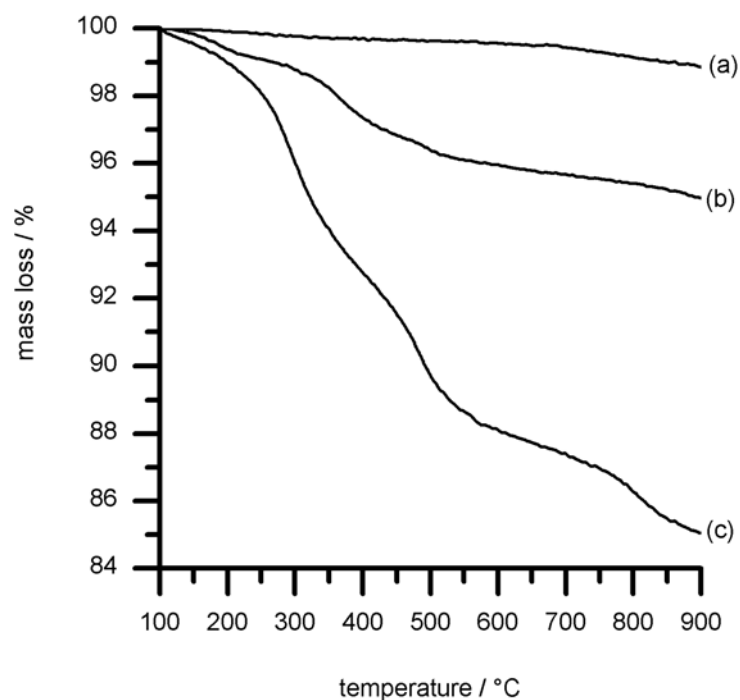


Figure 4.3.6 TGA curves for the samples (a) SBA-15, (b) SBA-Cl, and (c) SBA-trypsin.

While the unfunctionalized SBA-15 only shows a minor mass loss of less than 1 % (Figure 4.3.6 a), the mass loss of 5.0 % in sample SBA-Cl corresponds to 0.68 mmol g^{-1} of chloropropyl residues bound to the silica surface (Figure 4.3.6 b). Based on the mass loss of 15% in the sample SBA-trypsin (Figure 4.3.6 c), the amount of bound enzyme can be calculated to be 12 wt%. Detailed calculations of the obtained values from TGA can be found in the Appendix (A-2).

The results from TGA were confirmed by BCA-assay quantification of the remaining protein in the supernatant of the synthesis solution (see section 4.2.13 for experimental procedure, appendix A-3 for detailed calculation of the results).

Based on these results, the protein activity of the surface-bound enzyme in SBA-trypsin was determined. In order to prove the retention of the enzymatic activity, the assay developed by Hummel was applied.²⁰ The performance of trypsin, acteylene-modified trypsin (sp-trypsin), and silica-supported trypsin (SBA-trypsin) was photometrically quantified by the release of $N\alpha$ -p-tosyl-L-arginine methyl ester hydrochloride (TAME). In the following, one unit is

defined as the amount of enzymatic activity releasing 1 μmol of $\text{N}\alpha$ -p-tosyl-L-arginine per minute. The curves obtained from the assay can be found in the experimental section (4.3.14). Both sp-trypsin and SBA-trypsin remain biologically active. The activity found for trypsin was 346 units/mg, while sp-trypsin showed an activity of 334 units/mg. The high activity of SBA-supported trypsin was calculated to be 7.9 units/mg (host+enzyme), corresponding to 65.6 units/mg (enzyme), or retention of 20% of enzyme activity relative to aqueous solution. As a reference, nonporous silica aerogel was functionalized the same way, resulting in an enzymatic activity of 80 units/mg (enzyme) or 10.8 units/mg (host+enzyme). In comparison, the reported activity of chymotrypsin is reduced to 1.7 % upon cross-linking with glutaraldehyde in SBA-15.^{16,22} The results show that porous SBA-15 causes no substantial diffusion limitations compared to nonporous silica. The remaining pore diameter of 7 nm still allows efficient substrate transport to the reactive site of the enzyme molecules. The stabilizing role of SBA-15 is demonstrated by the exceptional conservation of activity during multiple recovery cycles (Figure 4.3.7).

Both enzyme-carrying materials SBA-trypsin and Cab-o-Sil-trypsin were compared in terms of reusability. After one catalytic cycle, both materials were centrifuged off (43500 rcf) and stored at 4 °C for 2 h. Then, the hosts were resuspended and the enzyme activity experiments were repeated. As can be seen in Figure 4.3.7, SBA-trypsin recovers 72 % of its initial catalytic activity after 4 recovering cycles. In contrast, Cab-o-Sil-trypsin recovers only 6 percent of its initial activity. This can be explained by the possibility of autodegradation in the case of Cab-o-Sil-trypsin, as the enzymes attached to the surface of non-porous silica nanoparticles are still able to degrade each other.

This experiment clearly demonstrates the beneficial role of SBA-15 in our approach.

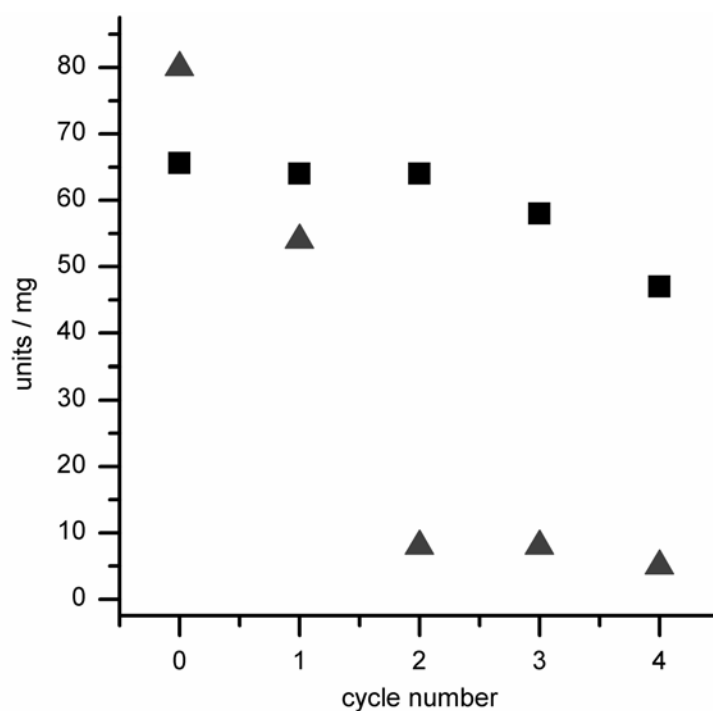


Figure 4.3.7 Reusability of the samples (■) SBA-trypsin and (▲) Cab-o-Sil-trypsin.

Leaching experiments were performed in order to show the stability of the covalent enzyme attachment. The amount of 1.1 mg SBA-trypsin was allowed to stir in 2 mL Tris buffer solution for 4 h. Then, the solid support was separated from the solution by centrifugation (5000 rpm for 10 min). Subsequently, the absorption of the supernatant solution was determined by UV-vis spectroscopy at 279 nm. The absorption value of 0.00673 implies that trypsin leaching has not occurred. This result was confirmed by BCA assay using 150 μ l of the supernatant of the leaching experiment described above. As a complementary approach, the catalytic activity of the supernatant was determined as described in 4.3.13. The obtained curve is shown in Figure 4.3.8. The resulting slope of zero implies that the measured solution does not contain any measurable amount of trypsin.

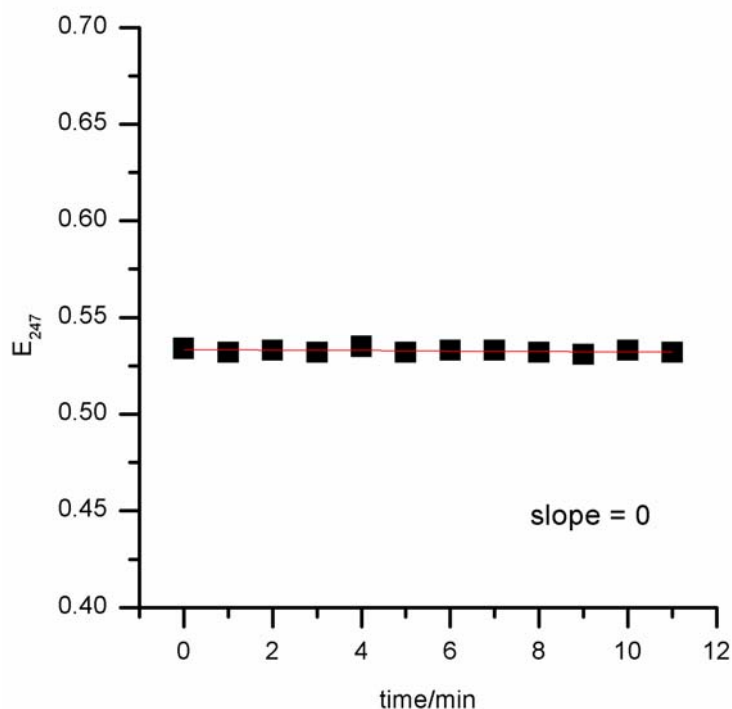


Figure 4.3.8 Obtained catalytic curve of the supernatant of the performed leaching experiment.

These data clearly prove that leaching does not occur under the experimental conditions.

4.4 Conclusion

In summary, we present a novel approach for the covalent modification of mesoporous silica with intact enzymes. The high covalent functionalization density under simultaneous retention of enzyme activity and the absence of leaching demonstrates the promising potential of this approach. This approach was chosen to demonstrate the applicability of the click reaction on mesoporous silica. Especially, the mild reaction conditions allow the immobilization of sensitive biomolecules. The findings are important not only in the field of applied biocatalysis, but also for the design for silica-based nanodevices for bio-related applications like drug delivery or biomolecule-based molecular machines.

4.5 References

- (1) Lummerstorfer, T.; Hoffmann, H. *Journal of Physical Chemistry B* **2004**, *108*, 3963.
- (2) Kacprzak, K. M.; Maier, N. M.; Lindner, W. *Tetrahedron Letters* **2006**, *47*, 8721.
- (3) Gallant, N. D.; Lavery, K. A.; Amis, E. J.; Becker, M. L. *Advanced Materials* **2007**, *19*, 965.
- (4) Prakash, S.; Long, T. M.; Selby, J. C.; Moore, J. S.; Shannon, M. A. *Analytical Chemistry* **2007**, *79*, 1661.
- (5) Mader, H. S.; Link, M.; Achatz, D. E.; Uhlmann, K.; Li, X.; Wolfbeis, O. S. *Chemistry-A European Journal* **2010**, *16*, 5416.
- (6) Armani, A. M.; Alabi, A. C.; Davis, M. E.; Flagan, R. C.; Fraser, S. E.; *US Patent No. 2009-214755*, **2009**, 39.
- (7) Govindaraju, T.; Jonkheijm, P.; Gogolin, L.; Schroeder, H.; Becker, C. F. W.; Niemeyer, C. M.; Waldmann, H. *Chemical Communications* **2008**, 3723.
- (8) Schlossbauer, A.; Warncke, S.; Gramlich, P. M. E.; Kecht, J.; Manetto, A.; Carell, T.; Bein, T. *Angewandte Chemie, International Edition* **2010**, *49*, 4734.
- (9) Huang, L.; Dolai, S.; Raja, K.; Kruk, M. *Langmuir* **2010**, *26*, 2688.
- (10) Yiu, H. H. P.; Wright, P. A. *Journal of Materials Chemistry* **2005**, *15*, 3690.
- (11) Won, Y.-H.; Aboagye, D.; Jang, H. S.; Jitianu, A.; Stanciu, L. A. *Journal of Materials Chemistry* **2010**, *20*, 5030.
- (12) Yiu, H. H. P.; Wright, P. A.; Botting, N. P. *Journal of Molecular Catalysis B: Enzymatic* **2001**, *15*, 81.
- (13) Vinu, A.; Murugesan, V.; Hartmann, M. *Journal of Physical Chemistry B* **2004**, *108*, 7323.
- (14) Hartono, S. B.; Qiao, S. Z.; Liu, J.; Jack, K.; Ladewig, B. P.; Hao, Z.; Lu, G. Q. M. *Journal of Physical Chemistry C* **2010**, *114*, 8353.

- (15) Hartmann, M. *Chemistry of Materials* **2005**, *17*, 4577.
- (16) Kim, M. I.; Kim, J.; Lee, J.; Shin, S.; Na, H. B.; Hyeon, T.; Park, H. G.; Chang, H. N. *Microporous and Mesoporous Materials* **2008**, *111*, 18.
- (17) Lu, Y.; Lu, G.; Wang, Y.; Guo, Y.; Guo, Y.; Zhang, Z.; Wang, Y.; Liu, X. *Advanced Functional Materials* **2007**, *17*, 2160.
- (18) Wang, Y.; Caruso, F. *Chemistry of Materials* **2005**, *17*, 953.
- (19) Katiyar, A.; Yadav, S.; Smirniotis, P. G.; Pinto, N. G. *Journal of Chromatography, A* **2006**, *1122*, 13.
- (20) Hummel, B. C. *Canadian Journal of Biochemical Physiology* **1959**, *37*, 1393.
- (21) Gole, A.; Murphy, C. J. *Langmuir* **2008**, *24*, 266.
- (22) Kim, J. D., R.; Dordick, J. S. *Biotechnological Progress* **2002**, *18*, 551.

5. Biotin-Avidin as Protease-Responsive Cap-System for Controlled Guest Release from Colloidal Mesoporous Silica

The following work is based on the publication indicated below:

Axel Schlossbauer, Johann Kecht, and Thomas Bein; *Angewandte Chemie, International Edition* 2009, 48, 3092-3095

5.1 Introduction

Recently, cap systems for colloidal mesoporous silica (CMS) acting as stimuli-responsive release mechanisms have been developed.^{1,2} Among other possible applications, the controlled release of molecules such as peptides or antibacterial agents has attracted growing attention in the design of smart detergents.^{3,4} CdS nanoparticles, polymers or large molecules, i.e., cyclodextrins and rotaxanes have been used as cap-systems to keep compounds from leaching out of porous hosts and to permit their controlled release.^{5,6} Opening stimuli include changes in pH value or temperature, as well as light-irradiation, esterase activity and redox reactions, depending on the system.^{5,7} However, many of the existing cap-systems still present challenges in terms of their biocompatibility or the toxicity of the capping agents used. One possible solution could be the direct use of native biomolecules, such as proteins, to block the pores of CMS reversibly. It is anticipated that such species would enable high biocompatibility and tailored interactions between the CMS and the locus of activity. Opening of the pore system is possible by removal of the capping system; that is, by the direct cleavage of a link or, as demonstrated in this study, through a decrease of protein-bonding interactions by proteolytic hydrolysis. Until now, the biotin-avidin system has mainly been used in biorecognition,⁸ biosensing,⁹ or biomedical applications.^{10,11} Here we describe the use of the well-studied biotin-avidin complex for a biomolecule-based, enzyme-responsive cap-system for CMS nanoparticles, and demonstrate the operability of this system by controlled release of

fluorescein molecules. Thus, it is possible to design a sophisticated biocompatible cap-system with protease-responsive properties by direct application of an existing biological system. The presence of proteases in modern detergents offers the possibility of a protease-responsive opening mechanism in order to release sensitive substances that benefit from protective encapsulation.¹²

Recently, we developed a strategy for integrating molecular functionality exclusively into the outer surface shell of CMS in precisely controlled amounts while leaving the inner pore system unfunctionalized.¹³ Here we use this method to design mesoporous nanospheres with protein coupling sites located exclusively on the outer particle surface. This approach enables the attachment of large proteins without uncontrolled pore clogging inside the mesoporous hosts, and the whole pore volume is available for cargo molecules. For reference experiments, unfunctionalized CMS was synthesized according to our previously published procedures.¹⁴

5.2 Experimental Section

5.2.1 Applied chemicals

Tetraethylorthosilicate (TEOS, Fluka, >99%), (3-mercaptopropyl)-triethoxysilane (MPTS, Gelest, 95%), cetyltrimethylammonium bromide (CTAC, Fluka, 25% in H₂O), triethanolamine (TEA, Aldrich, 98%), avidin from egg white (Sigma, lyophilized powder), trypsin from bovine pancreas (Sigma, lyophilized powder), fluorescein sodium salt (Fluka, standart for fluorescence), Saline-sodium citrate buffer, pH=7.0 (SSC-buffer, Sigma). All chemicals were used as received without further purification. Doubly distilled water from a Millipore system (Milli-Q Academic A10) was used for all synthesis and purification steps.

5.2.2 Preparation of colloidal mesoporous silica nanoparticles (CMS)

Mesoporous silica nanoparticles were prepared according to literature from reaction mixtures with a molar composition of 1 TEOS: 0.20 CTAC: 10.37 TEA: 130.15 H₂O.¹⁴ The combined TEOS (1.92 g, 9.22 mmol) and TEA (14.3 g, 95.6 mmol) were heated for 20 minutes at 90 °C without stirring in a 100 mL polypropylene reactor. A solution of CTAC (25 % in water, 2.41 mL, 1.83 mmol) and water (21.7 g, 1.21 mol) preheated to 60 °C was added, and the resulting mixture was stirred at room temperature for 12 hours. After addition of 100 mL ethanol, the mesoporous silica nanoparticles were separated by centrifugation, redispersed in ethanol and extracted according to the procedure described below.

5.2.3 General procedure for the selective functionalization of CMS with 3-mercaptopropyl moieties by co-condensation (CMS-SH)

The reactants were mixed following the previously published synthesis procedure for CMS.¹³ However, a second set of reactants was added at 30 minutes after combination of the initial TEOS/TEA and CTAC solutions. The reactants were added to the stirred reaction mixture with an Eppendorf micropipette and consist of TEOS and (3-mercaptopropyl)-triethoxysilane (MPTES) in the molar ratio 1 : 1. The combined amount of both silanes was 185 μmol, i.e. 2 % of the total amount of “Si” in the initial CMS synthesis. The resulting mixture was stirred at room temperature for 12 hours followed by purification and extraction as described for CMS.

5.2.4 Extraction of CMS

Extraction of the organic template from the CMS materials was performed by heating the colloidal suspensions containing 250 mg of CMS for 45 minutes under reflux at 90 °C in a solution containing 2 g ammonium nitrate in 100 mL ethanol, followed by 45 minutes under reflux in a solution of 4 g concentrated hydrochloric acid in 100 mL ethanol. The CMS

materials were separated by centrifugation and washed with ethanol after each extraction step. CMS materials were obtained as clear ethanolic suspensions.

5.2.5 Biotin-functionalized colloidal mesoporous silica nanoparticles (CMS-BIO)

20 mg CMS-SH was transferred into a 50 mL flask and redispersed in 20 mL SSC-buffer (pH = 7, 0.15 M sodium chloride, 15 mM trisodium citrate)). Subsequently, 1.1 mg (2.4 μ mol) of avidin from egg white was added to the reaction mixture. The resulting suspension was stirred for 12 hours at room temperature. The resulting colloidal suspension was washed by centrifugation and then redispersed in 20 mL of SSC-buffer.

5.2.6 Fluorescein-loaded CMS and CMS-BIO

The amount of 10 mg CMS-BIO or CMS was transferred to 20 mL of a 1 M fluorescein disodium salt solution in a saline-sodium citrate-buffer (pH = 7, 0.15 M sodium chloride, 15 mM trisodium citrate). The resulting mixtures were stirred for 1 hour. After centrifugation, CMS and CMS-BIO were both washed with 20 mL SSC-buffer. CMS was then directly subjected to the described release experiment after being redispersed in 200 μ L SSC-buffer. CMS-BIO was redispersed in 5 mL SSC-buffer solution and subsequently capped with avidin (see 5.2.7).

5.2.7 Avidin-capped, fluorescein loaded CMS (CMS-AVI)

To the amount of 10 mg fluorescein-loaded CMS-BIO redispersed in 5 mL SSC-buffer (pH=7, 0.15 M sodium chloride, 15 mM trisodium citrate), 7 mg avidin from egg white was added. The resulting mixture was stirred at room temperature for 12 hours. The suspension was centrifuged and washed three times with each 5 mL of SSC buffer. The product was then redispersed in 200 μ L SSC buffer solution. CMS-AVI was then subjected to the described release experiment (5.2.8).

5.2.8 Fluorescence spectroscopy setup

Fluorescence experiments were performed in order to show the time-dependent release of fluorescein from the mesopores of colloidal mesoporous silica spheres. Fluorescein sodium salt was excited with 490 nm and showed a maximum of emission at 511 nm (excitation slit 1.0 mm, emission slit 1.0 mm, integration 0.5 sec). For the release experiment, a ROTH Visking Typ 8/32 dialysis membrane with a molecular cut-off of 14.000 g/mol was used. A picture of our custom made Teflon container can be seen in Figure 5.5. The suspension is filled into the container, which is subsequently closed by a dialysis membrane. The closed container is then put onto a fluorescence cuvette, which is completely filled with water. The released dye is able to pass through the applied membrane while the relatively large particles are held back.

5.3 Results and Discussion

Colloidal mesoporous silica spheres with mercaptopropyl-functionalities exclusively on the outer particle surface were synthesized by applying our recently developed delayed co-condensation approach.¹³ Briefly, tetraethylorthosilicate (TEOS) was hydrolyzed in a reaction mixture containing cetyltrimethylammonium chloride (CTAC) and triethanolamine (TEA). A mixture of TEOS and (3-mercaptopropyl)-triethoxysilane equivalent to 2 % of the total silane content was added 30 minutes after the generation of the seeds, resulting in mesoporous silica nanoparticles bearing mercaptopropyl moieties exclusively on the outer particle surface (CMS-SH). As a reference sample, pure unfunctionalized CMS were synthesized as well (sample CMS). After 12 hours, the template-filled pores of both samples CMS and CMS-SH were extracted, resulting in clear suspensions featuring particle sizes around 80 nm, BET surfaces of approximately 1100 m²/g and NLDT pore sizes of about 3.8 nm. A representative TEM picture of the CMS is shown in Figure 5.3.1.

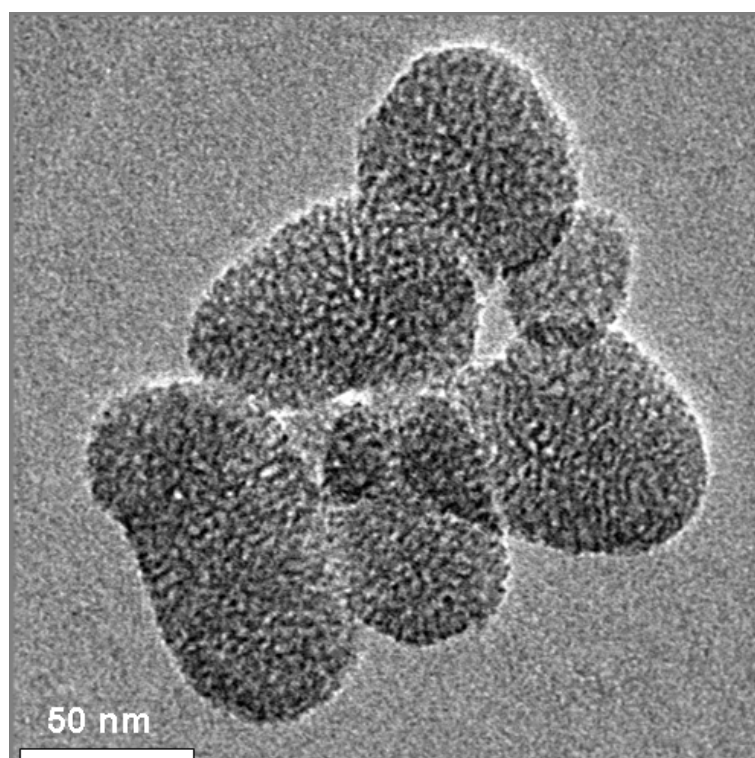


Figure 5.3.1 TEM picture of the sample CMS-SH.

The subsequent treatment of CMS-SH in aqueous solution at room temperature with biotin-maleimide (in 2-fold excess with respect to the thiol groups incorporated in the CMS) resulted in biotinylation of the outer surface of CMS-SH (to give CMS-BIO, Figure 5.3.2).

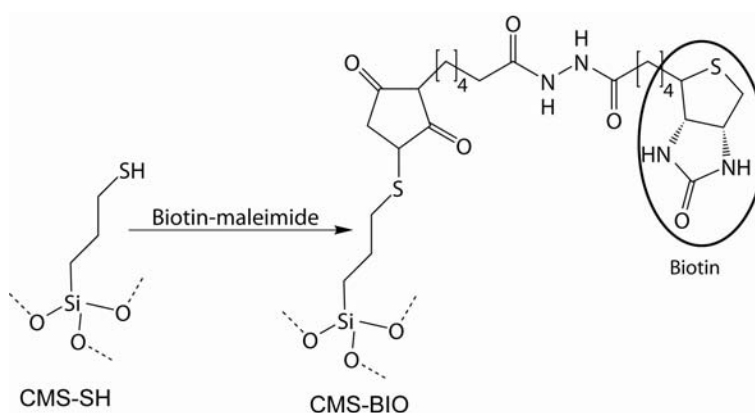


Figure 5.3.2 Attachment of biotin-maleimide to the thiol-functionalized CMS surface.

5. Biotin-Avidin as Protease-Responsive Cap-System for Controlled Release from CMS

CMS-BIO was then loaded with fluorescein by stirring CMS-BIO (10 mg) in 25 ml of a 1 M solution of fluorescein disodium salt for 1 hour. After centrifugation and redispersion in a citrate buffer solution (pH = 7), avidin (5 mg) was added to cap the filled pores (CMS-AVI, Figure 5.3.3).

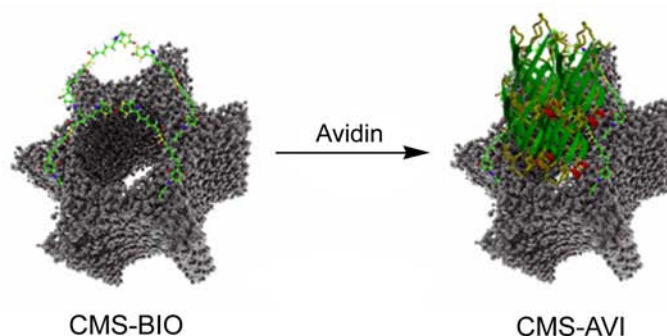


Figure 5.3.3 Attachment of avidin caps on the biotinylated CMS surface. The four subunits of avidin can each bind to one biotin moiety attached to the surface.

The closure reaction was performed by stirring at room temperature for 12 hours. The resulting material was washed three times to remove all dye molecules located outside the closed pores. Unfunctionalized CMS was loaded with dye as described for CMS-BIO, but only one washing step was performed. The results of the different reaction steps were monitored by IR spectroscopy (Figure 5.3.4).

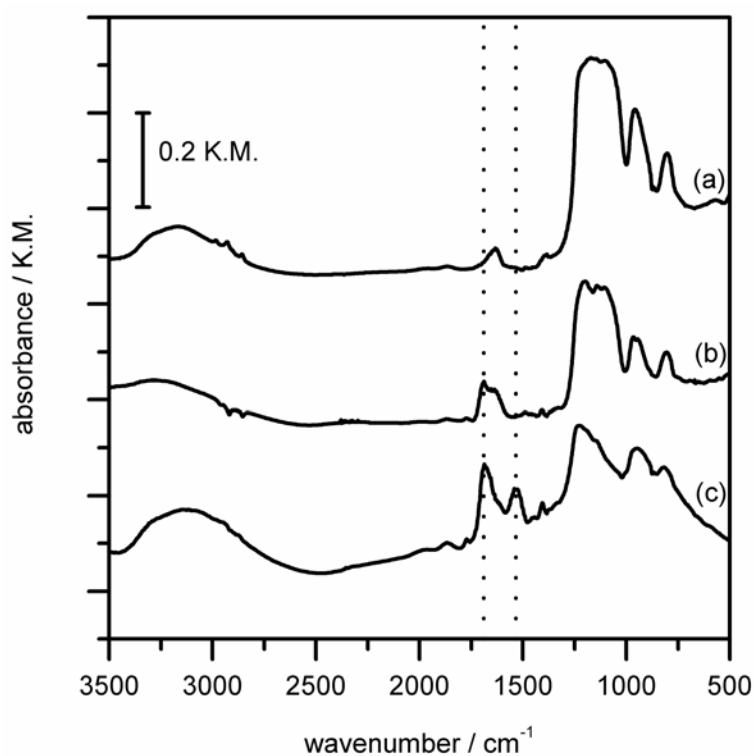


Figure 5.3.4 IR-spectra of the samples (a) CMS-SH, (b) CMS-BIO and (c) CMS-AVI. The absorbance is expressed in Kubelka-Munk (KM) units.

The emerging broad absorption band around 1680 cm^{-1} in sample CMS-BIO can be assigned to various vibrations of the hydrazide and cyclic urea structures contained within the attached biotin-maleimide molecules (Figure 5.3.4b). The typical amide vibrations in sample CMS-AVI are located at 1530 cm^{-1} and also around 1650 cm^{-1} (Figure 5.3.4c). Signals below 1500 cm^{-1} can be mainly attributed to the silica framework. Changes in pore volume and diameter were investigated by nitrogen sorption experiments (Figure 5.3.5).

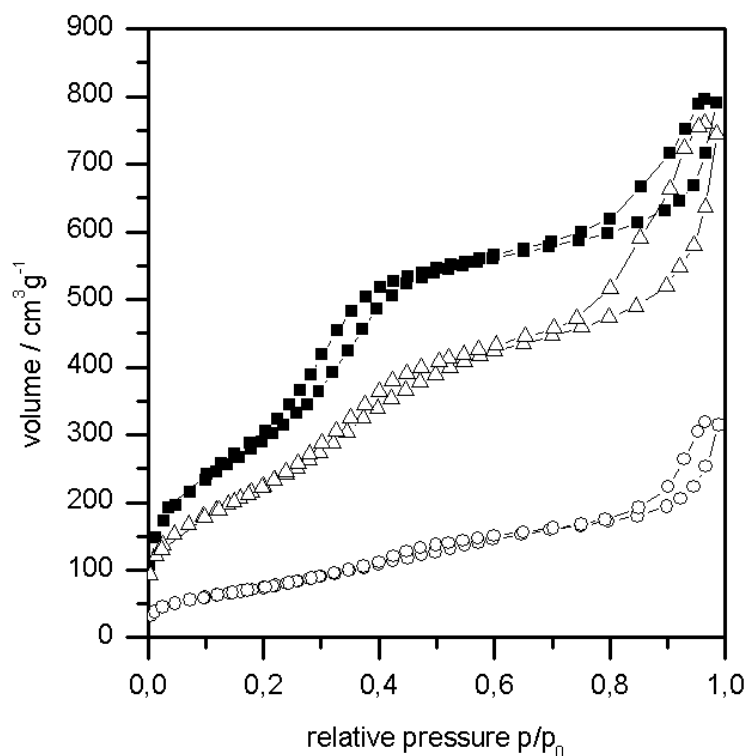


Figure 5.3.5 Nitrogen sorption isotherms of the samples CMS-SH (■), CMS-BIO (△), and CMS-AVI (○).

For BET and NLDFT calculations, only cumulative pore volumes are specified for pores smaller than 8 nm owing to the considerable textural porosity of the CMS samples. No decrease in pore diameter is observed in samples CMS, CMS-SH and CMS-BIO. This result indicates that the internal surface of the mesoporous particles remains unfunctionalized (Table 5.3.1). The corresponding pore size distribution graphs can be found in the Appendix (A-4).

Table 5.3.1 NLDFT pore diameters and pore volumes from the synthesized CMS samples.

	CMS	CMS-SH	CMS-BIO	CMS-AVI
Pore diameter (nm)	3.9	3.8	3.8	----
Pore volume (cm³ g⁻¹)	0.8	0.8	0.6	0.19

The decrease in surface area and pore volume by approximately 30 % in the sample CMS-BIO is attributed to partial pore blocking due to the large organic moieties on the outer shell of the CMS. In the case of CMS-AVI, a striking almost complete elimination of nitrogen-accessible mesopore volume was observed as a result of pore blocking of the mesopores by the large proteins. We take this observation as evidence of a very effective pore closure by the attached avidin.

Measurements of the zeta potential were made to show the effect of the different functionalization steps on the surface charge. As can be seen in Figure 5.3.6, the synthesized materials show characteristic surface potentials corresponding to the molecules covering the outer silica surface.

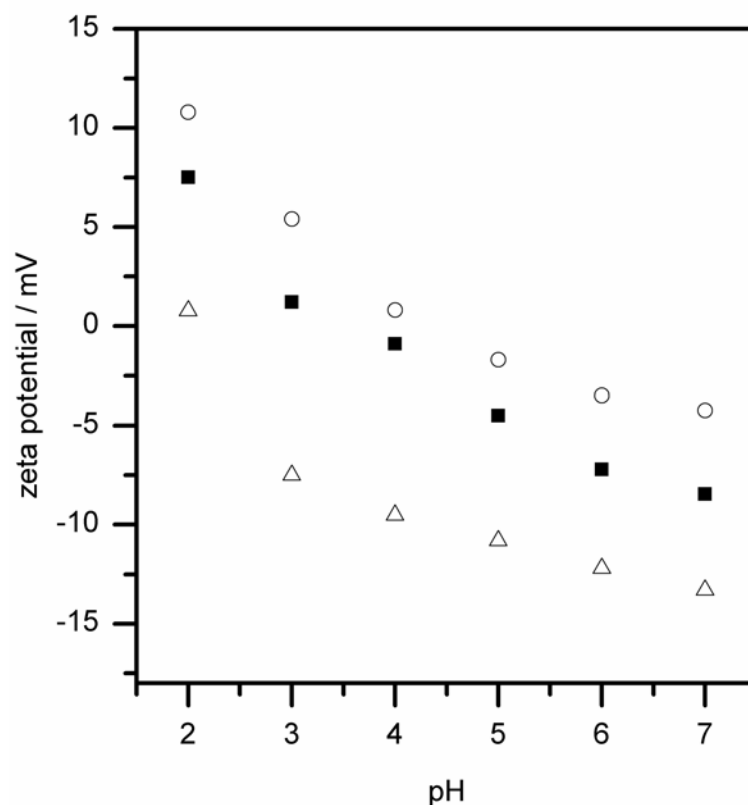


Figure 5.3.6 Zeta potential curves of the samples CMS-SH (filled squares), CMS-BIO (empty triangles), and CMS-AVI (empty circles).

The thiol-carrying surface of the sample CMS-SH is slightly protonated at $\text{pH} = 2$. At higher pH values, the acidic character of the thiol group leads to a deprotonation of SH and therefore leading to a more negative surface potential. The biotinylated surface of CMS-BIO shows a different behaviour (Figure 5.3.6, empty triangles). The structure of the biotin-maleimide molecule does not include possible protonation sites. Corresponding to the structure, the zeta potential of CMS-BIO at low pH is much lower than the values obtained for CMS-SH. However, the surface of CMS-AVI can be protonated at the aminogroups included in the structure of the attached protein thus leading to a higher zeta potential.

In order to show that we maintain the colloidal state of the samples after all synthesis steps, dynamic light scattering experiments were performed. The results show that we obtain colloidal samples after each functionalization reaction (Figure 5.3.7).

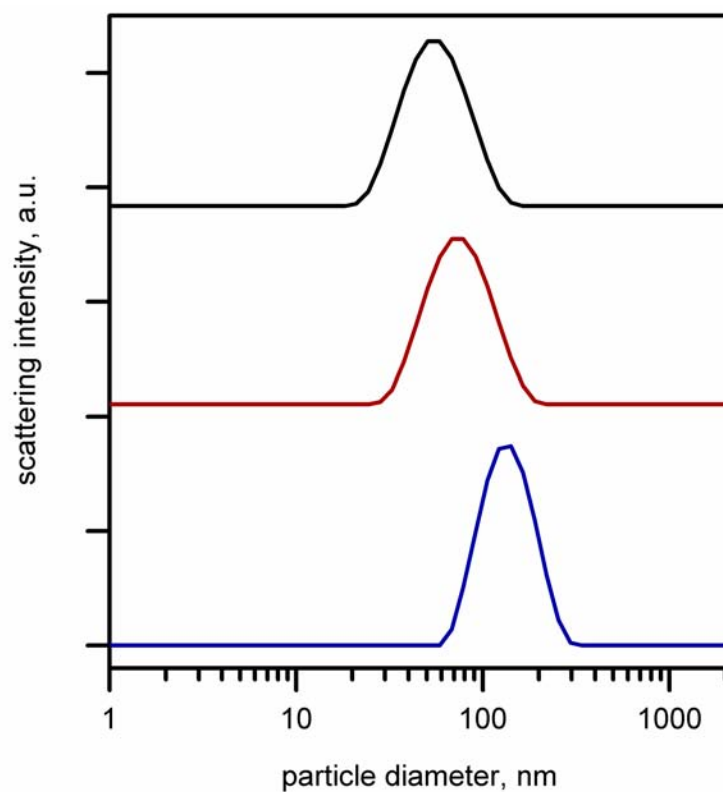


Figure 5.3.7 DLS measurements of the samples CMS-SH (black), CMS-BIO (red), and CMS-AVI (blue).

The enzyme-responsive release properties were investigated with fluorescence spectroscopy. An aqueous suspension containing either 2 mg of CMS-AVI or of loaded unfunctionalized CMS was transferred into a specially designed container, which could be closed by a holey lid lined with a dialysis membrane. This custom-made system fits on the opening of a fluorescence cuvette (see Figure 5.3.8).



Figure 5.3.8 Custom made release experiment setup featuring a 200 µl Teflon tube (a) which is closed by a dialysis membrane (b). This setup is put onto a fluorescence cuvette filled with water (c).

Whereas the colloidal particles are too large to diffuse through the dialysis membrane, fluorescein can enter the free cuvette volume readily and be observed by fluorescence spectroscopy at a temperature of 37 °C. In a reference experiment, it was shown that the dialysis membrane used (with a molecular weight cut-off of 16000 g/mol) does not act as a diffusion barrier for fluorescein (see Appendix A-5). Fluorescein was excited at 490 nm, which led to a fluorescence emission maximum at 511 nm. In another reference experiment, the unfunctionalized CMS host released the entire loaded amount of dye within minutes (Figure 5.3.9, ■). The concentration of fluorescein inside the cuvette remained stable after 30 minutes. This concentration was attributed to a relative release ratio of 100%. The attached avidin in sample CMS-AVI prevented the loaded fluorescein from escaping the pore system. After 60 minutes, no significant release of fluorescein was observed, which indicates that the new closure mechanism is highly efficient (Figure 5.3.9, △).

A very different result was obtained after the addition of the protease trypsin (1 mg) to the colloidal suspension. In an earlier study, trypsin had been used to hydrolyze avidin to obtain information about its amino acid sequence.¹⁵ In our case, the proteolytic digestion of avidin allows the loaded dye to escape from its host. The concentration of released fluorescein increased shortly after the addition of trypsin (Figure 5.3.9, △).

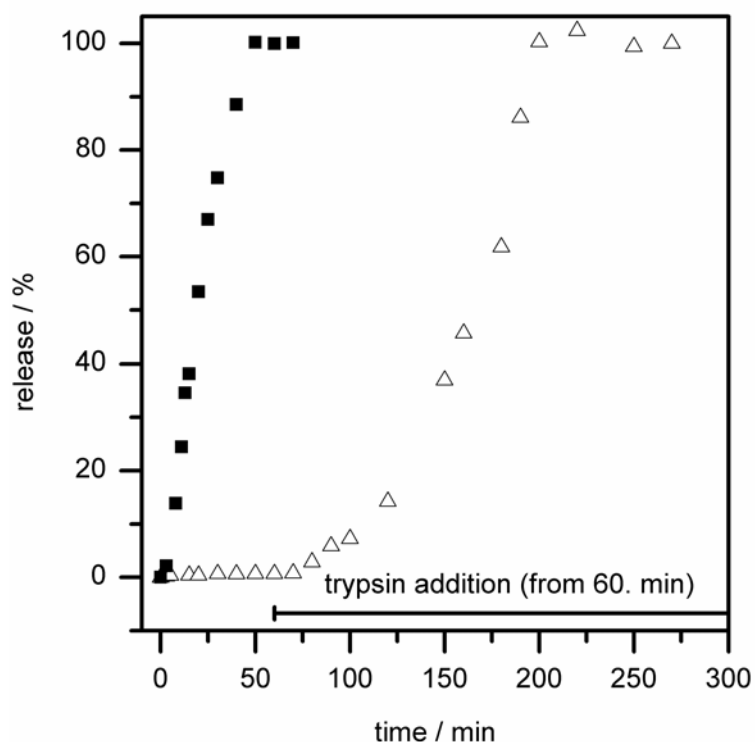


Figure 5.3.9 Protease-responsive release curve of the sample CMS-AVI (Δ) and release from unfunctionalized CMS (\blacksquare).

After 4 hours, no further increase in the concentration of released fluorescein was observed, a result that indicated the complete release of the loaded dye.

Interestingly, the enzyme-responsive release curve features a fairly slow release for the first hour after the addition of trypsin. This result can be explained by the tryptic hydrolysis process, in which an increasing number of caps are cleaved. After one hour, the capping proteins are effectively digested, which leads to a faster release of the guest molecules. After 140 minutes following the addition of the protease, the observed amount of fluorescein remained stable (100%). The absolute amounts of released dye were determined by UV-vis spectroscopy. All investigated samples released comparable amounts of fluorescence dye (around 0.03 mg per mg sample, see Appendix A-6 for calculations). These data clearly

demonstrate that we are able to close the pore system of CMS with the avidin-biotin system, and to subsequently release the loaded molecules by enzymatic hydrolysis of the caps.

We carried out a complementary thermoresponsive release experiment to compare the efficiency of the different cap-opening methods. In this case, the attached protein caps were opened by denaturation. Therefore, they were opened immediately and simultaneously. An increase in the temperature to 90 °C weakened the affinity of avidin for the biotinylated surface and led to the fast and fairly linear release of the loaded fluorescein molecules (Figure 5.3.10). In contrast to the enzyme-responsive opening mechanism, the thermoresponsive release occurs directly after the stimulation (temperature increase).

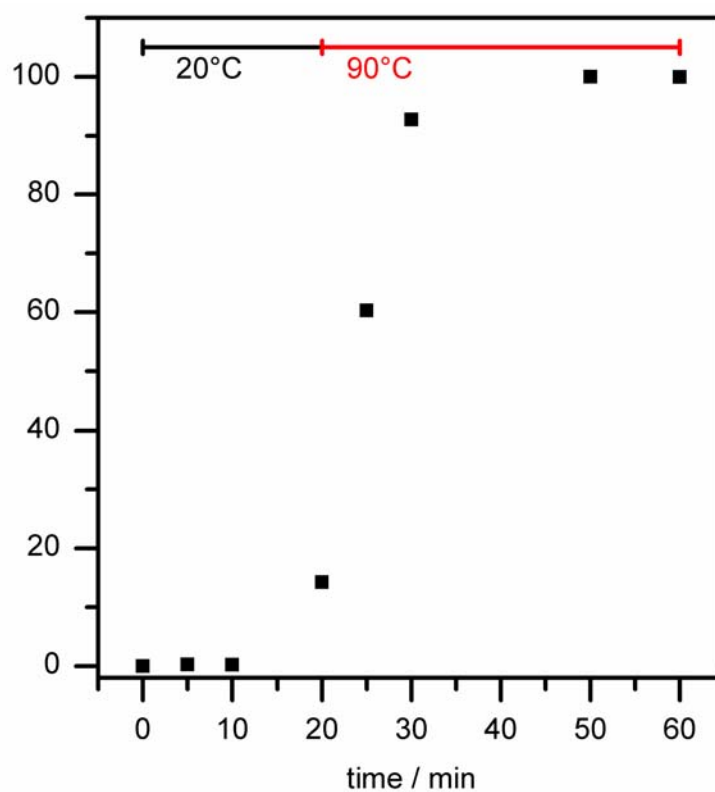


Figure 5.3.10 Thermoresponsive release of fluorescein from the sample CMS-AVI.

5.4 Conclusion

In summary, we have presented a biomolecule-based enzyme-responsive cap system for mesoporous silica. We show that the attachment of avidin to the outer surface of CMS can prevent the uncontrolled leaching of incorporated guest molecules. The tight closure of the pores can be explained by the structure of the avidin-biotin complex. The four subunits of avidin (molecule size $4.5 \times 5.5 \times 6 \text{ nm}^3$)¹⁶ can each bind to one biotin molecule; thus, a strong interaction between the avidin and the biotin-covered CMS surface results. We have demonstrated an opening mechanism based on the controlled enzymatic hydrolysis of the attached protein avidin. The advantage of this system lies in the use of native biomolecules. Thus, the creation of toxic or carcinogenic species can be avoided. This approach offers new possibilities for applications of mesoporous hosts in the fields of detergent design and drug delivery.

5.4 References

- (1) Giri, S.; Trewyn, B. G.; Lin, V. S. Y. *Nanomedicine (London, United Kingdom)* 2007, 2, 99.
- (2) Slowing, I. I.; Trewyn, B. G.; Giri, S.; Lin, V. S. Y. *Advanced Functional Materials* 2007, 17, 1225.
- (3) Dave, B. C.; Deshpande, K.; Gebert, M. S.; McAuliffe, J. C. *Advanced Materials (Weinheim, Germany)* 2006, 18, 2009.
- (4) Trewyn, B. G.; Whitman, C. M.; Lin, V. S. Y. *Nano Letters* 2004, 4, 2139.
- (5) Trewyn, B. G.; Giri, S.; Slowing, I. I.; Lin, V. S. Y. *Chemical Communications (Cambridge, United Kingdom)* 2007, 3236.
- (6) Izquierdo-Barba, I.; Manzano, M.; Colilla, M.; Vallet-Regi, M. *Key Engineering Materials* 2008, 377, 133.

- (7) Patel, K.; Angelos, S.; Dichtel, W. R.; Coskun, A.; Yang, Y.-W.; Zink, J. I.; Stoddart, J. F. *Journal of the American Chemical Society* 2008, *130*, 2382.
- (8) Prosperi, D.; Morasso, C.; Tortora, P.; Monti, D.; Bellini, T. *ChemBioChem* 2007, *8*, 1021.
- (9) Anzai, J.-i. *Chemical Sensors* 2002, *18*, 55.
- (10) Barat, B.; Wu, A. M. *Biomolecular Engineering* 2007, *24*, 283.
- (11) Kojima, N.; Matsuo, T.; Sakai, Y. *Biomaterials* 2006, *27*, 4904.
- (12) Maurer, K.-H. *Current Opinion in Biotechnology* 2004, *15*, 330.
- (13) Kecht, J.; Schlossbauer, A.; Bein, T. *Chemistry of Materials* 2008, *20*, 7207.
- (14) Moeller, K.; Kobler, J.; Bein, T. *Advanced Functional Materials* 2007, *17*, 605.
- (15) DeLange, R. J.; Huang, T. S. *The Journal of biological chemistry* 1971, *246*, 698.
- (16) Pugliese, L.; Coda, A.; Malcovati, M.; Bolognesi, M. *Journal of Molecular Biology* 1993, *231*, 698.

6. A Programmable DNA-Based Molecular Valve for Colloidal Mesoporous Silica

The following work is based on the publication indicated below:

Axel Schlossbauer, Simon Warncke, Philipp M. E. Gramlich, Johann Kecht, Antonio

Manetto, Thomas Carell, and Thomas Bein, *Angew. Chem., Int. Ed.* **2010**, *49*, 4734-4737

6.1 Introduction

Recently, stimuli-responsive gatekeepers or valves for the controlled release of guest molecules from mesoporous silica hosts have been developed.¹⁻⁴ Controlled release mechanisms are of great interest in many different fields such as drug delivery, detergent design, or additives in polymers. For example, inorganic nanoparticles, large molecules and also polymers have been applied to prevent guest molecules from leaving the pore system.⁵⁻⁷ The release mechanisms include those based on changes in the reduction potential, pH, UV irradiation, or temperature.⁸⁻¹⁰ For instance, gold nanoparticles were functionalized with photocleavable linkers and subsequently adsorbed onto the surface of MCM-41. Other systems utilize the external presence of enzymes for the controlled release of incorporated guests.^{11,12} One approach uses α -cyclodextrins fixed with ester-bound adamantyl-stoppers. Opening was achieved by the addition of porcine liver esterase, leading to a removal of the stoppers.¹² Our research has recently centered on systems using biomolecules as components for the design of the molecular valves. For example, we have demonstrated the applicability of the biotin-avidin complex as biomolecule-based valve on novel core-shell functionalized colloidal mesoporous silica, which opens by enzyme action or at high temperature (see chapter 5).³ The molecular valves reported so far are commonly based on one specific opening mechanism, which is determined by the chemical nature of the system. Here we

demonstrate that a molecular valve system can be made programmable by encoding the desired behavior in a DNA sequence that is part of the responsive system. We demonstrate this concept with the programmable opening temperature of a molecular valve on the pore mouths of novel core-shell colloidal mesoporous silica (CMS, Figure 6.1.1).

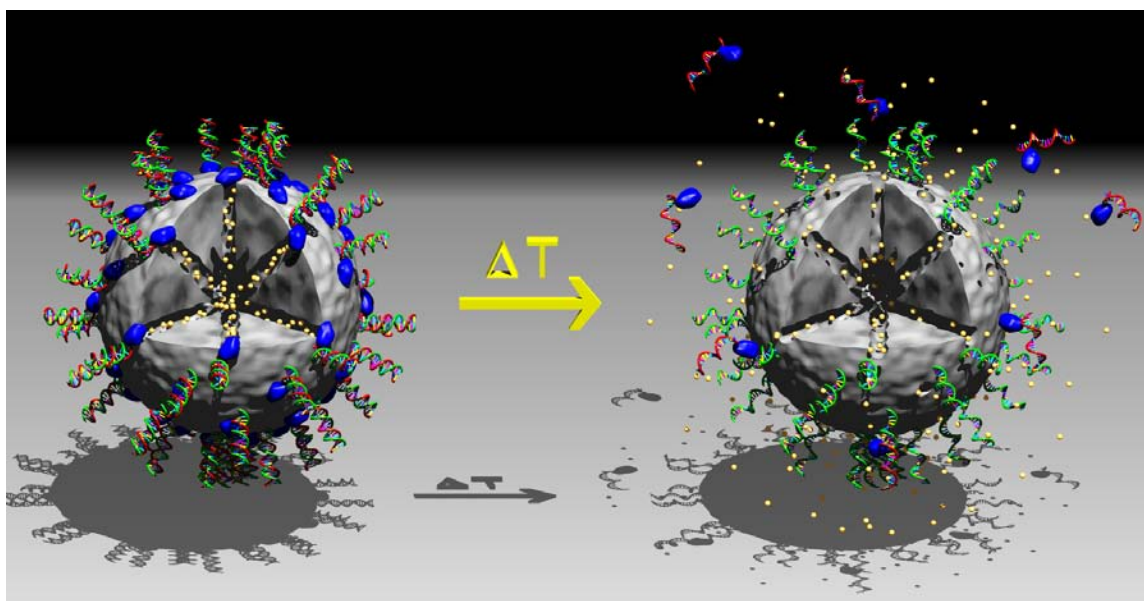


Figure 6.1.1 Concept of the programmable molecular valve system. Melting the DNA linkers at specifically encoded temperatures opens the avidin caps.

As discussed in Chapter 3, we have developed the controlled molecular core-shell functionalization of colloidal mesoporous silica, which is a prerequisite for the complex assembly of the different functionalities at different locations of the nanoscale porous particles.^{13,14}

As described below, we have selectively attached biotin-labeled DNA double strands to the pore mouths of the core-shell mesoporous nanoparticles. This procedure allows a subsequent closing of the pores by the protein avidin whilst leaving open the internal pore volume of the mesoporous nanoparticle. The opening of the valve is achieved by DNA strand melting at the

specific melting temperature of the oligonucleotide.

The work was carried out in cooperation with the research group of Prof. Thomas Carell, University of Munich, in particular with Philipp M. E. Gramlich and Simon Warneke and the Baseclick GmbH.

6.2 Experimental Section

6.2.1 Applied Chemicals

Tetraethylorthosilicate (TEOS, Fluka, >99%), (3-chloropropyl)-trimethoxysilane (CITMS, Fluka, 95%), cetyltrimethylammonium bromide (CTAC, Fluka, 25% in H₂O), triethanolamine (TEA, Aldrich, 98%), sodium azide (NaN₃, Fluka, 99%), avidin from egg white (Sigma, lyophilized powder), fluorescein sodium salt (Fluka, standard for fluorescence), N,N-dimethylformamide (DMF, Sigma, > 99.8 %). All chemicals were used as received without further purification. Doubly distilled water from a Millipore system (Milli-Q Academic A10) was used for all synthesis and purification steps. DNA oligomers and tris(benzyltriazolylmethylamine) ligand were received as a gift from Baseclick GmbH.

6.2.2 Preparation of colloidal mesoporous silica nanoparticles (CMS)

Mesoporous silica nanoparticles were prepared according to literature procedures.¹³ The combined TEOS (1.92 g, 9.22 mmol) and TEA (14.3 g, 95.6 mmol) were heated for 20 minutes at 90 °C without stirring in a 100 mL polypropylene reactor. A solution of CTAC (25 % in water, 2.41 mL, 1.83 mmol) and water (21.7 g, 1.21 mol) preheated to 60 °C was added, and the resulting mixture was stirred at room temperature for 30 minutes. A second set of reactants was added at 30 minutes after combination of the initial TEOS/TEA and CTAC solutions. The reactants were added to the stirred reaction mixture with an Eppendorf micropipette and consist of TEOS and (3-chloropropyl)-trimethoxysilane (CITMS) at the molar ratio 1 : 1. The combined amount of both silanes was 185 μmol, i.e., 2 % of the total

amount of “Si” in the initial CMS synthesis. The resulting mixture was stirred at room temperature for 12 hours. After addition of 100 mL ethanol, the mesoporous silica nanoparticles were separated by centrifugation, redispersed in ethanol and extracted according to the procedure described in 6.2.3.

6.2.3 Extraction of CMS

Extraction of the organic template from the CMS materials was performed by heating the colloidal suspensions containing 250 mg of CMS for 45 minutes under reflux at 90 °C in a solution containing 2 g ammonium nitrate in 100 mL ethanol, followed by 45 minutes under reflux in a solution of 4 g concentrated hydrochloric acid in 100 mL ethanol. The CMS materials were separated by centrifugation and washed with ethanol after each extraction step. CMS materials were obtained as clear ethanolic suspensions.

6.2.4 Synthesis of azide-functionalized CMS (CMS-N₃)

100 mg of the extracted sample CMS-Cl were washed with anhydrous DMF for three times by centrifugation. Finally, the particles were redispersed in 20 mL of anhydrous DMF and transferred into a 100 mL Schlenk flask equipped with a soxhlet extractor under nitrogen atmosphere. The Soxhlet extractor was filled with dried molecular sieve with a 4 Å pore size. The drying process was carried out for three hours at 90 °C. The resulting dried suspension was then saturated with 100 mg NaN₃. The reaction mixture was stirred at 80 °C for 5 hours. The amount of 50 mL water was then added. The particles were subsequently washed three times with 50 mL water followed by centrifugation and then redispersed in 20 mL of water, yielding sample CMS-N₃.

6.2.5 Attachment of alkyne-modified oligonucleotides to CMS-N₃ (CMS-DNA₁₅, CMS-DNA₂₅)

Alkyne-modified double-stranded DNA (0.70 mM, 71 μ L, 50.0 nmol in water) was added to 1 mg CMS-N₃. In a separate vial, 1 μ L CuBr solution (0.1 M in DMSO/ *t*BuOH 3:1) and 2 μ L of the tris(benzyltriazolylmethylamine) ligand (0.1 M in DMSO/ *t*BuOH 3:1) were mixed and added freshly to the DNA-particle mixture, which was then stirred overnight at room temperature. DNA-functionalized CMS was washed three times with 1 mL of MilliQ doubly distilled water followed by centrifugation. Subsequently, the particles were redispersed in 1 mL of water.

6.2.6 Fluorescein loading and avidin capping of CMS-DNA_x(CMS-DNA₁₅-AVI, CMS-DNA₂₅-AVI)

The amount of 2 mg fluorescein disodium salt was added to the respective suspensions of the samples CMS-DNA₁₅ and CMS-DNA₂₅ described in 6.2.5, and the resulting mixture was stirred at room temperature for two hours. Subsequently, the amount of 1 mg avidin from egg white was added to each of the suspensions. This capping process was carried out for two hours of stirring at room temperature. The samples were then washed five times with 1 mL of water by centrifugation, before each sample was redispersed in 200 μ L of water.

6.3 Results and Discussion

Colloidal mesoporous silica (CMS) with chloropropyl functionality exclusively on the outer shell of the nanoparticles was synthesized by using our recently developed delayed co-condensation method for the controlled synthesis of functionalized core-shell mesoporous nanoparticles.¹³ This approach avoids uncontrolled pore clogging of the nanoparticles upon the attachment of large organic moieties to the surface. Herein, the inner pore walls remain unfunctionalized, leaving the whole pore volume available for loading with guest molecules,

such as drugs or other organic molecules. A reaction mixture containing tetraethyl orthosilicate (TEOS), cetyltrimethylammonium bromide (CTAB), and triethanolamine (TEA) results in the spontaneous generation of seeds that grow further radially. After 30 min, a 1:1 mixture of 3-chloropropyltrimethoxysilane and TEOS was added to the reaction to yield organic functionality exclusively at the outer shell of the nanoparticles. CMS with particle sizes of about 50 nm were thus obtained as determined by transmission electron microscopy (TEM). A TEM image of the sample CMS-Cl can be found in Figure 6.3.1.

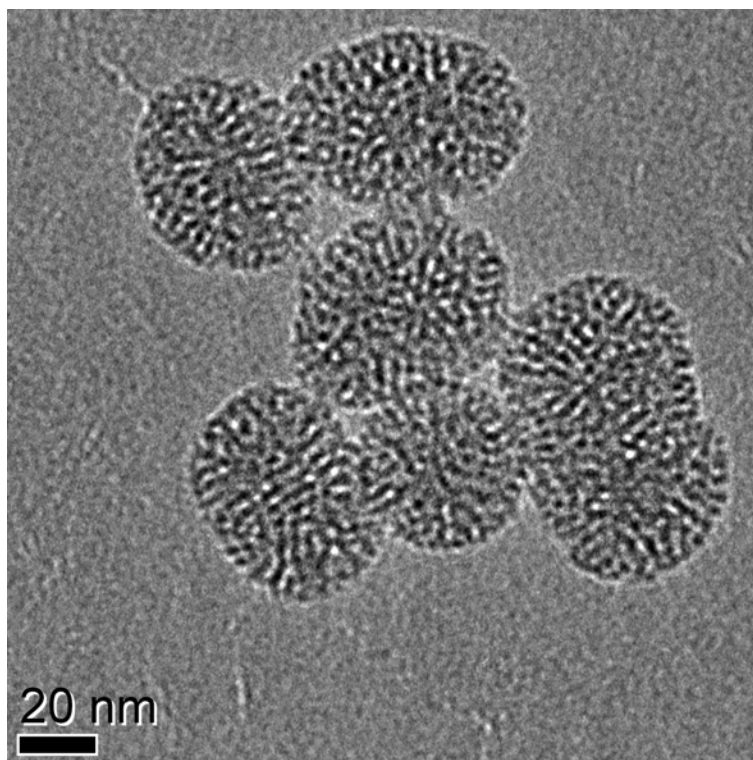


Figure 6.3.1 TEM-picture of the sample CMS-Cl

The functionalized mesoporous particles feature pore sizes of 3.8 nm and a pore volume of $0.99 \text{ cm}^3 \text{ g}^{-1}$, as determined from nitrogen sorption isotherms with non-local density functional theory (NLDFT). The corresponding isotherm is shown in Figure 6.3.2.

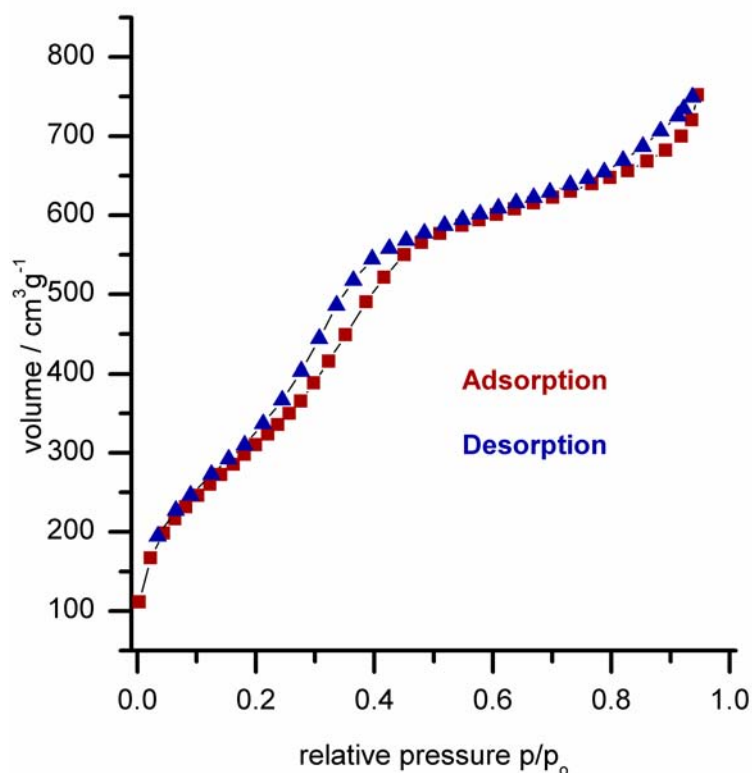


Figure 6.3.2 Nitrogen sorption isotherm of the sample CMS-Cl.

The colloids were then transferred into dry *N,N*-dimethylformamide. The remaining water from the pore system was removed under mild conditions according to our previously published vapor extraction procedure for 3 hours at 90 °C using molecular sieves.¹⁵ This approach protects the particles from temperature-induced agglomeration. The resulting water-free suspension was then saturated with sodium azide and heated to 85 °C for 5 hours to give an azide-carrying surface (sample CMS-N₃).

The azide- modified surface was used to attach biotin- and alkyne-functionalized DNA double strands by a click chemistry approach. The double strands act as a linker between the particle surface and the avidin protein caps. The applied DNA oligomers bear an alkyne functionality at their 5' end. Specifically, a C8-alkyne-desoxyuridine-phosphordiamidite that features a C8-alkyne linker at the 5-position of the base was incorporated at the 5' end of the DNA strands. This method was recently introduced by some of us.^{16,17} The functionalized DNA oligomers were then pre-hybridized with complementary strands carrying a biotin functionality at their

3' end by briefly heating a 1:1 mixture of the strands to 95 °C and slow cooling to room temperature in a 500 mM sodium chloride solution. For our experiments, two different double strands were synthesized, a 25 mer and a 15 mer. Along with the described alkyne and biotin functionality, the 15 mer is modified with two dyes (Cy3, Cy5), one on each end of the respective complementary oligomers. This allows for a fluorescence resonance energy transfer (FRET) between the two strands to further characterize the hybridization state of the DNA at different temperatures.¹⁸ Furthermore, the synthesized DNA strands were characterized by MALDI-TOF mass spectrometry. An overview of the DNA oligomers that were applied is given in Table 6.3.1.

Table 6.3.1 Sequences and MALDI-TOF analysis of the applied DNA strands.

Applied DNA double strands	
5' - XCA CGT CGC ATC TTG GCC TAC GCC C -3'	
$M_{\text{calc.}} = 7616.4$	$M_{\text{found}} = 7617.1$
3' -Bio-AGT GCA GCG TAG AAC CGG ATG CGG G - 5'	
$M_{\text{calc.}} = 8230.9$	$M_{\text{found}} = 8231.4$
5' - XCA CGT CGC ATC TTT Cy3 - 3'	
$M_{\text{calc.}} = 5404.8$	$M_{\text{found}} = 5405.6$
3' - Bio-AGT GCA GCG TAG AAA Cy5 - 5'	
$M_{\text{calc.}} = 5902.3$	$M_{\text{found}} = 5902.8$

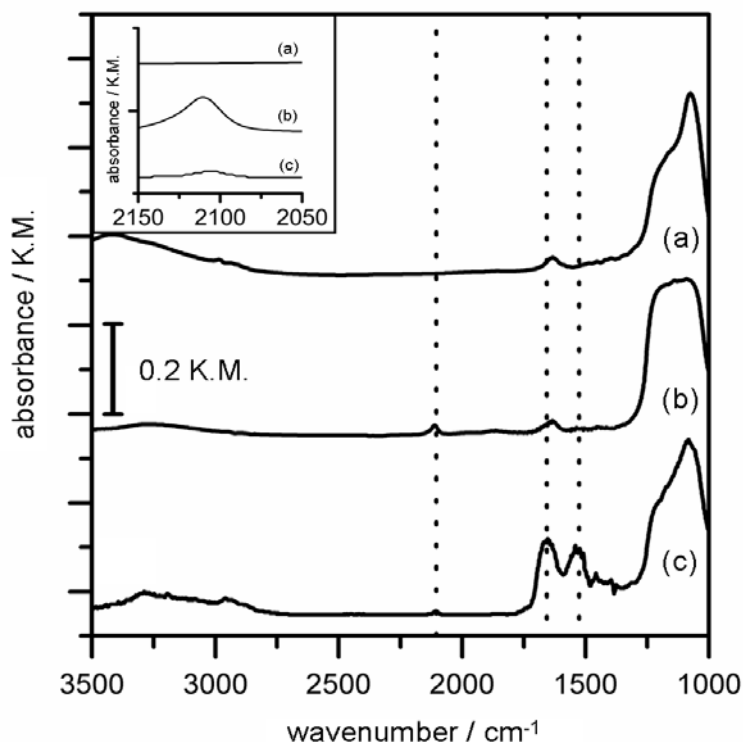


Figure 6.3.3 Infrared spectra of the samples (a) CMS-Cl, (b) CMS- N_3 , and (c) CMS-DNA₁₅-AVI (Inset shows a magnification of the azide stretch area).

The DNA oligomers were then attached to the particles using a click chemistry approach. We have elaborated in chapter 4 on the applicability of click chemistry on mesoporous silica surfaces.¹⁹ Samples were synthesized that carry the two different dsDNA introduced in Table 6.3.1 (CMS-DNA₁₅ and CMS-DNA₂₅). The sequence of building up the molecular DNA valve was followed by IR spectroscopy (Figure 6.3.3). Whereas the sample CMS-Cl (Figure 6.3.3a) only shows the silica framework vibrations, an azide band occurs in sample CMS- N_3 at 2105 cm^{-1} (Figure 6.3.3b). This band is strongly reduced in intensity upon DNA attachment during the click reaction. We take this result as evidence for the covalent DNA binding to the CMS sample. As can be seen in Figure 6.3.3, the sample CMS-DNA₁₅-AVI shows the typical amide vibrations at 1551 cm^{-1} and 1650 cm^{-1} of the attached protein, along with the silica vibrations. The weak signals between 1500 cm^{-1} and 1300 cm^{-1} in sample CMS-DNA₁₅-AVI

can be attributed to the carbonyl vibrations of the desoxyribose backbone and the amino groups of the incorporated DNA.

As described above, the attached strands have a biotin functionality that is now positioned closely to the surface of the nanoparticle pore mouth. The intact hybridization of the strands after the click reaction is indicated by a successful measurement of the FRET signal in the sample CMS-DNA₁₅-AVI (Figure 6.3.4).

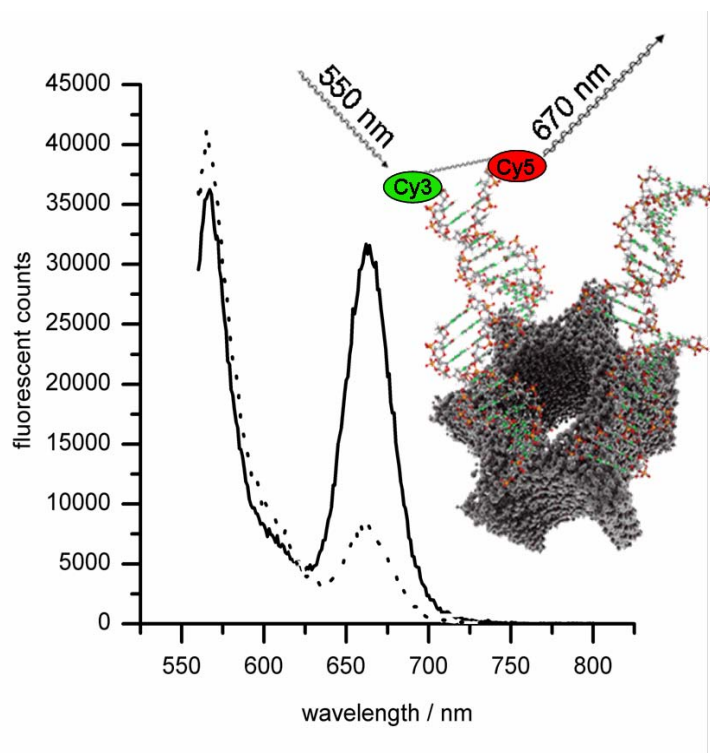


Figure 6.3.4 FRET measurements of the sample CMS-DNA₁₅-AVI in the closed state (line) and in the open state (dots).

A corresponding reference FRET experiment using the pure as-received 15mer DNA can be found in the Appendix (A-7). In analogy, it is assumed that the longer and more stable DNA-25mer is also in a hybridized state after the click reaction.

The samples CMS-DNA₁₅ and CMS-DNA₂₅ were then loaded with fluorescein as a model compound for guest molecules. To achieve the loading, 1 mg of each sample was stirred in 1 mL of a solution containing 2 mg fluorescein in water at room temperature for 2 hours.

Subsequently, 1 mg avidin from egg white was added and stirring was continued for another two hours. This leads to a coordination of the biotinylated DNA with the avidin protein and thus should close the pores of the colloidal particles. The subsequent release of fluorescein can be easily detected and quantified by fluorescence spectroscopy, as we have demonstrated in Chapter 5.³ After incorporation of the dye, the particles were centrifuged in a 1.5 mL vial and redispersed in water (pH 7). Thereafter three washing cycles were applied to remove free dye from the suspension, yielding the samples CMS-DNA₁₅-AVI and CMS-DNA₂₅-AVI. The samples were then transferred into a two-compartment fluorescence cuvette, which can be closed by a dialysis membrane and features a sample volume of 200 μL .³ With the two-compartment temperature-controlled fluorescence cuvette, the release of small fluorescent molecules can be detected by fluorescence spectroscopy. The silica nanoparticles are too large to diffuse through the dialysis membrane (featuring a molecular weight cut-off of 16.000 g mol^{-1}) The opening mechanism of the molecular valve was examined with FRET measurements. As described above, the sample CMS-DNA₁₅-AVI is equipped with the FRET pair Cy3-Cy5 on the complementary DNA strands (see Table 6.3.1). Cy3 has an absorption maximum around 550 nm and an emission at 570 nm that tails into the red. Cy5 is excited at 650 nm and emits at 670 nm. With the attached double strand in a hybridized state, an emission at 670 nm can be achieved upon excitation at 550 nm, owing to the energy transfer occurring between the two dyes in close contact (less than 10 nm; see Figure 6.3.4).^{18,20} After the thermoresponsive release experiment (see below), the sample was centrifuged and then redispersed in 2 mL of water. As can be seen in Figure 6.3.4 (dots), the FRET emission at 670 nm decreases substantially in intensity after the thermoresponsive release, indicating the opening of the molecular valve by separation of the DNA strands. Finally, the programmed thermoresponsive opening of the molecular DNA-avidin-biotin valves was demonstrated by quantification of the released fluorescein molecules with fluorescence spectroscopy in the two-compartment cuvette described above (Figure 6.3.5).

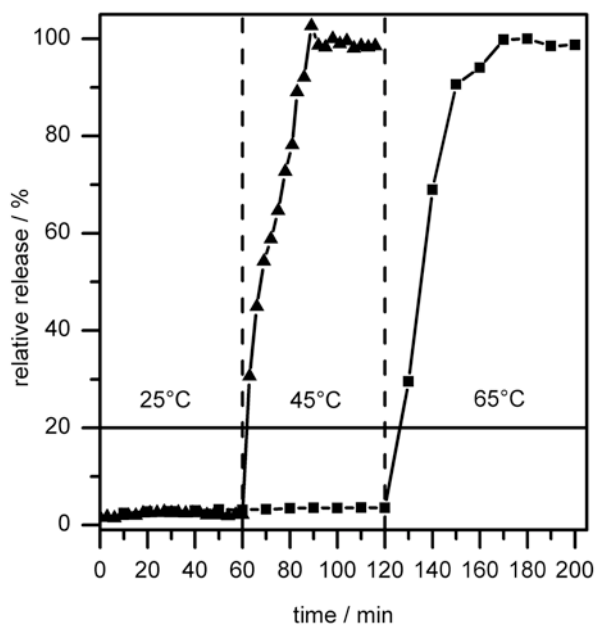


Figure 6.3.5 Release curves (normalized fluorescence intensity of fluorescein) of the samples CMS-DNA₁₅-AVI (triangles) and CMS-DNA₂₅-AVI (squares).

All intensity values are normalized to the highest obtained fluorescent count of the respective sample. Therefore, the highest released amount of fluorescein is set to 100% relative release. The raw data of the obtained release measurement before normalization can be found in the Appendix (A-8). The temperature-dependent release curves show the striking effect of the DNA-linker on the valve-opening behavior. Whilst the 15mer opens at 45 °C, the longer 25mer is still in a tightly sealed state at this temperature and thus keeps the avidin firmly bound to the CMS pore mouth. The sample CMS-DNA₂₅-AVI does not convert into the open state until further heating to 65°C. Quantification of the released amount of fluorescein by UV/Vis spectroscopy gives comparable amounts of dye released in both samples. Specifically, the sample CMS-DNA₁₅-AVI released 0.033 mg dye/mg CMS, whilst the sample CMS-DNA₂₅-AVI released 0.040 mg dye/mg CMS.

A calibration curve for the amount of released fluorescein and detailed calculations can be

found in the Appendix (Figure A-6.1, A-9)

6.4 Conclusion

In summary, we have shown how the incorporation of double-stranded DNA into a novel molecular valve can impart programmable, thermoresponsive release behavior at moderate temperatures. The successful assembly of this multifunctional nanodevice builds on the novel multifunctional core-shell colloidal mesoporous silica host with free available pore volume inside the host, selective functionalization of the pore mouths with dsDNA linker bearing two dyes for FRET monitoring, and biotin-avidin coupling for valve closure. These nanodevices allow the release temperature of incorporated guest molecules to be adjusted precisely for a desired application. The general concept of programmed release will be of significant importance in fields such as detergents or encapsulation of polymer hardeners.²¹ A further potential application is targeted drug release, although toxicological aspects have to be considered here as well.

6.5 References

- (1) Slowing, I. I.; Trewyn, B. G.; Giri, S.; Lin, V. S. Y. *Advanced Functional Materials* **2007**, *17*, 1225.
- (2) Slowing, I. I.; Vivero-Escoto, J. L.; Wu, C.-W.; Lin, V. S. Y. *Advanced Drug Delivery Reviews* **2008**, *60*, 1278.
- (3) Schlossbauer, A.; Kecht, J.; Bein, T. *Angewandte Chemie, International Edition* **2009**, *48*, 3092.
- (4) Coti, K. K.; Belowich, M. E.; Liong, M.; Ambrogio, M. W.; Lau, Y. A.; Khatib, H. A.; Zink, J. I.; Khashab, N. M.; Stoddart, J. F. *Nanoscale* **2009**, *1*, 16.
- (5) Lai, C.-Y.; Trewyn, B. G.; Jeftinija, D. M.; Jeftinija, K.; Xu, S.; Jeftinija, S.; Lin, V. S. Y. *Journal of the American Chemical Society* **2003**, *125*, 4451.

- (6) Ferris, D. P.; Zhao, Y.-L.; Khashab, N. M.; Khatib, H. A.; Stoddart, J. F.; Zink, J. I. *Journal of the American Chemical Society* **2009**, *131*, 1686.
- (7) Liu, R.; Zhao, X.; Wu, T.; Feng, P. *J. Am. Chem. Soc.* **2008**, *130*, 14418.
- (8) Vivero-Escoto, J. L.; Slowing, I. I.; Wu, C.-W.; Lin, V. S. Y. *Journal of the American Chemical Society* **2009**, *131*, 3462.
- (9) Aznar, E.; Marcos, M. D.; Martinez-Manez, R.; Sancenon, F.; Soto, J.; Amoros, P.; Guillem, C. *Journal of the American Chemical Society* **2009**, *131*, 6833.
- (10) Park, J.-H.; Lee, Y.-H.; Oh, S.-G. *Macromolecular Chemistry and Physics* **2007**, *208*, 2419.
- (11) Bernardos, A.; Aznar, E.; Marcos, M. D.; Martinez-Manez, R.; Sancenon, F.; Soto, J.; Barat, J. M.; Amoros, P. *Angewandte Chemie, International Edition* **2009**, *48*, 5884.
- (12) Patel, K.; Angelos, S.; Dichtel, W. R.; Coskun, A.; Yang, Y.-W.; Zink, J. I.; Stoddart, J. F. *J. Am. Chem. Soc.* **2008**, *130*, 2382.
- (13) Kecht, J.; Schlossbauer, A.; Bein, T. *Chemistry of Materials* **2008**, *20*, 7207.
- (14) Cauda, V.; Schlossbauer, A.; Kecht, J.; Zürner, A.; Bein, T. *Journal of the American Chemical Society* **2009**, *131*, 11361.
- (15) Kecht, J.; Bein, T. *Langmuir* **2008**, *24*, 14209.
- (16) Gramlich, P. M. E.; Warncke, S.; Gierlich, J.; Carell, T. *Angewandte Chemie, International Edition* **2008**, *47*, 3442.
- (17) Gierlich, J.; Burley, G. A.; Gramlich, P. M. E.; Hammond, D. M.; Carell, T. *Organic Letters* **2006**, *8*, 3639.
- (18) Fegan, A.; Shirude, P. S.; Balasubramanian, S. *Chemical Communications* **2008**, 2004.
- (19) Schlossbauer, A.; Schaffert, D.; Kecht, J.; Wagner, E.; Bein, T. *Journal of the American Chemical Society* **2008**, *130*, 12558.

- (20) Iqbal, A.; Arslan, S.; Okumus, B.; Wilson, T. J.; Giraud, G.; Norman, D. G.; Ha, T.; Lilley, D. M. J. *Proceedings of the National Academy of Science of the United States of America* **2008**, *105*, 11176.
- (21) McIlroy, D. A.; Blaiszik, B. J.; Braun, P. V.; White, S. R.; Sottos, N. R. *Polymer Reprints* **2008**, *49*, 963.

7. Role of Endosomal Escape for Disulfide-Based Drug Delivery from Colloidal Mesoporous Silica Evaluated by Live-Cell Imaging

The following work is based on the publication indicated below:

Anna M. Sauer, Axel Schlossbauer, Nadia Ruthardt, Valentina Cauda, Thomas Bein, and Christoph Bräuchle, *Nano Letters* **2010**, *10* (9), 3684-3691

7.1 Introduction

Controlled release of drugs from functionalized mesoporous materials has attracted great interest in recent years.¹⁻⁶ Triggers used to affect the controlled release include enzymatic digestion of gatekeepers,⁷⁻¹⁰ temperature,⁷ competitive binding,¹¹ light-irradiation,¹²⁻¹⁹ changes in the pH value,²⁰⁻²³ or changes in the redox potential.²⁴⁻²⁸ In Chapter 5 we have discussed an enzymatically triggered system, using tightly bound avidin proteins to seal the pores. An opening of these protein caps was shown by the release of fluorescein upon proteolytic digestion of the attached avidin. Most of the reported systems use valves or caps at the pore openings of the porous silica surface.^{7-9,11,13,20,24} Furthermore, redox-sensitive, disulfide-based mechanisms were applied in the field of drug delivery.²⁹ In the context of mesoporous silica, for example, poly(N-acryloxysuccinimide) was grafted on mesoporous silica nanoparticles and cross-linked by cystamine, resulting in a closure of the pores. Reopening was achieved by the addition of a reducing agent.¹⁸ As many therapeutic peptides carry thiol functions, and nucleic acid oligomers can be functionalized with such groups, redox-driven intracellular disulfide cleavage offers a high potential in drug delivery. This approach can also be transferred to the pore system of mesoporous hosts. Binding and releasing drug molecules from the inner volume of mesoporous silica nanoparticles allows one to avoid synthetically demanding molecular valve concepts while retaining the benefits of protecting sensitive or immunoresponsive drugs in porous host materials. Mortera *et al.* have initially studied the

7. Role of Endosomal Escape for Disulfide-Based Drug Delivery from Colloidal Mesoporous Silica Evaluated by Live-Cell Imaging

concept of disulfide bound agents attached to the pore system of mesoporous silica.²⁵ They showed that membrane-impermeable cysteine can be successfully delivered into cells. Cysteine delivery into cells promotes the synthesis of glutathione (GSH), which plays a central role in cell biology. A number of diseases including cancer as well as neurodegenerative and cardiovascular diseases are associated with GSH depletion and existing treatment strategies aim at promoting GSH synthesis by cysteine delivery.¹⁸ While Mortera *et al.*²⁵ have demonstrated that cell-induced release can be based on disulfide bridges in mesoporous silica, the cellular uptake mechanism and the specific locus as well as the time point of reduction inside the cell remains unknown. For a further development and optimization of this promising approach, it is of particular interest to focus on the details of nanoparticle entry and subsequent events after entry into the cell. Such processes can be followed effectively with highly sensitive live-cell imaging techniques, as they are available in the group of Prof. C. Bräuchle at the LMU. These techniques can monitor the uptake of a single particle and its trafficking inside the cell.³⁰⁻³² A well-known bottleneck for drug delivery into the cytosol of cells is the endosomal escape of macromolecular substances or drug conjugates.³³ Because of the low reductive or even oxidative milieu in endosomes, contact to the cytosol is essential for release of disulfide-bound agents.³⁴ The use of photoactive compounds to open the endosome is one possibility to overcome this challenge.^{35,36} Recently, our collaborators in this project from the laboratory of Prof. C. Bräuchle (LMU München) have used the disulphonated porphyrin derivative meso-tetraphenylporphine (TPPS_{2a}) for the study of photoinduced endosomal release dynamics of DNA-containing polyplexes and dextrans in living cells.³³ It was demonstrated that endosomal compartments could be damaged by activation of the membrane-bound photosensitizer to release the endosomal cargo. In the present work, photochemical release was used to study endosomal escape of colloidal mesoporous silica (CMS) nanoparticles in living HuH7 cells. HuH-7 is a well differentiated hepatocyte derived cellular carcinoma cell

line that was originally taken from a liver tumor in a 57-year-old Japanese male in 1982.³⁷ Core-shell functionalized CMS nanoparticles were obtained using the recently developed strategy described in Chapter 3. It allows integration of molecular functionalities at distinct locations within one mesoporous silica nanoparticle.^{38,39} We have synthesized CMS carrying a 3-mercaptopropyl-functionality at the inner pore walls of the core and 3-aminopropyl functionality on the outer particle surface. The outer surface was then labeled with N-hydroxysuccinimidyl-ATTO488 (ATTO488-NHS) fluorescent dye, while the inner core was functionalized with ATTO633-labeled cysteine by disulfide formation, leading to dual-color particles. The long-term intracellular integrity of the dual-color CMS nanoparticles measured by spinning disk confocal microscopy confirmed that endosomal escape is a bottleneck for drug delivery into cells. Endosomal release of the CMS nanoparticles was achieved by application of the photosensitizer meso-tetraphenylporphine (TPPS2a) and monitored by highly sensitive widefield fluorescence microscopy in living cells in collaboration with the group of Prof. Bräuchle. The endosomal collapse was verified by the release of the fluid phase marker Alexa Fluor 488 Dextran (AFD). After endosomal collapse, release of nanoparticles, cleavage of the disulfide-bond and release of fluorescently labeled cysteine into the cytosol of living cells was observed. The obtained results demonstrate that endosomal escape is a limiting factor for the redox-triggered intracellular release of disulfide-bound cysteine from core-shell functionalized colloidal mesoporous silica (CMS). The developed synthesis of the dye-labeled core-shell structured CMS was adapted to fulfill the special requirements of the highly sensitive live-cell imaging techniques used here.

7.2 Experimental Section

7.2.1 Applied Chemicals

Tetraethylorthosilicate (TEOS, Fluka, >99%), (3-mercaptopropyl)-triethoxysilane (MPTES, Gelest, 95%), (3-aminopropyl)-triethoxysilane (APTES, Fluka, >97%), cetyltrimethylammonium bromide (CTAC, Fluka, 25% in H₂O), triethanolamine (TEA, Aldrich, 98%), L-cysteine (97%, Sigma), ATTO488-NHS ester, ATTO633-NHS ester (both Atto-Tec), 2,2'-dithiopyridine (DTP, Fluka, >97%), *N,N*-dimethylformamide (DMF, Sigma, 99.8%), L-glutathione reduced (GSH, Sigma-Aldrich), Alexa Fluor 488 Dextran (AFD, MW 10 kDa, Invitrogen), cell culture media and fetal calf serum (Invitrogen), meso-tetraphenylporphine (TPPS2a, LumiTrans®, PCI Biotech).

All chemicals were used as received without further purification. Doubly distilled water from a Millipore system (Milli-Q Academic A10) was used for all synthesis and purification steps.

7.2.2 Synthesis of CMS-SH_{core}-NH_{2shell} by sequential co-condensation

The colloidal mesoporous silica particles were synthesized by using our sequential co-condensation approach discussed in Chapter 3.^{38,39} A mixture of TEOS (1.63 g, 7.82 mmol), MPTES (111.5 mg, 0.47 mmol), and TEA (14.3 g, 95.6 mmol) in a polypropylene reactor were heated for 20 minutes at 90 °C under static conditions. Then, a solution of CTAC (25 % in water, 2.41 mL, 1.83 mmol) and water (21.7 g, 1.21 mol) preheated to 60 °C was added and the mixture was allowed to cool to room temperature. The resulting mixture was stirred at room temperature for 20 minutes. The total amount of 138.2 mg TEOS (0.922 mmol) was added in four equal increments every three minutes, followed by another 30 minutes of stirring at room temperature. Next, a 1:1 mixture of TEOS (20.5 μL, 92.5 μmol) and APTES (21.6 μL, 92.5 μmol) was added to the reaction mixture (total volume 42.1 μL). The reaction was then allowed to stir for another 12 hours. After the addition of 100 mL ethanol, the CMS

were separated by centrifugation, redispersed in ethanol and subjected to the template extraction procedure described below.

7.2.3 Template extraction from CMS

The extraction of the organic template from the porous silica framework was achieved by heating 1 g of silica twice in 100 mL of an ethanolic solution of ammonium nitrate (2 g NH_4NO_3 in 100 mL ethanol), followed by 30 minutes under reflux in a solution of 4 g concentrated hydrochloric acid in 100 mL ethanol. After each step, the material was washed with 100 mL ethanol. After the extraction, the particles were collected by centrifugation and redispersed in 100 mL of absolute ethanol.

7.2.4 Fluorescence labeling procedure for CMS-SH_{core}-NH_{2shell}

The amount of 1 mg of CMS material was redispersed in 200 μL of absolute ethanol in a 1.5 mL Eppendorf tube. Then, 15 μL of a solution of ATTO488-NHS (1 mg dye in 500 μL dry DMF) was added and the resulting mixture was stirred for 2 hours at room temperature. Finally, the particles were washed 6 times with 1 mL ethanol each to remove remaining free dye, resulting in the sample CMS-SH_{core}-ATTO488_{shell}.

7.2.5 Fluorescence labeling procedure for the amino group of cysteine

Cysteine (1 mg, 8.25 μmol) was dissolved in 200 μL of 0.1 M sodium bicarbonate buffer (pH 8.3). Then, 62 μL of a solution of ATTO633-NHS (1 mg in 500 μL dry DMF) was added. The 50-fold excess of cysteine is intended to minimize the amount of remaining free dye, since no purification of the product was performed. The resulting mixture was stirred for 2 hours.

7.2.6 Attachment of ATTO633-labeled cysteine to CMS-SH_{core}-ATTO488_{shell} via disulfide bridge (CMS-CysATTO633_{core}-ATTO488_{shell})

The amount of 1 mg of CMS-SH_{core}-ATTO488_{shell} was redispersed in 200 μ L absolute ethanol. 2,2'-Dithiopyridine (1 mg, 4.5 μ mol) was added and the mixture was stirred for 30 minutes at room temperature. The colloids were collected by centrifugation. The successful activation of the bound thiol groups is indicated by the yellow color of the supernatant after centrifugation. After redispersion in 200 μ L absolute ethanol, 130 μ L of the prepared ATTO633-cysteine solution was added to the suspension. The resulting mixture was stirred for 2 hours at room temperature. The sample was washed six times by centrifugation and redispersion in water and was finally redispersed in 500 μ L of water. In order to remove larger aggregates from the suspension, the sample was filtered through a Rotband® filter before incubation with cells.

7.2.7 Attachment of ATTO633 to CMS-SH_{core}-ATTO488_{shell} (CMS-ATTO633_{core}-ATTO488_{shell})

The amount of 1 mg of CMS-SH_{core}-ATTO488_{shell} was redispersed in 200 μ L absolute ethanol. Then, 50 μ L of ATTO633-maleimide was added to the suspension and the resulting mixture was stirred for 2 hours at room temperature. The sample was washed six times by centrifugation and redispersion in water. In order to remove larger aggregates from the suspension, the sample was filtered through a Rotband® filter before incubation with cells, resulting in the sample (CMS-ATTO633_{core}-ATTO488_{shell}).

7.2.8 Cell culture

HuH7 cells were grown in Dulbecco's modified Eagle's medium (DMEM):F12 (1:1) with Glutamax I medium supplemented with 10% fetal calf serum at 37 °C in 5% CO₂ humidified atmosphere. To reduce autofluorescence of the cells, the medium was changed to DMEM:F12

supplemented with 10% B-27 two days before seeding. The cells were seeded on collagen A-coated LabTek chambered cover glass (Nunc).

7.2.9 Spinning disk confocal microscope

Confocal microscopy for live-cell imaging was performed on a setup based on the Nikon TE2000E and a spinning disk confocal microscope (Andor) utilizing a Yokogawa spinning disk unit CSU10. The system was equipped with a 1.49 NA 100x Plan Apo oil immersion objective from Nikon. For two color detection of ATTO488 and ATTO633, dichroic mirrors and band-pass filters HQ 525/50 and 730/140 were used (AHF Analysentechnik AG). Image sequences were captured with an electron multiplier charge coupled device (EMCCD) camera (iXon DV884; Andor).

7.2.10 Long-term incubation and imaging of CMS nanoparticles in living cells

In case of the long term (24 and 48 hours) incubations of HuH7 cells with dual-color CMS-CysATTO633_{core}-ATTO488_{shell} nanoparticles, the following procedure was applied. HuH7 cells were seeded in densities of $2 \cdot 10^4$ and $1 \cdot 10^4$ cells/cm² and exposed to nanoparticles after 9-12 hours. Measurements were performed on a spinning disk confocal microscope 24 and 48 hours after particle addition. Prior to imaging, the medium was replaced by CO₂-independent medium (Invitrogen) and the cells were kept on a heated microscope stage at 37°C.

Samples were illuminated in an alternating fashion with 488 nm and 635 nm lasers exciting ATTO488 and ATTO633, respectively. The movies were recorded in 3 z-planes (distance 0.5 μm) and are presented as z-projections. The exposure time per image was 300 ms, resulting in an actual frame rate of 0.5 frames per second for the movie showing the overlaid z-projections.

7.2.11 Wide-field fluorescence microscope

Wide-field fluorescence microscopy was performed on a custom-built setup based on the Nikon Ti microscope equipped with a 1.49 N.A. 60x Apo TIRF oil immersion objective (Nikon). The photosensitizer was excited by a 405 nm laser 1 min prior to imaging. Alexa Fluor 488 Dextran (AFD) and ATTO633 were excited by 488 and 642 nm laser light in alternating fashion. Fluorescence was collected in epifluorescence mode, split into two emission channels by a dichroic mirror (565 DCXR, Chroma) and passed through filter sets (525/50 and 725/150, Semrock). The green and red emission channels were projected onto two EMCCD cameras (DU-897 iXon+, Andor).

7.2.12 Dye release at single-particle level on glass

Redox-cleavable CMS-CysATTO633_{core} and the non-cleavable control CMS- ATTO633_{core} nanoparticles were measured on glass on a wide-field fluorescence microscope first in water, then in 10 mM GSH solution. Movies of the ATTO633 and background fluorescence were recorded before ($t < 0$ min) and after ($t > 0$ min) addition of the GSH solution. The exposure time per frame was 200 ms, resulting in an actual frame rate of 1.7 frames per second due to alternating illumination.

7.2.13 Photochemical release of CMS nanoparticles in HuH7 cells

The photochemical release experiments were performed on the basis of the experiments by de Bruin *et al.*³⁶ In brief, the cells were seeded at a density of $0.6\text{-}0.75 \cdot 10^4$ cells/cm², 3 to 4 days before imaging. 12-24 hours before imaging, the medium was replaced by a medium containing 0.025 $\mu\text{g/ml}$ TPPS_{2a}. AFD in a concentration of 0.24 mg/ml and the nanoparticles were added to the cells. Cells were incubated overnight, washed three times with CO₂-independent medium (Invitrogen) and subsequently transferred to a 37 °C heated microscope stage. The photosensitizer was activated by illumination with 405 nm laser light for 1 min.

After the activation of the photosensitizer, the measurement was performed with alternating excitation by 488 and 642 nm laser light with 200 ms exposure time resulting in a frame rate of 1.7 frames per second.

7.2.14 Evaluation of the fluorescence intensity of CMS nanoparticles in vitro and in cells

The fluorescence intensity of nanoparticles was obtained by calculating the mean fluorescence intensity of regions of interest (ROI) containing a single endosome or nanoparticle for all frames of a movie. To account for different laser excitation intensities and differing fluorescence intensities of individual movies, the mean fluorescence intensity was normalized to the initial background intensity defined by a ROI in a region without particles and plotted over time.

7.3 Results and Discussion

Axel Schlossbauer in the laboratory of Prof. Thomas Bein planned and performed all synthesis steps and non-microscopic characterization of the applied materials.

Core-shell functionalized CMS nanoparticles were synthesized according to the sequential co-condensation method described in Chapter 3 (Figure 7.3.1).³⁹ A mixture of TEOS and MPTES was hydrolyzed in an aqueous reaction mixture containing triethanolamine and cetyltrimethylammonium chloride. 30 minutes after seed generation, a shell of pure silica was grown by adding four small amounts of TEOS (each 2.5 mol % of total Si content) in three-minute steps. The mixture was stirred for another 30 minutes. Finally, a 1:1 mixture of TEOS: APTES (2% of total silica) was added to the reaction. The resulting mixture was stirred for another 12 hours at room temperature. After template extraction, colloidal mesoporous silica spheres featuring particle diameters of 80 nm (derived from transmission electron

microscopy) were obtained (sample CMS-SH_{core}-NH_{2shell}).

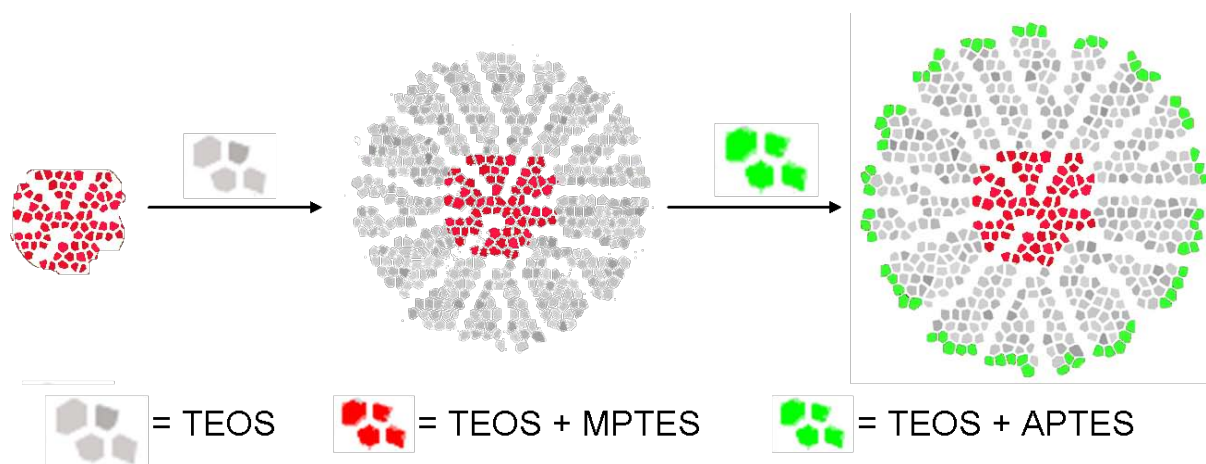


Figure 7.3.1 Synthesis scheme of core-shell functionalized colloidal mesoporous silica

To characterize the porous properties of the sample, nitrogen sorption measurements were performed, showing a Brunauer-Emmett-Teller surface area of $1160 \text{ m}^2\text{g}^{-1}$ (The isotherm can be found in the Appendix A-9, Figure A-9.1). The pore size and volume was calculated to 3.8 nm and $0.93 \text{ cm}^3\text{g}^{-1}$, respectively, according to nonlocal density functional theory. Subsequently, the amino-functionalized shell was labeled with ATTO488-NHS, yielding the sample CMS-SH_{core}-ATTO488_{shell}. After vigorous washing steps, the thiol-functionalized core of the particles was activated with 2-2'-dithiopyridine (DTP) and further reacted with ATTO633-labeled cysteine, resulting in a disulfide-bridged labeled cysteine attached to the inner core of the porous nanoparticle (sample CMS-CysATTO633_{core}-ATTO488_{shell}, Figure 7.3.2).

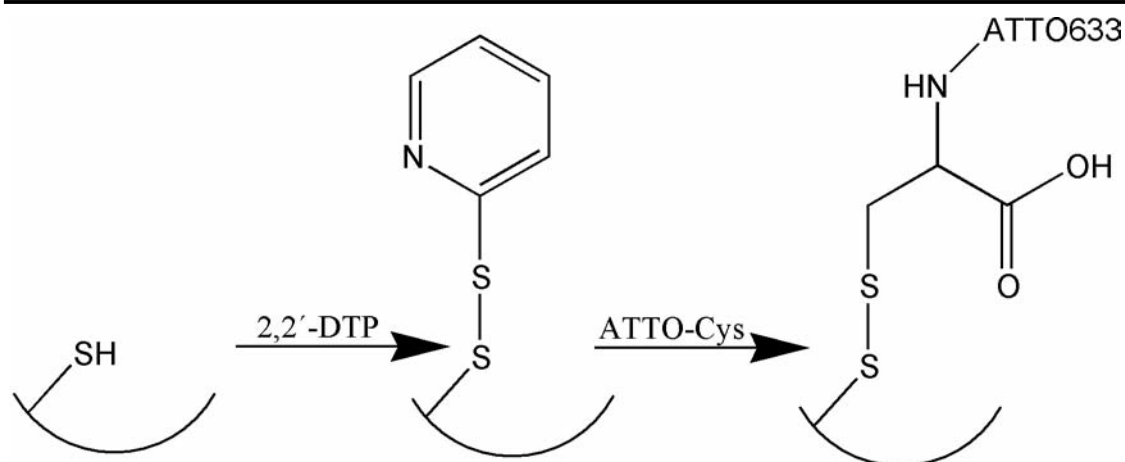


Figure 7.3.2 Attachment of ATTO633-labeled cysteine to the core of the colloidal mesoporous silica.

Additionally, a number of reference samples were prepared to perform all experiments described in the following. An overview of all prepared fluorescent CMS-samples is given in Table 7.3.1.

Table 7.3.1 Overview of all prepared fluorescent CMS samples

CMS sample name	Core functionality	Shell functionality
CysATTO633 _{core} -ATTO488 _{shell}	N-ATTO633-labeled, disulfide-bridged cysteine	ATTO488
ATTO633 _{core} -ATTO488 _{shell}	ATTO633	ATTO488
CysATTO633 _{core} -NH ₂ _{shell}	N-ATTO633-labeled, disulfide-bridged cysteine	Aminopropyl-
ATTO633 _{core} -NH ₂ _{shell}	ATTO633	Aminopropyl-

The progress of the increasing functionalization was monitored by Raman spectroscopy (Figure 7.3.3). The relevant peaks in the different spectra are marked with asterisks.

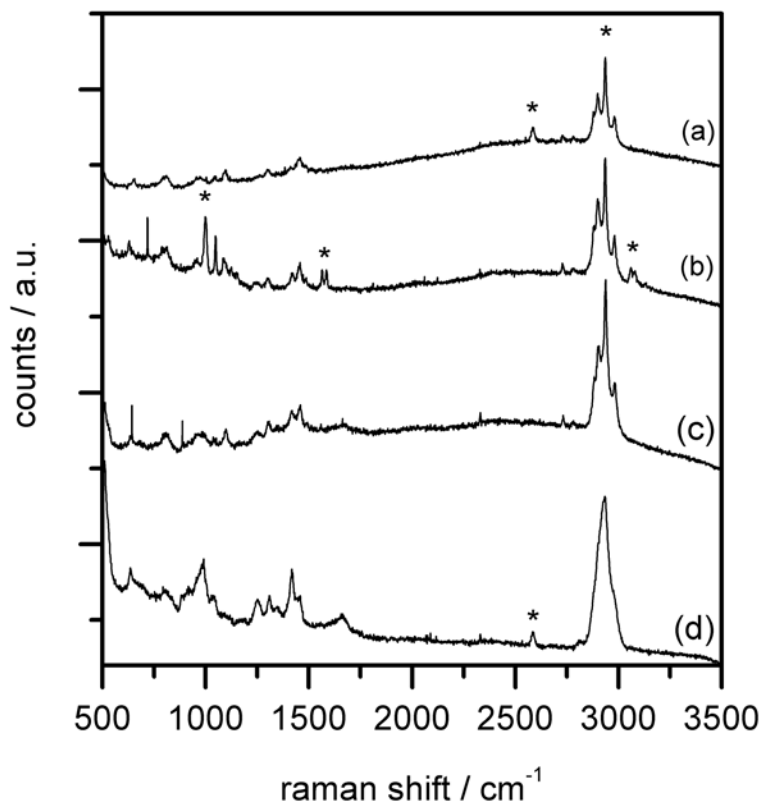


Figure 7.3.3 Raman spectra of the samples (a) CMS-SH_{core}-NH₂_{shell}, (b) DTP-activated CMS-SH_{core}-ATTO488_{shell}, (c) CMS-CysATTO633_{core}-ATTO488_{shell}, and (d) reduced CMS-SH_{core}-ATTO488_{shell}.

After the initial particle synthesis, the sample CMS-SH_{core}-NH₂_{shell} (Figure 7.3.3 a) shows the characteristic thiol vibration at 2584 cm^{-1} . The next synthesis step was the activation of the thiol-functionalities using DTP (Figure 7.3.3 b). The reaction is confirmed by Raman spectroscopy, by the emerging aromatic ring vibrations around 1000 cm^{-1} and the characteristic two bands for aromatic CN heterocycles at 1566 cm^{-1} and 1580 cm^{-1} . Additionally, the thiol vibration disappears upon disulfide formation. Further reaction of the activated thiols with dye-labeled cysteine leads to the removal of the aromatic vibrations in the Raman spectrum (Figure 7.3.3 c), and there are still no free thiol functionalities visible in the spectrum. After the reduction of the newly formed disulfides with 10 mM GSH in a reference experiment, the Raman spectrum shows the signal of free thiols again (Figure 7.3.3

d). The presence and absence of cysteine in the samples before and after the reduction are also confirmed with IR spectroscopy. The corresponding spectra can be found in Figure 7.3.4.

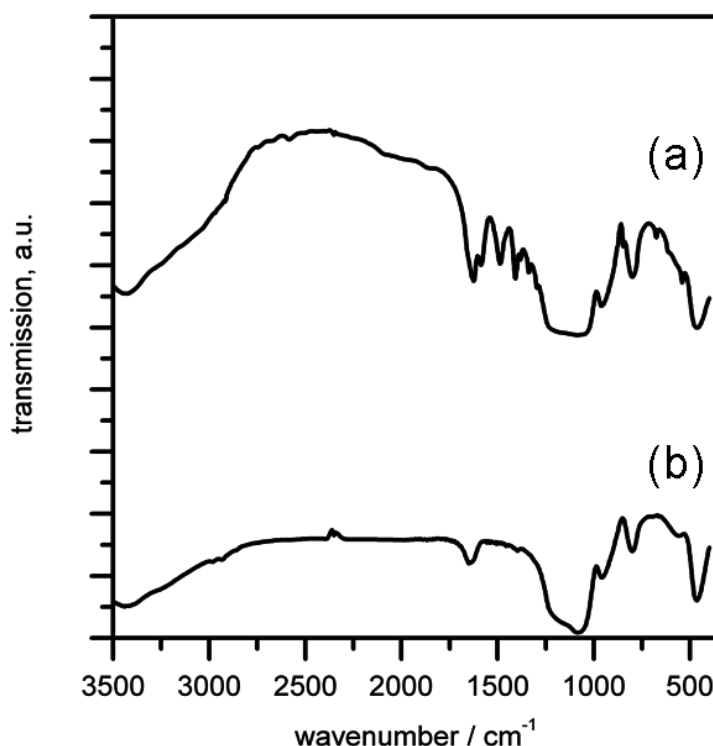


Figure 7.3.4 Infrared spectroscopy of (a) CMS with disulfide linked cysteine before reductive cleavage and (b) after reductive cleavage.

To examine the applicability of the system for GSH-responsive delivery, reference experiments were performed. For this purpose, the sample was transferred into our recently developed two-compartment fluorescence cuvette. A dialysis membrane separates the two compartments. While the CMS particles are too big to diffuse through the membrane, released, labeled cysteine can easily pass through the barrier and can be observed by fluorescence spectroscopy, applying an excitation wavelength of 633 nm. For the experiment, 1 mg of the sample in 200 μ L of water was separated by the membrane from 3 mL of water in the other compartment. While no detectable amount of cysteine was released before the addition of GSH, the release starts immediately after creation of the reductive milieu (10 mM GSH in both compartments, Figure 7.3.5). One hour after the GSH addition, the concentration

of cysteine remains stable. This maximum release was normalized to 100%.

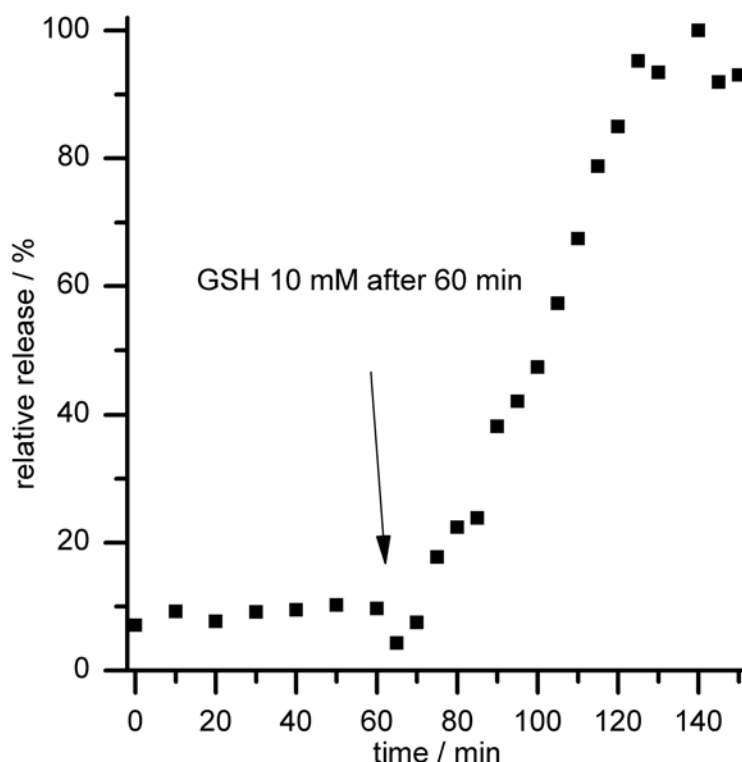


Figure 7.3.5 Release of CysATTO633 from the sample CMS-CysATTO633_{core}-ATTO_{488shell}.

The following analysis by microscopic methods was performed, analyzed and discussed in cooperation with Anna M. Sauer from the group of Prof. Christoph Bräuchle (LMU München).

To follow the release of dye-labeled cysteine at a single-particle level by fluorescence microscopy, the functionalized CMS nanoparticles were sedimented on glass coverslips and incubated with 10 mM GSH solution. Movies of the nanoparticles were recorded before ($t < 0$ min) and after ($t > 0$ min) addition of GSH solution. The mean fluorescence intensity of the ATTO633-labeled particles and the background was extracted and the intensity was plotted versus time as shown in Figure 7.3.6.

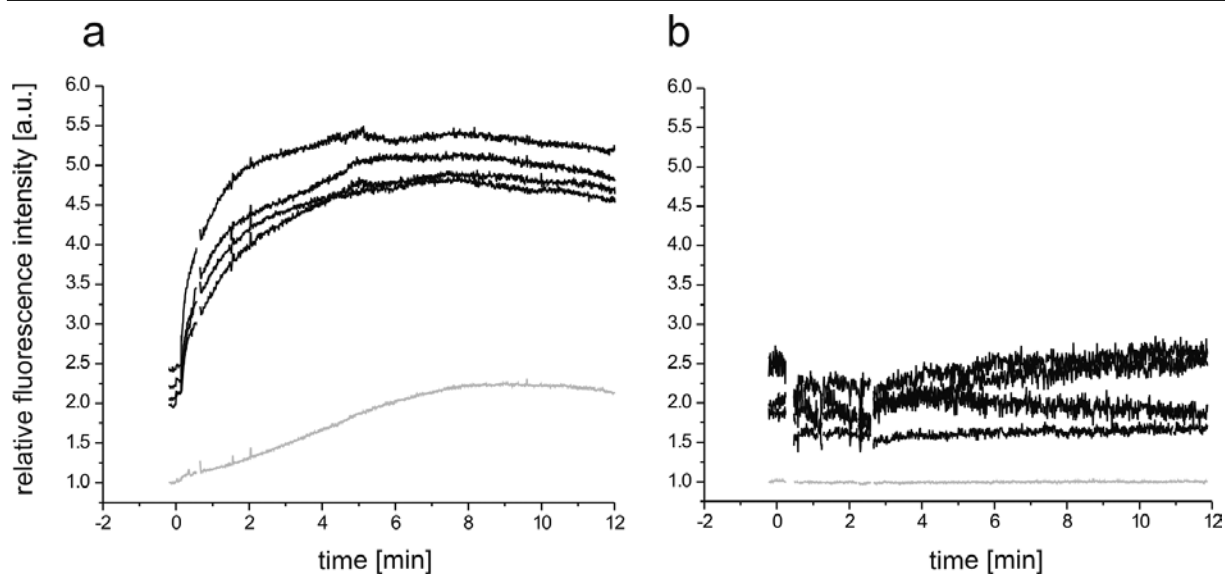


Figure 7.3.6 CysATTO633 release measured in vitro on a single-particle level. The mean fluorescence intensity of four single particles (black curves) on glass and background (gray curve) was extracted from a movie, normalized, and plotted versus time. The fluorescence intensity of ATTO633 was plotted for (a) redox cleavable CMS-CysATTO633_{core}-ATTO499_{shell} and (b) noncleavable control CMS-ATTO633_{core}-ATTO488_{shell} nanoparticles. GSH was added at $t = 0$ min. The movies were recorded at 642 nm illumination with an exposure time of 200 ms and a frame rate of 3.4 s^{-1} .

In Figure 7.3.6 a, the relative CysATTO633 fluorescence intensity of CMS-CysATTO633_{core}-ATTO488_{shell} nanoparticles (black) and background (gray) is displayed. After GSH addition the CysATTO633 fluorescence of the background (Figure 7.3.6 a, gray curve) increases up to a factor of 2.3 reaching a plateau after 8 min. The increase of CysATTO633 background fluorescence intensity indicates successful release of the dye from the functionalized CMS nanoparticles. Surprisingly, the CMS-CysATTO633_{core}-ATTO488_{shell} nanoparticles themselves (Figure 7.3.6 a, black curves) also showed an increase in Cys-ATTO633 fluorescence intensity. This increase by a factor of 2 or more occurred within two minutes and on a faster time scale than the increase in background fluorescence and was unexpected. Instead, we expected a decrease in the particle's CysATTO633 intensity after reductive dye

7. Role of Endosomal Escape for Disulfide-Based Drug Delivery from Colloidal Mesoporous Silica Evaluated by Live-Cell Imaging

release. However, the increase of nanoparticle-associated CysATTO633 intensity is easily explained by a de-quenching effect of the pore-bound CysATTO633. The tight packing of the dye molecules inside the pores promotes a self-quenching of CysATTO633 similar to tightly packed octadecyl rhodamine B or calcein in liposomes.⁴⁰ The release of dye lowers the dye concentration within the pores below the limit for self-quenching and the residual dye molecules start to fluoresce. The strong fluorescence of the nanoparticles also indicates that the disulfide-bound CysATTO633 is not completely released upon addition of GSH.

The self-quenching effect of tightly packed ATTO633 in a constrained environment such as mesoporous silica has not been reported before. In the present study, this self-quenching effect of CysATTO633 permits a well-detectable readout for dye release with excellent signal-to-noise ratio. As a control, CMS-ATTO633_{core}-ATTO488_{shell} nanoparticles without cleavable disulfide linker were examined under similar conditions (Figure 7.3.6 b). The fluorescence intensities of both the background and the particles remained constant and a de-quenching effect was not observed after addition of 10 mM GSH (at $t = 0$ min). This result confirms that only disulfide linker-bound dye is released by GSH and that the release is associated with a strong increase of nanoparticle fluorescence intensity. Another control experiment investigates the influence of TPPS_{2a} on the redox-sensitive bond between the particle and the labeled cysteine. It is shown, at a single particle level, that the disulfide bridge remains stable and the simple presence of the photosensitizer does not lead to a release of dye from the particle. The corresponding data of this experiment are plotted in the Appendix A-10, Figure A-10.1).

To summarize, we showed that release of disulfide bound CysATTO633 from CMS nanoparticles in 10 mM GSH can successfully be observed at a single-particle level. The release was accompanied by a de-quenching of the ATTO633 fluorescence and this effect permits a sensitive readout for the successful dye release.

To investigate whether the reductive milieu inside living cells is sufficient to induce dye

7. Role of Endosomal Escape for Disulfide-Based Drug Delivery from Colloidal Mesoporous Silica Evaluated by Live-Cell Imaging

release from CMS nanoparticles, we examined living cells exposed to CMS-CysATTO633_{core}-ATTO488_{shell} nanoparticles for up to 2 days. After 24 and 48 hours of exposure, confocal z-stacks of HuH7 cells were acquired by spinning disk confocal microscopy and the colocalization of CysATTO633_{core} with ATTO488_{shell} was evaluated. Successful cell entry and intracellular localization of the CMS nanoparticles was detected by their characteristic intracellular motion such as transport by motor proteins³⁰⁻³² (see movies 1 and 2 in the Appendix-CD) and the location within the z-stack. Transmission light images of the cells showed no morphological signs of toxicity within our observation time. After 49 hours, core-bound CysATTO633 and shell-bound ATTO488 signals of the intracellular particles were still colocalized. Additionally, fluorescence of free CysATTO633 in the cytoplasm was not detected. This indicates that within 49 hours, the disulfide-bound dye was not released. Two representative cells after 25 (Figure 7.3.7 a-c) and 49 hours (Figure 7.3.7 d-f) of incubation are displayed.

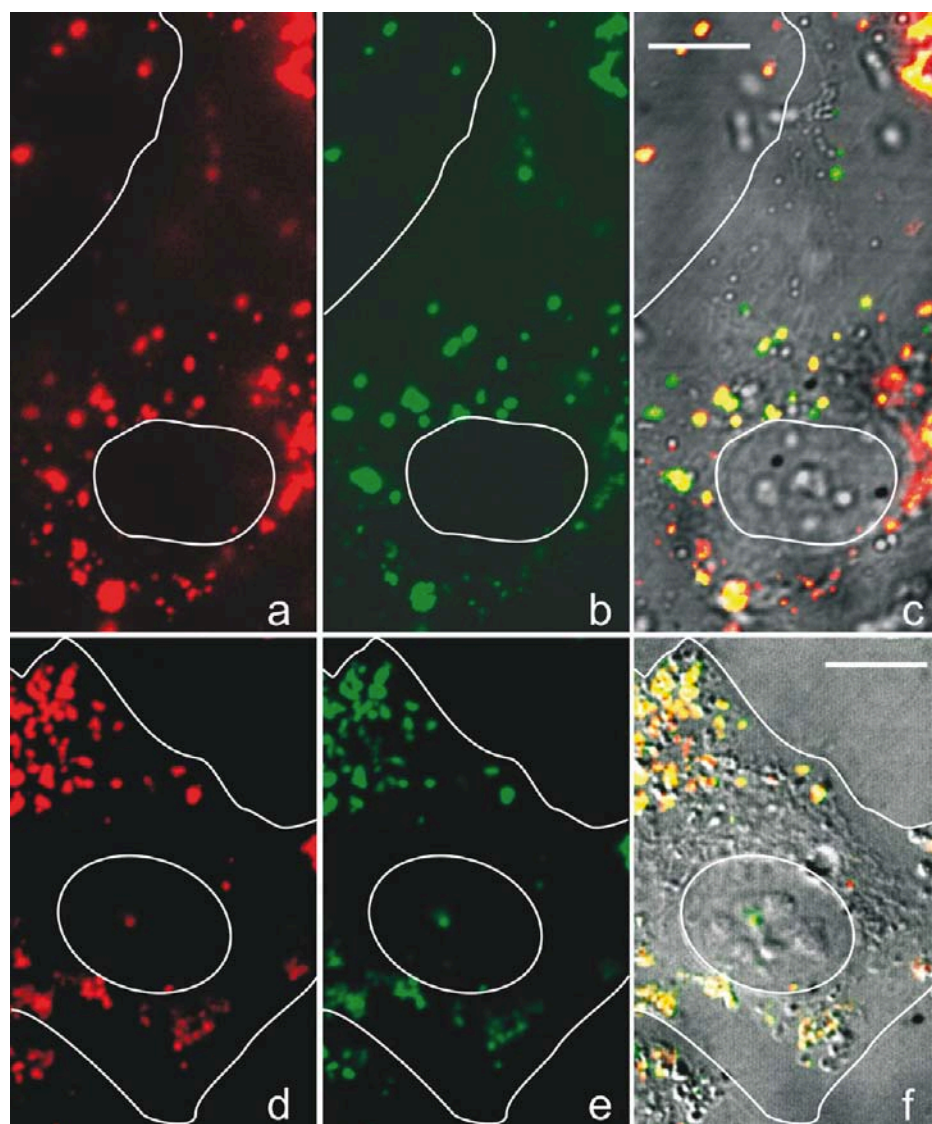


Figure 7.3.7 Confocal microscopy of living HuH7 cells exposed to CMS-CysATTO633_{core}-ATTO488_{shell} nanoparticles. Z-projections are shown consisting of the overlay of three planes inside an HuH7 cell exposed to CMS-CysATTO633_{core}-ATTO488_{shell} nanoparticles for 25 hours (a-c) and 49 hours (d-f). The cell nucleus is indicated by a white circle and the outer white line represents the cell border. Fluorescence of the particles' core (red a+d) and shell (green b+e) is highly colocalized as indicated by the yellow signal in the merged image (yellow c+f), which was superimposed on the transmitted light image of the cell. Scale bar: 10 μm . (Images recorded and analyzed by Anna M. Sauer, Group of Prof. Bräuchle).

7. Role of Endosomal Escape for Disulfide-Based Drug Delivery from Colloidal Mesoporous Silica Evaluated by Live-Cell Imaging

Fluorescence of the particle's CysATTO633-core (red a + d) and ATTO488-shell (green b + e) was colocalized as indicated by the yellow signal in the merged image (yellow c + f), which was superimposed on the transmission light image of the cell. Our results indicate that CMS-CysATTO633core-ATTO488shell nanoparticles are taken up into HuH7 cells without detectable signs of toxicity. Reductive release of ATTO633-labeled cysteine from internalized particles was not detected within 49 h of incubation. Our data and previous studies show that CMS nanoparticles are taken up into and transported within endosomes.²⁵ This implies that they are not accessible to the reductive milieu of the cytosol. Mortera et al. showed cytosolic fluorescence of reductively released cysteine.²⁵ However, they did not show the release process itself. In our mechanistic study, we could not detect reductive release of ATTO633 labeled cysteine.

To overcome the endosomal membrane barrier that separates CMS nanoparticles from the cytosol and to follow the release at a single cell level in real time, we employed photoinduced endosomal release. In this method, the photosensitizer TPPS_{2a} is incubated with the cells and incorporates into membranes via the endocytic pathway. TPPS_{2a} is excited into its singlet state by irradiation with 405 nm laser light, followed by intersystem crossing to its triplet state. This excited state is then quenched by triplet oxygen producing singlet oxygen. Singlet oxygen is able to oxidize unsaturated fatty acids, cholesterol, and amino acids and leads to a collapse of the endosomal membrane followed by release of the endosomal content into the cytosol. To label endosomes and monitor endosomal release, the fluid phase marker Alexa Fluor 488 Dextran (AFD) was added to the cells along with CMS-CysATTO633_{core}-NH₂_{shell} nanoparticles and the photosensitizer. AFD is internalized by fluid-phase endocytosis.⁴¹ After 18-24 hours of incubation, the cells were examined by wide-field fluorescence microscopy. All CMS nanoparticles that exhibit typical intracellular motion were found to be colocalized with AFD. This indicates successful internalization of the CMS nanoparticles into endosomes. The fluorescence intensity of the endosomes varied depending on the amount of internalized

AFD. However, the CysATTO633 fluorescence was quite weak, probably due to the self-quenching effect of the dye in the mesopores. Excitation of the photosensitizer was achieved by illumination of the sample with 405 nm laser for 1 minute (laser power density 0.2 W/cm²) this resulted in the termination of endosomal motion, as reported previously.³³ Depending on the amount of photosensitizer incorporated in the endosomal membrane, the endosomes were ruptured within 1-4 minutes, leading to a spontaneous release of AFD into the cytoplasm as indicated by a sudden drop in endosomal AFD fluorescence and increase in cytosolic fluorescence. Concomitant with endosomal rupture and AFD release, the fluorescence intensity of the CMS-CysATTO633_{core}-NH₂_{shell} nanoparticles increased due to the de-quenching effect as described above and presented in Figure 7.3.8 a.

Directly after photosensitizer activation the endosomes show still predominantly AFD fluorescence (Figure 7.3.8 b, depicted in green). Strikingly, only 4 minutes later the same endosomes show only CysATTO633 fluorescence (Figure 7.3.8 c, depicted in red). Please note that the diffuse red fluorescence within the nucleus area (big, white circle) is due to out of focus particle fluorescence.

7. Role of Endosomal Escape for Disulfide-Based Drug Delivery from Colloidal Mesoporous Silica Evaluated by Live-Cell Imaging

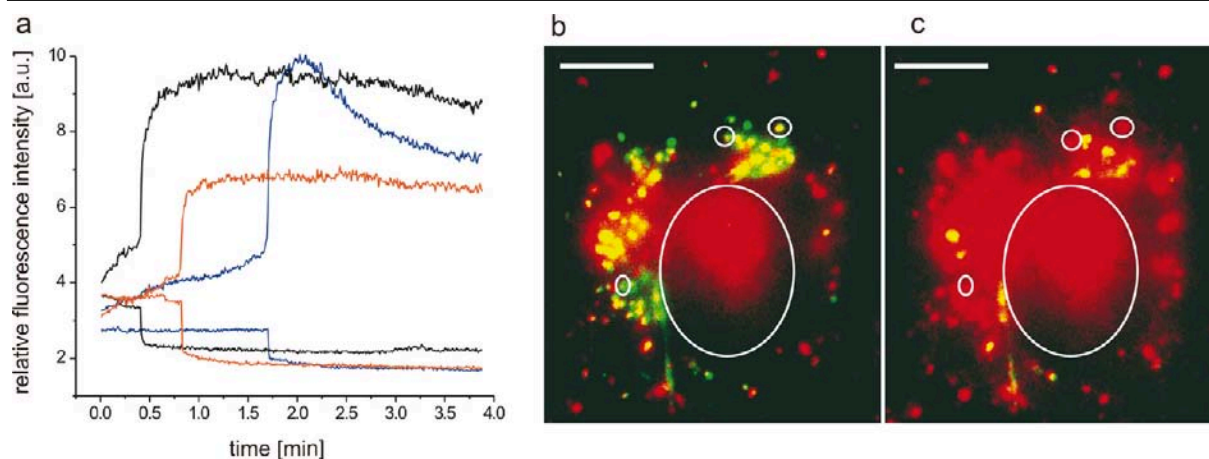


Figure 7.3.8 Photoinduced endosomal release of CMS-CysATTO633_{core}-NH_{2shell} and fluid phase marker AFD inside living HuH7 cells monitored by wide-field fluorescence microscopy. The cells were exposed to CMS-CysATTO633_{core}-NH_{2shell} overnight. (a) Intensity plot of three exemplary tracked endosomes (highlighted by small circles in b and c) over time. The fluorescence intensity of CysATTO633 (upper three curves) showed a sudden increase concomitant to the decrease in AFD fluorescence intensity (corresponding lower three curves) due to endosomal rupture and AFD-dye release. (b) Fluorescence microscopy image overlays of the CysATTO633 (red) and fluid phase marker AFD (green) signal at activation of the photosensitizer and (c) 4 min later. The cell nucleus is indicated with the large white circle. Scale bar: 10 μ m. (Data recorded and analyzed by Anna M. Sauer, Group of Prof. C. Bräuchle).

With a size of 10 kDa, AFD can diffuse almost freely after endosomal release, and it is dispersed within the cytosol.⁴² In contrast, due to their large size and impaired motion in the crowded cell interior the nanoparticles remain at their location. The corresponding movie is available as movie 3 in the Appendix-CD. We also performed a control measurement showing that activated TPPS_{2a} in solution has no influence on the fluorescence intensity of CMS-CysATTO633_{core}-NH_{2shell} particles on glass (see Figure A-10.1 in the Appendix). As a control measurement, non-cleavable CMS-ATTO633_{core}-NH_{2shell} nanoparticles without cysteine

linker were incubated with AFD and the photosensitizer for 12-24 hours. The internalized CMS-ATTO633_{core}-NH₂_{shell} nanoparticles showed colocalization with AFD until endosomal rupture. At endosomal rupture, the relative fluorescence intensity of AFD showed a sudden drop whereas the ATTO633 fluorescence remained largely constant with a slight intensity increase by a factor of 1.25 (Figure 7.3.9 a). This increase might be due to a small amount of unreacted dye inside the mesopores, which is released from the endosome after disruption of the endosomal membrane. The disruption of the endosomal membrane and release of AFD occurred within 4 min, and the CMS-ATTO633_{core}-NH₂_{shell} nanoparticle fluorescence remained at the former endosomal regions (Figure 7.3.9 c). Figure 7.3.9 a displays the fluorescence intensity of AFD and CMSATTO633_{core}-NH₂_{shell} nanoparticles of three representative endosomes (highlighted in Figure 7.3.9 b,c with small circles). The corresponding movie 4 is available in the Appendix-CD. The missing increase in ATTO633 fluorescence intensity of non-cleavable dye indicates that ATTO633 is maintained in the pores and did not escape into the cytosol as observed for the disulfide-bound dye.

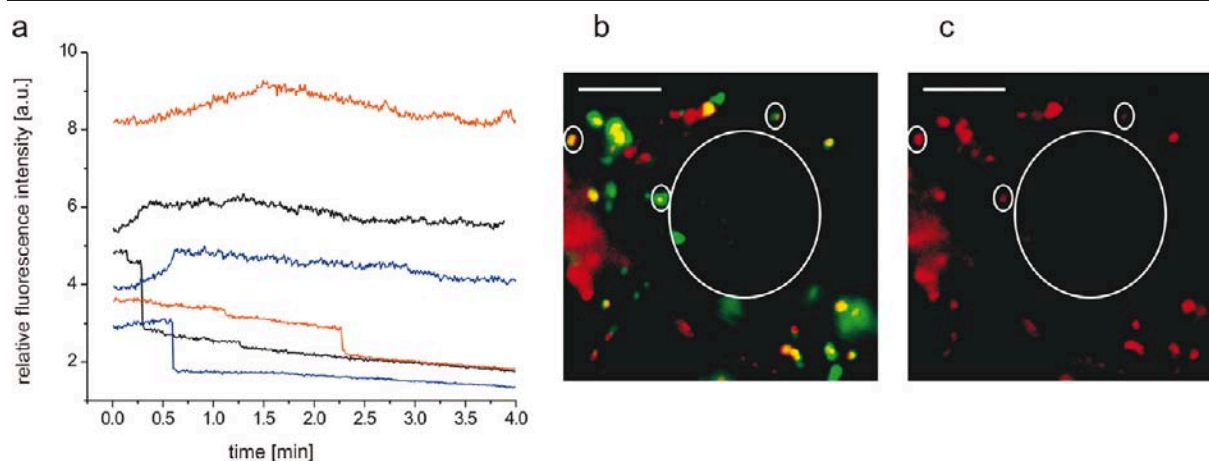


Figure 7.3.9 Photoinduced endosomal release of CMS-ATTO633_{core}-NH₂_{shell} and fluid phase marker AFD inside living HuH7 cells monitored by wide-field fluorescence microscopy. The cells were exposed to CMS-ATTO633_{core}-NH₂_{shell} overnight. (a) Intensity plot of three exemplary tracked endosomes (highlighted by small circles in b and c) over time. The fluorescence intensity of ATTO633 (upper three curves) showed no or only slight fluorescence increase concomitant to the decrease in AFD fluorescence intensity (corresponding lower three curves) due to endosomal rupture and AFD-dye release. (b) Fluorescence microscopy image overlays of the ATTO633 (red) and fluid phase marker AFD (green) signal at activation of the photosensitizer and (c) 4 min later. The cell nucleus is indicated with the large white circle. Scale bar: 10 μ m. (Data recorded and analyzed by Anna M. Sauer, Group of Prof. Bräuchle).

7.4 Conclusion

To conclude, our results show that CMS-CysATTO633_{core} nanoparticles were endocytosed by HuH7 cells without visible signs of toxicity. However, disulfide-bound dye in the pore system of internalized nanoparticles was not released within 49 hours of observation. Inefficient endosomal escape of the nanoparticles is generally a bottleneck for molecular delivery into the cytoplasm. After photochemical rupture of the endosomes by means of a photosensitizer, CMS-CysATTO633_{core} nanoparticles successfully released disulfide-bound CysATTO633

into the cytoplasm showing that the reducing milieu of the cytoplasm is sufficient to cleave the cysteine linker. In case of non-cleavable CMSATTO633_{core} nanoparticles without cysteine linker, release of ATTO633 was not observed. In addition, we show for the first time that linkage of ATTO633 at high concentration in the pores of silica nanoparticles results in quenching of the ATTO633 fluorescence. Release of dye from the pores promotes a strong de-quenching effect providing an intense fluorescence signal with excellent signal-to-noise ratio for single particle imaging.

7.5 References

- (1) Vallet-Regi, M.; Balas, F.; Arcos, D. *Angewandte Chemie, International Edition* **2007**, *46*, 7548.
- (2) Descalzo, A. B.; Martinez-Manez, R.; Sancenon, F.; Hoffmann, K.; Rurack, K. *Angewandte Chemie, International Edition* **2006**, *45*, 5924.
- (3) Aznar, E.; Martinez-Manez, R.; Sancenon, F. *Expert Opinion on Drug Delivery* **2009**, *6*, 643.
- (4) Trewyn, B. G.; Slowing, I. I.; Giri, S.; Chen, H.-T.; Lin, V. S. Y. *Accounts of Chemical Research* **2007**, *40*, 846.
- (5) Slowing, I. I.; Vivero-Escoto, J. L.; Wu, C.-W.; Lin, V. S. Y. *Advanced Drug Delivery Reviews* **2008**, *60*, 1278.
- (6) Saha, S.; Leung, K. C. F.; Nguyen, T. D.; Stoddart, J. F.; Zink, J. I. *Advanced Functional Materials* **2007**, *17*, 685.
- (7) Schlossbauer, A.; Kecht, J.; Bein, T. *Angewandte Chemie, International Edition* **2009**, *48*, 3092.
- (8) Patel, K.; Angelos, S.; Dichtel, W. R.; Coskun, A.; Yang, Y.-W.; Zink, J. I.; Stoddart, J. F. *Journal of the American Chemical Society* **2008**, *130*, 2382.

7. Role of Endosomal Escape for Disulfide-Based Drug Delivery from Colloidal Mesoporous Silica Evaluated by Live-Cell Imaging

- (9) Bernardos, A.; Aznar, E.; Marcos, M. D.; Martinez-Manez, R.; Sancenon, F.; Soto, J.; Barat, J. M.; Amoros, P. *Angewandte Chemie, International Edition* **2009**, *48*, 5884.
- (10) Park, C.; Kim, H.; Kim, S.; Kim, C. *Journal of the American Chemical Society* **2009**, *131*, 16614.
- (11) Climent, E.; Bernardos, A.; Martinez-Manez, R.; Maquieira, A.; Marcos, M. D.; Pastor-Navarro, N.; Puchades, R.; Sancenon, F.; Soto, J.; Amoros, P. *Journal of the American Chemical Society* **2009**, *131*, 14075.
- (12) Lu, J.; Choi, E.; Tamanoi, F.; Zink, J. I. *Small* **2008**, *4*, 421.
- (13) Nguyen, T. D.; Leung, K. C. F.; Liong, M.; Liu, Y.; Stoddart, F.; Zink, J. I. *Advanced Functional Materials* **2007**, *17*, 2101.
- (14) Mal, N. K.; Fujiwara, M.; Tanaka, Y. *Nature (London, United Kingdom)* **2003**, *421*, 350.
- (15) Mal, N. K.; Fujiwara, M.; Tanaka, Y.; Taguchi, T.; Matsukata, M. *Chemistry of Materials* **2003**, *15*, 3385.
- (16) Zhu, Y.; Fujiwara, M. *Angewandte Chemie (International ed. in English)* **2007**, *46*, 2241.
- (17) Angelos, S.; Choi, E.; Voegtle, F.; De Cola, L.; Zink, J. I. *Journal of Physical Chemistry C* **2007**, *111*, 6589.
- (18) Liu, R.; Zhao, X.; Wu, T.; Feng, P. *Journal of the American Chemical Society* **2008**, *130*, 14418.
- (19) Aznar, E.; Casassus, R.; Garcia-Acosta, B.; Marcos, M. D.; Martinez-Manez, R.; Sancenon, F.; Soto, J.; Amoros, P. *Advanced Materials (Weinheim, Germany)* **2007**, *19*, 2228.
- (20) Nguyen, T. D.; Leung, K. C. F.; Liong, M.; Pentecost, C. D.; Stoddart, J. F.; Zink, J. I. *Organic Letters* **2006**, *8*, 3363.

7. Role of Endosomal Escape for Disulfide-Based Drug Delivery from Colloidal Mesoporous Silica Evaluated by Live-Cell Imaging

- (21) Angelos, S.; Khashab, N. M.; Yang, Y.-W.; Trabolsi, A.; Khatib, H. A.; Stoddart, J. F.; Zink, J. I. *Journal of the American Chemical Society* **2009**, *131*, 12912.
- (22) Casasus, R.; Marcos, M. D.; Martinez-Manez, R.; Ros-Lis, J. V.; Soto, J.; Villaescusa, L. A.; Amoros, P.; Beltran, D.; Guillem, C.; Latorre, J. *Journal of the American Chemical Society* **2004**, *126*, 8612.
- (23) Casasus, R.; Climent, E.; Marcos, M. D.; Martinez-Manez, R.; Sancenon, F.; Soto, J.; Amoros, P.; Cano, J.; Ruiz, E. *Journal of the American Chemical Society* **2008**, *130*, 1903.
- (24) Lai, C.-Y.; Trewyn, B. G.; Jeftinija, D. M.; Jeftinija, K.; Xu, S.; Jeftinija, S.; Lin, V. S. Y. *Journal of the American Chemical Society* **2003**, *125*, 4451.
- (25) Mortera, R.; Vivero-Escoto, J.; Slowing, I. I.; Garrone, E.; Onida, B.; Lin, V. S. Y. *Chemical Communications (Cambridge, United Kingdom)* **2009**, 3219.
- (26) Hernandez, R.; Tseng, H.-R.; Wong, J. W.; Stoddart, J. F.; Zink, J. I. *Journal of the American Chemical Society* **2004**, *126*, 3370.
- (27) Nguyen, T. D.; Liu, Y.; Saha, S.; Leung, K. C. F.; Stoddart, J. F.; Zink, J. I. *Journal of the American Chemical Society* **2007**, *129*, 626.
- (28) Nguyen, T. D.; Tseng, H.-R.; Celestre, P. C.; Flood, A. H.; Liu, Y.; Stoddart, J. F.; Zink, J. I. *Proceedings of the National Academy of Sciences of the United States of America* **2005**, *102*, 10029.
- (29) West, K. R.; Otto, S. *Current Drug Discovery Technologies* **2005**, *2*, 123.
- (30) Bausinger, R.; von Gersdorff, K.; Braeckmans, K.; Ogris, M.; Wagner, E.; Braeuchle, C.; Zumbusch, A. *Angewandte Chemie, International Edition* **2006**, *45*, 1568.
- (31) de Bruin, K.; Ruthardt, N.; von Gersdorff, K.; Bausinger, R.; Wagner, E.; Ogris, M.; Braeuchle, C. *Molecular Therapy* **2007**, *15*, 1297.
- (32) Sauer, A. M.; de Bruin, K. G.; Ruthardt, N.; Mykhaylyk, O.; Plank, C.; Braeuchle, C. *Journal of Controlled Release* **2009**, *137*, 136.

- (33) de Bruin, K. G.; Fella, C.; Ogris, M.; Wagner, E.; Ruthardt, N.; Braeuchle, C. *Journal of Controlled Release* **2008**, *132*, e1.
- (34) Austin, C. D.; Wen, X.; Gazzard, L.; Nelson, C.; Scheller, R. H.; Scales, S. J. *Proceedings of the National Academy of Sciences of the United States of America* **2005**, *102*, 17987.
- (35) Berg, K.; Selbo, P. K.; Prasmickaite, L.; Tjelle, T. E.; Sandvig, K.; Moan, J.; Gaudernack, G.; Fodstad, O.; Kjolsrud, S.; Anholt, H.; Rodal, G. H.; Rodal, S. K.; Hogset, A. *Cancer Research* **1999**, *59*, 1180.
- (36) Berg, K.; Selbo, P. K.; Weyergang, A.; Dietze, A.; Prasmickaite, L.; Bonsted, A.; Engesaeter, B. O.; Angell-Petersen, E.; Warloe, T.; Frandsen, N.; Hogset, A. *Journal of Microscopy (Oxford, United Kingdom)* **2005**, *218*, 133.
- (37) Nakabayashi, H., Taketa, T., Miyano, K., Yamane, T., and Sato, J. *Cancer Research* **1982**, *42*, 3858.
- (38) Kecht, J.; Schlossbauer, A.; Bein, T. *Chemistry of Materials* **2008**, *20*, 7207.
- (39) Cauda, V.; Schlossbauer, A.; Kecht, J.; Zurner, A.; Bein, T. *Journal of the American Chemical Society* **2009**, *131*, 11361.
- (40) Pollock, S.; Antrobus, R.; Newton, L.; Kampa, B.; Rossa, J.; Latham, S.; Nichita, N. B.; Dwek, R. A.; Zitzmann, N. *FASEB Journal* **2010**, *24*, 1866.
- (41) Berlin, R. D.; Oliver, J. M. *The Journal of cell biology* **1980**, *85*, 660.
- (42) Dauty, E.; Verkman, A. S. *Journal of Biological Chemistry* **2005**, *280*, 7823.

8. Photosensitizer-Functionalized PEGylated Colloidal Mesoporous Silica

8.1 Introduction

In recent years, mesoporous silica materials were investigated for new and advanced applications like targeted cancer therapy or other biomedical challenges.¹⁻³ It was demonstrated that multifunctional constructions of silica nanocarriers are able to release cargo only under defined conditions. Once in the cell, the released cargo is able to induce metabolic processes within these cells. For example, the release of insulin and cyclic adenosine monophosphate was shown upon sugar-induced removal of endcaps from mesoporous silica nanoparticles.⁴ Another approach uses the reductive cleavage of disulfide-bridged compounds bound to the pore walls of mesoporous silica nanoparticles.⁵ As the intracellular milieu is referred to be reductive, a cleavage of these disulfide bridges occurs in the cells. However, we have recently shown that endosomal escape represents a bottleneck for this approach,⁶ since the intra-endosomal milieu does not have these reductive properties.⁷ Using photoactive compounds that induce the endosomal escape by creating singlet oxygen has been demonstrated to be a powerful tool to overcome this barrier.

The concept of photodynamic therapy includes the use of photosensitizers (PS) to induce oxidative stress by light irradiation. The generation of singlet oxygen leads to the oxidation of membrane structures and thus induces the cell death.⁸⁻¹¹ However, most of the approaches to incorporate PS into mesoporous silica lack control over the spatial distribution of the PS, as they are not covalently fixed to the particles. This leads to an uncontrolled leaching of the compounds, leading to immediate cell death by oxidation of the cellular membranes. For a more precise function of PS-equipped nanodevices that have the aim to solely giving access of the applied drug carrier to the cytosol, it is desirable to bind the PS directly to the surface of the mesoporous particles. This approach would concentrate photoactivity to the direct environment of the nanoparticles and thus would not impact endosomes not loaded with

particles. A first approach to covalently incorporate porphyrin-functionality in/on mesoporous silica structures was demonstrated very recently.¹² For the synthesis, the authors of this study describe the creation of a hematoporphyrin-silane precursor, but no analytical evidence for the described product was given. A similar approach was published shortly thereafter by another group.¹³ The obtained material was used in photodynamic therapy. This publication centers on the synthesis of an anionic, sulfonated porphyrin derivative featuring one free amino group. This amino group was further reacted with isocyanatopropyltriethoxysilane, resulting in a water-soluble porphyrin sol-gel precursor. However, analytical data of the reaction product were not provided.

In this Chapter, we present the synthesis of outer-surface porphyrin-functionalized, colloidal mesoporous silica particles (CMS). For this purpose, an amino-terminated derivative of protoporphyrin-IX was synthesized and characterized. Subsequently, it was covalently attached to a shell of poly(ethylene glycol) (PEG) attached to dye-labeled colloidal mesoporous silica nanoparticles. As indicated in the literature, PEG shells around nanomaterials enhance their colloidal and structural stability in biological environments.^{14,15} Additionally, PEGylation was reported to protect against capture by the reticuloendothelial system in the blood stream (stealth effect).¹⁶

The functionality of the obtained nanomaterial was investigated in HuH7 cancer cells by confocal fluorescence microscopy on a single cell level. An important prerequisite for the design of the particles is our recently developed delayed co-condensation approach in order to achieve functionality exclusively on the outer surface of the particle.¹⁷ This work was carried out as a joint project with Anna M. Sauer from the laboratory of Prof. Christoph Bräuchle (LMU München), who performed all microscopic investigations.

8.2 Experimental Section

8.2.1 Applied chemicals

Tetraethylorthosilicate (TEOS, Fluka, >99%), (3-mercaptopropyl)-triethoxysilane (MPTES, Gelest, 95%), (3-aminopropyl)-triethoxysilane (APTES, Fluka, >97%), cetyltrimethylammonium bromide (CTAC, Fluka, 25% in H₂O), triethanolamine (TEA, Aldrich, 98%), Atto488-NHS ester and Atto633-NHS ester (both Atto-Tec), tetrahydrofuran (THF, Acros, 99.8%), protoporphyrin IX (Sigma, >95%), p-phenylenediamine (Sigma, 95%), triethylamine (Sigma, 99%), ethyl chloroformate (Fluka, >98%), ammonium nitrate (Sigma, 99%), 1-maleinimido-3-oxo-7,10,13,16,19,22,25,28-octaoxa-4-azahentriacontan-31-oic acid (mal-dPEG(8)-COOH, Iris Biotech), N-hydroxysuccinimide (NHS, Aldrich, 98%), N-(3-dimethylaminopropyl)-N'-ethylcarbodiimide (EDC, Sigma, 97%), Alexa Fluor 488 Dextran (AFD, MW 10 kDa, Invitrogen), cell culture media and fetal calf serum (Invitrogen). All chemicals were used as received without further purification. Doubly distilled water from a Millipore system (Milli-Q Academic A10) was used for all synthesis and purification steps.

8.2.2 Synthesis of CMS-NH₂_{core}-SH_{shell} by sequential co-condensation

The colloidal mesoporous silica particles were synthesized by using our recently developed sequential co-condensation approach, as described in Chapter 3.^{17,18} A mixture of TEOS (1.63 g, 7.82 mmol), APTES (104 mg, 0.47 mmol), and TEA (14.3 g, 95.6 mmol) in a polypropylene reactor were heated for 20 minutes at 90 °C under static conditions. Then, a solution of CTAC (25 % in water, 2.41 mL, 1.83 mmol) and water (21.7 g, 1.21 mmol) preheated to 60 °C was added and the mixture was allowed to cool to room temperature. The resulting mixture was stirred at room temperature for 20 minutes. The total amount of 138.2 mg TEOS (0.922 mmol) was added in four equal increments every three minutes, followed by another 30 minutes of stirring at room temperature. Next, a 1:1 mixture of TEOS and MPTES (each 92.5 μmol, 19.27 mg TEOS, 22.8 mg MPTES) was added to the reaction mixture. The

reaction was then allowed to stir for another 12 hours. After the addition of 100 mL ethanol, the CMS were separated by centrifugation, redispersed in ethanol and subjected to the template extraction procedure described below.

8.2.3 Template extraction from CMS

The extraction of the organic template from the porous silica framework was achieved by heating 1 g of silica twice in 100 mL of an ethanolic solution of ammonium nitrate (2 g NH_4NO_3 in 100 mL ethanol), followed by 30 minutes under reflux in a solution of 4 g concentrated hydrochloric acid in 100 mL ethanol. After each step, the material was washed with 100 mL ethanol. After the extraction, the particles were collected by centrifugation and redispersed in 100 mL of absolute ethanol.

8.2.4 PEGylation of CMS-NH₂_{core}-SH_{shell} with maleinimido-3-oxo-7,10,13,16,19,22,25,28-octaoxa-4-azahentriacontan-31-oic acid (Mal-dPEG(8)-COOH, sample CMS-NH₂_{core}-PEG_{shell})

An ethanolic suspension containing 1 mg of CMS-NH₂_{core}-SH_{shell} was centrifuged and redispersed in 500 μL of water. Subsequently, 100 μL of a solution of Mal-dPEG(8)-COOH (10 mg/mL, 1.69 μmol) in water was added. The reaction mixture was stirred for 14 hours at room temperature. In order to remove the excess of Mal-dPEG(8)-COOH, the particles were washed three times with each 1 mL of water, followed by centrifugation. Finally, the sample was redispersed in 500 μL of absolute ethanol, yielding the sample CMS-NH₂_{core}-PEG_{shell}.

8.2.5 Dye Labeling of CMS-NH₂_{core}-PEG_{shell} (sample CMS-Atto488_{core}-PEG_{shell}; sample CMS-Atto633_{core}-PEG_{shell})

The amount of 15 μL of a solution of the respective Atto-NHS-ester (1 mg dye in 500 μL dry DMF) was added to the as-synthesized sample CMS-NH₂_{core}-PEG_{shell}. The resulting mixture

was stirred for 4 hours at room temperature. Subsequently, the sample was washed by several cycles of centrifugation with 1 mL absolute ethanol each, until no free dye was visible in the supernatant. Finally, the sample was dispersed in 500 μ L of THF for further functionalization.

8.2.6 Synthesis of Protoporphyrin-IX-bis(phenyleneaminoamide) (PP-NH₂)

In a dry and darkened 100 mL three-neck flask, protoporphyrin-IX (100 mg, 0.178 mmol, 1 eq.) was dissolved in 20 mL of water-free tetrahydrofuran and cooled to 0 °C under nitrogen atmosphere. Then, triethylamine (2.45 mL, 17.7 mmol, 100 eq.) was added to the solution. Ethyl chloroformate (1.7 mL, 17.9 mmol, 100 eq.) was added slowly (30 minutes) under stirring to the solution by using a dropping funnel. The resulting mixture **1** was stirred for 2 hours at 0 °C.

In a second dried and darkened 100 mL three-neck flask, finely powdered p-phenylene diamine (1.95 g, 17.9 mmol, 100 eq.) was dissolved in 10 mL THF under nitrogen atmosphere. To this solution, mixture **1** was added slowly with a syringe. The resulting mixture was stirred for 24 hours at room temperature in the dark. The solvent was removed *in vacuo*. The resulting precipitate was suspended in 15 mL of ice-cold water. The resulting suspension was filtered and washed three times with 15 mL each of ice-cold water. PP-NH₂ was obtained as a brown precipitate (85 mg, 0.114 mmol, 64%).

Analytcs: MS (ESI, acetonitrile/water): $m/z = 743.38 [m+H]^+$, $765.36 [m+Na]^+$; exact formula mass: 742.37 g/mol; IR (emerging amide vibrations 1550 cm^{-1} , 1634 cm^{-1})

8.2.7 Attachment of PP-NH₂ to CMS-Atto_{core}-PEG_{shell}

The as-synthesized sample CMS-Atto_{core}-PEG_{shell} (based on 1 mg silica particles, approximately 0.17 μ mol –COOH) was mixed with PP-NH₂ (2 mg, 2.7 μ mol). Subsequently, *N*-hydroxysuccinimide (2.3 mg, 20 μ mol) and EDC (3.5 μ l, 20 μ mol) were added. The resulting mixture was stirred at room temperature in the dark for 14 hours. Subsequently, the

sample was washed 3 times with 1 mL THF each and 1 mL water. Finally, the sample was redispersed in 500 μ L water and filtered through a Rotband[®] filter in order to remove large aggregates, yielding the samples CMS-Atto488_{core}-PS_{shell} or CMS-Atto633_{core}-PS_{shell}.

8.2.8 Cell culture

HuH7 cells were grown in Dulbecco's modified Eagle's medium (DMEM):F12 (1:1) with Glutamax I medium supplemented with 10% fetal calf serum at 37 °C in 5% CO₂ humidified atmosphere. To reduce autofluorescence of the cells, the medium was changed to DMEM:F12 supplemented with 10% B-27 two days before seeding. The cells were seeded on collagen A-coated LabTek chambered cover glass (Nunc).

8.3 Results and Discussion

Functionalized CMS with 3-mercaptopropyl functionality on the outer surface of the particles and 3-aminopropyl-groups in the core were synthesized according to our recently published procedure (see also Chapter 3; sample CMS-NH₂_{core}-SH_{shell}).¹⁷ The particles feature diameters around 80 nm (derived from dynamic light scattering, DLS), NLDT pores sizes around 4 nm and BET surface area of 1000 m²g⁻¹. The corresponding isotherm and pore size distribution is displayed in the Appendix (Figure A-11.1, A-11.2). The obtained number-weighted particle size distribution, as derived from DLS, is plotted in Figure 8.3.1.

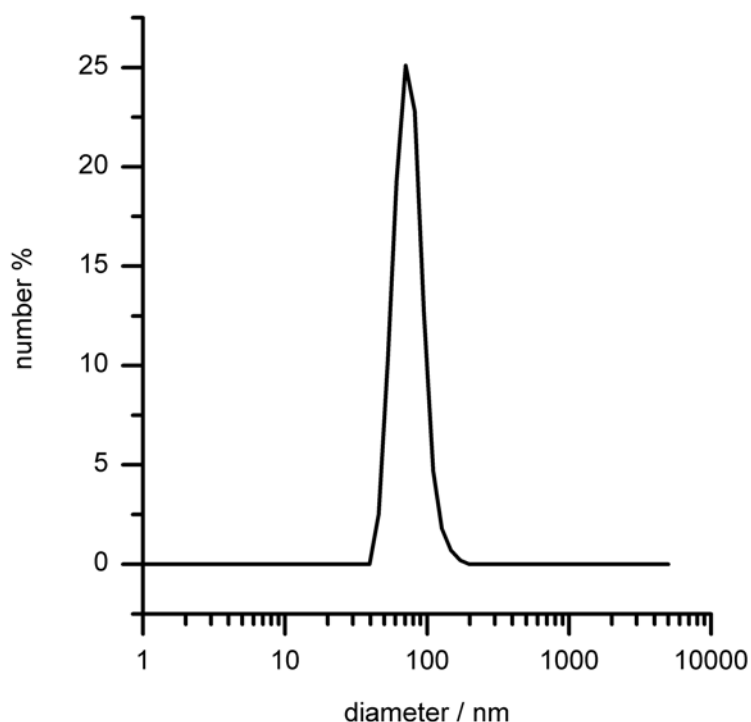


Figure 8.3.1 Number-weighted particle size distribution of the sample CMS-NH₂core-SH_{shell}.

Subsequently, the particles were covered with a bifunctional polyethyleneglycol linker (maleimide-dPEG₈-COOH) featuring eight ethylene glycol units. One end of the applied linker features a maleimide group, which attaches to the thiol-carrying surface of the CMS *via* Michael-addition, giving the sample CMS-NH₂core-PEG_{shell}. The opposite carboxylic acid terminus of the linker protrudes into the solvent. The next synthesis step includes the fluorescent labeling of the amino-functionalized core of CMS-NH₂core-PEG_{shell} with Atto488 fluorescence dye (Sample CMS-Atto488_{core}-PEG_{shell}). The attached fluorescent dye allows further investigation of the synthesized materials by fluorescence microscopy.

In order to react protoporphyrin IX as photosensitizer (PS) *via* an amide bond to the surface of CMS-Atto488_{core}-PEG_{shell}, an amino-modified protoporphyrin-IX (PP-NH₂) is needed. The synthesis scheme of a modified literature procedure for the synthesis of PP-NH₂ can be found in Figure 8.3.2.¹⁹

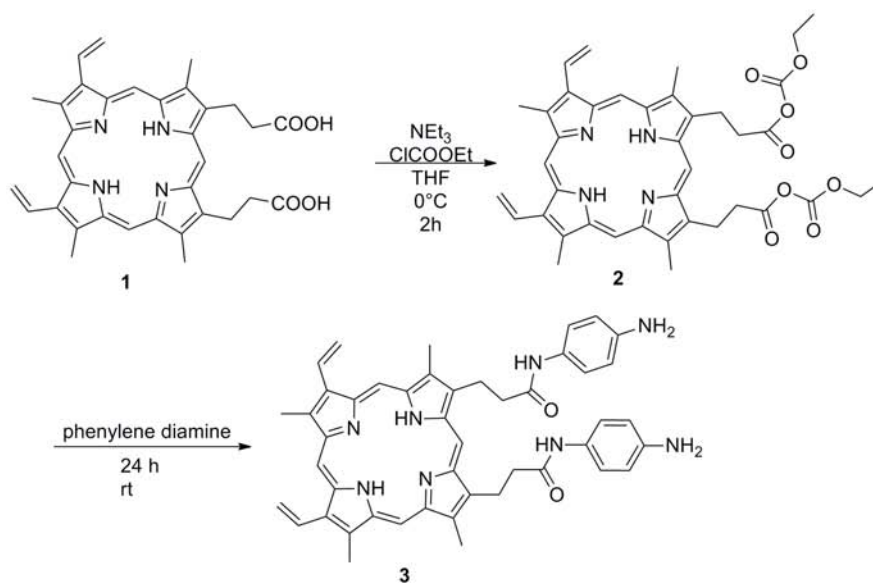


Figure 8.3.2 Synthesis scheme for PP-NH₂.

Protoporphyrin IX (PP-IX, **1**) is reacted with ethyl chloroformate to give the mixed anhydride **2**. Further reaction of **2** with a large excess of *p*-phenylene diamine yields the amide **3** (PP-NH₂). The obtained compound PP-NH₂ was characterized by IR spectroscopy and ESI mass spectrometry. The IR-spectrum shows a shift of the C=O stretching vibration from 1702 cm⁻¹ to 1648 cm⁻¹ due to the amide formation (Figure 8.3.3 a,b). Correspondingly, the N-H bending signal (amide II-band) appears at 1515 cm⁻¹ in the sample PP-NH₂ (Figure 8.3.3b).

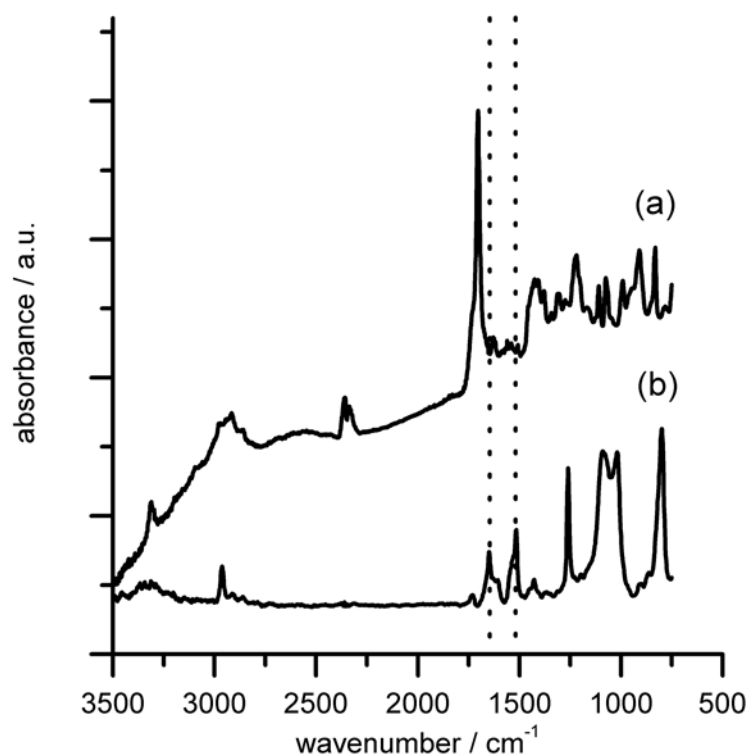


Figure 8.3.3 ATR-IR spectra of the samples (a) PP-IX and (b) PP-NH₂ (spectra are offset).

The successful synthesis was also confirmed by electron spray ionization mass spectrometry (ESI-MS). The corresponding spectrum can be found in the appendix (A-12).

CMS-Atto488_{core}-PEG_{shell} and PP-NH₂ were subsequently reacted in a *N*-(3-dimethylaminopropyl)-*N'*-ethylcarbodiimide (EDC) assisted amidation to yield the photosensitizer-functionalized sample CMS-Atto488_{core}-PS_{shell} (Figure 8.3.3).

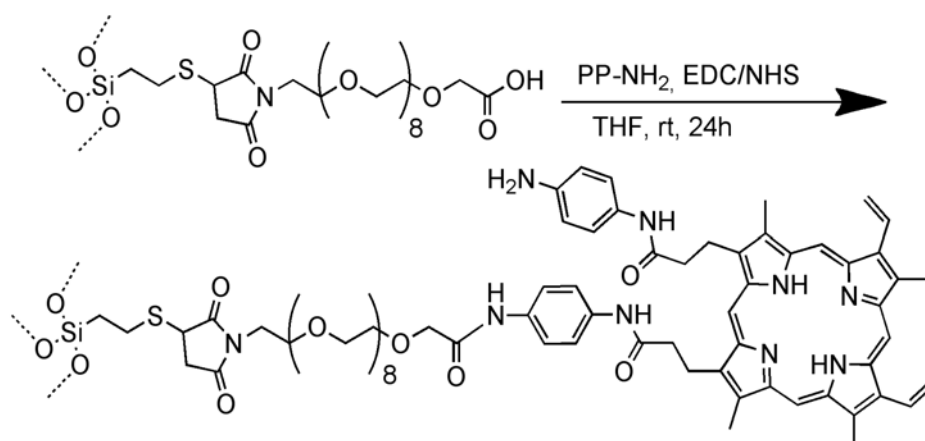
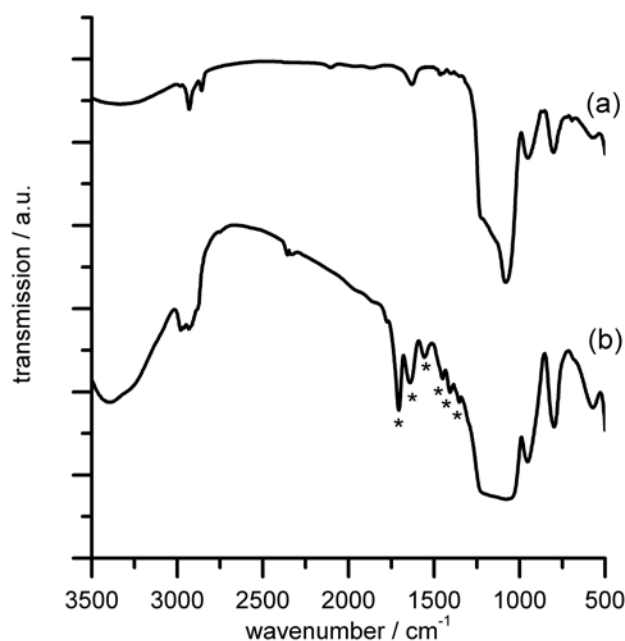


Figure 8.3.3 Attachment of PP-NH₂ to the PEGylated mesoporous silica nanoparticle.

The PEGylation reaction step (CMS → CMS-PEG) was characterized by IR-Spectroscopy (Figure 8.3.4).

**Figure 8.3.4** IR-spectra of the samples (a) CMS and (b) CMS-NH₂core-PEG_{shell}. The bands discussed in the text are marked with asterisks

The sample CMS shows the typical bands expected for organofunctionalized silica structures (Figure 8.3.4a). The band below 1300 cm⁻¹ can be attributed to silica framework vibrations. The organic functionality (mercaptopropyl- and aminopropyl-) is observed between 2800 cm⁻¹ and 2900 cm⁻¹, visible as CH₂ stretching vibrations. Signals between 2900 cm⁻¹ and 3000 cm⁻¹ occur due to ethoxy-groups on the surface attached mainly during the extraction procedure. The origin of these bands has been described earlier in the literature.²⁰ However, the signals of the sample CMS-NH₂core-PEG_{shell} clearly show the increasing functionalization (Figure 8.3.3b). The typical CH₂ deformation- and wagging-vibrations of aliphatic ethers are visible as emerging bands at 1456 cm⁻¹, 1411 cm⁻¹ and 1362 cm⁻¹. The strong amide bands at 1637 cm⁻¹ and 1550 cm⁻¹ (amide I and amide II) are attributed to the maleimide-functions included

in the applied maleimide-dPEG₈-COOH linker. The signal at 1710 cm⁻¹ can be assigned to the C=O stretch of the terminal carboxylic acid.

The successful covalent attachment of PP-NH₂ to the particle (Figure 8.3.2, Sample CMS-Atto488_{core}-PS_{shell}) was demonstrated by fluorescence spectroscopy after several washing steps in THF (Figure 8.3.5).

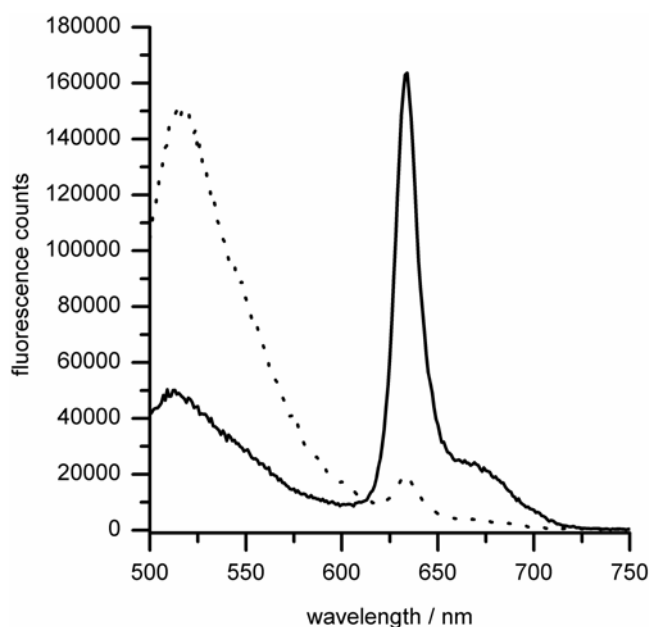


Figure 8.3.5. Fluorescence emission spectra of the sample CMS-Atto488_{core}-PS_{shell} with an excitation wavelength of 488 nm (dotted line) and 405 nm (solid line).

Excitation with 488 nm gives an emission maximum at 515 nm, corresponding to the particles' fluorescence dye label. Excitation of the same sample 408 nm shows a sharp emission maximum at 632 nm, which is characteristic for the protoporphyrin IX emission.¹⁹ As a reference, a suspension of CMS-Atto488_{core}-PEG_{shell} in THF was mixed with PP-NH₂ in the absence of EDC. In contrast to the sample CMS-Atto488_{core}-PS_{shell}, PP-NH₂ in the reference sample was simply removed by a few washing cycles in THF. This simple test additionally implies the covalent bonding of PP-NH₂ to the PEGylated CMS-surface.

In order to demonstrate the functionality of the nanodevice in living cells with confocal fluorescence microscopy, another sample was prepared. The core of the particle intended as sample for live cell investigations was carrying an Atto633 dye instead of the Atto488 dye. The resulting sample CMS-Atto633_{core}-PS_{shell} was used in a confocal fluorescence microscopy investigation in combination with Alexa Fluor 488 Dextran (AFD). This water-soluble, fluorescently-labeled polysaccharide has a molecular weight of 10 kDa and can act as a fluid phase marker in live cell investigations. An uptake of the dextran *via* endocytosis leads to fluorescence-labeled intra-endosomal liquids. The endosomal release of the nanocarriers can be observed by using this approach. The collapse of the endosomal membrane leads to an abrupt loss of fluorescence intensity in the region of the formerly intact endosome in the observed fluorescence channel of AFD. We have recently applied this method to exactly determine the time point of endosomal release.⁶ Figure 8.3.6 shows a representative cell. The cell was exposed to the sample CMS-Atto633_{core}-PS_{shell} and AFD for 14 hours. The successful cell entry and the intracellular localization was detected by their characteristic motion such as transport by motor proteins.^{21,22} The signal of AFD is displayed in Figure 8.3.6a, Atto633 fluorescence is shown in Figure 8.3.6b. For the characterization of the light-induced endosomal disruption, areas with colocalized signal of the two channels were investigated (see overlay, Figure 8.3.6c).

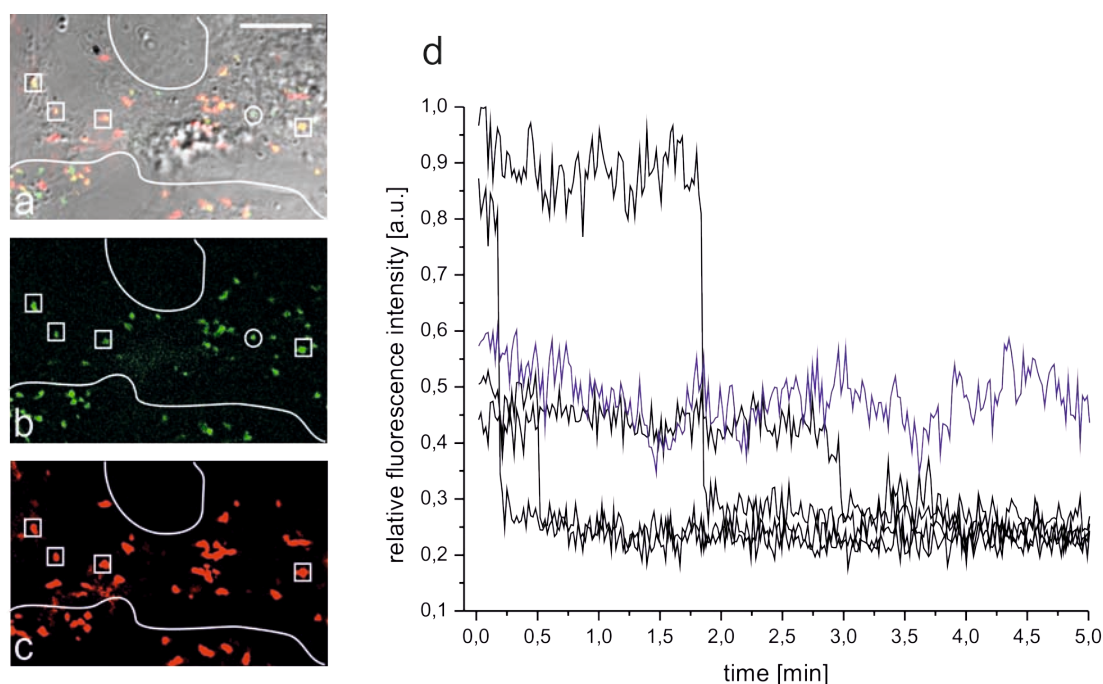


Figure 8.3.6 Photoinduced release of AFD from endosomes filled with CMS-Atto633-PS nanoparticles. The cell was exposed to the nanoparticles and AFD overnight. (a) shows an Image overlay of the AFD (green, b) and particle-bound Atto633 (red, c) signal superimposed on the transmitted light image of the cell directly after activation of the photosensitizer. A white circle indicates the cell nucleus; the white line represents the cell border. Scale bar: 10 μm . (d) shows fluorescence intensity plots of the AFD from 5 different endosomes; black lines correspond to the endosomes in boxes (a-c, filled with particles), the purple curve corresponds to the endosome in the circle (a-b, empty). The data were recorded and analyzed by Anna M. Sauer from the group of Prof. Bräuchle, LMU Munich.

The squares in Figures 8.3.6 a-c highlight the exemplary tracked endosomes. The time-related fluorescence intensity plots are displayed in Figure 8.3.6d. The cells were irradiated with 405 nm light (0.2 W/cm^2) for 1 minute for singlet oxygen production induced by the attached porphyrin-derivative. As can be seen from the intensity plots (Figure 8.3.6d), the AFD fluorescence suddenly drops, indicating the endosomal release of AFD. It should be noted that only particle-loaded endosomes collapse after light-irradiation. Endosomes that are not loaded

with CMS stay intact (Figure 8.3.6d, purple curve). We take this observation as a proof for the functionality of the synthesized nanostructures.

8.4 Conclusion

In summary, a novel synthetic route for the generation of photoactive nanocarriers as potential drug delivery devices is presented. In the synthesis, protoporphyrin IX was functionalized with p-phenylene diamine to give an amino-terminated structure. This derivative was subsequently attached to PEGylated CMS nanoparticles featuring a terminal carboxylic acid group. In contrast to earlier publications in this field, a different functionalization route was chosen and every step of the synthesis was characterized in detail. Another advantage compared to earlier work is the use of a poly(ethylene glycol) shell around the particles. As indicated in the literature, PEGylation of nanomaterials leads to stealth properties in the blood stream and results in enhanced colloidal and structural stability in biological fluids. Co-incubation of the CMS with AFD confirms the endocytotic pathway of the cellular particle uptake. The obtained nanoparticles can directly induce endosomal escape upon light irradiation at 405 nm. This is of major importance for the application of such particles in drug delivery, where endosomal trapping is one of the key issues to be overcome.

8.5 References

- (1) Saha, S.; Leung, K. C. F.; Nguyen, T. D.; Stoddart, J. F.; Zink, J. I. *Advanced Functional Materials* **2007**, *17*, 685.
- (2) Vallet-Regi, M.; Balas, F.; Arcos, D. *Angewandte Chemie, International Edition* **2007**, *46*, 7548.
- (3) Trewyn, B. G.; Slowing, I. I.; Giri, S.; Chen, H.-T.; Lin, V. S. Y. *Accounts of Chemical Research* **2007**, *40*, 846.

- (4) Zhao, Y.; Trewyn, B. G.; Slowing, I. I.; Lin, V. S. Y. *Journal of the American Chemical Society* **2009**, *131*, 8398.
- (5) Mortera, R.; Vivero-Escoto, J.; Slowing, I. I.; Garrone, E.; Onida, B.; Lin, V. S. Y. *Chemical Communications* **2009**, 3219.
- (6) Sauer, A. M.; Schlossbauer, A.; Ruthardt, N.; Cauda, V.; Bein, T.; Braeuchle, C. *Nano Letters* **2010**, *10*, 3684.
- (7) Austin, C. D.; Wen, X.; Gazzard, L.; Nelson, C.; Scheller, R. H.; Scales, S. J. *Proceedings of the National Academy of Sciences of the United States of America* **2005**, *102*, 17987.
- (8) de Bruin, K. G.; Fella, C.; Ogris, M.; Wagner, E.; Ruthardt, N.; Braeuchle, C. *Journal of Controlled Release* **2008**, *130*, 175.
- (9) Yang, Y.; Song, W.; Wang, A.; Zhu, P.; Fei, J.; Li, J. *Physical Chemistry Chemical Physics* **2010**, *12*, 4418.
- (10) Zhang, R.; Wu, C.; Tong, L.; Tang, B.; Xu, Q.-H. *Langmuir* **2009**, *25*, 10153.
- (11) Guo, H.; Qian, H.; Idris, N. M.; Zhang, Y. *Nanomedicine (Philadelphia, PA, United States)* **2010**, *6*, 486.
- (12) Zhao, T.; Wu, H.; Yao, S. Q.; Xu, Q.-H.; Xu, G. Q. *Langmuir*, ACS ASAP.
- (13) Brevet, D.; Gary-Bobo, M.; Raehm, L.; Richeter, S.; Hocine, O.; Amro, K.; Loock, B.; Couleaud, P.; Frochot, C.; Morere, A.; Maillard, P.; Garcia, M.; Durand, J.-O. *Chemical Communications (Cambridge, United Kingdom)* **2009**, 1475.
- (14) He, Q.; Zhang, J.; Shi, J.; Zhu, Z.; Zhang, L.; Bu, W.; Guo, L.; Chen, Y. *Biomaterials* **2010**, *31*, 1085.
- (15) Cauda, V.; Schlossbauer, A.; Bein, T. *Microporous and Mesoporous Materials* **2010**, *132*, 60.
- (16) Rio-Echevarria, I. M.; Selvestrel, F.; Segat, D.; Guarino, G.; Tavano, R.; Causin, V.; Reddi, E.; Papini, E.; Mancin, F. *Journal of Materials Chemistry* **2010**, *20*, 2780.

- (17) Kecht, J.; Schlossbauer, A.; Bein, T. *Chemistry of Materials* **2008**, *20*, 7207.
- (18) Cauda, V.; Schlossbauer, A.; Kecht, J.; Zurner, A.; Bein, T. *J. Am. Chem. Soc.* **2009**, *131*, 11361.
- (19) Sahoo, S. K.; Sawa, T.; Fang, J.; Tanaka, S.; Miyamoto, Y.; Akaike, T.; Maeda, H. *Bioconjugate Chemistry* **2002**, *13*, 1031.
- (20) Kecht, J.; Bein, T. *Microporous and Mesoporous Materials* **2008**, *116*, 123.
- (21) Bausinger, R.; von Gersdorff, K.; Braeckmans, K.; Ogris, M.; Wagner, E.; Braeuchle, C.; Zumbusch, A. *Angew. Chem., Int. Ed.* **2006**, *45*, 1568.
- (22) de Bruin, K.; Ruthardt, N.; von Gersdorff, K.; Bausinger, R.; Wagner, E.; Ogris, M.; Braeuchle, C. *Molecular Therapy* **2007**, *15*, 1297.

9. Light-Induced Delivery of Chromobodies from Lipid-Bilayer Coated Colloidal Mesoporous Silica

9.1 Introduction

In the previous Chapter 8 we have discussed the design of integrated multifunctional mesoporous nanoparticles that carry a covalently bound photosensitizer for light-induced endosomal escape. In the present Chapter, we want to show a first step towards an application of the photosensitizer-carrying nanoparticles as carrier-materials for intracellular release of biologically active compounds. In the literature, functional molecules like drugs or model compounds were incorporated into the pores of mesoporous silica nanoparticles and were released in cancer cells upon activating several types of triggers. For example, fluorescent dyes were delivered into cells by mesoporous silica nanoparticles additionally loaded with a photosensitizer.¹ Nel *et al.* have shown the intracellular delivery of doxorubicin in combination with P-glycoprotein siRNA to drug-resistant KB-V1MDR cancer cells.² They were able to increase the intracellular doxorubicin concentration compared to the incubation with free doxorubicin together with a downregulation of the P-glycoprotein (Pgp) expression. Another group used G-insulin-capped mesoporous silica nanoparticles loaded with membrane-impermeable cyclic adenosine monophosphate (cAMP).³ They showed a release of the cAMP that is selectively responsive to the presence of fructose *in vitro* and in cells. The same group showed a release of disulfide-bound cysteine upon cell uptake.⁴ They explain the release by the reductive milieu present in the cytosol. In contrast, we have recently demonstrated by live cell imaging methods on a single cell level, that endosomal escape is the essential step in the process of redox-driven controlled release from mesoporous silica (see Chapter 7).⁵ In order to demonstrate this mechanism, photosensitizers (porphyrine derivatives) that induce an endosomal collapse upon light irradiation were applied. The

applied photosensitizers were able to oxidize the membranes from the endosomes. As a result, uptaken particles were released into the cytosol.

Supported lipid bilayers on mesoporous silica nanoparticles (MSN) were investigated. Brinker *et al.* demonstrated the release of calcein into Chinese hamster ovary cells from lipid-bilayer coated MSN.⁶ Our group in cooperation with others has investigated the delivery of the plant toxin colchicine with such a system, followed by the effective depolymerization of the microtubules of cancer cells.⁷

A combination of the two approaches (incorporation of photosensitizers and supported lipid bilayers as diffusion barrier for guest molecules) can lead to the construction of a powerful, light-driven drug delivery system.

In the present Chapter, the successful delivery of dye-labeled, tubulin-GFP-binding heavy-chain antibodies from *Camelidae* sp. (so-called chromobodies)⁸ is demonstrated by confocal fluorescence microscopy on a single cell level. Chromobodies are up to ten times smaller than conventional antibodies and labeled with either fluorescent proteins or a fluorescent dye. Heavy-chain antibodies are devoid of light chains and recognize antigens via their variable domain (referred to as V_HH, see Figure 9.1.1).

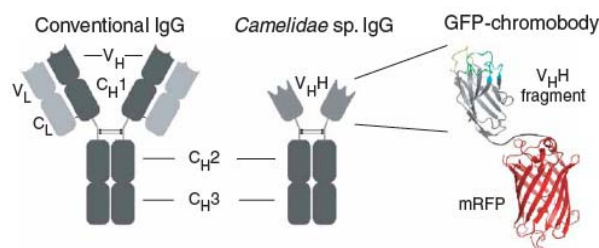


Figure 9.1.1 Schematic outline of a conventional antibody in comparison with a *Camelidae*-derived heavy-chain antibody and a generic chromobody. Picture taken from Ref. 8.

For target cells, a tubulin-GFP expressing HeLa liver cancer cell line was chosen. A multifunctional mesoporous silica nanoparticle was developed as nanosized carrier, based on

our earlier work. Rothbauer et al. have initially studied the chromobodies, as they were isolated from GFP-immunized alpacas.⁸ They have co-transfected HeLa cells with GFP- β -actin and GFP-chromobody expression vectors and analyzed them by live cell microscopy. It was shown that the GFP chromobodies co-localize with the GFP- β -actin on cytoskeletal actin filaments. For the present work, the group of Prof. H. Leonhardt (LMU) provided Atto594-labeled chromobodies.

Here we demonstrate the carrier-mediated delivery of these membrane-impermeable chromobodies from outside the cell by using highly functionalized mesoporous silica nanoparticles.

Additionally, the enrichment of fluorescent structures along the microtubuli serves to show the functionality of our release mechanism.

For this purpose, the chromobodies are loaded into photosensitizer-functionalized colloidal mesoporous silica spheres, which are subsequently surrounded by a supported lipid bilayer. After endocytotic uptake in GFP-tubulin expressing HeLa cells, the cells are irradiated with a 405 nm laser in order to induce the creation of singlet oxygen, as demonstrated in Chapter 8. The singlet oxygen will lead to the collapse of both the supported lipid bilayer and the endosomal membrane, followed by the release of the chromobodies (experimental scheme, see Figure 9.1.1).

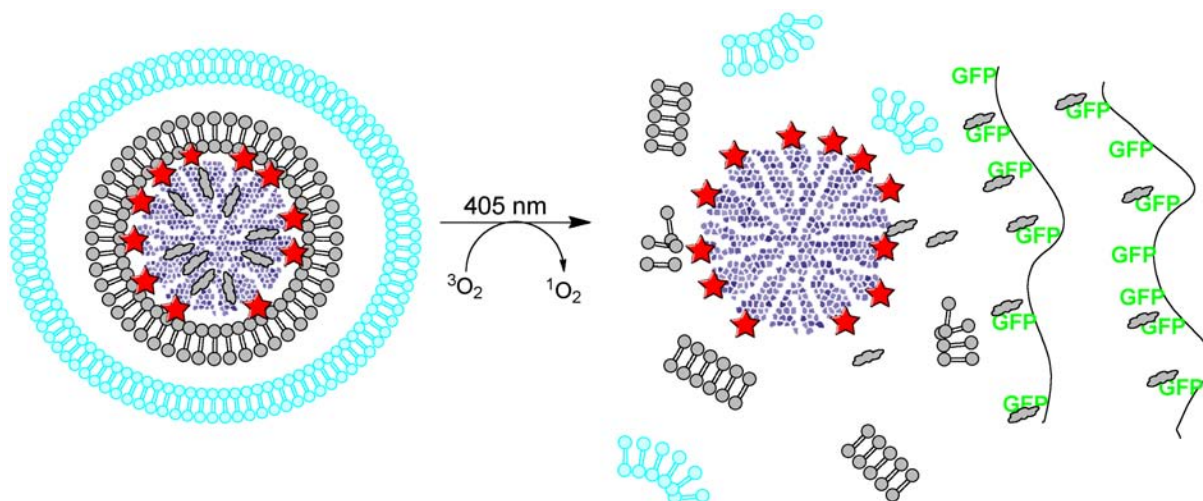


Figure 9.1.1 Photosensitizer functionalized (stars), chromobody-loaded colloidal mesoporous silica nanoparticles release the chromobodies in HeLa cells upon irradiation with a 405 nm laser. The process can be monitored by the fluorescence of the chromobodies attaching to GFP-labeled tubulin, which is directly expressed in the HeLa cells.

A successful release of chromobodies is indicated by the coordination of GFP-tubulin, as characterized by confocal fluorescence microscopy in cooperation with the group of Prof. Bräuchle, LMU Munich. The work is a joint project within the Center for NanoScience (CeNS Munich). The collaborators are members of the groups of Prof. Leonhardt (Biology, LMU Munich), Prof. Bein and Prof. Bräuchle (Chemistry, LMU Munich), and Prof. Rädler (Physics, LMU Munich). The obtained results imply that this method can serve as an alternative approach to a technically demanding genetic transfection.

The synthesis and characterization of the multifunctional nanoparticles was carried out in our laboratory and is my contribution to this interdisciplinary work.

9.2 Experimental Section

9.2.1 Applied chemicals

Tetraethylorthosilicate (TEOS, Fluka, >99%), (3-mercaptopropyl)-triethoxysilane (MPTES, Gelest, 95%), (3-aminopropyl)-triethoxysilane (APTES, Sigma, 98 %) cetyltrimethylammonium bromide (CTAC, Fluka, 25% in H₂O), Phenyltriethoxysilane (PhTES, Sigma, 98%) triethanolamine (TEA, Aldrich, 98%), Atto488-NHS ester and Atto633-NHS ester (both Atto-Tec), tetrahydrofuran (THF, Acros, 99.8%), protoporphyrin IX (Sigma, >95%), *p*-phenylenediamine (Sigma, 95%), triethylamine (Sigma, 99%), ethyl chloroformate (Fluka, >98%), ammonium nitrate (Sigma, 99%), 1-maleinimido-3-oxo-7,10,13,16,19,22,25,28-octaoxa-4-azahentriacontan-31-oic acid (mal-dPEG(8)-COOH, Iris Biotech), N-hydroxysuccinimide (NHS, Aldrich, 98%), N-(3-dimethylaminopropyl)-N'-ethylcarbodiimide (EDC, Sigma, 97%), toluene (Aldrich, 99.8 %) (1,2-dioleoyl-sn-glycero-3-phosphocholine (DOPC, Avanti Polar Lipids), Alexa Fluor 488 Dextran (AFD, MW 10 kDa, Invitrogen), cell culture media and fetal calf serum (Invitrogen). The group of Prof. Heinrich Leonhardt provided Atto594-chromobodies. All chemicals were used as received without further purification. Doubly distilled water from a Millipore system (Milli-Q Academic A10) was used for all synthesis and purification steps.

9.2.2 Synthesis of bi-functionalized colloidal mesoporous silica (CMS-NH₂_{core}-SH_{shell})

The colloidal mesoporous silica particles were synthesized according to our previously published procedure, see also Chapter 3.⁹ A mixture of TEOS (1.63 g, 9.22 mmol), PhTES (57 mg, 0.24 mmol), APTES (53.1 mg, 0.24 mmol), and TEA (14.3 g, 95.6 mmol) was heated for 20 at 90°C without stirring in a 100 mL polypropylene reactor. A solution of CTAC (25 % in water, 2.41 mL, 1.83 mmol) in water (21.7 g, 1.21 mol) preheated to 60 °C was added quickly. The resulting reaction mixture with a molar composition of 1 TEOS: 0.20 CTAC: 10.37 TEA: 130.15 H₂O was stirred at room temperature for 30 minutes. Then, a mixture of

TEOS (19.3 mg, 92.5 μmol) and MPTES (22 mg, 92.5 μmol) was added to the reaction. The resulting mixture was stirred at room temperature for another 12 hours. After the addition of 100 mL ethanol, the mesoporous silica nanoparticles were collected by centrifugation, redispersed in 100 mL of ethanol and extracted according to the procedure described below.

9.2.3 Extraction of the CMS samples

Extraction of the organic template from the CMS materials was performed by heating the colloidal suspensions containing 250 mg of CMS for 45 minutes under reflux at 90 °C in a solution containing 2 g ammonium nitrate in 100 mL ethanol, followed by 45 minutes under reflux in a solution of 4 g concentrated hydrochloric acid in 100 mL ethanol. The CMS materials were separated by centrifugation and washed with ethanol after each extraction step. CMS materials were obtained as clear ethanolic suspensions.

9.2.4 Preparation of non-porous, aminofunctionalized silica nanoparticles (Stöber-NH₂)

Silica nanoparticles were prepared according to a previously published procedure.¹⁰ To a mixture of water (17.7 mL, 0.98 mol), methanol (100 mL, 2.47 mol) and ammonia (8.86 mL, 25 %wt. in H₂O, 0.13 mol), TEOS was added under stirring (0.368 mL, 1.65 mmol) divided in two aliquots (0.184 mL each). The second aliquot was added 10 minutes after the first. The resulting mixture was stirred at room temperature for 120 minutes. The resulting particles were centrifuged and washed with 100 mL of ethanol followed by centrifugation. Finally, the washed silica nanoparticles were dispersed in 100 mL of ethanol. For the subsequent functionalization with (3-aminopropyl)triethoxysilane (APTES), a suspension containing 2 mg of silica nanoparticles was transferred in toluene (5 mL, 47.2 mmol) by centrifugation. To the resulting suspension, APTES (281 μL , 1.2 mmol) was added. The resulting mixture was stirred under reflux conditions for 4 hours. The functionalized nanoparticles were washed in 10 mL of ethanol by centrifugation and finally dispersed in 5 mL of ethanol.

9.2.5 PEGylation of CMS-NH₂core-SH_{shell} with maleinimido-3-oxo-7,10,13,16,19,22,25,28-octaoxa-4-azahentriacontan-31-oic acid (Mal-dPEG(8)-COOH, sample CMS-NH₂core-PEG_{shell})

The following synthesis was carried out as described in chapter 8. An ethanolic suspension containing 1 mg of CMS-NH₂core-SH_{shell} was centrifuged and redispersed in 500 μ L of water. Subsequently, a 100 μ L of solution of Mal-dPEG(8)-COOH (10 mg/mL) was added. The reaction mixture was stirred for 14 hours at room temperature. In order to remove the excess of Mal-dPEG(8)-COOH, the particles were washed three times with 1 mL of water followed by centrifugation. Finally, the sample was redispersed in 500 μ L of absolute ethanol, yielding the sample CMS-NH₂core-PEG_{shell}.

9.2.6 Synthesis of protoporphyrin-IX-bis(phenyleneaminoamide) (PP-NH₂)

Protoporphyrin-IX-bis(phenyleneaminoamide) was prepared according to a modified literature procedure, see also Chapter 8.¹¹ In a dry and darkened 100 mL three-neck flask, protoporphyrin-IX (100 mg, 0.178 mmol, 1 eq.) was dissolved in 20 mL of water-free tetrahydrofuran and cooled to 0 °C under nitrogen atmosphere. Then, triethylamine (2.45 mL, 17.7 mmol, 100 eq.) was added to the solution. Ethyl chloroformate (1.7 mL, 17.9 mmol, 100 eq.) was added slowly (30 minutes) under stirring to the solution by using a dropping funnel. The resulting mixture **1** was stirred for 2 hours at 0 °C.

In a second dried and darkened 100 mL three-neck flask, finely powdered p-phenylene diamine (1.95 g, 17.9 mmol, 100 eq.) was dissolved in 10 mL THF under nitrogen atmosphere. To this solution, mixture **1** was added slowly with a syringe. The resulting mixture was stirred for 24 hours at room temperature in the dark. The solvent was removed *in vacuo*. The resulting precipitate was suspended in 15 mL of ice-cold water. The resulting suspension was filtered and washed three times with each 15 mL of ice-cold water. PP-NH₂ was obtained as a brown precipitate (85 mg, 0.114 mmol, 64%).

Analytics: MS (ESI, acetonitrile/water): $m/z = 743.38 [m+H]^+$, $765.36 [m+Na]^+$; exact formula mass: 742.37 g/mol; IR (emerging amide vibrations 1550 cm^{-1} , 1634 cm^{-1})

9.2.7 Attachment of PP-NH₂ to CMS-NH₂core-PEG_{shell} (sample CMS-NH₂core-PS_{shell}, see also chapter 8)

The as-synthesized sample CMS-NH₂core-PEG_{shell} (based on 1 mg silica particles, approximately 0.17 μmol -COOH) was mixed with PP-NH₂ (2 mg, 2.7 μmol). Subsequently, *N*-hydroxysuccinimide (2.3 mg, 20 μmol) and EDC (3.5 μl , 20 μmol) were added. The resulting mixture was stirred at room temperature in the dark for 14 hours. Subsequently, the sample was washed 3 times with 1 mL THF and 1 mL water each.

9.2.8 Loading of silica nanoparticles with Atto594-labeled chromobodies

To a suspension containing 1 mg of the respective silica sample (CMS or Stöber) in 500 μL of sterile water, 50 μL of a solution containing chromobodies was added. The resulting mixture was shaken for 16 hours at room temperature in a darkened 1.5 mL polypropylene vial.

9.2.9 Supported lipid bilayer preparation (samples CMS-NH₂core-PS_{shell}-DOPC)

The amount of 2.5 mg DOPC was dissolved in a mixture of 40 %vol ethanol / 60 %vol water. The chromobody-loaded CMS from 9.2.7 were centrifuged (14.000 rpm, 5 minutes) and 100 μL of the lipid solution was added to the centrifuged pellet. Upon the addition of 700 μL of sterile water followed by a 3 minute treatment in an ultrasonic bath, the supported lipid bilayer was formed on the CMS samples. The samples were centrifuged and redispersed again in order to remove freely diffusing lipids and the ethanol. Before incubation with cells, the samples were filtered through a 250 nm filter to remove aggregates. The obtained samples were subsequently incubated with HeLa cells expressing tubulin-GFP.

9.2.10 Spinning disc confocal microscope

As explained in chapter 7.2.9, confocal microscopy for live-cell imaging was performed on a setup based on the Nikon TE2000E and a spinning disk confocal microscope (Andor) utilizing a Yokogawa spinning disk unit CSU10. The system was equipped with a 1.49 NA 100x Plan Apo oil immersion objective from Nikon. For two color detection of ATTO488 and ATTO633, dichroic mirrors and band-pass filters HQ 525/50 and 730/140 were used (AHF Analysentechnik AG). Image sequences were captured with an electron multiplier charge coupled device (EMCCD) camera (iXon DV884; Andor).

9.3 Results and Discussion

The synthesis of the core-shell functionalized colloidal mesoporous silica was carried out by applying a previously published procedure, see also Chapter 3.^{12,13} For this purpose, tetraethyl orthosilicate (TEOS) was hydrolyzed together with (3-aminopropyl)-triethoxysilane and phenyltriethoxysilane in a mixture containing cetyltrimethylammounium chloride as a template and triethanolamine (TEA) as base. A shell of TEOS was grown on the initial seeds after 30 minutes of stirring at room temperature in order to gain a spatial separation between the core and the shell functionality. Thiol-functionality exclusively placed on the outer surface of the porous nanoparticles was achieved by subsequently adding a 1:1 mixture of TEOS and (3-mercaptopropyl)triethoxysilane equivalent to 2 % of the total silane content. After twelve hours of condensation, the template was extracted. The obtained nanoparticles showed pore sizes around 3.9 nm and a BET surface area around $1000 \text{ m}^2\text{g}^{-1}$, as derived from nitrogen sorption. The corresponding isotherm and NLDFT pore size distribution can be found in Figure 9.3.1.

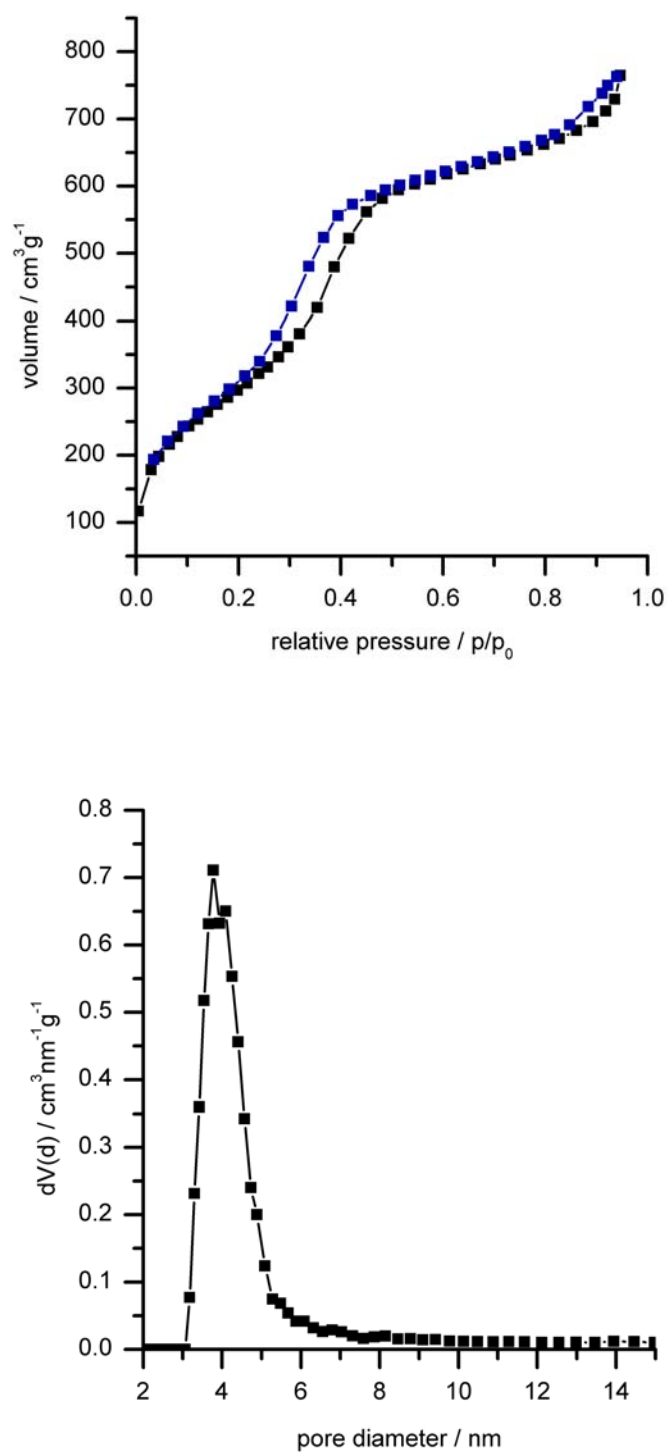


Figure 9.3.1 Nitrogen sorption isotherm (upper panel, adsorption plotted in black, desorption plotted in blue) and NLDFT pore size distribution (lower panel) of the sample CMS-NH₂core-SH_{shell}.

Next, the particles were reacted with maleinimido-3-oxo-7,10,13,16,19,22,25,28-octaoxa-4-azahentriacontan-31-oic acid (Mal-dPEG(8)-COOH), yielding a carboxylic acid-terminated polyethylene glycol shell around the particles, as reported earlier in Chapter 8. The material was further functionalized with the previously synthesized protoporphyrin-IX-bis(phenyleneaminoamide) (PP-NH₂, refer to Chapter 8) in order to covalently attach the photosensitizer as additional function to the particle. A detailed analysis of these reaction steps can be found in Chapter 8.

Another important aspect of this work was to evaluate the beneficial role of using mesoporous particles compared to non-porous silica nanoparticles. As the chromobodies have a molecular mass of around 13 kDa¹⁴ it is unclear if they can fit completely into the 4 nm pores of our mesoporous particles. A chromobody uptake experiment was made to demonstrate that the porous structure of our nanoparticle allows a higher loading with the chromobodies compared to surface-adsorbed chromobodies on the surface of non-porous amino-functionalized silica nanoparticles.

For the experiments, non-porous silica nanoparticles featuring an aminopropyl-grafted surface with a diameter of 80 nm were synthesized according to the literature (Stöber-NH₂).¹⁰ A dynamic light scattering characterization of the sample Stöber-NH₂ can be found in the Appendix (A-13). The amount of 1 mg of the respective samples was each subsequently soaked in 150 μ L of a solution with Atto594-labeled chromobodies (CB) with a CB-concentration of 5 μ g/mL (total amount of CB 0.75 μ g). After 14 hours, the samples were centrifuged and the residual solution was investigated by fluorescence spectroscopy. In parallel, a fluorescence intensity calibration curve was recorded to correlate known concentrations with the maximum fluorescence emissions at 620 nm of the supernatants of the investigated samples. The obtained calibration curve can be found in Figure 9.3.2.

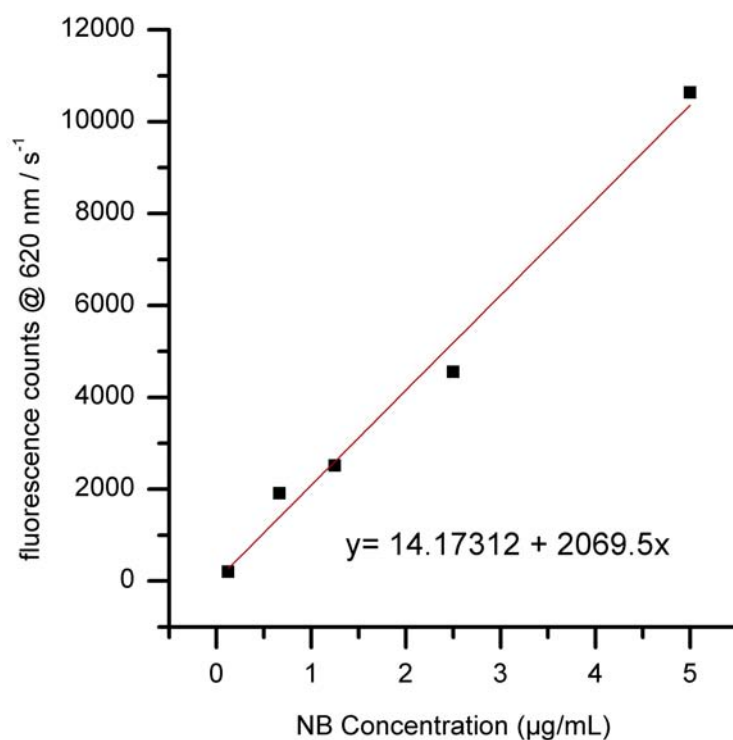


Figure 9.3.2 Chromobody fluorescence intensity calibration curve (excitation at 594 nm). The red curve represents the linear regression of the obtained data points. The linear equation of the regression curve is displayed as an inset.

The obtained CB concentrations and absolute CB uptake values per mg silica were calculated by using the linear regression from the calibration curve are displayed in Table 9.3.1.

Table 9.3.1 Fluorescence intensities of the three samples subjected to chromobody adsorption

	CMS-NH ₂ core-SH _{shell}	Stöber-NH ₂
Measurement 1	790.165	4128.509
Measurement 2	666.117	4385.087
Average	728.141	4256.798
Conc. of CB in supernatant [$\mu\text{g/ml}$]	0.345	2.050
Sample Volume [μL]	150	150
Absolute uptake values [$\mu\text{g/mg silica}$]	0.70	0.44

As can be seen, the porous structure of the particle allows the loading with higher amounts of chromobodies than using non-porous silica as carrier material. With these values, the amount of loaded CB per particle can be calculated as follows.

Calculation of CB-loading level

Particle diameter: 80 nm

Particle Volume (sphere): $2.14 \cdot 10^{-15} \text{ cm}^3$

Density assumption: 1.1 g cm^{-3}

→ particle weight: $2.35 \cdot 10^{-15} \text{ g}$

Adsorbed amount of CB (Sample CMS-NH₂core): 0.7

$\mu\text{g/mg silica}$

→ $1.65 \cdot 10^{-18} \text{ g CB/ particle}$

Molecular weight of CB: 13 kDa

→ $1.27 \cdot 10^{-22} \text{ mol CB/ particle}$

→ 76 CB per particle can be assumed

For live-cell investigations, the sample CMS-NH₂core-PS_{shell} was loaded with Atto594-labeled chromobodies before being encapsulated in a supported lipid bilayer consisting of 1,2-dioleoyl-*sn*-glycero-3-phosphocholine (DOPC). The encapsulation was carried out according to our previously reported procedures, yielding the sample CMS-NH₂core-PS_{shell}-DOPC.¹¹

The encapsulated Atto594-chromobodies specifically bind to green fluorescent protein (GFP) and were provided by the group of Heinrich Leonhardt (LMU Munich). The live-cell investigations were carried out by fluorescence microscopy in the group of Prof. Bräuchle, in particular by Anna M. Sauer.

The GFP-tubulin expressing HeLa cells were exposed to small aliquots (several μg) of the CB-loaded sample CMS-NH₂core-PS_{shell}-DOPC and studied by confocal z-stacks after 24 hours of incubation time. The endosomes were labeled by using Alexa Fluor 488 Dextran (AFD) as fluid phase marker by adding it to the cells along with the particles. From earlier work it is known that the cells take up the lipid bilayer-coated particles within that time period and that they do not show significant cytotoxicity.⁷ 24 hours after the addition of AFD and the particles to the cells, the well plate was irradiated with 405 nm laser light (0.2 W/cm^2) for one minute in order to stimulate the formation of singlet oxygen by the attached porphyrine derivative and thus, induce the endosomal release and the disruption of the supported lipid bilayer. This irradiation step is essential for the CB-release.

Subsequently, the cells were investigated by confocal z-stack fluorescence microscopy. Figure 9.3.3 shows two representative images of single cells, consisting of an overlay of two fluorescence channels. In the red channel, the Atto594-labeled chromobodies and the fluorescence of the protoporphyrin derivative is displayed. In the green channel, the microtubuli-GFP appears as a filamentous structure and the fluorescence of the intra-endosomal fluid phase marker AFD can be seen in the form of spots.

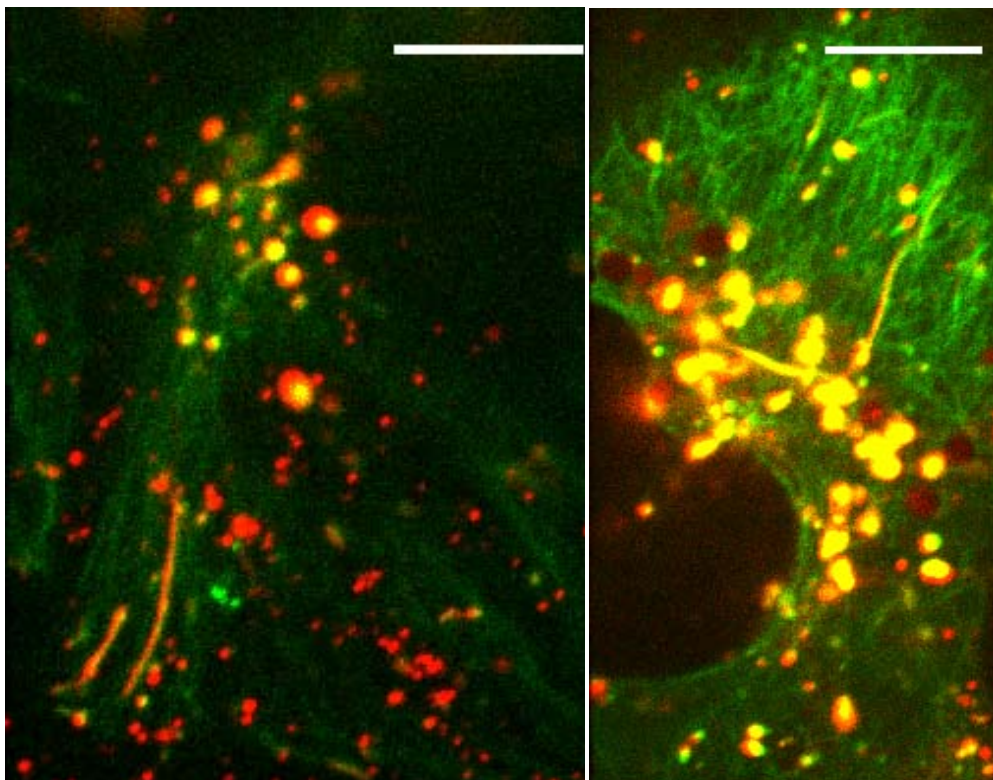


Figure 9.3.3 Fluorescence microscopy images of two single cells (left and right) treated with the sample CMS-NH₂core-PS_{shell}-DOPC (spinning disc confocal microscopy). The red channel shows fluorescence of the Atto594-chromobodies and protoporphyrin IX. The green channel shows microtubuli-GFP (filamentous) and fluid phase marker Alexa 488 Fluor Dextran (spots). Scale bar 10 μ m. The data were recorded and analyzed by Anna M. Sauer from the group of Prof. Bräuchle (LMU Munich).

As can be seen in Figure 9.3.3, some of the filamentous GFP-microtubule structures are clearly covered by the nanoparticle-delivered chromobodies. This can be explained by the photochemical action of the attached porphyrin-derivative followed by a release of the loaded CB. The irradiation of the samples with 405 nm laser light induces the formation of singlet oxygen. This effect leads to a rupture of the surrounding supported lipid bilayer and the destruction of the endosomal membrane.

The moderate overall coverage of the microtubuli by the CB can be explained by the small loading capacity for these large molecules ($M_w = 13$ kDa). Compared to direct genetic

production of CBs in earlier work, a similar amount of intracellular CB cannot be reached by our method. However, carrier-mediated delivery of chromobodies has not yet been reported in the literature. This method allows the incorporation of chromobodies into cells without the biological know-how of gene transfection. Additionally, the carrier-mediated approach seems to be less stressful to the living cells compared to microinjection.

In order to underline these findings, a sample without photosensitizer activation at 405 nm was investigated. Following our argumentation above, no CB should be released, as they are encapsulated by the supported lipid bilayer in the porous carriers. Secondly, the endosomal membrane should represent an additional barrier to the CB. As expected, no structures of the GFP-tubulin were covered by the chromobodies (Figure 9.3.4, showing a representative cell sample). This negative control underlines the key role of the photosensitizer, which is directly attached to the outer surface of our particles.

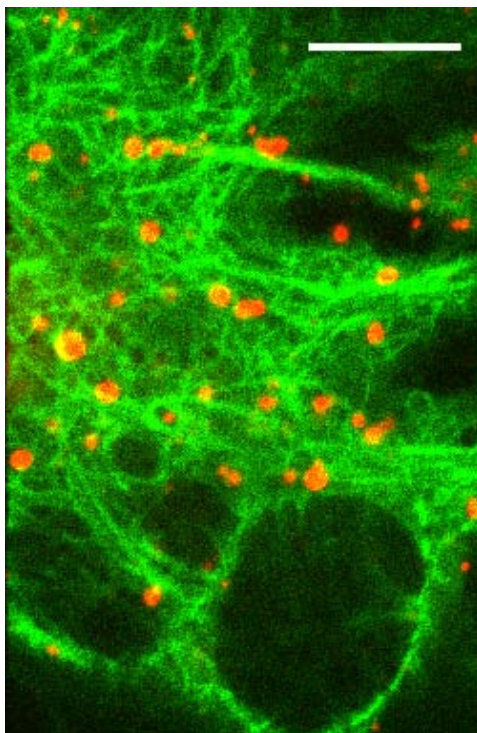


Figure 9.3.4 Fluorescence microscopy image of a single cell incubated with the sample CMS-NH₂core-PS_{shell}-DOPC. No activation at 405 nm prior to investigation. Green channel shows tubulin-GFP, red channel shows Atto594-chromobodies and protoporphyrin IX fluorescence. Scale bar 10 μ m. The image was recorded and analyzed by Anna M. Sauer from the group of Prof. Bräuchle (LMU Munich).

9.4 Conclusion

To summarize, we have shown the applicability of our recently developed photoactive colloidal mesoporous silica nanoparticles as carriers for antibodies for the light-induced delivery in living cells. It was shown by *in vitro* measurements that the porous structure is beneficial for the amount of chromobodies adsorbed in/on the carrier. To achieve this, our recently developed pathway for the attachment of a protoporphyrin IX derivative to the outer surface of CMS was applied. Irradiation of the samples with 405 nm light is necessary for the singlet-oxygen generation, which leads as a consequence to the rupture of the surrounding lipid membranes (artificial DOPC and endosomal membranes). In a control experiment, it was

shown that the photoinduced endosomal escape plays a key role in the delivery of the Atto594-chromobodies to the microtubuli-GFP.

9.5 References

- (1) Febvay, S.; Marini, D. M.; Belcher, A. M.; Clapham, D. E. *Nano Letters* **2010**, *10*, 2211.
- (2) Meng, H.; Liong, M.; Xia, T.; Li, Z.; Ji, Z.; Zink, J. I.; Nel, A. E. *ACS Nano* **2010**, *4*, 4539.
- (3) Zhao, Y.; Trewyn, B. G.; Slowing, I. I.; Lin, V. S. Y. *Journal of the American Chemical Society* **2009**, *131*, 8398.
- (4) Mortera, R.; Vivero-Escoto, J.; Slowing, I. I.; Garrone, E.; Onida, B.; Lin, V. S. Y. *Chemical Communications (Cambridge, United Kingdom)* **2009**, 3219.
- (5) Sauer, A. M.; Schlossbauer, A.; Ruthardt, N.; Cauda, V.; Bein, T.; Braeuchle, C. *Nano Letters* **2010**, *10*, 3684.
- (6) Liu, J.; Stace-Naughton, A.; Jiang, X.; Brinker, C. J. *Journal of the American Chemical Society* **2009**, *131*, 1354.
- (7) Cauda, V.; Engelke, H.; Sauer, A.; Arcizet, D.; Braeuchle, C.; Raedler, J.; Bein, T. *Nano Letters* **2010**, *10*, 2484.
- (8) Rothbauer, U.; Zolghadr, K.; Tillib, S.; Nowak, D.; Schermelleh, L.; Gahl, A.; Backmann, N.; Conrath, K.; Muyldermans, S.; Cardoso, M. C.; Leonhardt, H. *Nature Methods* **2006**, *3*, 887.
- (9) Cauda, V.; Schlossbauer, A.; Kecht, J.; Zurner, A.; Bein, T. *Journal of the American Chemical Society* **2009**, *131*, 11361.
- (10) Stoeber, W.; Fink, A.; Bohn, E. *Journal of Colloid and Interface Science* **1968**, *26*, 62.
- (11) Sahoo, S. K.; Sawa, T.; Fang, J.; Tanaka, S.; Miyamoto, Y.; Akaike, T.; Maeda, H. *Bioconjugate Chemistry* **2002**, *13*, 1031.

- (12) Kecht, J.; Schlossbauer, A.; Bein, T. *Chemistry of Materials* **2008**, *20*, 7207.
- (13) Schlossbauer, A.; Kecht, J.; Bein, T. *Angewandte Chemie, International Edition* **2009**, *48*, 3092.
- (14) Hamers-Casterman, C.; Atarhouch, T.; Muyldermans, S.; Robinson, G.; Hamers, C.; Songa, E. B.; Bendahman, N.; Hamers, R. *Nature (London, United Kingdom)* **1993**, *363*, 446.

10. pH-Responsive Release of Acetal-Linked Mellitin from SBA-15

Mesoporous Silica

The following work is based on the publication indicated below:

Axel Schlossbauer, Christian Dohmen, David Schaffert, Ernst Wagner, and Thomas Bein;

submitted

10.1 Introduction

In the previous chapters, controlled release concepts based on triggers like temperature, enzymatic action or redox chemistry were introduced. Other concepts for delivery-on-demand systems based on mesoporous silica are presented in the literature. In most cases, large molecules or nanoparticles were attached reversibly to the pore mouths in order to sterically hinder loaded guest molecules (drugs or model compounds) from leaving the pores. For example, one study uses acetal-gated mesopores as pH- responsive gatekeeper for mesoporous silica.¹ Another approach demonstrates that coumarin-derivatives can act as photo-responsive gatekeeper molecules for MCM-41. UV-light irradiation ($\lambda > 310$ nm) of the coumarin-functionalized silica surface causes a [2+2] photocycloaddition between two coumarin molecules, leading to an efficient closing of the pores. Reopening is achieved by irradiation at higher energy ($\lambda \approx 250$ nm).²

Another approach to create delivery-on-demand systems based on mesoporous materials is to directly attach the therapeutic molecules to the silica pore walls using reversible chemistry. One recent approach uses disulfide-bridged linkers between the pore wall and cysteine in mesoporous silica nanoparticles in order to generate a redox-responsive delivery mechanism.³

We have contributed to this field by studying the cell uptake and drug release mechanism of

this method in great detail (see Chapter 7).⁴ As an additional option for biomedical applications, it would be highly desirable to have pH-responsive linkers between the substance to be delivered and the porous host, since the pH drops from 7.4 to 5.5 upon endosomal uptake.⁵

Here we describe the use of acetal-linkers for a pH-responsive release study of mellitin from SBA-15 type mesoporous silica. Mellitin, the active component of bee venom, is a small peptide containing 26 amino acids. Currently this compound is widely investigated in the field of nanomedicine due to its lytic or apoptosis-inducing properties.^{6,7} It acts as a membrane-invading agent, leading to a local disruption of lipid membranes. It has been used earlier as endosomolytic peptide for siRNA-polymer-conjugates.⁸ Here we evaluate the release of the peptide by an erythrocyte lysis assay. A triggered release of the peptide leads to lysis of mouse erythrocyte cells (Figure 10.1.1).

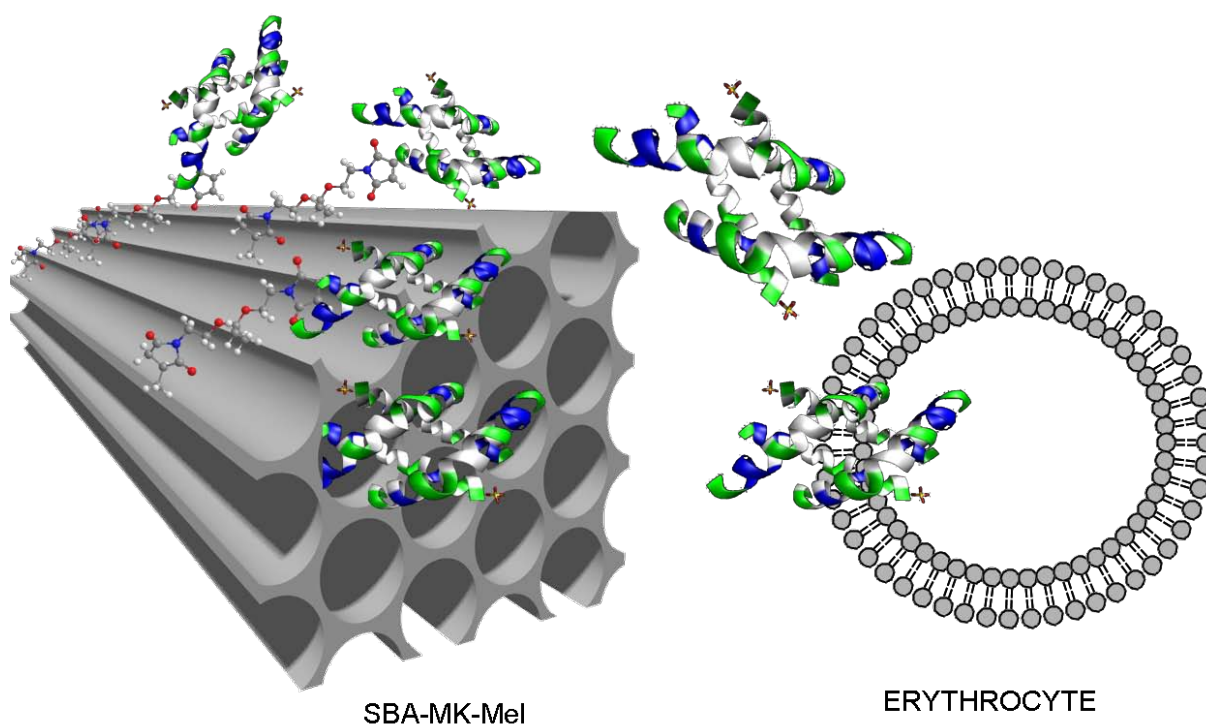


Figure 10.1.1 Released mellitin peptides from mesoporous structure intercalate the membranes of erythrocytes (schematic).

The structure of certain acetals offers a reasonable stability under extracellular conditions while undergoing fast hydrolysis in an acidic milieu. The applicability of acetals for controlled release systems has been recently demonstrated with oligoethyleneimine conjugates.⁹ It was shown that acetal-linked oligoethyleneimines can be used as efficient pH-sensitive gene carriers. Another group has applied this chemistry to create pH-sensitive polyethyleneoxide conjugates of model drugs.¹⁰ For protein delivery from mesoporous structures, acetal-linked proteins have not yet been reported. This work is the result of a joint project with Christian Dohmen from the group of Prof. Ernst Wagner (LMU).

10.2 Experimental Section

10.2.1 Applied Chemicals

Tetraethyl orthosilicate (TEOS, Sigma-Aldrich, >98%), cetyltrimethylammonium bromide (CTAB, Aldrich, 95%), (3-mercaptopropyl)trimethoxysilane (MPTS, ABCR, 95%), mesitylene (Aldrich, 98%), 1,8-bis-maleimidodiethyleneglycol (BM-Linker, Pierce Biotechnology, Inc.), 2,2-Bis(N-maleimidoethoxy)propane (MK-Linker, Organix, Inc.); Pluronic 123 block copolymer was received as a gift from BASF Company. Cysteine-terminated mellitin was synthesized and purchased from Biosynthan. Doubly distilled water from a Millipore system (Milli-Q Academic A10) was used for buffer preparation and synthesis steps. All solvents and buffer contents were purchased from Sigma-Aldrich. All chemicals were used as received without further purification.

10.2.2 Preparation of large-pore SBA-15 spherical particles

For the synthesis of the applied SBA-15 material, a procedure from the literature was used.¹¹ To a solution of Pluronic 123 (3.0g) in hydrochloric acid (HCl, 60 mL, 1.5 M), another solution of cetyltrimethylammonium bromide (CTAB, 0.6 g) and mesitylene (1.5 g) in 25 mL

water was added. Subsequently, the amount of 20 mL ethanol (absolute) was added. Then, 10 mL of tetraethyl orthosilicate (TEOS) were added dropwise and the resulting mixture was vigorously stirred at 35 °C for 45 minutes. The solution was subsequently transferred into a Parr autoclave for hydrothermal treatment at 75°C for 12 hours under static conditions. For aging, the reaction mixture was heated up to 125 °C for another 12 hours. The resulting powder was filtered and washed with both 100 mL of water and ethanol. The resulting powder was dried at 60 °C overnight. Removal of the template was performed by calcination at 550 °C for 5 hours (heating rate 1°C / min).

10.2.3 Preparation of mercaptopropyl-functionalized SBA-15 (SBA-SH)

The amount of 200 mg of freshly calcined SBA-15 was dried at 110 °C under vacuum conditions for 90 minutes. Afterwards, dry toluene was added under nitrogen atmosphere. Subsequently, 3-mercaptopropyltrimethoxysilane (MPTS, 1.5 mmol,) was added. The resulting mixture was stirred for 4 hours under nitrogen atmosphere while being heated to reflux temperature (oil bath temperature 120°C). The functionalized SBA-15 (SBA-SH) was filtered and subsequently washed with each 50 mL of toluene, methanol and water before being dried at 60 °C for 12 hours.

10.2.4 Maleimide-linker attachment (samples SBA-MK, SBA-BM)

The amount of 5 mg of the sample SBA-SH was dried at 110 °C under nitrogen atmosphere for 2 hours. After cooling to room temperature, the amount of 5 mL water-free dimethylsulfoxide (DMSO) was added. 33.5 μmol of the respective linker (MK-linker or BM-linker, 10-fold excess) was then added to the resulting suspension. The mixture was stirred at room temperature under nitrogen atmosphere for 14 hours. The samples were filtered off and

washed with DMSO and PBS buffer (pH 7.4). Drying was performed under high vacuum conditions. The resulting white powder gave the sample SBA-MK or SBA-BM, respectively.

10.2.5 Attachment of mellitin to SBA-15 (samples SBA-MK-Mel and SBA-BM-Mel)

To a solution of mellitin ($2893.6 \text{ g mol}^{-1}$, 3 mg, $1.58 \text{ }\mu\text{mol}$) in 1.5 mL DMSO, 1 mg of linker functionalized SBA-15 was added. The reaction mixture was stirred for 60 minutes at room temperature. The samples were washed with PBS buffer solution (pH 7.4) by centrifugation. The resulting samples were named SBA-MK-Mel or SBA-BM-Mel, respectively.

10.2.6 Erythrocyte leaching assay

Mouse erythrocytes were isolated from fresh, citrate-treated blood and washed in phosphate buffered saline (PBS) by four centrifugation cycles, each at 800 g for 10 min at 4 °C. The erythrocyte pellet was diluted in PBS buffer to get a final cell concentration of $5.0 \cdot 10^7$ cells/mL. The samples SBA-BM-Mel and SBA-MK-Mel were serially diluted in phosphate-buffered saline (PBS), resulting in theoretical mellitin concentrations of 5, 1, and 0.1 μM , respectively. As a control, pure mellitin solutions having the same concentrations were prepared, 75 μL of a mouse erythrocyte solution ($3.75 \cdot 10^6$ cells) was mixed with 75 μL of the sample suspensions and mellitin solution as reference. To define 100% lysis, erythrocytes were incubated with 1% Triton-X100 in PBS. For samples that were pre-incubated at acidic conditions (MK-acidic, BM-acidic), the pH was adjusted to 5.0. The resulting acidic samples were incubated for 30 min before dilution. 75 μL erythrocyte suspension ($3.75 \cdot 10^6$ cells) was added per well of a V-bottomed 96-well plate and mixed with 75 μL of the different mellitin dilutions. For 100% lysis, cells were treated with 75 μL of buffer containing 1% Triton X-100. After incubation for 60 min at 37 °C under constant shaking, cells were centrifuged at 800 g for 10 min. The volume of 80 μL supernatant was analyzed for hemoglobin release at 405 nm using a microplate reader.

10.3 Results and Discussion

As host material for the reversible encapsulation of mellitin, we used large-pore SBA-15-type mesoporous silica. The material was produced following previously published procedures.¹⁰ A mixture of Pluronic 123, cetyl-trimethylammonium bromide (CTAB), mesitylene, potassium chloride and hydrochloric acid was prepared to hydrolyze tetraethylorthosilicate (TEOS) and assemble the mesoporous structure. After calcination, the nitrogen sorption isotherm gave pore diameters of about 11.1 nm (according to non-local density functional theory) and a Brunauer-Emmett-Teller (BET) surface area of about 700 m²/g⁻¹. The corresponding isotherm and NLDFT pore size distribution graph can be found in Figure 10.3.1.

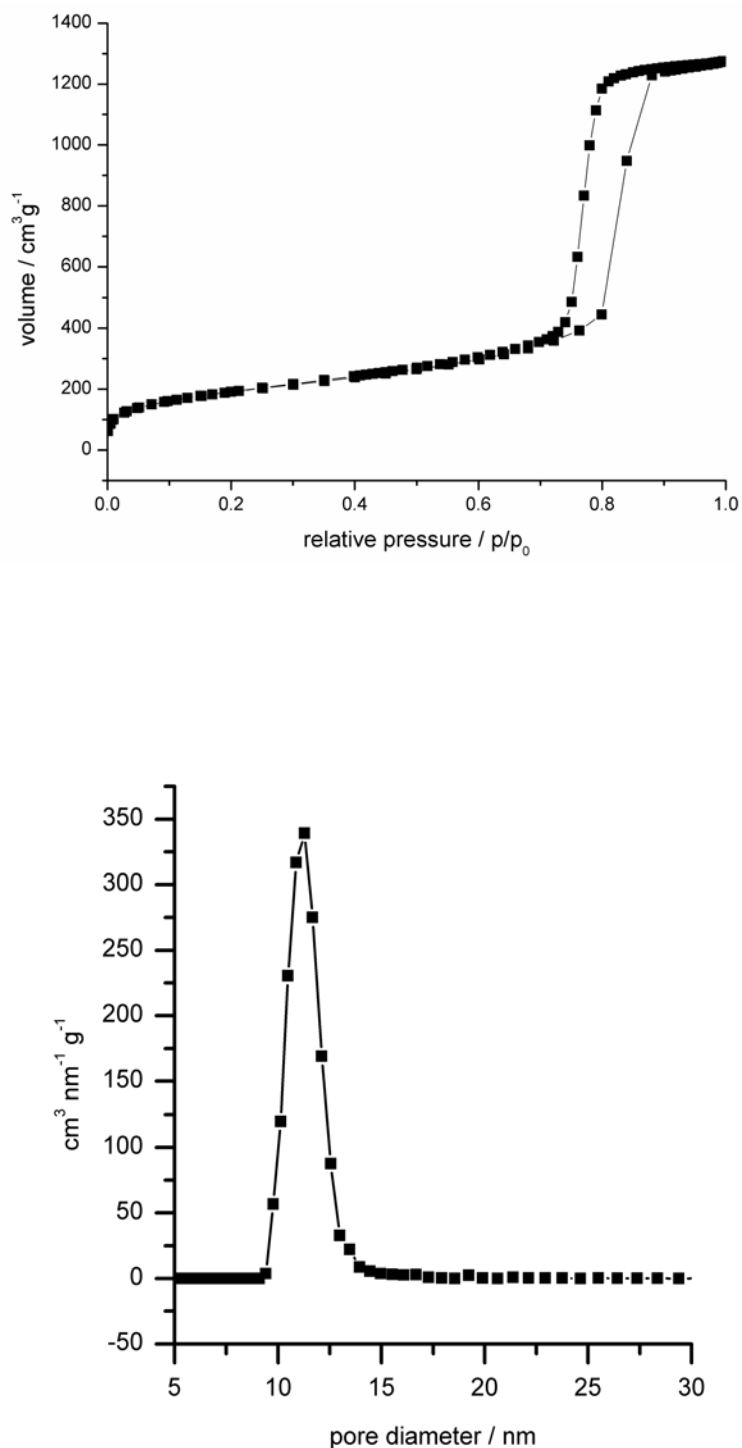


Figure 10.3.1 Nitrogen sorption isotherm (upper graph) and NLDFT pore size distribution (lower graph) of the sample SBA-15.

The resulting material was subsequently functionalized with 3-mercaptopropyltrimethoxysilane (MPTS) by post-synthetic grafting in toluene under nitrogen

atmosphere and reflux conditions, yielding sample SBA-SH. Thermogravimetric analysis (TGA) was performed in order to determine the amount of functionalization grafted to the mesoporous host. The obtained curve can be found in Figure 10.3.2.

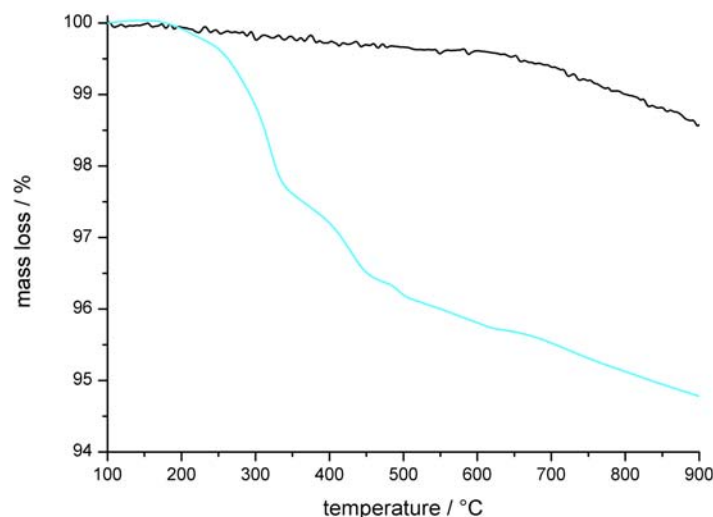


Figure 10.3.2 Thermogravimetric analysis for the samples SBA-15 (black) and SBA-SH (blue).

A mass loss of 5 % during heating to 900°C was evaluated to correspond to a thiol content of 0.67 mmol of mercaptopropyl moieties per gram material. It should be noted, that the resulting mass loss from dehydroxylation processes (>700°C) was not taken into account. The presence of thiols was also confirmed by the cleavage of 2,2'-dithiopyridine, releasing the yellow colored 2-thiopyridon (Ellman's assay), as described in the literature.¹¹ In the following, SBA-SH was dried under vacuum and was then suspended in water-free dimethylsulfoxide (DMSO) under nitrogen atmosphere. The sample was divided in two aliquots of 5 mg each. The samples were incubated with a 10-fold excess of MK- or BM-linker relative to the thiol-content as evaluated by TGA, respectively (samples SBA-MK, SBA-BM, Figure 10.3.3).

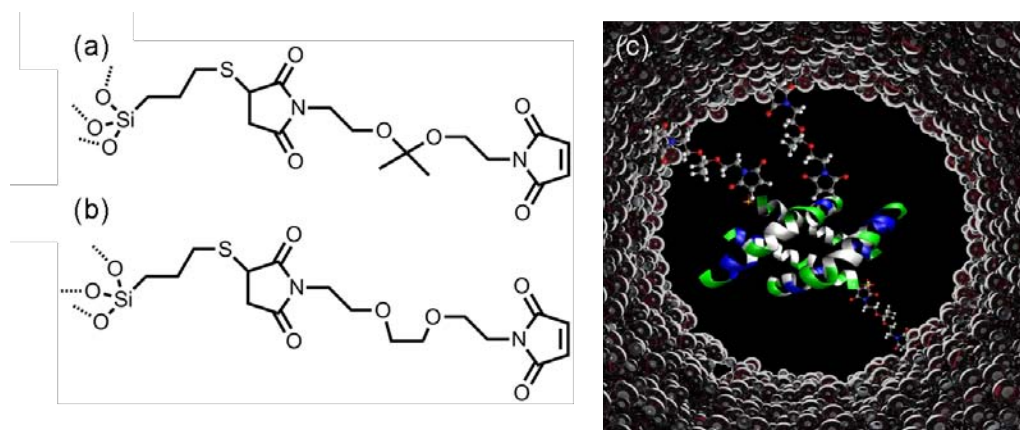


Figure 10.3.3 Attached linkers in the sample (a) SBA-MK, (b) SBA-BM; (c) shows a 3D scheme of the pH-sensitive attachment of mellitin in the pores of SBA-15

The reactions were carried out for 14 hours under nitrogen at room temperature, followed by washing with DMSO. The increasing functionality of the material can be monitored by IR-spectroscopy (see Figure 10.3.4). The presence of the maleimide-linked MK-moiety can be observed by the emerging C=O stretch signal at 1707 cm^{-1} (Figure 10.3.4b). In contrast, the sample SBA-BM shows also aliphatic ether vibrations around 1450 cm^{-1} (Figure 10.3.4c). Additionally, the C=C stretch of the maleimide is visible in the sample SBA-MK. The signals below 1250 cm^{-1} can be attributed to silica framework vibrations. IR-spectra from the pure linkers can be found in the Appendix (A-14) as a reference.

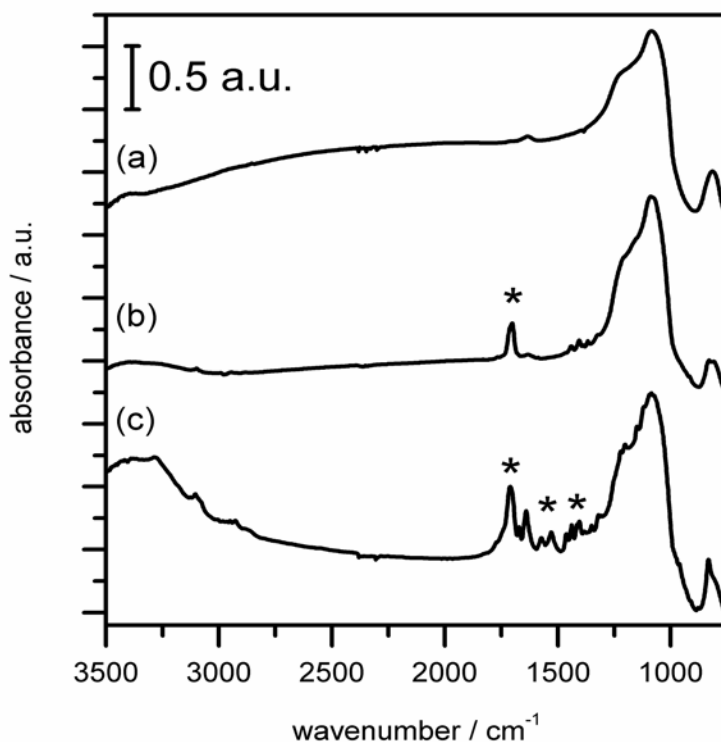


Figure 10.3.4 IR spectra (offset, normalized to the Si-O stretch) of the samples (a) SBA-SH, (b) SBA-MK and (c) SBA-BM; Bands discussed in the text are marked with asterisks.

A negative Ellman's assay also implies the reaction of the free thiol-groups with the maleimide-groups of the respective linkers. Subsequently, 1.0 mg of each sample was incubated with a 1.5-fold excess (relative to the incorporated amount of thiols) of synthetically produced, cysteine-terminated mellitin at room temperature for 4 hours (Samples SBA-MK-Mel, and SBA-BM-Mel).

The conjugation reaction was carried out under water-free conditions in DMSO in order to avoid unwanted cleavage of the acetal linker. After intense washing and centrifugation, the samples were exposed to an erythrocyte leakage assay.

For this purpose, pure mellitin and the suspensions of the samples SBA-BM-Mel and SBA-MK-Mel were serially diluted in phosphate-buffered saline (PBS), resulting in theoretical mellitin concentrations of 5, 1, and 0.1 μM , respectively. 75 μL of a mouse erythrocyte solution (3.75×10^6 cells) were mixed with 75 μL of the respective sample suspension and

mellitin solution as reference. To define 100% lysis, erythrocytes were incubated with 1% Triton-X100 in Phosphate-buffered saline. The acidic samples were pre-incubated at pH 5 for 30 minutes before dilution. In Figure 10.3.5, the results of the leakage assay are shown.

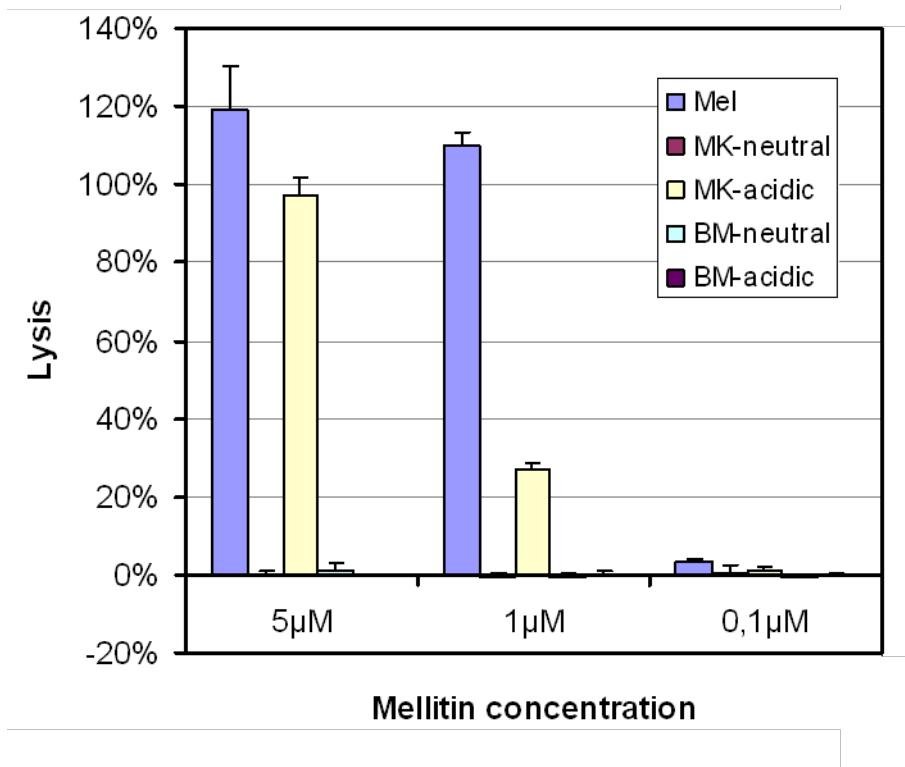


Figure 10.3.5 Results of the erythrocyte leakage assay. The five experiments listed in the figure are plotted in the same sequence from left to right at each different global concentration.

It can be seen that the MK linker shows the desired behavior and remains stable at pH 7. However, when the pH is lowered, the MK-linker is cleaved, resulting in a release of the encapsulated mellitin. In contrast, the applied BM-linker remains stable upon pH decrease, keeping mellitin covalently bound to the pore walls.

In order to quantify the amount of incorporated or released mellitin, a photometric approach was used.¹² This approach is based on the prediction of the molar extinction coefficient ϵ of a peptide by taking into account the number of tryptophanes and tyrosines in the primary structure of the peptide and the disulfide bridges present. According to reference 18, every

tryptophane contributes $5500 \text{ M}^{-1}\text{cm}^{-1}$ to ϵ . Since the primary structure of mellitin contains only one tryptophane and none of the other relevant groups, we can set ϵ to $5500 \text{ M}^{-1}\text{cm}^{-1}$. For the experiment, 1 mg of SBA-MK was incubated with 3 mg of mellitin in 1.5 mL water-free DMSO for 4 hours. The silica was separated from the suspension by centrifugation. Absorption measurements of the supernatant at 280 nm gave an amount of 1.85 mg peptide in solution, or 1.15 mg ($0.4 \mu\text{mol}$) mellitin of the uptaken mellitin, respectively. Relative to the initial amount of 3-mercaptopropyl-moieties, the occupation of the potential binding sites for the mellitin peptide can be calculated to 60 %. The centrifugate was re-suspended in 1.5 mL of PBS buffer (pH 7.4). Subsequently, the resulting suspension was separated into two equal aliquots. One of the two resulting samples was centrifuged down, the other one was filled up with $750 \mu\text{L}$ of PBS-buffer (pH 7.4). The resulting pellet was resuspended in 1.5 mL PBS buffer (pH 5.5). The two resulting samples are defined as Quant-MK-7.4 and Quant-MK-5.5. After 60 minutes of incubation, the samples were centrifuged off and the absorption at 280 nm of the supernatant was determined. It was found that the sample Quant-MK-5.5 has released the amount of 0.615 mg of mellitin, while the sample Quant-MK-7.4 only released 0.015 mg. The observed value of released peptide corresponds well to the determined amount of incorporated mellitin. A detailed calculation of the UV-absorption using Lambert-Beer's law can be found in the Appendix (A-15).

10.4 Conclusion

To summarize, we have shown that acetals can be applied as pH-sensitive linkers for the delivery of a biomedically relevant peptide from mesoporous silica. The obtained results represent an interesting alternative for the release of bioactive compounds from mesoporous hybrid materials. The investigated acetal linkers attached between the pore walls and the peptides clearly show an on/off mechanism in the observed time intervals for the release. The investigated pH-values represent the pH values in the human blood stream (7.4) and late

endosomes in cells (5.5), respectively. This implies that the obtained results are of significant importance in the field of targeted drug delivery.

10.5 References

- (1) Liu, R.; Zhang, Y.; Zhao, X.; Agarwal, A.; Mueller, L. J.; Feng, P. *Journal of the American Chemical Society* **2010**, *132*, 1500.
- (2) Mal, N. K.; Fujiwara, M.; Tanaka, Y. *Nature (London, United Kingdom)* **2003**, *421*, 350.
- (3) Mortera, R.; Vivero-Escoto, J.; Slowing, I. I.; Garrone, E.; Onida, B.; Lin, V. S. Y. *Chemical Communications (Cambridge, United Kingdom)* **2009**, 3219.
- (4) Sauer, A. M.; Schlossbauer, A.; Ruthardt, N.; Cauda, V.; Bein, T.; Braeuchle, C. *Nano Letters* **2010**, *10*, 3684.
- (5) Killisch, I.; Steinlein, P.; Roemisch, K.; Hollinshead, R.; Beug, H.; Griffiths, G. *Journal of Cell Science* **1992**, *103*, 211.
- (6) Raghuraman, H.; Chattopadhyay, A. *Bioscience Reports* **2007**, *27*, 189.
- (7) Park, H. J.; Lee, Y. K.; Song, H. S.; Kim, G. J.; Son, D. J.; Lee, J. W.; Hong, J. T. *Journal of Toxicology and Public Health* **2006**, *22*, 31.
- (8) Meyer, M.; Dohmen, C.; Philipp, A.; Kiener, D.; Maiwald, G.; Scheu, C.; Ogris, M.; Wagner, E. *Molecular Pharmaceutics* **2009**, *6*, 752.
- (9) Knorr, V.; Russ, V.; Allmendinger, L.; Ogris, M.; Wagner, E. *Bioconjugate Chemistry* **2008**, *19*, 1625.
- (10) Gillies, E. R.; Goodwin, A. P.; Frechet, J. M. J. *Bioconjugate Chemistry* **2004**, *15*, 1254.
- (11) Katiyar, A.; Yadav, S.; Smirniotis, P. G.; Pinto, N. G. *Journal of Chromatography, A* **2006**, *1122*, 13.
- (12) Pace, C. N.; Vajdos, F.; Fee, L.; Grimsley, G.; Gray, T. *Protein Science* **1995**, *4*, 2411.

11. General Conclusions and Outlook

In the present work, new pathways for the construction of nanosized drug delivery devices based on mesoporous silica were developed.

First, a sequential co-condensation approach was developed in order to obtain multiple functionality within single colloidal mesoporous silica particles. It was shown that a spatial separation of two different molecular functions can be achieved by adding the functionalized precursors at different time-points of the particle growth.

Click-chemistry was evaluated as a mild synthetic tool for the covalent attachment of sensitive biomolecules in the pores of mesoporous silica. It was demonstrated that the activity of enzymes can be conserved in the protected environment of a mesoporous silica host and that the enzyme can be exposed to many recovery cycles. The careful investigation of this strategy was necessary as it was further applied as a synthesis step in the construction of a DNA-based molecular valve.

Controlled release of model compounds or bioactive molecules was also investigated. Molecular valves that open upon enzymatic digestion were developed. By placing avidin proteins that act as molecular caps on the pore mouths of mesoporous silica nanoparticles, fluorescein was encapsulated inside the pores. The addition of trypsin caused opening of the caps and the dye was able to leach out of the particle.

Attaching DNA-linkers between the silica surface and the protein caps successfully extended this capping concept. This approach allowed us to impart a programmable release temperature to the colloidal mesoporous silica. It was shown that the length of the DNA-linker and thus its melting temperature defines the temperature for the guest release.

Other approaches do not use external caps on the outer surface of the pores, but directly link the guest (or cargo) molecules to the inner pore walls. Mesoporous silica nanoparticles with disulfide-linked cysteine inside the pores were synthesized and investigated during the course of this work. It was shown that the amino acid is released upon creation of a reductive milieu

in vitro. However, studies in living cancer cells have demonstrated that the reductive potential in an endosome is not sufficient to release the guest. This issue was investigated in cooperation with the group of Prof. Bräuchle, and we could show that photosensitizers producing singlet oxygen induce the endosomal escape of the drug carriers and therefore lead to a successful drug delivery.

Taking into account these results, we designed particles that carry a modified derivative of protoporphyrin IX covalently attached to the outer surface of the mesoporous nanoparticles. The biological activity of these systems was again demonstrated by live-cell imaging at a single cell level in cooperation with the group of Prof. Bräuchle.

Encouraged by these results, we applied this approach to the light-induced delivery of small antibodies (chromobodies) from lipid-bilayer coated mesoporous silica nanoparticles. GFP-labeled microtubuli in HuH7 cells were successfully labeled with the chromobodies. This demonstrates the applicability of our mesoporous silica nanoparticles as carriers for these biomolecules.

Finally, another way to use reversible chemistry in drug delivery is to utilize the dramatic pH drop from cell medium (around 7.4) to late endosomes (around 5.4). In this context, acetal linkers were integrated into the mesopores to trigger the release of the apoptotic peptide mellitin from SBA-15 mesoporous silica. In a joint project with the group of Prof. Wagner we could show that the membrane intercalating peptide destroys mouse erythrocytes only at low pH values around 5, while it stays encapsulated in the host at a neutral pH.

Further experiments based on the findings from this work will provide multifunctional mesoporous silica nanoparticles with larger pores than 4 nm. A larger pore diameter enables the encapsulation of therapeutic biomolecules like siRNA, peptide nucleic acids (PNA) or peptides into nanosized carriers. Another next step will be the use of the introduced DNA-

based cap system (Chapter 6) in living cells. A possible release trigger in cells can be a concurrent hybridization with intracellular single stranded oligonucleotides.

The attachment of targeting ligands in order to provide a specialized affinity to a cancer cell should also be one of the next steps. Interesting molecules to be bound to the particle's surface are the RGD peptide, the epidermal growth factor (EGF), folic acid, or even a combination of the three.

Another interesting aspect to investigate is the *in vivo* behavior of the synthesized silica nanoparticles, for example, in a mouse model. The blood circulation time is an important factor for the efficiency of nanosized drug delivery and imaging devices. Different surface functionalities can have a dramatic influence on the behavior of the particles in a biological system.

The findings of this work are the product of a successful cooperation of different fields of science, such as chemistry, physics, pharmaceuticals and medicine. It can be seen that the interdisciplinary cooperation of different fields of science opens the gate to new materials with striking properties. Thus, the integration of functional biomolecules in inorganic structures can lead to novel macroscopic functions of the synthesized material.

12. Appendix

A-1 Isotherms and NLDFIT pore size distribution of the samples synthesized in Approach A and B

The nitrogen sorption values shown in Table 3.3.1 and Table 3.3.2 were derived from the data shown in Figures A-1.1, A-1.2, and A-1.3

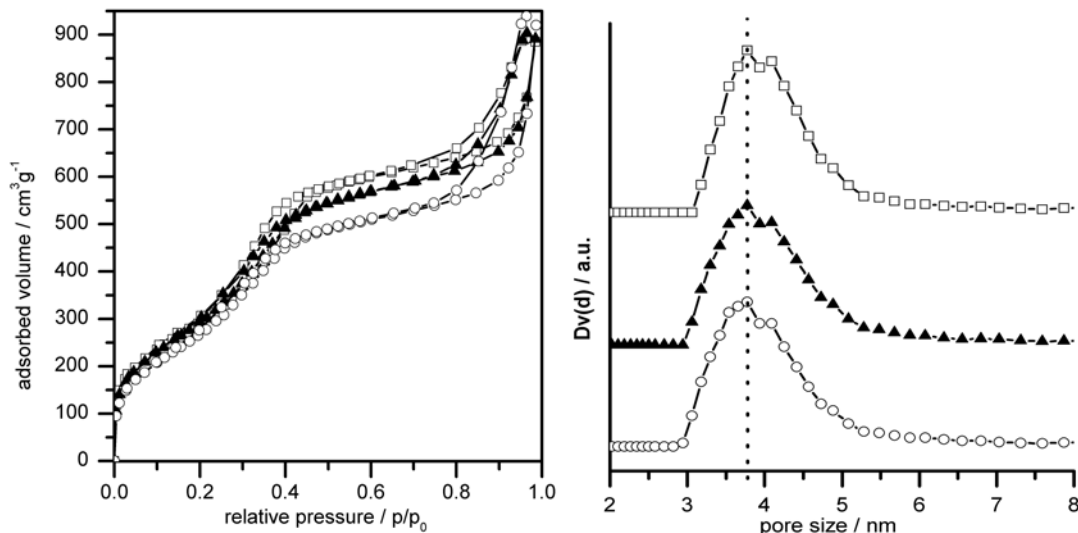


Figure A-1.1 Nitrogen sorption isotherms (left) and NLDFIT pore size distributions (right, offset) of the samples Un-CMS (□), CMS(A)-Cl_{OUT} (▲), and CMS(A)-Cl_{OUT}-NH_{IN} (○)

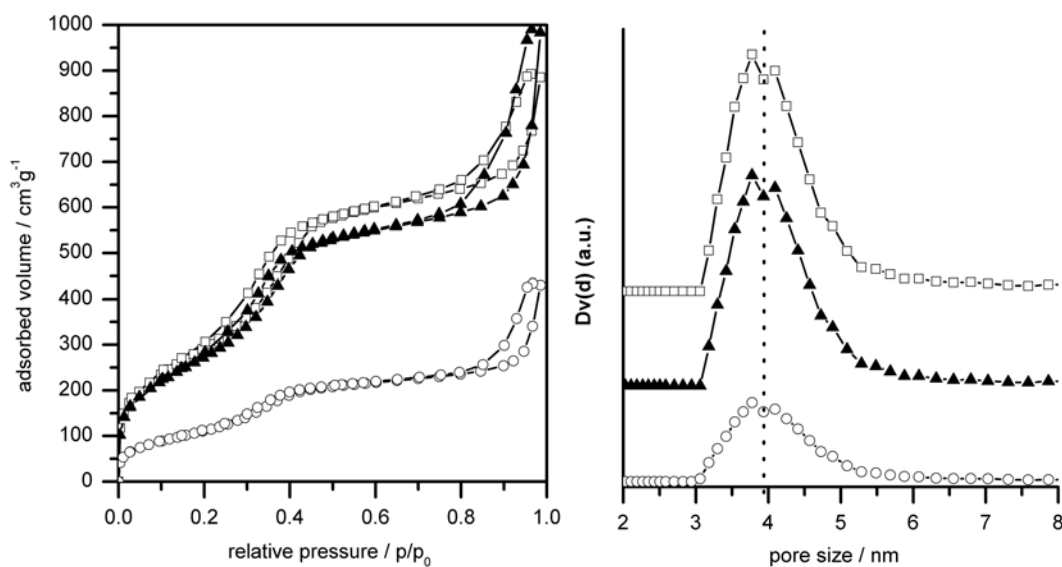


Figure A-1.2 Nitrogen sorption isotherms (left) and NLDFIT pore size distributions (right, offset) of the samples Un-CMS (□), CMS(A)-NH_{OUT} (▲) and CMS(A)-NH_{OUT}-Cl_{IN} (○)

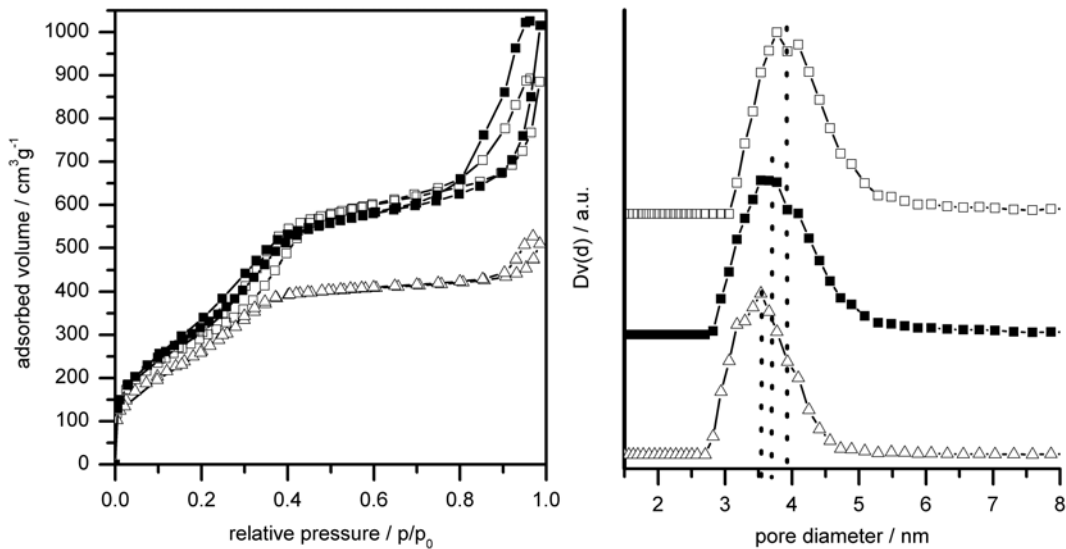


Figure A-1.3 Nitrogen sorption isotherms (left) and NLDFT pore size distributions (right, offset) of the samples Un-CMS (□), CMS(B)-Ph_{IN}-NH_{OUT} (■) and CMS(B)-(Ph/NH)_{IN} (△)

A-2 Detailed calculations for thermogravimetric analysis (TGA) of the samples SBA-Cl and SBA-trypsin

(a) TGA-Calculations for SBA-Cl

1 g sample contains 50 mg of chloropropyl-residues (C_3H_6Cl , 77.53 gmol^{-1}).

$$\frac{0.05 \text{ g}}{77.53 \text{ gmol}^{-1}} = 6.45 \cdot 10^{-4} \text{ mol pro g SBA-Cl}$$

$$\rightarrow 1 \text{ g silica has bound } \frac{6.45 \cdot 10^{-4} \text{ mol}}{0.95 \text{ g}} = 6.79 \cdot 10^{-4} \text{ mol chloropropyl-residues}$$

(b) TGA calculation for SBA-trypsin

1 g sample contains 150 mg of organic compounds. Thus, 1 g SBA-15 has bound

$$\frac{0.15 \text{ g}}{0.85 \text{ g}} = 0.176 \text{ g organic compounds.}$$

The amount of chloropropyl residues is subtracted in order to get the amount of enzyme attached to the surface.

$$0.176 \text{ g} - 0.053 \text{ g} = 0.12 \text{ g of trypsin attached to 1 g of SBA-15}$$

A-3. Detailed calculations for the protein quantification from BCA-assay for the samples SBA-trypsin and Cab-o-Sil-trypsin

The supernatants of the reactions 3.2.6 (preparation of SBA-trypsin) and 3.2.9 (preparation of Cab-o-Sil-trypsin) were analyzed in order to determine the amount of enzyme that reacted with SBA-N₃. In both reactions 3.2.6 and 3.2.9, the amount of 7.0 mg protein was used. The presence of 1.0 mg protein in the supernatant in reaction 3.2.6 implies that 6.0 mg protein have bound to 50 mg of SBA-N₃. This value confirms the results from TGA of the sample SBA-trypsin (12%). In reaction 3.2.9, no protein could be detected by the BCA method. The applied amount of enzyme was completely attached to the surface.

A-4. NLDFT pore size distributions of the samples prepared in chapter 5

The pore size distribution curves are shown in Figure A-4.1

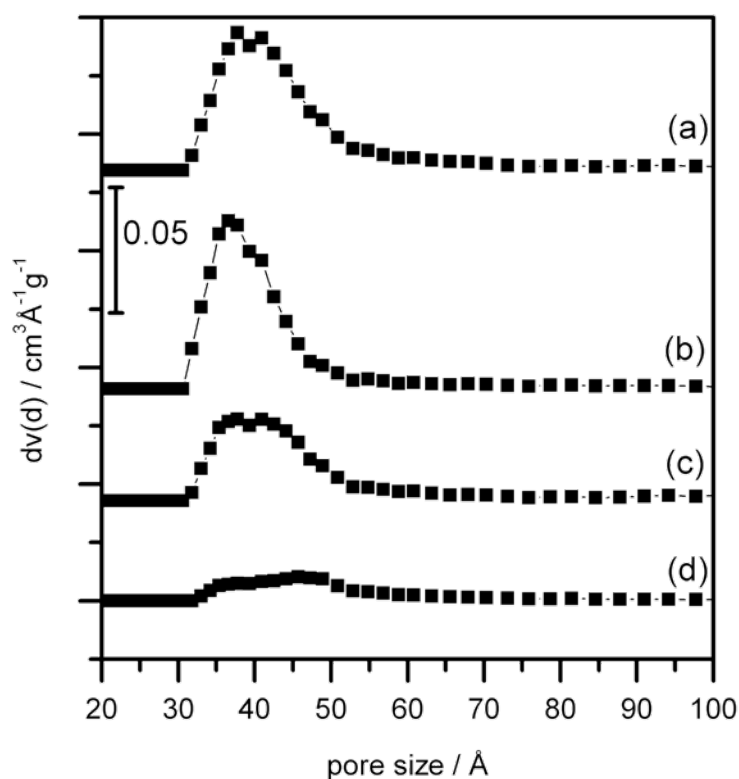


Figure A-4.1 NLDFT pore size distribution of the samples (a) CMS, (b) CMS-SH, (c) CMS-BIO and (d) CMS-AVI

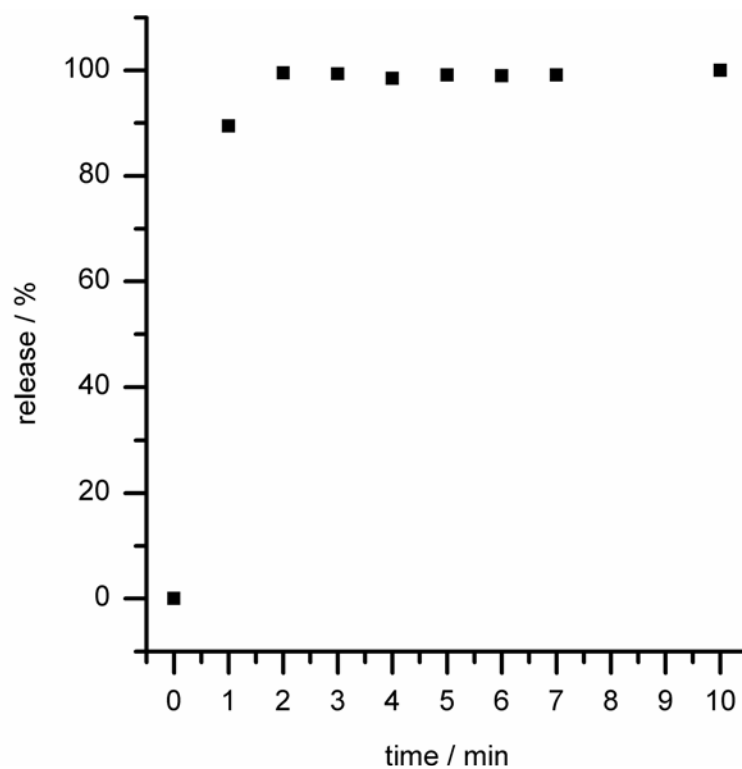
A-5. Reference experiment from unfucntionalized CMS (Chapter 5)

Figure A-5.1 Release of non-encapsulated fluorescein through a dialysis membrane

A-6. Fluorescein release quantification of the samples prepared in Chapter 5 and 6.

For quantification, a calibration curve for fluorescein was recorded (Figure A-6.1) in the UV-vis spectrometer and the released fluorescein was quantified.

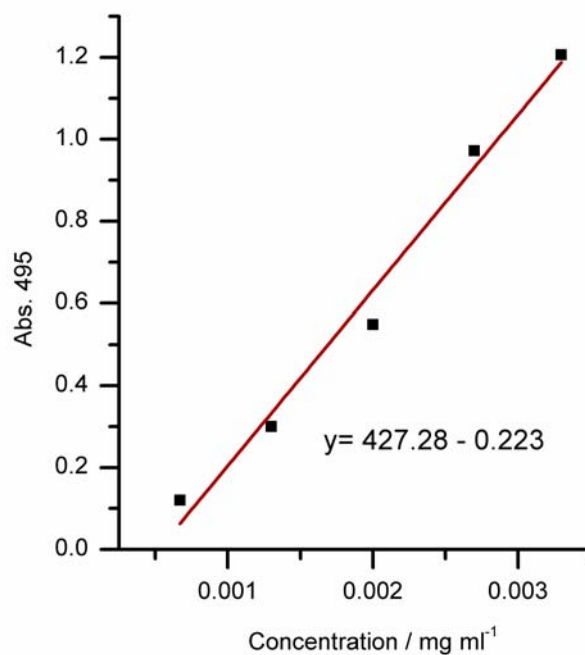


Figure A-6.1 Calibration curve for fluorescein concentration determination

The fluorescein solutions from the release experiment were diluted by the factor of 10. The absorption at 495 nm was recorded and the amount of released dye was quantified (Table A-6.1).

Table A-6.1 Quantification of release of fluorescein from CMS samples

Sample	CMS	CMS-AVI	
		Thermoresponsive	Protease-responsive
Abs. at 495 nm	0.760	0.689	0.702
Concentration (mg ml⁻¹)	0.0023	0.0021	0.0022
Released fluorescein [mg/mg sample]	0.035	0.031	0.033

Example for the calculation (CMS):

An absorbance of 0.760 leads to a sample concentration of 0.0023 mg/ml using the calibration curve.

The sample was diluted by the factor of 10. → Original sample concentration: 0.023 mg/ml.

Sample volume is 3 ml → Total amount of released fluorescein: is 0.069 mg.

The fluorescein was released from 2 mg of CMS: Released fluorescein is 0.035 mg/mg CMS

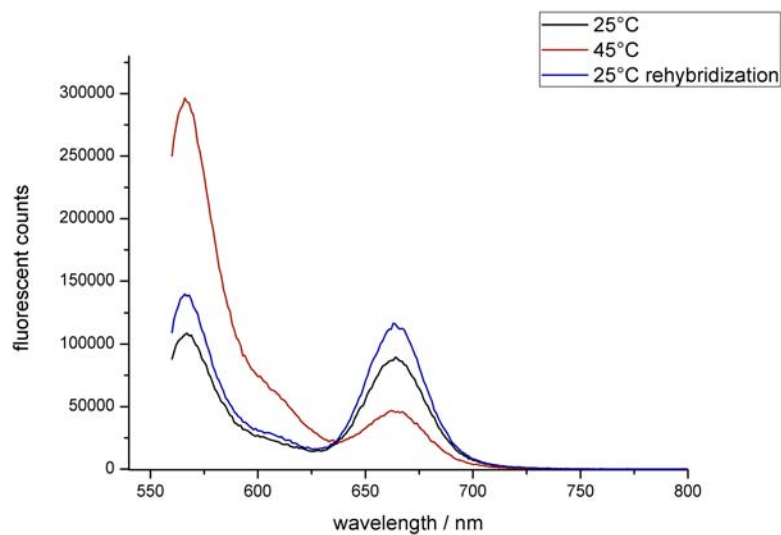
A-7. FRET-experiment with pure as-received 15mer DNA-strands

Figure A-7.1 FRET measurement of the pure as-received 15mer DNA double strand at 25°C (black), at 45 °C (red), and after rehybridization at 25°C (blue)

A-8. Raw data for the programmed thermoresponsive release experiments

The raw data for the investigated fluorescein release are displayed in the Figures A-8.1, A-8.2, A-8.3, and A-8.4.

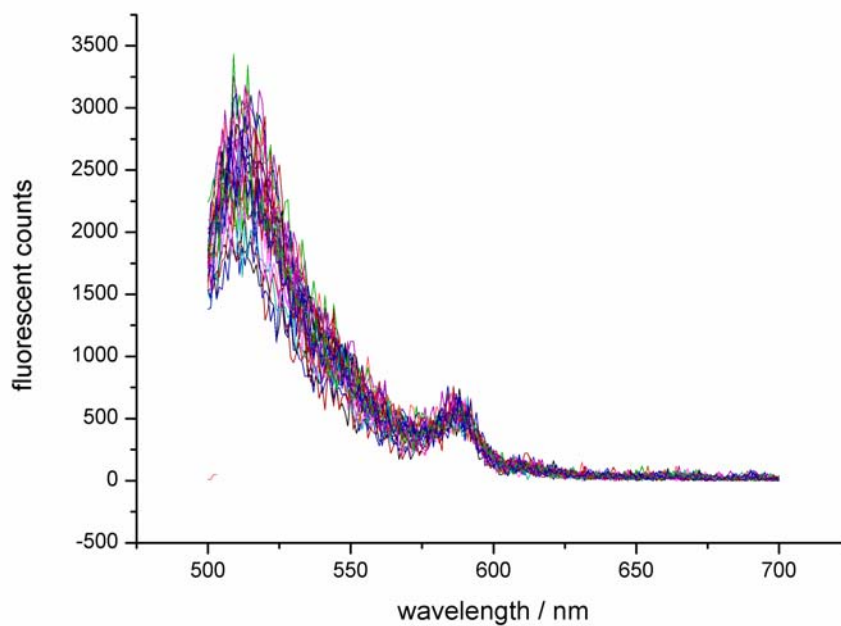


Figure A-8.1 Series of emission spectra of sample CMS-DNA₁₅-AVI at 25°C. Data was collected for 1 hour in 5 minutes intervals.

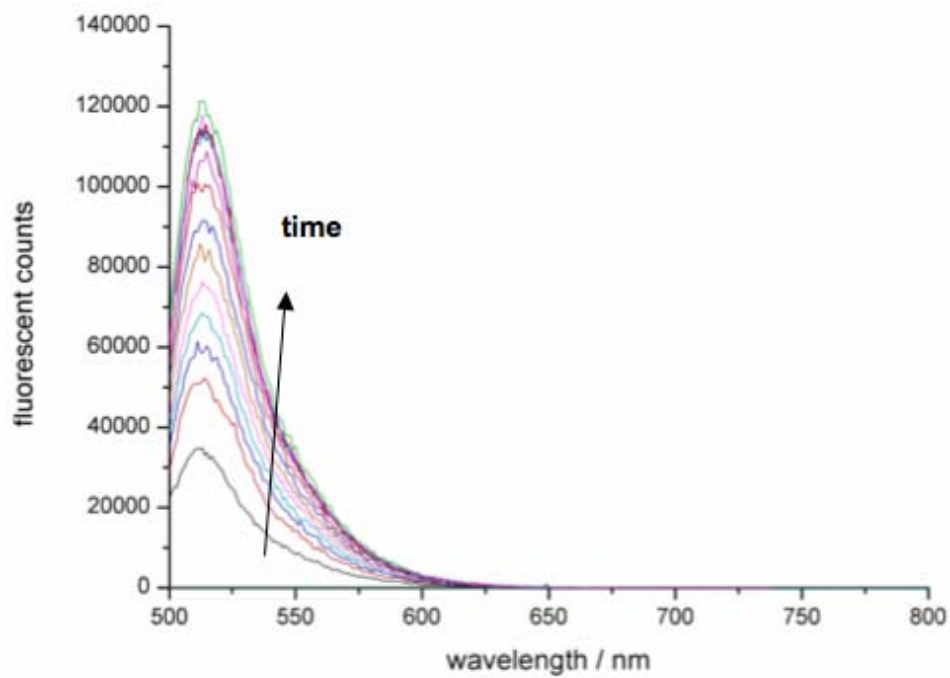


Figure A-8.2 Series of emission spectra of sample CMS-DNA₁₅-AVI at 45°C.

Acquisition every 2 minutes

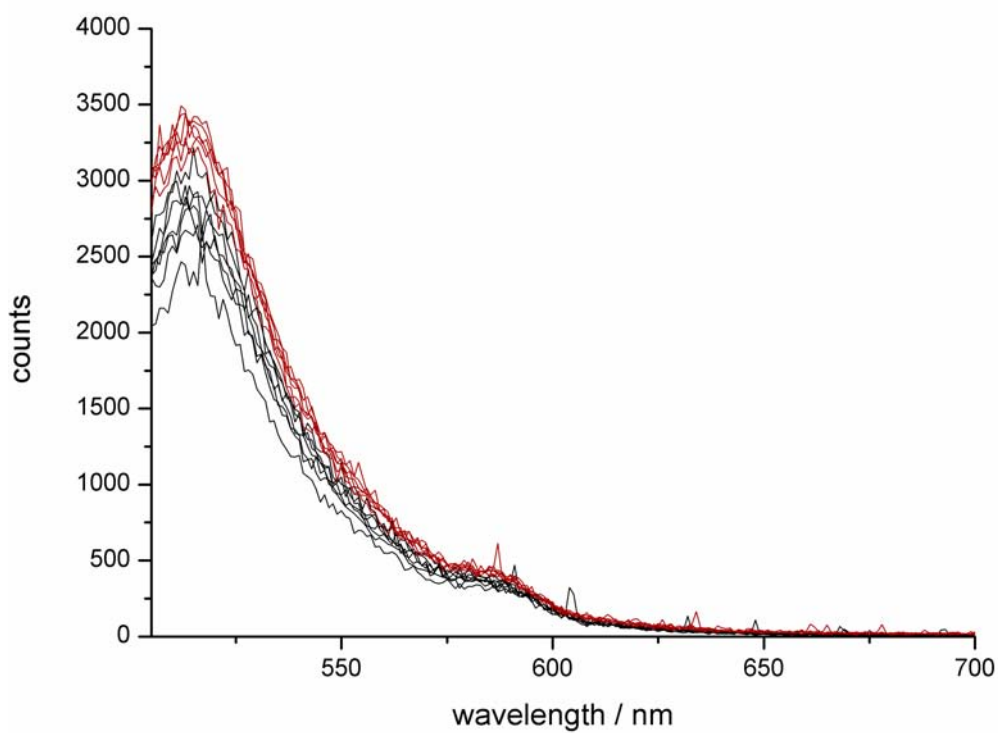


Figure A-8.3 Series of emission spectra of sample CMS-DNA₂₅-AVI, ten minutes between the acquisitions. (Black lines: 25°C; Red lines: 45°C)

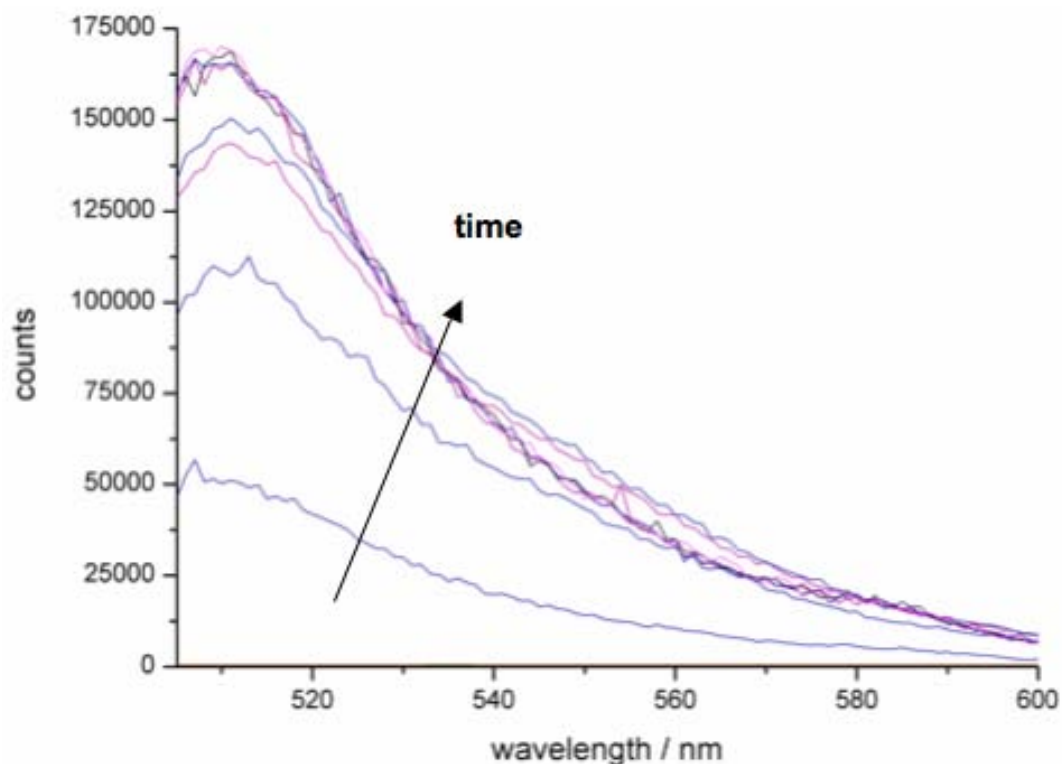


Figure A-8.4 Series of emission spectra of sample CMS-DNA₂₅-AVI, ten minutes between the acquisitions. Temperature 65 °C (open state)

A-9. UV-vis calculation for the released amounts of fluorescein from the CMS-DNA-AVI samples

Fluorescein solutions showing the corresponding maximum fluorescent counts released from the samples CMS-DNA₁₅-AVI and CMS-DNA₂₅-AVI were prepared and then diluted by the factor of ten. The absorption at 495 nm of the prepared samples can be used to determine the exact fluorescein content of the solution (A calibration curve is shown in Figure A-6.1).

Table A-9.1 Quantification of release of fluorescein from CMS samples

Sample	CMS-DNA₁₅-AVI	CMS-DNA₂₅-AVI
Abs. at 495 nm	0.344	0.348
Concentration (mg ml⁻¹)	0.0011	0.0013
Released fluorescein [mg/mg sample]	0.033	0.040

Example for the calculation (CMS):

An absorbance of 0.344 leads to a sample concentration of 0.0011 mg/ml by using the calibration curve's linear regression.

The sample was diluted by the factor of 10. → Original sample concentration: 0.011 mg/ml.

Sample volume is 3 ml → Total amount of released fluorescein: is 0.033 mg.

The fluorescein was released from 1 mg of CMS: Released fluorescein is 0.033 mg/mg CMS

A-10. Nitrogen Sorption Isotherm of the sample CMS-SH_{core}-NH₂shell (Chapter 7)

The nitrogen sorption isotherm of the sample CMS-SH_{core}-NH₂shell can be found in Figure A-10.1.

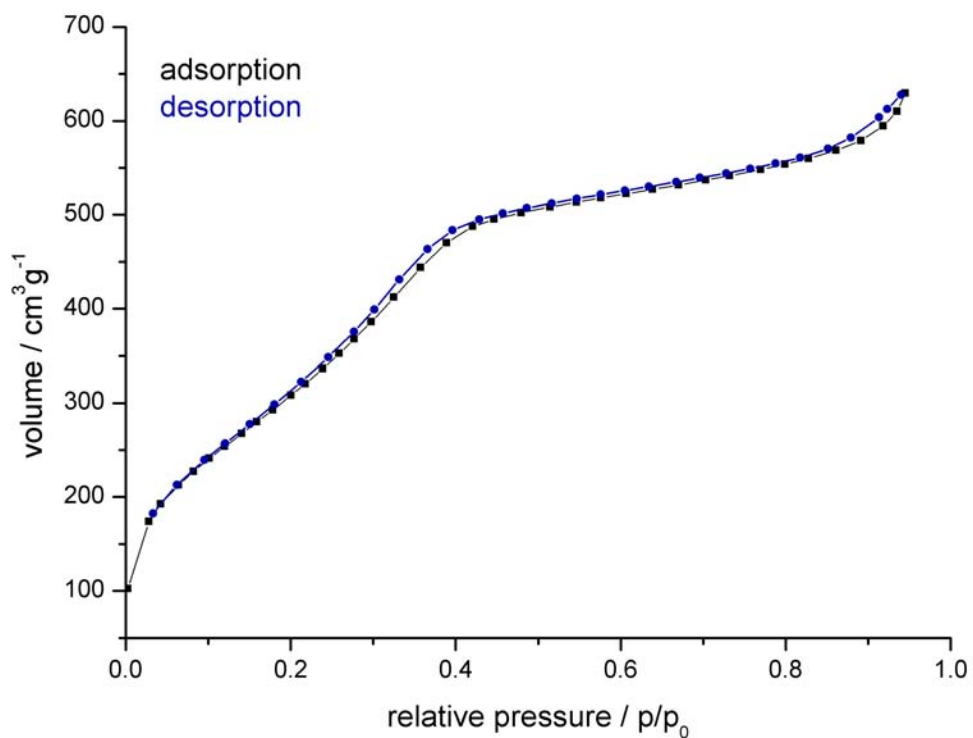


Figure A-10.1 Nitrogen sorption isotherm of the sample CMS-SH_{core}-NH₂shell

A-11. Reference microscopy measurements of Chapter 7

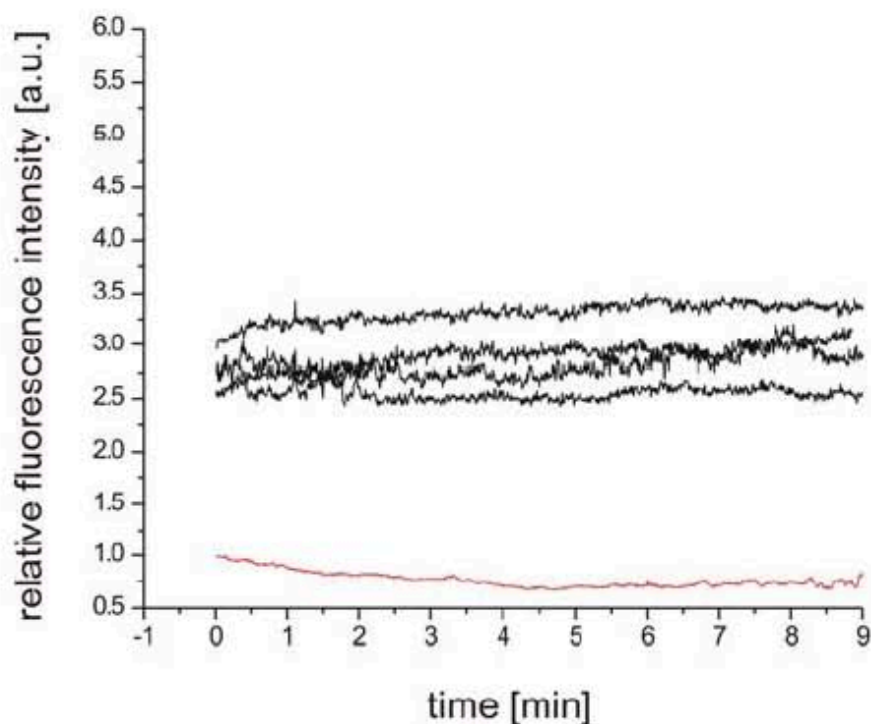


Figure A-11.1. Influence of a TPPS_{2a} solution on redox-cleavable CMS-CysATTO633_{core}-NH_{2shell} measured at a single particle level

Redox-cleavable CMS-CysATTO633_{core}-NH_{2shell} nanoparticles were incubated in a TPPS_{2a} solution on glass coverslips on the microscope. TPPS_{2a} was activated with a 405 nm laser. A movie was recorded at 642 nm illumination with an exposure time of 200 ms and a frame rate of 3.4 s⁻¹. The CysATTO633 intensity of single particles (black curves) on glass and background (red curve) was extracted from the movie, normalized and plotted versus time. The control measurement shows that activated TPPS_{2a} in solution has no influence on the fluorescence intensity of CMS-CysATTO633_{core}-NH_{2shell} particles.

A-12. Nitrogen sorption isotherm of the sample CMS-NH₂core-SH_{shell}

The isotherm of the sample CMS-NH₂core-SH_{shell} can be found in Figure A-12.1, the corresponding NLDFT pore size distribution can be found in Figure A12-2.

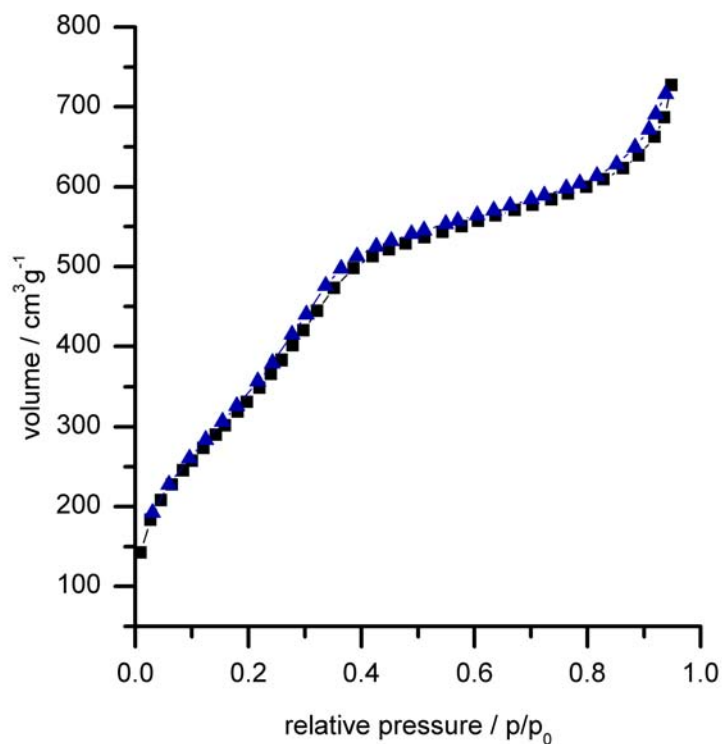


Figure A-12.1 Nitrogen sorption isotherm of the sample CMS-NH₂core-SH_{shell}. Adsorption is plotted in black, desorption is plotted in blue.

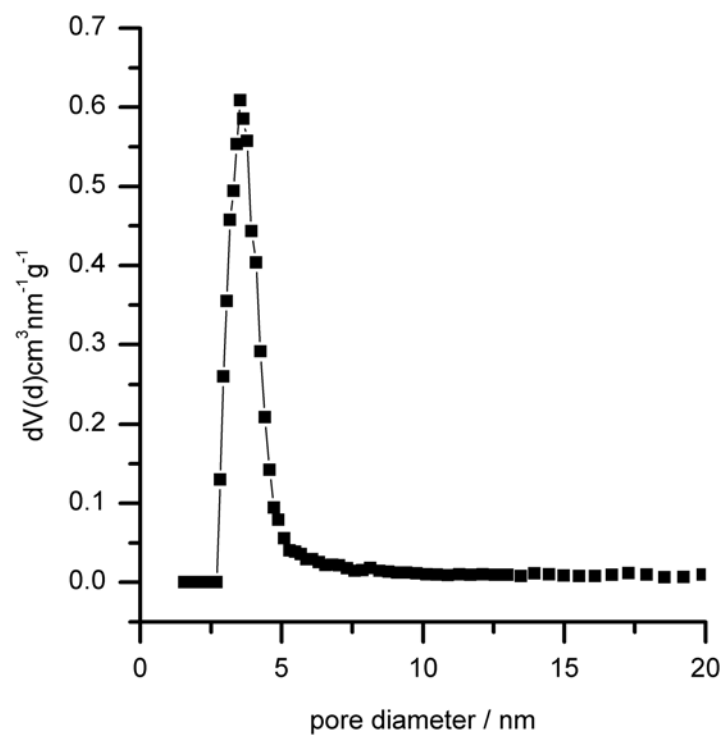


Figure A-12.2 NLDTF pore size distribution of the sample CMS-NH₂_{core}-SH_{shell}

A-13. ESI-MS of the sample PP-NH₂

A scan of the obtained sheet from ESI-MS can be seen in Figure A-13.1. The $[m+H]^+$ peak at 743.38 and the $[m+Na]^+$ peak at 765.36 clearly show the successful synthesis of PP-NH₂.

(exact formula mass: 742.37g/mol)

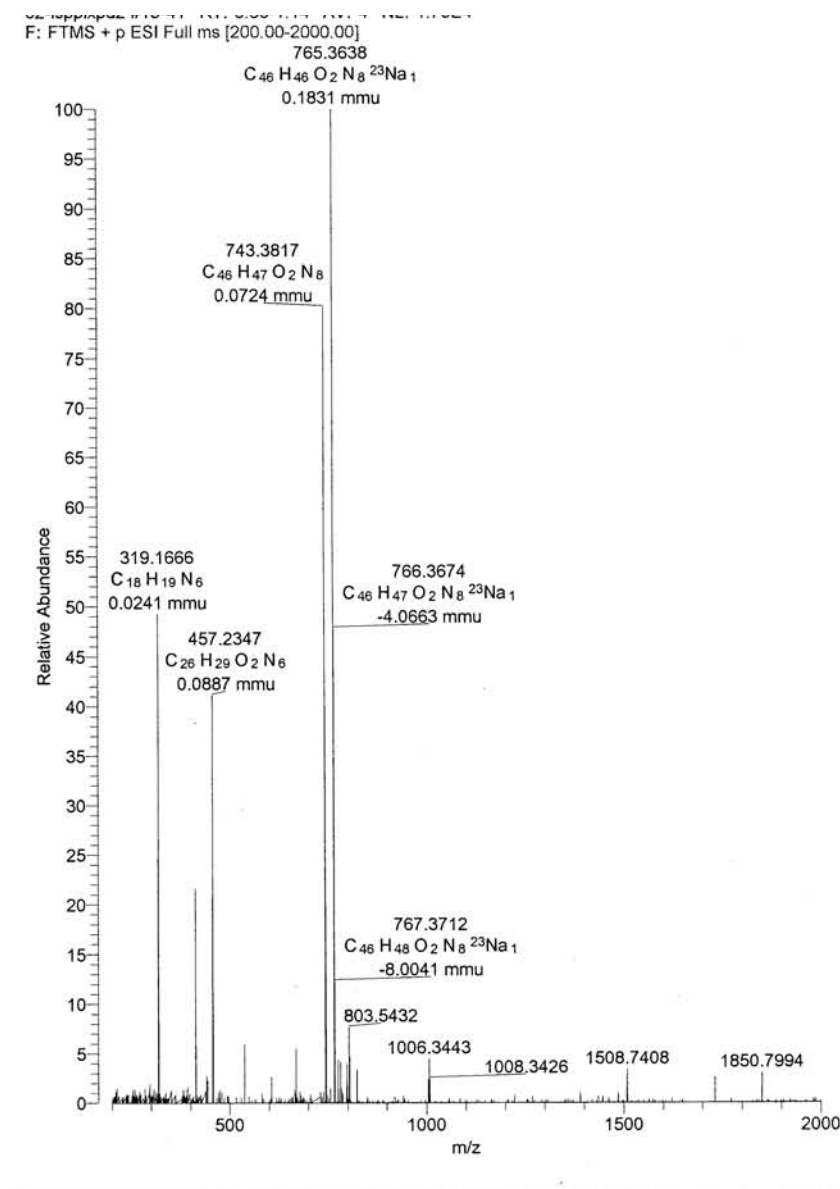


Figure A.13-1 Scan of the obtained spectra from ESI-MS

A-14. DLS of the sample Stöber-NH₂ (Chapter 9)

A number-weighted statistics graph of the sample Stöber-NH₂ can be found in Figure A-14.1.

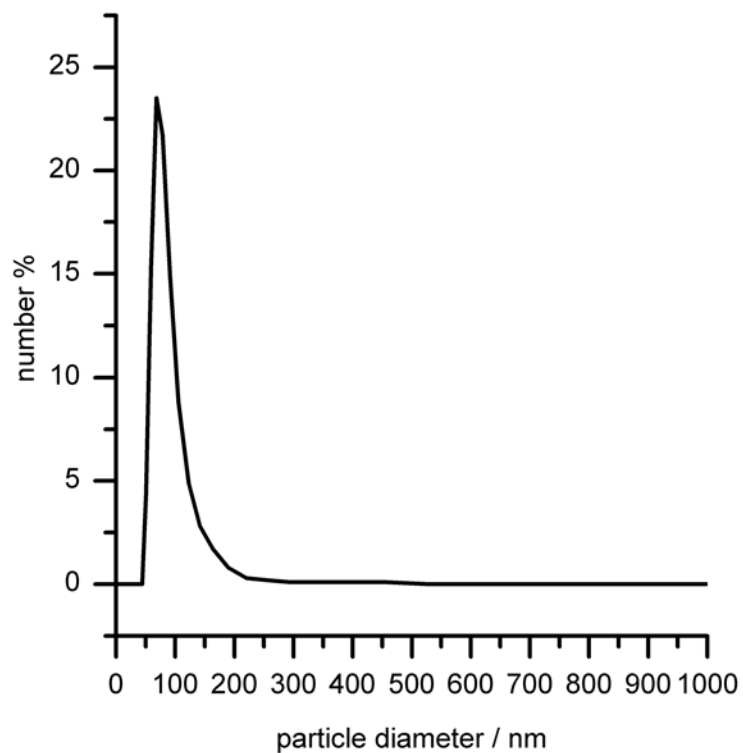


Figure A-14.1 DLS-measurement of the sample Stöber-NH₂

A-15. IR-spectra of the applied bismaleimide linkers (Chapter 10)

The reference spectra of the applied linkers and the mellitin peptide are displayed in Figure A-15.1.

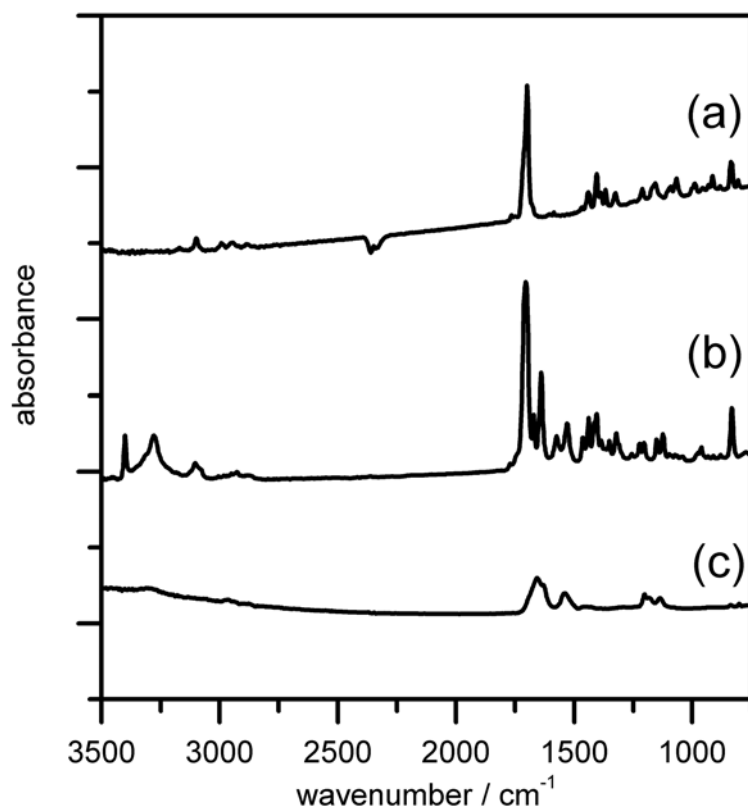


Figure A-15.1 IR-spectra of (a) MK-linker, (b) BM-linker, and (c) mellitin

A-16 Mellitin quantification with UV-vis spectroscopy (Chapter 10)

For quantification of the uptaken and released amount of mellitin, the samples Quant-MK-7.4 and Quant-MK-5.5 were prepared. For the synthesis, the procedure described in 10.2.6 was followed, using the MK-linker. After mellitin attachment, the sample was centrifuged down and the pellet was washed and resuspended in PBS buffer at pH 7.4. Then, the sample was divided in two equal aliquots. For the sample Quant-MK-7.4, the amount of 750 μL of PBS-buffer (7.4) was added, to give a resulting sample volume of 1.5 mL. For the preparation of the sample Quant-MK-5.5, the respective aliquot was centrifuged and redispersed in PBS buffer (5.5). Incubation time for the release was one hour.

12. Appendix

The theoretical calculated extinction coefficient of the mellitin can be calculated according to reference 13 (Formula A-16.1).

$$\varepsilon(280)(M^{-1}cm^{-1}) = (\#Trp)(5500) + (\#Tyr)(1490) + (\#cystines)(125)$$

Formula A-16.1. Calculation of the molar extinction coefficient ε according to ref. 13.

The primary structure of our cysteine-terminated mellitin is:

CIGA VLKV LTTG LPAL ISWI KRKR QQ-OH; all D-amino acid, M_w : 2893.6 Da

For the quantification of the uptake, 10 μ L of the supernatant was diluted with 100 μ L PBS buffer. The absorption was $A_{280} = 0.213$

According to Lambert-Beer's law, the concentration can be calculated as follows.

$$c = \frac{0.213 \text{ mol}}{5500 \text{ l}} = 0.0387 \frac{\mu\text{mol}}{\text{mL}}$$

→ Under consideration of the dilution factor of 11, the Mellitin concentration in the observed sample can be calculated to 0.4257 μ mol/mL or 1.85 mg of mellitin in 1.5 mL supernatant.

This results in an uptaken amount of mellitin of 1.15 mg per mg SBA-MK or a linker occupancy of about 60 %.

The loaded SBA-MK-Mel was separated in two equal aliquots.

The amount of released Mellitin in the sample Quant-MK-5.5 was quantified as follows.

$$A_{280}=0.779 \text{ (no dilution!)}$$

$$c = 0.615 \text{ mg in 1.5 mL solution}$$

This value is multiplied by 2, since only one of the aliquots was transferred to pH 5.5.

According to our measurements, we have released 1.23 mg Mellitin from 1 mg SBA-MK at a pH of 5.5 within 60 Minutes.

The other aliquot was incubated at pH of 7.4 for 60 minutes. Again, absorption at 280 nm was measured.

$$A_{280} = 0.020$$

12. Appendix

This value can further be calculated to a mellitin release of 0.030 mg per 1 mg of SBA-MK within one hour at a pH of 7.4.

13. Curriculum vitae

Persönliche Daten

Geb. am 15.12.1981 in München
Familienstand: ledig
Staatsangehörigkeit: deutsch

Schule

05/2001: Abitur am Carl-Spitzweg-Gymnasium Unterpfaffenhofen

Zivildienst

09/2001-09/2002: Zivildienst (Labortätigkeit) an der LMU München, Medizinische
(ab 06/2002-09/2002: Fakultät (Prof. Gerbes, PD Dr. Manfred Bilzer)
angestellter
Mitarbeiter)

Studium und Promotion

10/2002 – 12/2007: Studium der Chemie an der Ludwig-Maximilians-Universität
München
09/2002 – 10/2004: Grundstudium
28.10.2004 Vordiplom (2.98)
10/2004-12/2007: Hauptstudium
6/2007 – 12/2007: Diplomarbeit: „*Biofunctionalized colloidal mesoporous silica*“
bei Prof. Thomas Bein (1.0)
14.12.2007: Diplom-Chemiker Univ. (1.84)
Seit 01/2008: Promotion bei Prof. Thomas Bein: “*Functionalized colloidal
mesoporous silica for controlled release applications*”
Vorr. ab 01/2011 Post-Doc bei Prof. Craig Hawker, UC Santa Barbara

Sonstige Tätigkeiten

Seit 01/2008: Verantwortlicher wissenschaftlicher Angestellter für die Infrarot-
und Ramanspektroskopie, Zentrifugen, Fluoreszenzspektroskopie
und Dynamische Lichtstreuung im Arbeitskreis Bein
Seit 01/2008: Fachliche Anleitung und Ausbildung von Diplomanden und
Studenten im Hauptstudium, Betreuung von Praktika in der
Anorganischen und Physikalischen Chemie

Sonstiges

12/2007: Preis der Dr. Klaus Römer Stiftung (Diplomarbeit)
12/2008: Center for NanoScience Publikationpreis 2008
12/2009: Center for NanoScience Publikationpreis 2009

Zusatzqualifikationen

Sprachen: Englisch (verhandlungssicher)
Französisch (gut)
EDV: Microsoft Office Produkte (sehr gut)
Adobe Illustrator und Photohop (gut)

14. Publications and Presentations

14.1 Publications

1. "Selective Functionalization of the Outer and Inner Surfaces in Mesoporous Silica Nanoparticles"
J. Kecht, A. Schlossbauer, and T. Bein; *Chem. Mater.* **2008**, 20 (23), 7207-7214
2. "Click Chemistry for High-Density Biofunctionalization of Mesoporous Silica"
A. Schlossbauer, D. Schaffert, J. Kecht, E. Wagner, and T. Bein; *J. Am. Chem. Soc.* **2008**, 130, 12558-12559
3. "Biotin-Avidin as a Protease-Responsive Cap System for Controlled Guest Release from Colloidal Mesoporous Silica"
A. Schlossbauer, J. Kecht, and T. Bein; *Angew. Chem. Int. Ed.* **2009**, 48(17), 3092-3095
4. "Multiple Core-Shell Functionalized Colloidal Mesoporous Silica Nanoparticles"
V. Cauda, A. Schlossbauer, J. Kecht, A. Zürner, and T. Bein; *J. Am. Chem. Soc.* **2009**, 131 (32), 11361-11370
5. "Bio-degradation study of colloidal mesoporous silica nanoparticles: effect of surface functionalization with organo-silanes and poly(ethylene glycol)"
V. Cauda, A. Schlossbauer, and T. Bein; *Microporous Mesoporous Mater.* **2010**, 132, 60-71
6. "A Programmable DNA-based Molecular Valve for Colloidal Mesoporous Silica"
A. Schlossbauer, S. Warncke, P. M. E. Gramlich, J. Kecht, A. Manetto, T. Carell and T. Bein; *Angew. Chem. Int. Ed.* **2010**, 49 (28), 4734-4737
7. "pH-Sensitive Gate Controlling the Delivery Kinetics from Colloidal Mesoporous Silica Nanoparticles"
V. Cauda, C. Argyo, A. Schlossbauer, and T. Bein; *J. Mater. Chem.* **2010**, 20, 4305-4311
8. "Role of Endosomal Escape for Disulfide-Based Drug Delivery from Colloidal Mesoporous Silica Evaluated by Live-Cell Imaging"
A. M. Sauer, A. Schlossbauer, N. Ruthardt, V. Cauda, T. Bein, and C. Bräuchle, *Nano Lett.* **2010**, 10(9), 3684-3691
9. "Immobilizing Glycopranose on Mesoporous Silica via "Click Chemistry" for Borate Adsorption"
D. I. Fried, A. Schlossbauer, and T. Bein, *Microporous Mesoporous Mater.* **2010**, *accepted*
10. "pH-responsive Release of Mellitin from SBA-15 Mesoporous Silica"
A. Schlossbauer, C. Dohmen, D. Schaffert, E. Wagner, and T. Bein, *submitted*

14.2 Poster Presentations

1. A. Schlossbauer, D. Schaffert, J. Kecht, E. Wagner, and T. Bein
„Click-Chemistry for High-Density Biofunctionalization of Mesoporous Silica“
Third International Symposium „Advanced micro- and mesoporous materials“, **2009**, Albena,
Bulgarien

14.3 Oral Presentations

1. A. Schlossbauer, J. Kecht, and T. Bein
„Biotin-Avidin as Protease-Responsive Cap-System for Colloidal Mesoporous Silica“
21. Deutsche Zeolith Tagung, **2009**, Kiel

2. A. Schlossbauer, A. M. Sauer, V. Cauda, N. Ruthardt, C. Bräuchle, and T. Bein
„Synthesis Strategies for stimuli-responsive release mechanisms from colloidal mesoporous
silica“
22. Deutsche Zeolith Tagung, **2010**, München

3. A. Schlossbauer, S. Warncke, T. Carell, and T. Bein
„Molecular Valves for Controlled Guest Release from Colloidal Mesoporous Silica Based on
Biotin-Avidin Binding“
16th International Zeolite Conference/7th International Mesostructured Materials Symposium
, **2010**, Sorrento, Italien

4. A. Schlossbauer and T. Bein
„Synthesestrategien zur Kontrollierten Freisetzung von Substanzen aus Kolloidalem,
Mesoporösen Silikatnanopartikeln“, **2010**, Nano4Lifescience, Planegg

14. Publications and Presentations

14. Publications and Presentations
